

Technical Performance of EHV Power Transmission Systems with Long Underground Cables

Khalilnezhad, Hossein

DOI

[10.4233/uuid:1a7bbcd9-e0d8-489d-9c0f-67b8595fb945](https://doi.org/10.4233/uuid:1a7bbcd9-e0d8-489d-9c0f-67b8595fb945)

Publication date

2018

Document Version

Final published version

Citation (APA)

Khalilnezhad, H. (2018). *Technical Performance of EHV Power Transmission Systems with Long Underground Cables*. [Dissertation (TU Delft), Delft University of Technology].
<https://doi.org/10.4233/uuid:1a7bbcd9-e0d8-489d-9c0f-67b8595fb945>

Important note

To cite this publication, please use the final published version (if applicable).
Please check the document version above.

Copyright

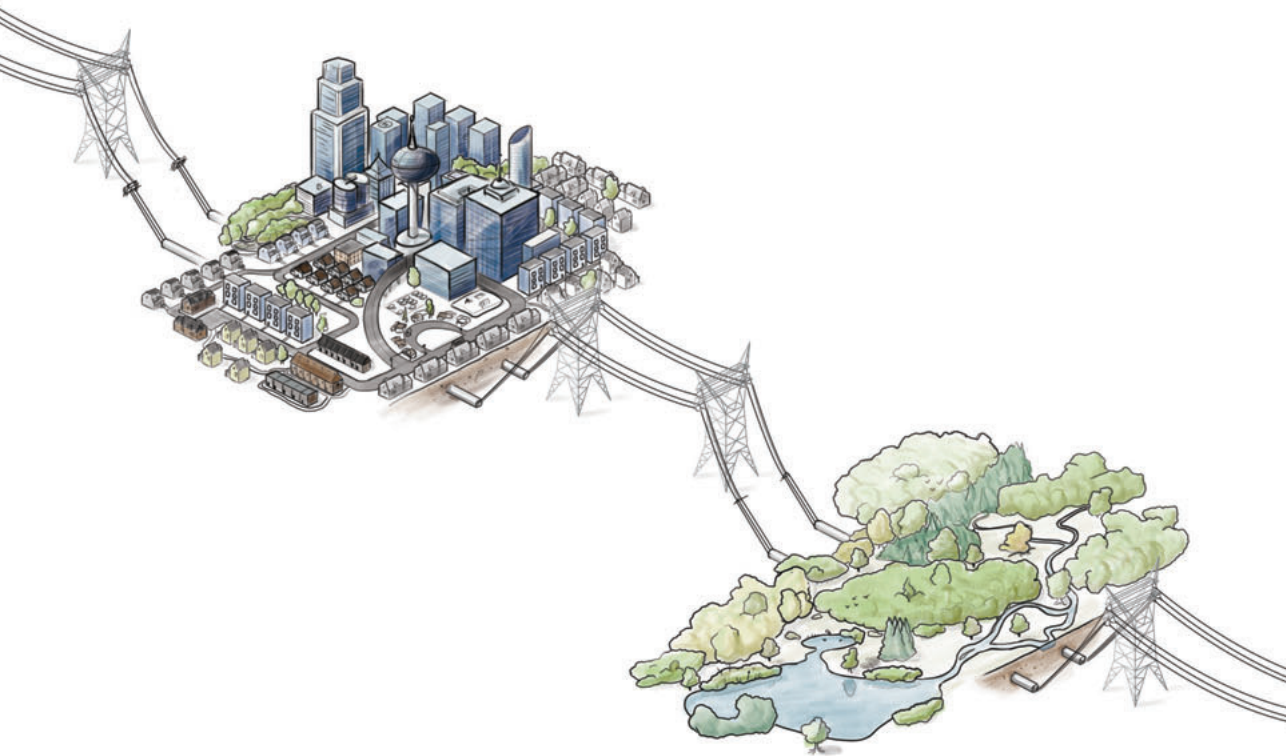
Other than for strictly personal use, it is not permitted to download, forward or distribute the text or part of it, without the consent of the author(s) and/or copyright holder(s), unless the work is under an open content license such as Creative Commons.

Takedown policy

Please contact us and provide details if you believe this document breaches copyrights.
We will remove access to the work immediately and investigate your claim.

Technical Performance of EHV Power Transmission Systems with Long Underground Cables

Hossein Khalilnezhad



**TECHNICAL PERFORMANCE OF EHV POWER
TRANSMISSION SYSTEMS WITH LONG
UNDERGROUND CABLES**

TECHNICAL PERFORMANCE OF EHV POWER TRANSMISSION SYSTEMS WITH LONG UNDERGROUND CABLES

DISSERTATION

for the purpose of obtaining the degree of doctor
at Delft University of Technology
by the authority of the Rector Magnificus, Prof. dr. ir. T. H. J. J. van der Hagen
chair of the Board for Doctorates
to be defended publicly on
Tuesday 11 December 2018 at 10:00 o'clock

by

HOSSEIN KHALILNEZHAD

Master of Science in Electrical Engineering
Delft University of Technology, the Netherlands

Born in Birjand, Iran

This dissertation has been approved by the promoters.

Composition of the doctoral committee:

Rector Magnificus	Chairperson
Prof. ir. L. van der Sluis	Delft University of Technology, promotor
Dr. dipl.-ing. M. Popov	Delft University of Technology, promotor

Independent members:

Prof. dr. ir. A. Ametani	Doshisha University, Japan
Prof. dr. ir. E. F. Steennis	Eindhoven University of Technology
Prof. dr. P. Palensky	Delft University of Technology
Prof. dr. J. J. Smit	Delft University of Technology
Ir. J. Smit	TenneT TSO B.V.

This research was financially supported by TenneT TSO B.V. within the framework of the 380 kV cable research program.



Keywords: Hybrid OHL-Cable grids, EHV underground cables, Power system transients, Power system planning and design

ISBN 978-94-6375-217-6

Copyright © 2018 Hossein Khalilnezhad, the Netherlands
Cover design copyright © 2018 Hossein Khalilnezhad, the Netherlands
Cover design by Arie de Kam, the Netherlands

All rights reserved. No part of the material protected by this copyright notice may be reproduced or utilized in any form or by any means, electronic or mechanical, including photocopying, recording or by any information storage and retrieval system, without written permission of the author.

An electronic version of this dissertation is available at: <http://repository.tudelft.nl/>

Printed by Ridderprint B.V., Ridderkerk, the Netherlands

*To my beloved family,
my parents Zahra and Mahmood,
my sisters Parisa and Pardis,
and my brother Reza.*

SUMMARY

Extra high voltage (EHV) power transmission systems have been traditionally constructed by using overhead lines (OHL) to transfer power over long distances. During the last decade, the opposition against the construction of new OHLs has significantly increased due to societal and environmental concerns, which has caused major obstacles for the grid development. Under this circumstance, system operators have been urged to find solutions and alternatives for the future grid developments.

A promising solution of this challenge is to underground the transmission grids (fully or partially) by means of EHV AC underground cables. In this regard, the future transmission grids will be composed of OHLs in non-sensitive areas and underground cables in sensitive areas like populated neighbourhoods and environmentally sensitive locations, which implies on a large-scale utilization of long cables in future EHV grids. These grids are known as hybrid OHL-Cable grids. Although this is very encouraging from the societal and environmental points of view, new challenges arise mainly from the technical perspective and high capital cost.

Regarding the technical perspective, the large-scale application of long cables in transmission grids is not yet a well-practiced technique for system operators. In fact, cables have been widely used in low and medium voltage distribution grids, but not in EHV transmission grids. The electrical, thermal, and mechanical characteristics of cables and OHLs are significantly different. These differences can cause various technical problems in the grid, which in return may increase the chance of damage to system components and reduce the reliability of the power supply. Therefore, a decision for the large-scale utilization of EHV cables will be very risky without gaining the complete knowledge and insight of the expected hazards and their countermeasures. This was the main driving force for system operators and manufacturers to carry out research and investigation on the technical performance of EHV grids with long cables.

So far, lots of researches have been performed to investigate the design and operation of long EHV cables in transmission grids. These studies have answered many questions and unknowns, but there are still several important scientific gaps that have to be tackled. As a result, the Dutch transmission system operator, TenneT, began an extensive ten-year cable research program together with the Technical Universities of Delft and Eindhoven to investigate the technical possibilities of utilizing long EHV underground cables in the future transmission projects.

This thesis, as the last part of the Dutch cable research program, provides robust and comprehensive answers to the most crucial scientific gaps and addresses the required techniques for the reliable operation of cable projects. These techniques can be used in practice by system operators since they are based on realistic assumptions and reliable

simulations on an accurate model of an actual power transmission system. This thesis focuses on crucial phenomena related to the steady-state operation, harmonic behaviour, and transient operation of hybrid OHL-Cable systems. A hypothetical future project in the Dutch 380 kV grid with 80 km transmission length was selected as the case study, for which all phenomena were studied according to the most recent standards and grid code.

The main scientific contribution of this thesis is the rigorous and comprehensive analysis of a hybrid OHL-Cable system to identify the impact of long cables, system parameters and topology on the system operation. The thesis proposes a methodology for optimal compensation of the cable reactive power in order to enhance the system performance. Moreover, the significance of energization overvoltages is investigated by a robust statistical analysis, which is the first of its kind for hybrid OHL-Cable grids. Last but not the least, two new countermeasures for the zero-missing phenomenon have been developed and several other countermeasures have been also investigated.

The main conclusion of the thesis is that the large-scale application of underground cables in transmission systems is technically possible under the condition that all technical phenomena and issues are properly addressed in the planning and designing phases of each project. A case-by-case study for cable projects is a “must” as each project has its own electrical and geographical characteristics. System parameters and topology are different in different areas and consequently the severity of phenomena and challenges will be different. Several countermeasures are available for each technical issue, where the most optimal one should be selected by conducting an in-depth technical analysis. The decision to choose the right countermeasure is highly dependent on the project specifications.

Finally, for each cable project, it is always recommended to perform a step-by-step study similar to the presented approach in this thesis, in which all the relevant phenomena from the steady-state operation to the electromagnetic transient behaviour are investigated. The study should follow the guidelines, grid code, manufacturer requirements, and standards in order to guarantee that all requirements for a reliable system operation are met accordingly.

SAMENVATTING

Het hoogspanningstransportnet maakt traditiegetrouw gebruik van bovengrondse hoogspanningsverbindingen. De laatste jaren echter is de weerstand tegen nieuw aan te leggen bovengrondse verbindingen, vanuit maatschappelijke en milieuoverwegingen, toegenomen en dit is een aanzienlijk obstakel geworden bij de uitbreiding van het hoogspanningsnet.

Een veel voorgestelde oplossing voor deze problematiek is het geheel of gedeeltelijk vervangen van de bovengrondse lijnen door ondergrondse kabels. Als gevolg daarvan zullen toekomstige transportnetten bestaan uit bovengrondse hoogspanningslijnen en, in dicht bevolkte gebieden, als dit mogelijk is uit ondergrondse hoogspanningskabels. Dit brengt een grootschalig gebruik van EHV-kabels met zich mee. Deze netten worden als gemengde lijn-kabel netten aangeduid. Alhoewel dit tegemoet komt aan de wensen van de burgers en de lokale overheden levert dit voor de netbeheerder, van uit technisch oogpunt bezien, nieuwe uitdagingen op en het brengt tevens hogere investeringen met zich mee. Het op grote schaal toepassen van grote lengtes EHV-kabel is heden ten dage nog geen praktijk. In laagspanningsnetten en hoogspanningsdistributie netten worden ondergrondse kabels echter wel veelvuldig toegepast.

Het thermisch en elektrisch gedrag en hoe zij zich gedragen bij mechanische belasting is voor kabels verschillend van dat voor lijnen. Deze verschillen zorgen voor een verscheidenheid aan technische problemen bij vervanging van lijnen door kabels en die kunnen zelfs uitmonden in schade aan andere hoogspanning componenten en daardoor de betrouwbaarheid van de elektriciteitsvoorziening in negatieve zin beïnvloeden. Dientengevolge is besluitvorming over het op grote schaal toepassen van EHV-kabels zonder uitgebreide verkennende systeemstudies, om eventuele knelpunten aan het licht te brengen en de daarvoor te nemen maatregelen in kaart te brengen, sterk af te raden. Deze stellingname is voor netbeheerders en fabrikanten de drijvende kracht om onderzoek te doen naar en metingen te verrichten aan het systeem gedrag van EHV-netten met lange kabel tracés.

Er zijn in de loop der jaren een aantal studies verricht naar de bedrijfsvoering van transportnetten met EHV-kabels. Deze studies hebben een antwoord kunnen geven op veel van de voorliggende vragen, maar er blijven desalniettemin nog een significant aantal vragen onbeantwoord. Dit laatste was voor de netbeheerder TenneT tien jaar geleden aanleiding om met de Technische Universiteiten van Delft en Eindhoven een grootschalig onderzoeksproject te definiëren met als doel inzicht te verkrijgen in het systeemgedrag van gemengde lijn-kabel verbindingen.

Dit proefschrift vormt het sluitstuk van dit Randstad-380kV onderzoeksproject en geeft antwoorden op een aantal nog openstaande vragen en geeft tevens in voorkomende gevallen

richtlijnen voor een betrouwbare bedrijfsvoering van het transportnet, gebaseerd op simulaties met een op de praktijk afgestemd computermodel van het huidige Nederlandse 380 kV transportnet. Het proefschrift beschrijft de belangrijkste verschijnselen die zich bij de dagelijkse bedrijfsvoering kunnen voordoen, de invloed van hogere harmonischen op de netcomponenten en de schakelverschijnselen die in gemengde lijn-kabel verbindingen kunnen optreden.

Een in de toekomst mogelijke uitbreiding van het 380 kV net met een denkbeeldige transport verbinding van 80 kilometer is gekozen als onderwerp voor een casestudie waarbij de optredende verschijnselen bestudeerd zijn in relatie tot de geldende voorschriften en de net-code.

De wetenschappelijke bijdrage van dit proefschrift vindt zijn grondslag in de uitgebreide en diepgaande analyse van gemengde lijn-kabel verbindingen waarbij de invloed van de kabellengte, de systeemvariabelen en de topologie van het transportnet op de bedrijfsvoering zijn bestudeerd. Het proefschrift beschrijft de werkwijze om tot een optimale compensatie van het door de kabels gegenereerde blindvermogen te komen.

Middels een uitgebreide statistische analyse is het ontstaan van schakeloverspanningen onderzocht, hetgeen voor gemengde lijn-kabel verbindingen niet eerder is gedaan. Tot slot worden twee nog niet eerder in de literatuur beschreven maatregelen tegen het verschijnsel van uitblijvende stroom-nul doorgangen voorgesteld en andere reeds bekende maatregelen tegen dit fenomeen zijn beschreven en onderzocht.

Het op wat grotere schaal opnemen van kabels in bovengrondse EHV-transportverbindingen is technisch mogelijk, met dien verstande dat aan alle voorkomende verschijnselen bij de planning en in de ontwerpfase van elk project zorgvuldig aandacht wordt besteed. Elk project is als zodanig uniek en heeft daarom zijn eigen geografische en elektrische aspecten. Voor de zich voordoende technische aandachtspunten zijn oplossingen voorhanden van waaruit de voor de desbetreffende situatie de meest optimale gekozen kan worden. Voor elk kabelproject dient vanaf het begin bij voorkeur de stap-voor-stap benadering, als beschreven in dit proefschrift, gevolgd te worden, waarbij de voorschriften, de net-code en de eisen van de fabrikant als harde randvoorwaarde worden meegenomen.

CONTENTS

Summary	vii
Samenvatting.....	ix
1 Introduction	1
1.1 Background	1
1.2 Hybrid OHL-Cable Transmission Grids	2
1.3 Problem Definition	3
1.4 Technical Issues and State-of-the-Art	3
1.4.1 Steady-State Operation	5
1.4.2 Harmonic Resonance	6
1.4.3 Transient Operation	6
1.4.4 Reliability	9
1.4.5 Power System Stability	9
1.5 Dutch 380 kV Cable Research Program	10
1.6 Research Objectives	11
1.7 Thesis Outline	12
References	14
2 Case Study Project and Grid Modelling.....	19
2.1 Introduction	19
Part I: Case Study Project.....	19
2.2 Dutch Power Transmission Grid	20
2.3 Spaak Project.....	20
2.3.1 Mixed-Line Configuration.....	22
2.3.2 Cable Scenarios	26
Part II: Grid Modelling	28
2.4 Grid Modelling for Steady-State Studies.....	28
2.5 Grid Modelling for Transient Studies.....	30
2.5.1 Modelling Depth.....	30
2.5.2 Overview of the Dutch 380 kV Grid Model	32
2.5.3 Transmission Lines Modelling	32
2.5.4 Transformer and Shunt Reactor Modelling	42
2.5.5 Capacitor Banks Modelling	42
2.5.6 Lower Voltage Grids Modelling.....	43
2.6 Conclusions	43

References.....	44
3 Shunt Compensation Allocation in Hybrid OHL-Cable Systems	49
3.1 Introduction	49
3.2 Cable Capacitive Behaviour	50
3.3 Negative Effects of Cable Reactive Power.....	50
3.4 Reactive Power Compensation.....	52
3.5 Study of the Spaak Project	53
3.5.1 Sizing Criteria	53
3.5.2 Load-Flow Scenarios	55
3.5.3 Global Compensation	55
3.5.4 Most Decisive Sizing Criterion	58
3.5.5 Distributed Compensation	61
3.5.6 Impact of Mixed-Line Configuration	62
3.6 Cable Overloading.....	64
3.7 Conclusions	67
References.....	68
4 Resonance Behaviour of Hybrid OHL-Cable Systems.....	71
4.1 Introduction	71
4.2 Resonance in Electrical Circuits.....	72
4.3 Typical Grid Topologies Leading to Resonance in Cable Systems.....	74
4.3.1 Series Resonance Topologies	75
4.3.2 Parallel Resonance Topologies.....	76
4.4 Resonance Behaviour of the Dutch 380 kV Grid with the Spaak Connection	77
4.4.1 Parameter Selection	78
4.4.2 Evaluation Criteria.....	79
4.4.3 Impact of the Spaak Connection.....	79
4.4.4 Impact of Shunt Compensation	82
4.4.5 Impact of Shunt Compensation Location	83
4.4.6 Impact of Mixed-Line Configuration	84
4.5 Conclusions	86
References.....	86
5 Energization Overvoltages in Hybrid OHL-Cable Systems	89
5.1 Introduction	89
5.2 Simulation Considerations	90
5.3 Energization Overvoltages	92
5.4 Statistical Analysis of Overvoltages.....	95
5.4.1 Statistical Behaviour of Circuit Breaker	96
5.4.2 Statistical Simulation Approach	97
5.4.3 Simulation Results and Analysis	98

5.5 Conclusions	111
References	112
6 Zero-Missing Phenomenon in Cable Systems	115
6.1 Introduction	115
6.2 Zero-Missing Phenomenon	116
6.3 Operation Criteria	119
6.4 Countermeasures	120
6.5 Simulation Results	121
6.5.1 Simultaneous Cable and Reactors Energization at the Voltage Peak	122
6.5.2 Energization in Sequence	126
6.5.3 Sequential Switching	131
6.5.4 Opening Faulted Phase(s)	132
6.5.5 Increasing DC-Offset Damping	132
6.6 Discussions	135
6.7 Conclusions	137
References	137
7 De-Energization Transients of Hybrid OHL-Cable Systems	139
7.1 Introduction	139
7.2 Capacitive Current Interruption	139
7.3 De-Energization Transients of the Spaak Connection	142
7.3.1 Switching-off Both the Circuit and Shunt Reactors	143
7.3.2 Switching-off the Circuit	146
7.4 Conclusions	152
References	152
8 Conclusions and Recommendations	155
8.1 Social and Scientific Relevance	155
8.2 Scientific Contributions	156
8.3 Findings and Conclusions	157
8.4 Recommendations for Future Research	162
A Study Flowchart for the Technical Performance Assessment and Design of Long EHV Cable Connections	165
Glossary	167
Acknowledgements	171
Biography and Publications	173

CHAPTER 1

INTRODUCTION

1.1 BACKGROUND

Extra high voltage (EHV) power transmission grids are responsible for transferring bulk amounts of electric power along long distances from production to consumption sites. These grids are the backbones of the electric energy supply system and their proper functionality is directly related to the national security of every country. This means that these grids should be designed and operated for maximum reliability and efficiency.

Nowadays, transmission grids are often operated close to the limits of their transfer capacity. This highlights the necessity of grid expansions and reinforcements to increase the available transfer capacity and to guarantee the reliability of future power supply. This upgrade is required in the near future due to several reasons, notably the higher power demand, fast increase of cross-border trades, and production of bulk amount of renewable energy at the edges of grids. Upgrading power grids can be realized by constructing new facilities and/or replacing aging grid components.

Power transmission grids are traditionally based on the overhead lines (OHL) and any increase in the grid transfer capacity has been traditionally realized by building new OHLs. In 2007, over 98% of the onshore EHV transmission grids in Europe (European Union, Norway and Switzerland) were of OHL construction [1]. This technology has been used for decades since it is relatively cheap to construct, easy to maintain, reliable in operation, and well-known by transmission system operators (TSOs) and manufactures. However, OHLs sometimes cross through populated or environmentally sensitive areas, causing several problems and adverse consequences.

The main problem with developing new OHLs is widespread public opposition and environmental impacts. People are reluctant to have OHLs and transmission towers in their surroundings due to their negative impacts; most notably, visual effect, land price decrement, land occupation (right-of-way), effects on forests and territories, health concerns related to exposure to electromagnetic fields, radio interference, and audible noise [2]. These negative impacts have caused strong political and environmental pressure by governments and non-governmental organizations on system operators and have made the construction of new OHLs more difficult than before. This situation is mostly noticeable in densely populated countries in Europe and south Asia. In some countries like the

Netherlands and Denmark, governments have passed laws to limit or ban the construction of new OHLs and, in some cases, to oblige system operators to find alternatives for existing OHLs. As a result, system operators have to find and implement solutions to overcome these obstacles of the grid development.



Figure 1.1: Overhead power transmission lines (OHLs) in sensitive areas.

1.2 HYBRID OHL-CABLE TRANSMISSION GRIDS

A promising solution for the mentioned obstacles is to extend the grids by means of alternating current (AC) underground cables. There are many factors that make cables attractive alternatives of OHLs. In underground cable systems, the electromagnetic field attenuates much faster with distance from the centre of the installation compared to those in OHL systems, although they are higher in cable systems right above the centre of the installation [2], [3]. In addition, underground cables have limited visual impact and no audible noise. The right-of-way for cables is also narrower compared to that of OHLs. Further, cables are stronger against earthquakes, storms, and freezing temperature. Therefore, cables can limit or remove the negative impacts of OHLs in locations like densely populated areas and national parks. This enables system operators to develop transmission grids with reduced social and environmental impacts. Grids with full or partial cable-based connections are known as hybrid OHL-Cable grids, where transmission connections are composed of OHLs in non-sensitive areas and underground cables in sensitive (and maybe non-sensitive) areas.



Figure 1.2: Power transmission by underground cables, (a) Randstad 380 kV project in the Netherlands, (b) 132 kV City West Cable Tunnel project in Sydney, Australia.

1.3 PROBLEM DEFINITION

The science of underground cables has developed steadily in recent decades. Underground cables have been so far widely used in low and medium voltage (i.e. distribution) grids [1]. However, usage of long EHV cables in transmission grids has not been common. This tendency has been changed during recent years due to social and political supports as well as successful development and operation of cross-linked polyethylene (XLPE) cables [1], [3].

Cables have been used here and there in EHV power transmission grids, but so far, their application has been limited to short lengths and a few locations. One of the longest cable connections in the world is in operation in Japan, consisting of two parallel circuits with a length of 40 km and at a voltage level of 500 kV [1], [3], [4]. A couple of cable projects with transmission lengths up to 35 km are in operation or under construction in the Netherlands and Germany. In Denmark, due to the government's decision in 2008, the system operator has to put all 132 kV and 150 kV grids under the ground by 2030. In addition, all new 400 kV power lines will be constructed by underground cables [5-7]. Cable projects are also in operation in Italy, notably the 400 kV AC submarine cable connection between the mainland and Sicily and the 380 kV double-circuit hybrid OHL-Cable line between Turbigo and Rho [5].

Despite the advantages of transmission systems undergrounding, negative aspects of cable application in these systems should be also taken into account, most notably the high capital cost and technical challenges of cable systems. The capital cost of an EHV cable connection is several times higher than that of an OHL with an equivalent transfer capacity [8]. In addition, a large-scale application of cables in EHV transmission grids has several technical issues and can cause undesirable system operating conditions. Therefore, it is crucial to properly address these challenges and devise countermeasures in the design stage of cable projects to improve the system performance and reliability.

1.4 TECHNICAL ISSUES AND STATE-OF-THE-ART

The large-scale application of cables in transmission grids is not yet a well-practiced technique from the technical point of view. Both system operators and equipment suppliers do not possess much experience with the technical performance of transmission systems with long cables as they are very different from OHLs from electrical, thermal, and mechanical perspectives [3], [9]. Cables that need reactive power shunt compensation are generally considered as long cables (for a three-phase 380 kV cable circuit with a single cable per phase, a long cable is associated to cables roughly longer than 10 km transmission length).

From the electrical point of view, major challenges are caused by significant differences between the electrical characteristics of cables and OHLs. The electrical characteristics of cables and OHLs are different since their structure and physical properties are not the same. The conductor in OHLs is surrounded and insulated by air, whereas cables have a

multi-layer structure consisting of at least four layers, including a core conductor, an insulating material with semiconductor layers at the interfaces, a sheath (screen) conductor, and an outer insulation layer (it may also have an extra layer of conductor, called armour, with an outer insulation layer). As a result, per unit length, the series inductance of a cable can be up to five times smaller and the shunt capacitance to earth can be up to thirty times larger than those of an equivalent-rated OHL [3].

The application of cables influences the behaviour of a traditionally OHL-based grid in several aspects due to the large cable capacitance and its interaction with the inductive grid. Several undesirable operating conditions are expected in hybrid OHL-Cable systems, which increase the risk of damage to system components and reduce the reliability of the power supply [3], [5-11]. Therefore, all the technical issues should be investigated before realization of a cable project.

Before explaining the most important technical issues, it is useful to elaborate on the classification of overvoltages in transmission grids. A transmission grid can experience overvoltages with frequencies up to 100 MHz, which can be classified to four categories based on the amplitude, shape, and duration of overvoltage waveforms [12-14]:

- *Temporary overvoltages* (TOV): temporary overvoltages are recognized by low-frequency oscillations below 500 Hz and long duration up to several minutes. These overvoltages can be caused by several events like transformer energization, line energization/de-energization, fault, fault clearing, switching of capacitive and inductive currents, resonance, and load rejection. TOVs are important in determining stresses on equipment related to power-frequency withstand voltage. Ferro-resonance is a particular type of temporary overvoltages [15].
- *Slow-front overvoltages* (SFO): these overvoltages are with frequencies up to 20 kHz and duration of some milliseconds. Slow-front overvoltages can be caused by events like transformer energization, line energization/de-energization, fault, fault clearing, and switching of capacitive/inductive current. Slow-front overvoltages are used to determine withstand voltage of equipment insulation.
- *Fast-front overvoltages* (FFO): fast-front overvoltages are with much larger amplitudes than other voltages and with frequencies from 10 kHz to 3 MHz and the duration of tens of microseconds. They are mainly caused by lightning strokes and sometimes caused by switching of capacitive/inductive currents and back flashover. These types of overvoltage should be studied to determine the risk of equipment failure and selection of protective devices, mainly surge arresters.
- *Very-fast front overvoltages* (VFFO): these overvoltages are with frequencies up to 100 MHz and duration of tens of nanoseconds. They are associated with GIS switching actions, vacuum circuit breaker switching in medium voltage levels, and SF6 circuit breaker re-ignition.

The major technical issues related to the performance of transmission grids with long cables can be sorted in five categories as below:

1.4.1 STEADY-STATE OPERATION

The steady-state operation is related to the performance of the grid in the normal condition when no disturbance has occurred (i.e. 50 Hz or 60 Hz frequency operation). In this case, the main technical challenge of long cables operation is the cable surplus reactive power, which is a consequence of the large surge impedance loading of cables.

The surge impedance loading (SIL) is the power loading at which reactive power is neither produced nor absorbed by a line. When a line is loaded above its SIL, it acts like a shunt reactor and absorbs reactive power and when it is loaded below its SIL, it acts like a shunt capacitor and generates reactive power. SIL of a cable is several times larger than that of an OHL. During the normal operation, because the cable SIL is several times larger than its thermal rating, cables are always loaded below their SIL and produce reactive power like capacitors. On the contrary, SIL of an OHL is smaller than its thermal rating and therefore OHLs are normally operated above their SIL and behave as inductors consuming reactive power [16], [17].

The capacitive behaviour of cables means that a loaded cable injects reactive power into the grid. As a result, a portion of the cable ampere capacity (ampacity) is occupied by the capacitive (charging) current. By increasing the cable length, a larger portion of the cable ampacity is occupied by the capacitive current and the remaining transfer capacity for active power decreases. At a critical length, the capacitive current equals the cable ampacity so that no transfer capacity is left for active power. This is one of the main limitations in application of long AC cables, which is elaborated and analysed in [17-20]. In addition, the large surplus reactive power produced by cables results in steady-state voltage rise and under-excitation of synchronous generators (in severe cases self-excitation), which can cause severe stresses on power system equipment and higher risk of system transient instability [3], [17], [21]. Another risk of long cables operation is the large capacitive current in the line circuit breakers, which may exceed the breaking capability of the breaker [17], [22].

The above-mentioned limitations and problems can be removed by an optimal shunt compensation of cable reactive power. This is realized by using fixed or variable size shunt reactors connected to the hybrid circuit at the two ends or distributed at multiple locations along the circuit. Alternatively, shunt reactors can be installed at substation busbars or at power transformer tertiary windings when the cable is not long. When the increase of active power transfer capacity is required, shunt reactors should be distributed along the cable especially for cables longer than the critical length. The distributed compensation can also reduce the required degree of compensation and boost the system transient stability [21], [22]; however, it may not be possible to utilize a distributed compensation in some situations due to the land occupation and visual impact of reactor banks [17].

As mentioned, shunt reactors should be sized and located optimally. Otherwise, in case of under compensation, the discussed problems may not be completely removed and in case of overcompensation, the risk of other negative phenomena like zero-missing currents may increase [3], [17], [22], [23]. References [3], [17-20], [22], [24], [25] proposed techniques for optimal sizing of shunt reactors, where they have considered different sizing criteria for

shunt compensation sizing. In addition, the power transmission limits of cable lines are analytically assessed in [25], where the AC load-flow simulations of the transmission network referring to severe loading conditions are evaluated.

Another problem with the utilization of long cables is the cable overloading when it is operated in parallel with OHLs. The lower series impedance of cables compared to that of OHLs may lead to an unequal power flow in parallel circuits with higher power flowing through the circuits with cables. To solve this problem, series reactors or phase shifting transformers can be installed to control the power flow.

1.4.2 HARMONIC RESONANCE

The use of long EHV cables in transmission systems raises serious concerns regarding the resonance behaviour of systems. The large cable capacitance leads to low-order series and parallel resonance frequencies, lower than those in the systems without cables. In addition to the order of the first resonance frequency, the number and the magnitude of resonance frequencies can increase when cables are applied in transmission systems [3], [10], [26-28]. In shunt-compensated cable connections, a parallel-resonance circuit is formed by the cable capacitance and the shunt reactor inductance. The combination of the cable capacitance and transformer leakage inductance forms a series-resonance circuit [5], [9].

Resonance temporary overvoltages occur when a resonance circuit is excited by a current or voltage with an equal frequency to that of the resonance circuit. Harmonic currents and voltages can be originated from switching actions or short-circuits in the system (leading to damped oscillations) and/or from existing background harmonic sources (leading to driven oscillation) [29], [30]. In the latter case, the existing background harmonics produced by sources like frequency controllers of motors, HVDC connections, and convertors can be amplified when long cables are added to the system. The background harmonic amplification can cause power quality issues and is unequal among the three phases when the cable system is electrically asymmetrical [31].

Temporary overvoltages produced by a resonance in a cable system are weakly damped and last long. In fact, the system resistance damps the oscillations especially at higher resonance frequencies (because it is directly proportional to frequency), but in cable systems, the resonance frequencies are low and as the result the system resistance is also low. On the other hand, the probability of exciting the low-order resonance frequencies is higher due to the presence of larger harmonic pollution in the low-order frequency spectrum than the high-order range [3], [5]. Thus, the sustained nature and the higher probability of resonance overvoltages in cable systems can impose a high-risk situation for system equipment.

1.4.3 TRANSIENT OPERATION

One of the main technical concerns regarding the application of long cables in transmission levels is the system transient performance. Transients are initiated by switching actions (energization and de-energization), faults or lightning events [32], [33]. The occurrence probability and severity of a phenomenon depends on the system parameters and topology

at the point of interest. Each transient phenomenon can result in steep and high overvoltages, high inrush currents, and/or severe transient recovery overvoltages (TRV) across the circuit breakers. These negative consequences impose high stress on system equipment causing either an immediate breakdown or a gradual damage of equipment.

A. ENERGIZATION OVERVOLTAGES

Energization overvoltages after connection of an unloaded transmission line to the grid are temporary or slow-front [34]. Several phenomena are associated with energization of cables. Statistical studies show that the energization overvoltages of a cable are lower than those of an OHL with an equal length [32], [35]. A hybrid OHL-Cable circuit with a given transmission length produces energization overvoltages higher than those of a fully-cable circuit and most likely lower than those of a fully-OHL circuit with the same transmission lengths [36-38]. However, still high energization overvoltages are expected in hybrid OHL-Cable circuits. Energization overvoltages are very dependent on the number, location, and lengths of cable and OHL sections because of the consequent changes in reflections and refractions of the propagating voltage/current waves at locations with surge impedance mismatch (cable joints and OHL-Cable transition points). It should be noted that other system parameters also affect energization overvoltages; most notably, the power-frequency voltage, system short-circuit power, shunt compensation degree, and switching instant [32], [39].

The cable energization with trapped charges on the cable can generate even higher overvoltages on both the core and sheath conductors, which increases the risk of equipment failure. Excessive sheath voltage limiters (SVL) failures in 275 kV cable circuits were reported [40]. In cables longer than 1 km, the sheath conductor is generally grounded to decrease the induced current, power losses, and overvoltages on the sheath [32], [41]. The travelling surges are reflected and refracted at the sheath-bonding joints due to impedance mismatch, which may lead to overvoltages across the sheath section insulation and the sheath to earth insulation [42], [43]. The SVL energy absorption rating, as a function of the voltage magnitude and duration of which it remains in conduction state, can be exceeded in case of high energization overvoltages [40].

Energization of long cables in parallel is categorized among slow-front events and is usually associated with high inrush currents. It is a similar phenomenon as back-to-back energization of capacitor banks [3], [23], [44], [45]. When two or more cable connections are in parallel (i.e. connected to the same busbar), energization of a cable causes a part of the charge on the already energized cable(s) flowing to the cable being energized and cause a high and steep inrush current. The amplitude and frequency of the inrush current are higher than those of a stand-alone cable with no parallel cables. High inrush currents may put a severe stress on the line circuit breaker and decreases its lifetime, therefore mitigation measures should be considered if the circuit breaker ratings are exceeded.

B. ZERO-MISSING PHENOMENON

Energization of shunt-compensated cable connections may also result in the zero-missing phenomenon. The simultaneous energization of the cable and reactors may cause a zero-missing current, which means that the current through the line breaker does not cross the zero value for several cycles. In this situation, it is difficult or even impossible to safely open the healthy phases if a fault occurs in the circuit at the instant of, or just after, energization when the zero-missing current is still present. Therefore, the system is more vulnerable and unprotected against faults if proper countermeasures are not devised at the design stage of the cable project. Several countermeasures have been addressed in [23], [32], [46] to prevent or mitigate the zero-missing current, whereas the effectivity of a countermeasure is strongly dependent on the system parameters and topology like the configuration of the hybrid OHL-Cable circuit, power-frequency voltage, and short-circuit power.

C. DE-ENERGIZATION TRANSIENTS

The de-energization of a cable connection is associated with several phenomena. The required time for the complete discharge of a cable depends on the system configuration and characteristics, mainly the connection of shunt reactors and voltage transformers (VT). Normally, it takes a very long time to discharge the charge of a long cable without direct shunt compensation due to the high resistance of the discharge circuit; however, when the shunt reactors remain connected to the disconnected cable, the discharge time is only a few tens of seconds [3], [32], [47]. When inductive VTs are present, cable discharges in several hundred milliseconds due to the quick saturation of VTs [3].

When a hybrid OHL-Cable circuit is de-energized with shunt reactors connected to the phases, the residual voltages on the disconnected phases are decaying oscillatory voltages with superimposed frequencies. A de-energized reactor-connected cable phase oscillates with its natural frequency determined by the cable capacitance and the shunt reactor inductance. The natural resonance frequency will be close to 50 Hz in circuits with long cables due to the high degree of compensation close to 100%. When the circuit is even slightly unsymmetrical, each phase has a slightly different resonance frequency. Due to the mutual inductive coupling between shunt reactor phases and the capacitive coupling between circuit phases, the resulting voltage on each phase is the sum of its own voltage and the two induced voltages by the other phases. In this situation, adding up three different voltages with different frequencies and phase shifts results in voltage amplification or attenuation [48], [49].

Resonance overvoltages are also expected in disconnected shunt-compensated hybrid OHL-Cable circuits. Resonance may occur between the reactor inductance, the inter-phase/inter-circuit capacitance, and the cable capacitance if reactors remain connected to the disconnected phase(s) which have a capacitive coupling with the energized phase(s). Ferroresonance may also occur when magnetic-core shunt reactors are used for the reactive power compensation. These risks can be minimized by connecting the shunt reactors via breakers to the line, so they can be disconnected from the de-energized phase(s) [15], [50].

Another issue with de-energization of cables is the risk of circuit breaker restrike due to the large cable capacitance, despite the probability of this incident is low. When a restrike occurs, very high slow-front or fast-front overvoltages with the risk of severe damages to the cable and system equipment are expected [51]. It should be stressed that the probability of breaker restrike is very dependent on the breakdown voltage of the dielectric between the breaker contacts.

High frequency transients may also originate from the energization and de-energization of the shunt reactors. When a reactor is switched-in, high magnitude unsymmetrical phase energization currents with large decay time will occur. Opening of a reactor breaker involves interruption of inductive currents, which may result in a high transient recovery voltage across the breaker contact gap and cause re-ignition [52], [53]. Transient overvoltages due to a re-ignition are steep and dangerous for system equipment.

D. LIGHTNING TRANSIENTS

A lightning strike is another origin of transients in power systems and can induce very high and fast-front overvoltages in the line. The behaviour of hybrid OHL-Cable circuits under lightning events is of importance since high overvoltages may lead to insulation breakdown and equipment failure [54]. Surge arresters are normally applied at transition points and/or both ends of the hybrid connection to protect the equipment against lightning overvoltages. The analysis of lightning transients requires an accurate model of the grid including a detailed representation of the grounding systems and high voltage towers.

1.4.4 RELIABILITY

An important issue related to operation of long cables is the reliability of transmission systems. Fault locating and repairing is more challenging and time consuming in cable systems compared to OHL systems, although several online and off-line methods for fault location in cable systems are addressed in literature [11]. According to the analysed failure statistics presented in [55], it takes a few hours to locate and repair a failure in OHLs, whilst this can take up to a month for underground cables. Although the failure frequency of a cable is lower than that of an OHL, existence of cable joints and terminations as the additional components of a cable system increase the failure frequency and decrease the reliability of the whole cable system [55]. Long outage of an important transmission line can lead to overloading of other transmission lines, load-shedding, and even in extreme cases power blackout in a part of the grid [56], [57].

1.4.5 POWER SYSTEM STABILITY

The application of long EHV cables can also impact the transient stability of transmission grids. The critical clearing time of a synchronous generator depends on the X/R ratio and the ratio between the line and generator impedances, which are different for cables and OHLs [3]. The X/R ratio of a cable can be an order of magnitude lower than that of an equivalent OHL [58]. Thus, replacing OHLs with cables results in a higher critical clearing time, especially when faults are close to substations [3].

The impact of a generator power factor on its critical clearing time should be also taken into account. When the cable share in a system increases, the operating point of the generator may shift to unity power factor or even in some cases to a lagging power factor (i.e. reactive power absorption), depending on the degree of reactive power compensation and the operating mode of the generator. The shift of the generator operating point to a lagging power factor reduces the critical clearing time and adversely affects the transient stability [3].

Generators under-excitation and in severe cases self-excitation may occur when the cable reactive power is not sufficiently compensated [3], [21]. In this situation, the uncompensated reactive power generated by a long cable may push the nearby synchronous generators to the under-excitation mode (or self-excitation mode in extreme cases) as they absorb the surplus reactive power in the grid. According to [21] and from the transient stability point of view, the main risks of long cables operation when the reactive power is not sufficiently compensated are: synchronous generators under-excitation and self-excitation, high-amplitude rotor angle oscillations, and high temporary overvoltages. The self-excitation phenomenon can cause an uncontrolled voltage rise at the generator terminal as well as equipment failure since the generator loses its control on the terminal voltage [3], [21].

These problems can be avoided by an appropriate allocation (both size and location) of shunt reactors and use of an optimal sequence for circuit breakers switching when cables are being connected or disconnected from the grid. Moreover, the system stability can considerably be improved by connecting shunt reactors directly to the line at the both remote ends or distributed along the line, instead of installing them at substation busbars or transformers [21], [22].

1.5 DUTCH 380 kV CABLE RESEARCH PROGRAM

In 2009, the transmission system operator of the Netherlands, TenneT, began an extensive research program to study the possibilities of underground cables application in the future transmission projects. This program has been conducted in collaboration with Delft University of Technology and Eindhoven University of Technology. The ten-year 380 kV cable research program has covered major technical issues associated with long EHV cables in order to increase the knowledge and experience of TenneT in the design and operation of hybrid OHL-Cable transmission systems.

Currently, the partially undergrounded Randstad 380 kV connection is in operation/under construction in the Dutch transmission grid. This is a double-circuit transmission line consisting of a south ring and a north ring. The south ring with 20.1 km length is between the substations Wateringen and Bleiswijk in the south-west of the Netherlands, out of which 10.8 km is realized by 2500 mm² single-core copper XLPE cables with two cables per phase. This part of the connection is in operation since 2015 and is composed of two OHL sections and a cable section in the middle (OHL-Cable-OHL) with lengths of 4.4, 10.8, and 6.8 km, respectively. The north ring is still under construction

between the substations Bleiswijk and Beverwijk with the total transmission length of 58 km, out of which 9.3 km will be realized by single-core copper and aluminium XLPE cables of different diameters. Currently, the first part of this connection between the Vijfhuizen and Beverwijk substations is in service. This connection includes five OHL and four cable sections placed in an intermediate sequence, where the shortest cable section will be 1 km long.

Within the Dutch cable research program, several Ph.D. and M.Sc. researches have been conducted on 380 kV cable systems. Reference [59] developed the models of key components of cable systems for transient studies and conducted transient analysis on the Randstad 380 kV South-Ring project. In [60], the steady-state power flow, the transmission line model validation, and the transient behaviour of the mixed OHL-Cable circuits of the Randstad South-Ring project were investigated. The transient stability of the Dutch transmission grid with long cables was studied in [61] and [21], in which the influence of long cables in three different locations of the grid on the transient stability was analysed. The reliability of EHV transmission lines consisting of OHLs and underground cables was studied in [62], where an investigation of failure statistics of the cable connection components has been presented too. Based on the research in [62], a complementary study was performed in [63] on the reliability modelling and assessment of the Dutch transmission grid to find out the impacts of future EHV cable installations on the overall reliability level. In 2016, a summary of the studies related to the shunt compensations sizing, reliability analysis, and condition monitoring of cable systems was published in [56].

1.6 RESEARCH OBJECTIVES

The operation of underground cables should have minimal negative effects on the characteristics and the behaviour of a power system. Despite of the gained knowledge and experiences during recent years about the technical performance of transmission systems with long cables, there are still several crucial scientific gaps that have to be addressed, especially related to hybrid OHL-Cable systems.

The aim of this thesis is to cover the most important scientific gaps and unanswered questions in this area with the use of a reliable model and a comprehensive approach, which make the findings of this thesis applicable to any transmission system. In fact, this thesis seeks for the techniques required for the reliable design and operation of cable projects in transmission systems. Therefore, the main objective of the thesis is to answer the following question:

From the technical perspective, how should EHV transmission systems be designed and operated for the large-scale utilization of underground cables?

To answer this question, this thesis focuses on phenomena related to the steady-state operation, harmonic behaviour, and transient operation of hybrid OHL-Cable systems. A possible future project in the Dutch 380 kV transmission grid is selected as the case study

project. The impact of cable length on system frequency, voltage, and current are analysed with regard to the IEC standards and grid code. Moreover, countermeasures for preventing or handling unwanted situations are devised whenever it is necessary.

With respect to the steady-state issues, this thesis provides an approach for optimal sizing and locating of shunt reactors. The influence of load-flow on the optimal size of reactors is determined by means of representing different load-flow scenarios during a year. In addition, sensitivity analyses are performed on distributed compensation and mixed-line structure.

With regard to the harmonic behaviour issues, the thesis addresses the impacts of the large-scale cable application on the frequency-scan of the grid. The changes in the number and the order of the resonance frequencies are recorded to determine the risk of resonance overvoltages.

Regarding the transient operation issues, three aspects are studied: energization transients, de-energization transients, and fault transients. In energization transients, this thesis carries out an in-depth study to determine how the overvoltages change with the large-scale application of cables. An extensive statistical analysis is presented to show how the distribution of energization overvoltages changes with the use cables. Moreover, effective and practical countermeasures of zero-missing phenomenon are provided. Finally, de-energization transients including voltage on the disconnected cables, TRV across the breaker contacts, and restrike are studied for different system operating conditions.

1.7 THESIS OUTLINE

The structure of this thesis is illustrated by the research flowchart shown in Figure 1.3, where the topics discussed in each chapter are as follows:

Chapter 2 is divided into two parts, where the first part describes the Spaak project, as the case study project of this research. The location of the project and the cable scenarios in addition to some general information about the Dutch transmission grid are provided in this part. The second part of this chapter elaborates on the developed models of the Dutch transmission grid. It is explained how the grid components are modelled for simulation of each technical issue. The developed models are used in the rest of the thesis for the simulation of the grid operation.

Chapter 3 deals with the shunt compensation allocation in EHV cable systems. The proposed method for the shunt compensation sizing is elaborated in this chapter. Four sizing criteria are used to find the required size of compensation. Moreover, different compensation arrangements including line-end and distributed arrangements are compared in terms of the required compensation size. In addition, the influence of the mixed-line configuration (i.e. different number and location of cable sections) on the required compensation size is investigated by simulating five mixed-line configurations. Finally, the cable overloading is discussed. All simulations are performed for two load-flow scenarios in the future planning of the Dutch transmission grid.

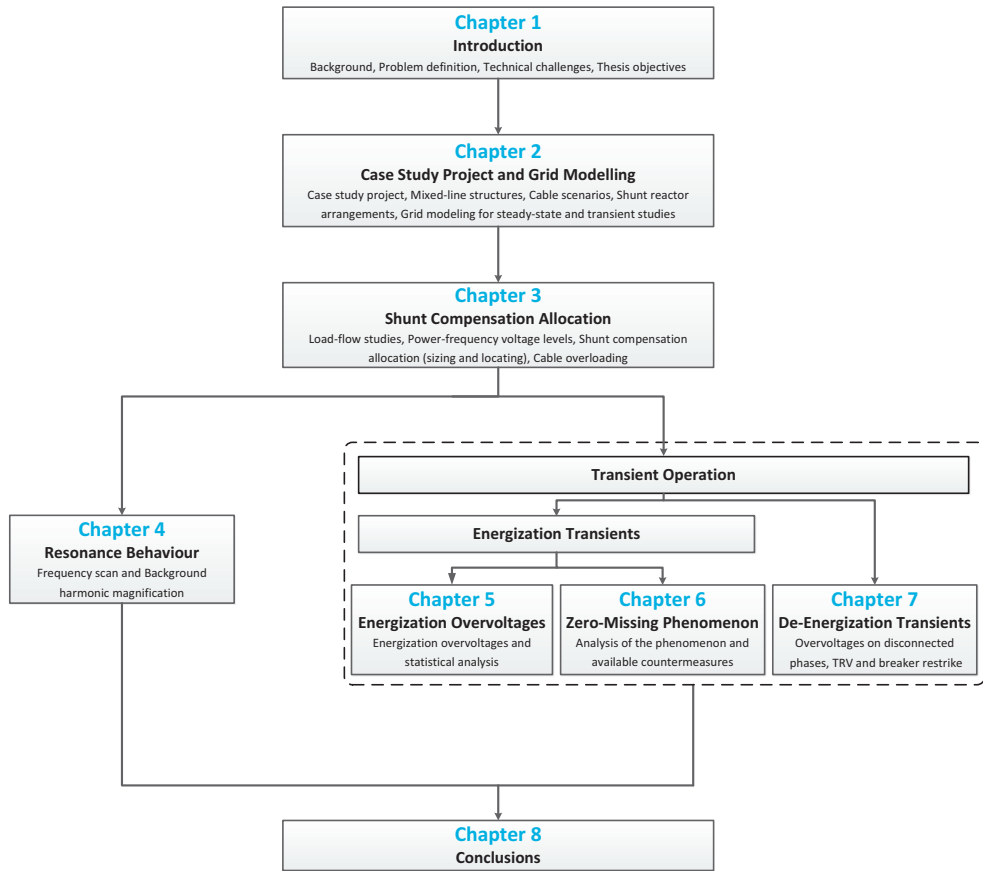


Figure 1.3: Research flowchart.

Chapter 4 presents the study on the resonance effects of long EHV cables. The frequency scan is performed on the frequency-dependent parameter model of the whole Dutch 380 kV grid with and without cables in the case study project. The analysis is carried out for different cable scenarios (i.e. different cable lengths) and with several sensitivity analyses to find the impact of the compensation size, the compensation location, and the mixed-line configuration on the resonance behaviour of the grid. The results are compared in terms of the order of first harmonic resonance frequency and the number of resonance frequencies.

Chapter 5 is dedicated to the analysis of transient overvoltages due to the energization of long cables. Time-domain simulations together with statistical switching analysis are performed on the case study project to investigate how energization overvoltages are distributed in hybrid OHL-Cable systems. Statistical distribution of energization overvoltages is addressed in the literature only for OHLs and cables, but it is not available for hybrid systems consisting of OHL and cable combined. The study is performed for different cable lengths in the case study project to identify how the increasing cable share influences the distribution of energization overvoltages. Moreover, the impact of

short-circuit power, compensation size and location, trapped charges, and mixed-line configuration on overvoltages are also addressed.

Chapter 6 deals with the zero-missing phenomenon in shunt compensated cable systems, in which a thorough investigation on countermeasures of the phenomenon is performed. The study determines the requirements, benefits, and risks of each countermeasure. Results are analysed based on three criteria related to the IEC standards and the Dutch grid code. In addition, the switching sequence of circuit breakers is specified to maximize the effectiveness of the countermeasures. A statistical switching analysis is performed for the insulation coordination study since the application of some countermeasures increases the probability of high transient switching overvoltages. Moreover, the permissible operating delay of the line circuit breaker, required for a successful countermeasure, is calculated.

Chapter 7 is dedicated to the analysis of de-energization transients in cable systems. Voltages of the disconnected phases and the transient recovery voltages across the breakers are analysed to determine how severe the risk of breaker re-ignition and restrike after the current interruption is.

Chapter 8 is summarizing the conclusions of this thesis and provides several recommendations for future researches.

REFERENCES

- [1] CIGRE Working Group B1.07, "Statistics of AC underground cables in power networks," *CIGRE Technical Brochure no. 338*, December 2007.
- [2] K. Burges, J. Bomer, C. Nabe and G. Papaefthymiou, "Study on the comparative merits of overhead transmission lines versus underground cables," Ecofys Germany GmbH, May 2008.
- [3] CIGRE Working Group C4.502, "Power system technical performance issues related to the application of long HVAC cables," *CIGRE Technical Brochure no. 556*, October 2013.
- [4] Y. Ohki and S. Yasufuku, "The world's first long-distance 500 kV-XLPE cable line, part 2: joints and after-installation test," *IEEE Electrical Insulation Magazine*, vol. 18, no. 3, pp. 57-58, 2002.
- [5] C. L. Bak and F. F. da Silva, "High voltage AC underground cable systems for power transmission-A review of the Danish experience, part 1," *Electric Power Systems Research*, vol. 140, pp. 987-994, 2016.
- [6] F. M. F. da Silva, "Analysis and simulation of electromagnetic transients in HVAC cable transmission grids," Ph.D. dissertation, Department of Energy Technology, Aalborg University, Aalborg, Denmark, 2011.
- [7] U. S. Gudmundsdottir, "Modelling of long high voltage AC cables in transmission systems," Ph.D. dissertation, Department of Energy Technology, Aalborg University, Aalborg, Denmark, 2010.
- [8] R. Benato and D. Napolitano, "Overall cost comparison between cable and overhead line including the costs for repair after random failures," *IEEE Transactions on Power Delivery*, vol. 27, no. 3, pp. 1213-1222, 2012.

- [9] R. Smeets, L. van der Sluis, M. Kapetanovic, D. Peelo and A. Janssen, *Switching in Electrical Transmission and Distribution Systems*, Hoboken, NJ, USA: Wiley, 2015.
- [10] Tokyo Electric Power Company, "Assessment of the technical issues relating to significant amounts of EHV underground cable in the all-island electricity transmission system," November 2011.
- [11] C. L. Bak and F. F. da Silva, "High voltage AC underground cable systems for power transmission-A review of the Danish experience, part 2," *Electric Power Systems Research*, vol. 140, pp. 995-1004, 2016.
- [12] "Insulation Co-Ordination-Part 1: Definitions, Principles and Rules," IEC 60071-1, 2006.
- [13] "Insulation Co-Ordination-Part 2: Application Guide," IEC 60071-2, 1996.
- [14] CIGRE Working Group 02, Committee 33, "Guidelines for representation of network elements when calculating transients," *CIGRE Technical Brochure no. 39*, 2000.
- [15] CIGRE Working Group C4.307, "Resonance and ferroresonance in power networks," *CIGRE Technical Brochure no. 569*, February 2014.
- [16] J. J. Grainger and W. D. Stevenson Jr., *Power System Analysis*, Singapore: McGraw-Hill, Inc., 1994.
- [17] F. M. Gatta, A. Geri, S. Lauria and M. Maccioni, "Steady-state operation conditions of very long EHVAC cable lines," *Electric Power Systems Research*, vol. 81, pp. 1525-1533, 2011.
- [18] L. Colla, F. M. Gatta, A. Geri, S. Lauria and M. Maccioni, "Steady-state operation of very long EHV AC cable lines," in *IEEE Power Technology Conference*, Bucharest, Romania, June-July 2009.
- [19] F. M. Gatta and S. Lauria, "Very long EHV cables and mixed overhead-cable lines. Steady-state operation," in *IEEE Power Technology Conference*, St. Petersburg, Russia, June 2005.
- [20] L. Colla, F. M. Gatta, F. Iliceto and S. Lauria, "Design and operation of EHV transmission lines including long insulated cable and overhead section," in *IEEE Power Engineering Conference*, November-December 2005.
- [21] H. Khalilnezhad, M. Popov, J. A. Bos and K. P. J. Jansen, "Influence of partial undergrounding on the transient stability of EHV power transmission systems," *Electric Power Systems Research*, vol. 131, pp. 126-138, 2016.
- [22] H. Khalilnezhad, S. Chen, M. Popov, J. A. Bos, J. P. W. de Jong and L. van der Sluis, "Shunt compensation design of EHV double-circuit mixed OHL-cable connections," in *IET International Conference on Resilience of Transmission and Distribution Networks*, Birmingham, UK, 2015.
- [23] H. Khalilnezhad, M. Popov, L. van der Sluis, J. A. Bos, J. P. W. de Jong and A. Ametani, "Countermeasures of zero-missing phenomenon in (E)HV Cable Systems," *IEEE Transactions on Power Delivery*, vol. 33, no. 4, pp. 1657-1667, August 2018.
- [24] S. Lauria, F. M. Gatta and L. Colla, "Shunt compensation of EHV cables and mixed overhead-cable lines," in *IEEE Power Technology Conference*, Lausanne, Switzerland, July 2007.
- [25] F. M. Gatta, A. Geri, S. Lauria and M. Maccioni, "Steady-state operation conditions of very long EHVAC cable lines: Two case studies," *Electric Power Systems Research*, vol. 83, pp. 160-169, 2012.
- [26] H. Khalilnezhad, M. Popov, L. van der Sluis, J. A. Bos and J. P. W. de Jong, "Influence of long EHV AC underground cables on the resonance behavior of the Dutch transmission system," in *IEEE Power and Energy Society (PES) General Meeting*, Boston, MA, USA, July 2016.

- [27] M. Bollen, S. Aceky, H. Jansson and M. Jonsson, "Using transfer impedance to study harmonic resonance due to AC cables in a transmission system," in *CIGRE*, Lund, Sweden, 2015.
- [28] F. F. da Silva, C. L. Bak and P. B. Holst, "Study of harmonics in cable-based transmission networks," in *44th CIGRE Session*, Paris, France, 2012.
- [29] CIGRE Working Group B1.47, "Implementation of long AC HV and EHV cable systems," *CIGRE Technical Brochure no. 680*, March 2017.
- [30] L. Colla, S. Lauria and F. M. Gatta, "Temporary overvoltages due to harmonic resonance in long EHV cables," in *International Conference on Power System Transients (IPST)*, Lyon, France, June 2007.
- [31] C. F. Jensen, "Harmonic background amplification in long asymmetrical high voltage cable systems," in *International Conference on Power System Transients (IPST)*, Seoul, Republic of Korea, June 2017.
- [32] A. Ametani, T. Ohno and N. Nagaoka, *Cable System Transients: Theory, Modeling and Simulation*, Hoboken, NJ, USA: Wiley, July 2015.
- [33] F. F. da Silva and C. L. Bak, *Electromagnetic Transients in Power Cables*, London, UK: Springer, 2013.
- [34] Y. Itoh, N. Nagaoka and A. Ametani, "Transient analysis of a crossbonded cable system underneath a bridge," *IEEE Transactions on Power Delivery*, vol. 5, no. 2, pp. 527-532, April 1990.
- [35] T. Ohno, C. L. Bak, A. Ametani, W. Wiechowski and T. K. Sorensen, "Statistical distribution of energization overvoltages of EHV cables," *IEEE Transactions on Power Delivery*, vol. 28, no. 3, pp. 1423-1432, July 2013.
- [36] H. Khalilnezhad, M. Popov, L. van der Sluis, J. A. Bos and A. Ametani, "Statistical analysis of energization overvoltages in EHV hybrid OHL-cable systems," *IEEE Transactions on Power Delivery*, DOI:10.1109/TPWRD.2018.2825201, April 2018.
- [37] H. Khalilnezhad, M. Popov, J. A. Bos, J. P. W. de Jong and L. van der Sluis, "Investigation of statistical distribution of energization overvoltages in 380 kV hybrid OHL-cable systems," in *International Conference on Power System Transients (IPST)*, Seoul, Republic of Korea, June 2017.
- [38] H. Khalilnezhad, M. Popov, L. van der Sluis, J. P. W. de Jong, N. Nenadovic and J. A. Bos, "Assessment of line energization transients when increasing cable length in 380 KV power grids," in *IEEE International Conference on Power System Technology (POWERCON)*, Wollongong, Australia, September 2016.
- [39] T. Ohno, "Dynamic study on the 400 kV 60 km Kyndbyværket-Asnæsværket line," Ph.D. dissertation, Department of Energy Technology, Aalborg University, Aalborg, Denmark, 2012.
- [40] F. Ghassemi, "Effect of trapped charges on cable SVL failure," *Electric Power Systems Research*, vol. 115, pp. 18-25, 2014.
- [41] N. Nagaoka, A. Ametani, K. Yoshida and T. Karasaki, "Transient sheath voltage characteristics of a crossbonded cable installed within a tunnel," *Electrical Engineering in Japan*, vol. 112, no. 5, pp. 36-45, 1992.
- [42] W. Kersten, "Surge arresters for sheath protection in crossbonded cable system," *Proc. of the Institution of Electrical Engineers (IEE)*, vol. 126, no. 12, pp. 1255 - 1262, December 1979.
- [43] N. Nagaoka and A. Ametani, "Transient calculations on crossbonded cables," *IEEE Transactions on Power Apparatus and Systems*, Vols. PAS-102, no. 4, pp. 779-787, April 1983.

- [44] "IEEE Guide for the Application of Capacitance Current Switching for AC High-Voltage Circuit Breakers Above 1000 V," IEEE Standard C37.012, 2014.
- [45] F. F. da Silva and C. L. Bak, "Energization of long HVAC cables in parallel-Analysis and estimation formulas," *Electric Power Systems Research*, vol. 96, pp. 150-156, 2013.
- [46] F. F. da Silva, C. L. Bak, U. S. Gudmundsdottir, W. Wiechowski and M. R. Knardrupgard, "Methods to minimize zero-missing phenomenon," *IEEE Transactions on Power Delivery*, vol. 25, no. 4, pp. 2923-2930, October 2010.
- [47] I. Lafaia, F. Ghassemi, A. Ametani, J. Mahseredjian, S. Dennis, A. M. Haddad and S. Robson, "Experimental and theoretical analysis of cable discharge," *IEEE Transactions on Power Delivery*, vol. 32, no. 4, pp. 2022-2030, August 2017.
- [48] C. L. Bak, W. Wiechowski, K. Søgaard and S. D. Mikkelsen, "Analysis and simulation of switching surge generation when disconnecting a combined 400 kV cable/overhead line with shunt reactor," in *International Conference on Power System Transients (IPST)*, Lyon, France, June 2007.
- [49] C. L. Bak, H. Baldursson and A. M. Oumarou, "Switching overvoltage in 60 kV reactor compensated cable grid due to resonance after disconnection," in *8th International Conference on Electric Power Systems, High Voltages, Electric Machines (POWER '08)*, 2008.
- [50] F. Iliceto, E. Cinieri and A. Di Vita, "Overvoltages due to open-phase occurrence in reactor compensated EHV lines," *IEEE Transactions on Power Apparatus and Systems*, Vols. PAS-103, no. 3, pp. 474-482, March 1984.
- [51] F. F. da Silva, C. L. Bak and P. B. Holst, "Switching restrikes in HVAC cable lines and hybrid HVAC cable/OHL lines," in *International Conference on Power System Transients (IPST)*, Delft, The Netherlands, June 2011.
- [52] D. F. Peelo and E. M. Ruoss, "A new IEEE application guide for shunt reactor switching," *IEEE Transactions on Power Delivery*, vol. 11, no. 2, pp. 881-887, April 1996.
- [53] I. Uglešić, M. Krepela, B. Filipović- Grčić and F. Jakl, "Transients due to switching of 400 kV shunt reactor," in *International Conference on Power System Transients (IPST)*, 2011.
- [54] F. Massaro, G. Morana and R. Musca, "Transient behavior of a mixed overhead-cable EHV line under lightning events," in *44th International Universities Power Engineering Conference (UPEC)*, Glasgow, UK, September 2009.
- [55] B. W. Tuinema, J. L. Rueda, L. van der Sluis and M. A. M. M. van der Meijden, "Reliability of transmission links consisting of overhead lines and underground cables," *IEEE Transactions on Power Delivery*, vol. 31, no. 3, pp. 1251-1260, June 2016.
- [56] H. Khalilnezhad, F. Barakou, N. Kandalepa, J. Wu, L. Wu, M. Popov, E. F. Steennis, P. A. A. F. Wouters, S. Mousavi Gargari, J. A. Bos, J. P. W. de Jong, C. P. J. Jansen, J. Smit and R. Kuik, "Shunt compensation sizing, reliability analysis, and condition monitoring measurements and simulations for an EHV mixed OHL-cable connection," in *46th CIGRE Session*, Paris, France, 2016.
- [57] N. Kandalepa, B. W. Tuinema, J. L. Rueda and M. A. M. M. van der Meijden, "Reliability modeling of transmission networks: An explanatory study on further EHV underground cabling in the Netherlands," in *IEEE International Energy Conference (ENERGYCON)*, Leuven, Belgium, April 2016.
- [58] CIGRE Working Group B1.30, "Cable systems electrical characteristics," *CIGRE Technical Brochure no. 531*, April 2013.
- [59] L. Wu, "Impact of EHV/HV underground power cables on resonant grid behavior," Ph.D.

- dissertation, Department of Electrical Engineering, Eindhoven University of Technology, Eindhoven, The Netherlands, October 2014.
- [60] G. Hoogendorp, "Steady state and transient behavior of underground cables in 380 kV transmission grids," Ph.D. dissertation, Department of Electrical Sustainable Energy, Delft University of Technology, Delft, The Netherlands, October 2016.
- [61] H. Khalilnezhad, "Influence of 380 kV AC cables on the dynamic stability of the Dutch transmission system," M.Sc. dissertation, Department of Electrical Sustainable Energy, Delft University of Technology, Delft, The Netherlands, September 2013.
- [62] B. W. Tuinema, "Reliability of transmission networks: impact of EHV underground cables & interaction of offshore onshore network," Ph.D. dissertation, Department of Electrical Sustainable Energy, Delft University of Technology, Delft, The Netherlands, November 2017.
- [63] N. Kandalepa, "Reliability modeling of transmission networks-An explanatory study on further EHV underground cabling in the Netherlands," M.Sc. dissertation, Department of Electrical Sustainable Energy, Delft University of Technology, Delft, The Netherlands, 2015.

CHAPTER 2

CASE STUDY PROJECT AND GRID MODELLING

2.1 INTRODUCTION

As mentioned in Chapter 1, the main objective of this thesis is to study the major technical issues associated with the increasing cable length in transmission grids. To achieve this objective, it is required to define a robust study approach based on realistic assumptions, so that the obtained results can be interpreted to a set of guidelines and instructions for development and operation of future hybrid OHL-Cable transmission grids. In addition to a robust approach, a precise set of input parameters and a detailed and accurate grid model are required to ensure the reliability of the obtained simulation results.

The aim of this chapter is to elaborate on the research approach and the grid modelling, where it is divided in two parts. Part I describes the case study project of the thesis. The location of the project in the Dutch 380 kV grid and the defined cable scenarios for this project are explained. In addition, some general information about the Dutch transmission grid is provided in this part. Part II discusses the developed models of the Dutch transmission grid for simulation of different technical issues. It is explained which models are used for steady-state and transient analyses. The defined approach and developed models in this chapter are used for the rest of this thesis to study the Dutch grid performance.

This chapter is structured as follows: first, an overview of the Dutch power transmission grid is provided in Section 2.2. Afterwards, the case study project is described in Section 2.3, where the location of the project, mixed-line configurations, and the cable scenarios are explained. The grid models used for the steady-state and transient studies are elaborated in Sections 2.4 and 2.5, respectively. Finally, conclusions are discussed in Section 2.6.

PART I: CASE STUDY PROJECT

The case study project of this thesis is a hypothetical 380 kV double-circuit transmission line for which different cable scenarios are defined. The influence of long cables on the

system performance can be determined by analysing the technical issues of cable operation in this project.

2.2 DUTCH POWER TRANSMISSION GRID

Figure 2.1 shows the map of the Dutch (E)HV transmission grid including the interconnections with the neighbouring countries. The future projects are shown by dotted lines in this map. The large-scale power generations are concentrated in the west and north, where conventional power plants and renewable resources like wind parks are located. This creates potential bottlenecks in the grid due to the large amounts of power that should be transferred from the west and north to the rest of the grid.

The Dutch transmission system is composed of four main voltage levels of 110, 150, 220, and 380 kV. The 220 kV and 380 kV grids are constructed and operated in a ring structure to increase the system reliability and serve as backbones for the meshed 110 kV and 150 kV grids. The present availability of the grid is 99.99%, which implies on the high reliability of the power supply. Moreover, the grid has four AC connections with Germany, two AC connections with Belgium, and HVDC connections with Norway (NorNed), Great Britain (BritNed), and Denmark (COBRACable).

To keep pace with the rapidly developing energy landscape, TenneT should expand the transfer capacity of the grid by making new transmission lines. Several transmission connections are at this moment under study or construction, among which some should be partially undergrounded by the use of underground cables. This raises new challenges for the grid developers and strategists from the technical perspective.

2.3 SPAAK PROJECT

The Spaak project is the case study of this thesis. It is a hypothetical future transmission line connecting the western side of the 380 kV ring to the eastern side. This would be a double-circuit connection between substations Krimpen aan den IJssel (KIJ) and Dodewaard (DOD) with the transmission length of 80 km.

Figure 2.2 shows the single-line diagram of the Dutch 380 kV grid and the Spaak project. The hybrid OHL-Cable circuits of the Randstad South-Ring project (from the Wateringen substation to the Bleiswijk substation with 10.8 km cable) and the Randstad North-Ring project (from the Bleiswijk substation to the Vijfhuizen substation and then to the Beverwijk substation with 9.3 km cable in total) are one substation away from the Spaak project. The Spaak and the Randstad projects are shown with the red and the green colours, respectively. The conventional power generation sites are shown by blue circles, where the sizes are proportional to the aggregated generation capacity of all units at each site.



Figure 2.1: Map of the Dutch (E)HV transmission grid. [Source: TenneT TSO, 2018]

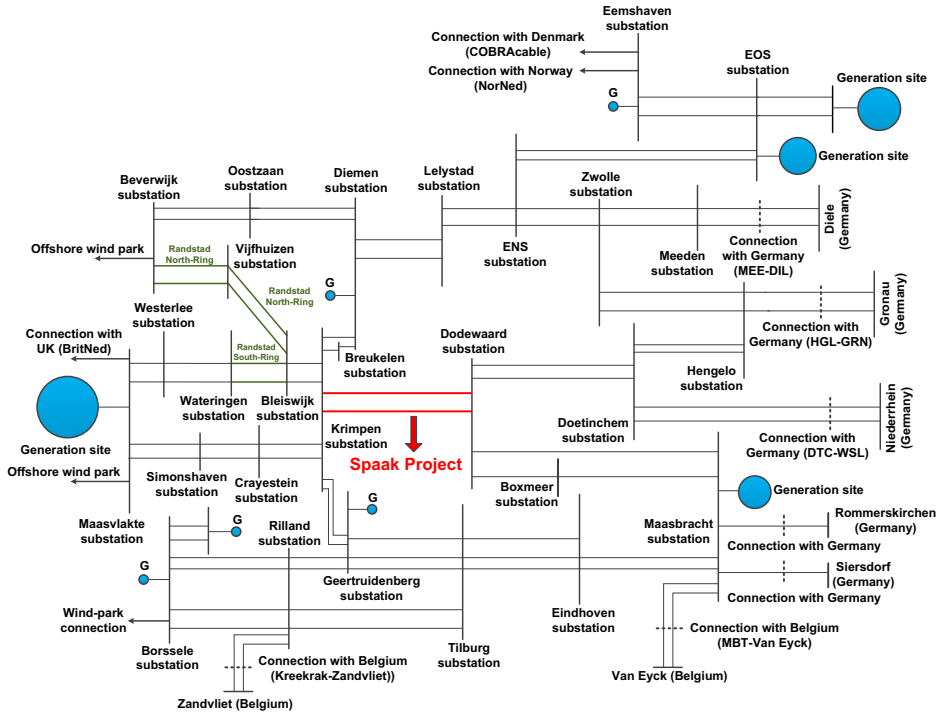


Figure 2.2: Single-line diagram of the Dutch 380 kV transmission grid in the reference year 2025. The Spaak project is shown with the red colour and the Randstad cable projects are shown with the green colour.

2.3.1 MIXED-LINE CONFIGURATION

The first important step is to determine the mixed-line configuration, which is specified by the number and the location of OHL and cable sections in the connection. A mixed transmission line is made of series-connected OHL and cable sections. Different configurations can be derived as the result of various possibilities for the number and location of sections.

In this research, a study case mixed-line configuration was determined in order to investigate all the technical issues for this configuration. In addition, four other configurations are also taken into account to find out the influence of the mixed-line configuration on the system operation. In other words, since the number and the location of cable sections are determined in the planning and design stages of a cable project, it is important to compare various mixed-line configurations from the system operation perspective.

A. STUDY CASE MIXED-LINE CONFIGURATION

As a practical approach, cable sections are expected to be utilized mainly at sensitive areas like cities and national parks, where the importance of undergrounding is highlighted. Therefore, it was assumed that each circuit of the Spaak connection includes seven sections as shown in Figure 2.3. There are three cable sections and four OHL sections per circuit

and the two circuits are identical. In the Dutch 380 kV grid, the continuous current ratings (ampacity) of a typical OHL, consisting of a bundle of four sub-conductors, and a typical single-core cable are respectively 4 kA and 1.5 kA (see Table 2.8). Therefore, the cable sections require two parallel cables per phase to have almost the same transmission capacity as the OHL sections. In this research, this is the default mixed-line configuration, used for the analysis of the technical issues, unless a different configuration is mentioned.

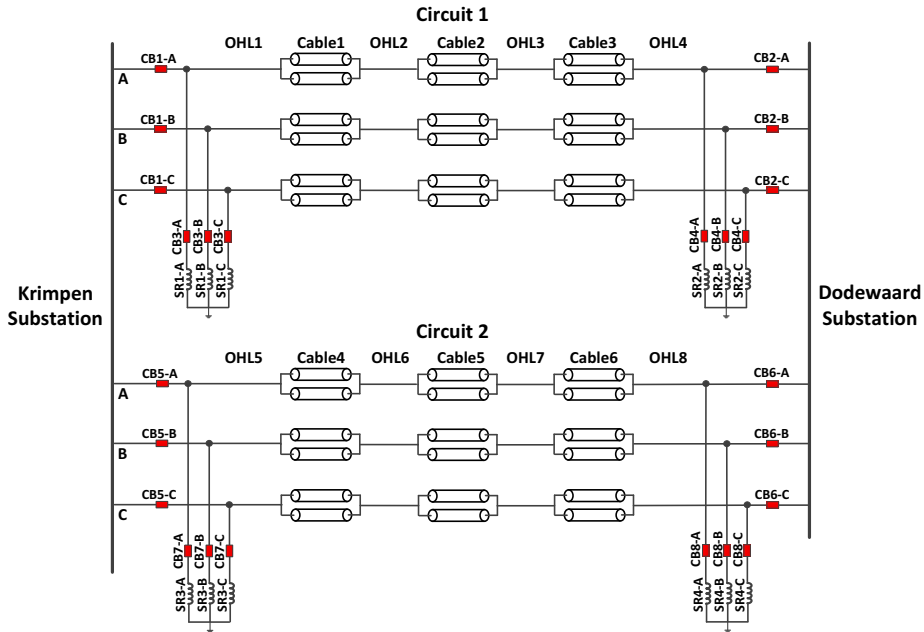


Figure 2.3: Study case mixed-line configuration for the Spaak connection (CB: circuit breaker, SR: shunt reactor).

B. SHUNT REACTORS LOCATION

At the sending and receiving terminals, the three-phase shunt reactors (SR) are connected through breakers to the circuit right behind the line breakers. This type of compensation is known as line-end compensation (LEC). It should be noted that each SR, i.e. SR1 to SR4, is representing a compensation bank. A measure of flexibility will be provided by installing switchable variable reactors or parallel combination of smaller fixed reactors with the unit size (typical unit sizes are 100 Mvar or 150 Mvar), which can be switched in/out separately.

The connection of shunt reactors to the circuit and behind the line breakers helps to limit post-switching steady-state energization overvoltages in the circuit (especially at the open-end of the circuit due to the Ferranti effect) and to minimize the capacitive current flowing through the line breaker during energization. These benefits are not achieved when the shunt reactors are connected to busbars or to tertiary windings of power transformers at substations. However, for some cable lengths, shunt reactors can be connected to busbars or to tertiary windings if energization overvoltages and capacitive currents are not very large. In this case, the inductive voltage transformer connected to the cable should have enough

discharge capability and also the leading current interruption capability of the line breaker should be checked [1].

The installation of separate breakers for the shunt reactors results in an added switching flexibility as well as minimizing the risk of line resonance by decoupling reactors from the disconnected phase(s). Resonance may occur between the reactor inductance, the inter-phase/inter-circuit capacitance, and the cable capacitance if reactors remain connected to the disconnected phase(s) in uneven open-phase conditions (e.g. one phase is disconnected and the other two are energized) [2], [3]. In fact, the induced power-frequency voltage in the disconnected phase(s) by the capacitive coupling with the energized phase(s) can trigger the resonance circuit. The risk of ferroresonance also exists when shunt reactors have a magnetic core. Thus, these risks can be minimized by disconnecting the shunt reactors from the disconnected phase(s) when they are connected via breakers.

C. ALTERNATIVE MIXED-LINE CONFIGURATIONS

It is of importance to investigate the influence of other mixed-line configurations on the system operation. Different configurations can be derived by varying the number and the location of OHL and cable sections. In addition to the study case configuration, four mixed-line configurations were selected to be compared with the study case configuration in terms of their influence on the system operation. These configurations are:

1. Configuration 1: OHL-Cable
2. Configuration 2: Cable-OHL
3. Configuration 3: OHL-Cable-OHL
4. Configuration 4: OHL-Cable-OHL-Cable-OHL

Figure 2.4 shows the four alternative configurations. Only one circuit is depicted due to the identical configuration of the two circuits.

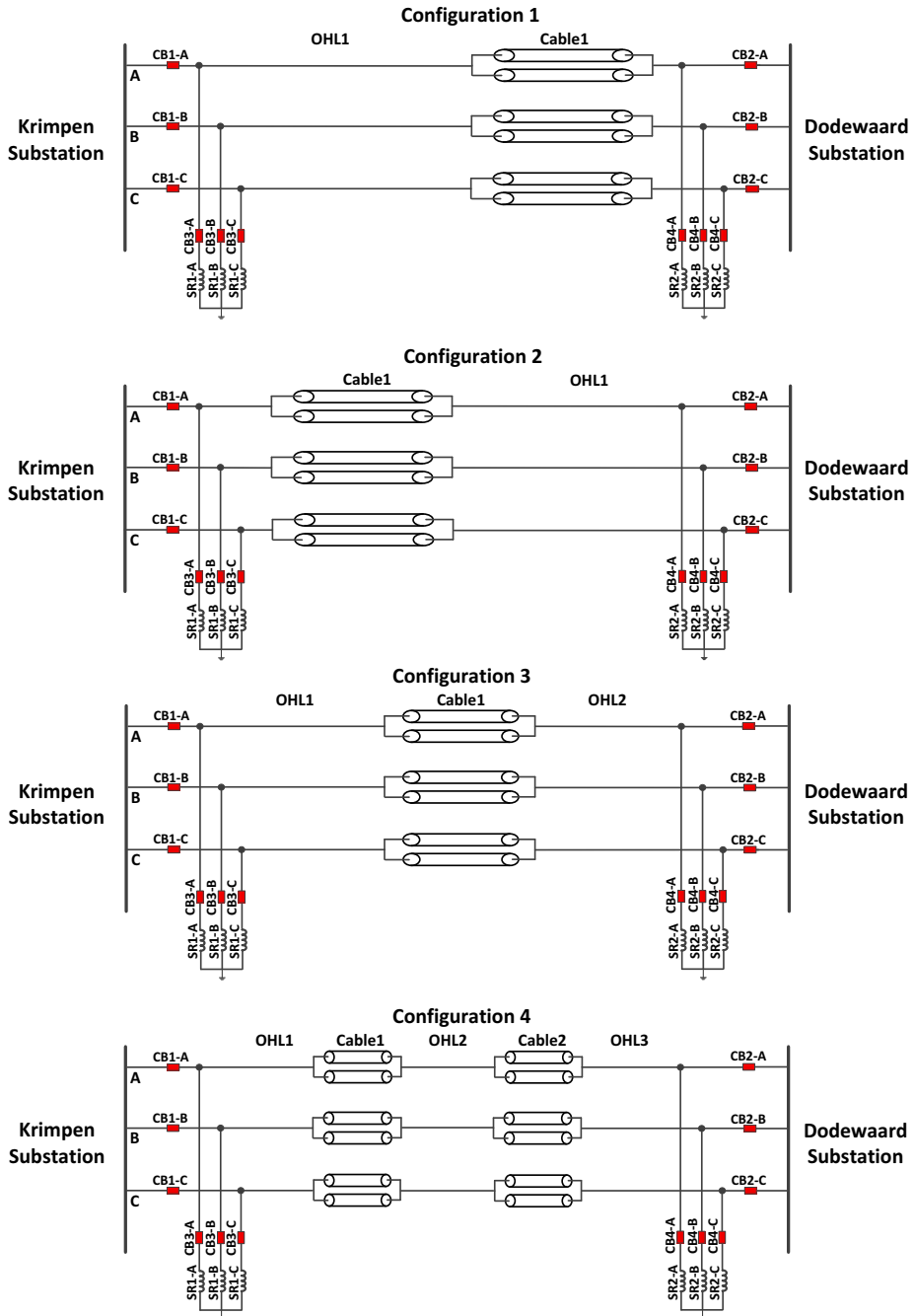


Figure 2.4: Alternative mixed-line configurations of the Spaak connection. Only one circuit is shown because the two circuits are identical (CB: circuit breaker, SR: shunt reactor).

2.3.2 CABLE SCENARIOS

Six cable scenarios were defined to determine the impact of the cable length on the system operation. In each scenario, it is specified how many kilometres of the total transmission length is realized by the cables. The total transmission length of the Spaak connection from the sending substation to the receiving substation is 80 km. By these scenarios, the cable share varies from 0% (fully OHL) to 100% (fully cable) of the transmission length. The cable scenarios are presented in Table 2.1.

The cable portion is increasing from zero to 100% in five steps, which means in total six scenarios: 0% cable (fully OHL), 15% cable, 25% cable, 50% cable, 75% cable and 100% cable (fully cable). Different percentages of cable length are chosen to show the influence of the cable length increase on the system operation.

In this research, when it is mentioned L km cable, it is meant that the total transmission length of the cable sections is L km. Thus, each phase is composed of $2 \times L$ km cable (two cables per phase), each circuit $3 \times 2 \times L$ km cable, and the two circuits $12 \times L$ km cable. Table 2.1 presents the total transmission length of the OHL and cable sections. In the next step, the length of each section should be determined.

TABLE 2.1
CABLE SCENARIOS OF THE SPAAK PROJECT

Scenario	OHL length (km)	Cable length (km)
0% Cable (Fully OHL)	80	0
15% Cable	68	12
25% Cable	60	20
50% Cable	40	40
75% Cable	20	60
100% Cable (Fully Cable)	0	80

A. SECTION LENGTHS OF THE STUDY CASE MIXED-LINE CONFIGURATION

For the study case configuration represented in Figure 2.3, the section lengths can be determined in a way that the mixed-line becomes symmetrical or asymmetrical with respect to the midpoint of the line. In a symmetrical configuration, the cable and OHL sections are equally distributed along the route of the line, meaning that the line is identical at the two sides of its mid-point in terms of the lengths of the OHL and cable sections (i.e. the left and right sides of the line mid-point are mirroring each other). In practice, an asymmetrical mixed-line is a more realistic assumption than a symmetrical structure since the realization of a completely symmetrical mixed-line can be difficult due to practical limitations. However, it may be in some situations possible to realize a symmetrical hybrid circuit. According to [4] and [5], an unsymmetrical configuration leads to a non-optimal reactive power flow to line-end terminals as well as the decrease of first resonance frequency compared to that of a symmetrical configuration.

Tables 2.2 and 2.3 present lengths of the OHL and cable sections, respectively for the asymmetrical and symmetrical study case mixed-line configurations. There are several

combinations of section lengths that can result in an asymmetrical configuration, so those presented in Table 2.2 are only one of the possible combinations. In contrary, there is only one combination for the symmetrical configuration. In the fully-OHL and fully-cable scenarios the whole circuit is either totally OHL or cable, therefore the section lengths are not applicable.

TABLE 2.2
OHL AND CABLE SECTION LENGTHS IN EACH CABLE SCENARIO FOR THE STUDY CASE MIXED-LINE CONFIGURATION, ASYMMETRICAL CONFIGURATION

Scenario	Section length (km)						
	OHL1	Cable1	OHL2	Cable2	OHL3	Cable3	OHL4
Fully OHL	---	---	---	---	---	---	---
15% Cable	5	2	21	5	28	5	14
25% Cable	4	4	20	7	24	9	12
50% Cable	2	13	13	17	14	10	11
75% Cable	0	22	8	18	7	20	5
Fully Cable	---	---	---	---	---	---	---

TABLE 2.3
OHL AND CABLE SECTION LENGTHS IN EACH CABLE SCENARIO FOR THE STUDY CASE MIXED-LINE CONFIGURATION, SYMMETRICAL CONFIGURATION

Scenario	Section length (km)						
	OHL1	Cable1	OHL2	Cable2	OHL3	Cable3	OHL4
Fully OHL	---	---	---	---	---	---	---
15% Cable	17	4	17	4	17	4	17
25% Cable	15	7	15	6	15	7	15
50% Cable	10	13	10	14	10	13	10
75% Cable	5	20	5	20	5	20	5
Fully Cable	---	---	---	---	---	---	---

B. SECTION LENGTHS OF THE ALTERNATIVE MIXED-LINE CONFIGURATIONS

The assumed OHL/cable section lengths for the alternative mixed-line configurations, as depicted in Figure 2.4, are presented in Tables 2.4 to 2.7. For configurations 3 and 4, symmetrical configurations are considered. This is due to the fact that the symmetrical configurations are necessary to have a comparison between the study case mixed-line configuration (symmetrical version) and the alternative configurations.

TABLE 2.4
OHL AND CABLE SECTION LENGTHS IN EACH CABLE SCENARIO FOR CONFIGURATION 1

Scenario	Section length (km)	
	OHL1	Cable1
Fully OHL	---	---
15% Cable	68	12
25% Cable	60	20
50% Cable	40	40
75% Cable	20	60
Fully Cable	---	---

TABLE 2.5
OHL AND CABLE SECTION LENGTHS IN EACH CABLE SCENARIO FOR CONFIGURATION 2

Scenario	Section length (km)	
	Cable1	OHL1
Fully OHL	---	---
15% Cable	12	68
25% Cable	20	60
50% Cable	40	40
75% Cable	60	20
Fully Cable	---	---

TABLE 2.6
OHL AND CABLE SECTION LENGTHS IN EACH CABLE SCENARIO FOR CONFIGURATION 3, SYMMETRICAL CONFIGURATION

Scenario	Section length (km)		
	OHL1	Cable1	OHL2
Fully OHL	---	---	---
15% Cable	34	12	34
25% Cable	30	20	30
50% Cable	20	40	20
75% Cable	10	60	10
Fully Cable	---	---	---

TABLE 2.7
OHL AND CABLE SECTION LENGTHS IN EACH CABLE SCENARIO FOR CONFIGURATION 4, SYMMETRICAL CONFIGURATION

Scenario	Section length (km)				
	OHL1	Cable1	OHL2	Cable2	OHL3
Fully OHL	---	---	---	---	---
15% Cable	23	6	22	6	23
25% Cable	20	10	20	10	20
50% Cable	13	20	14	20	13
75% Cable	7	30	6	30	7
Fully Cable	---	---	---	---	---

PART II: GRID MODELLING

This part elaborates on the developed models of the Dutch 380 kV grid for the steady-state and transient studies of the hybrid OHL-Cable circuits of the Spaak connection. It is explained how the grid components are modelled for each of the technical issues and to which extend the grid should be modelled to ensure sufficiently fast and accurate simulations. The developed grid models in this chapter are used in the rest of the thesis for technical studies.

2.4 GRID MODELLING FOR STEADY-STATE STUDIES

In this research, the steady-state simulations are based on the positive-sequence representation of the whole Dutch transmission grid (110 kV, 150 kV, 220 kV, and 380 kV voltage levels) in the DiGSILENT PowerFactory environment. This model includes representations of substations, transmission lines (OHLs and cables), transformers, shunt reactors, capacitor banks, and loads together with all interconnections to the neighbour

grids and a simplified representation of European transmission grids. By this means, realistic load-flow scenarios and short-circuit powers can be simulated based on the expected future dispatch scenarios.

In the steady-state analysis, the wavelength of currents and voltages (6000 km in a 50 Hz system) is much larger than the network physical dimensions. Therefore, a lumped-parameter model can be used to simulate the steady-state behaviour of the transmission lines [6]. Two types of lumped-parameter models are studied here: nominal pi-model and exact (or equivalent) pi-model, where both are two-port models.

The nominal pi-model, as shown in Figure 2.5, is a very simple representation of a line at power-frequency, in which the total resistance (R), inductance (L), capacitance (C), and usually conductance (G) of the line are represented by lumped-parameters. Z is the total series impedance and Y is the total shunt admittance of the line:

$$Z = R + j\omega L \quad (2.1)$$

$$Y = G + j\omega C \quad (2.2)$$

This model is only accurate for steady-state simulations and for short and medium length lines (lengths up to 240 km). For long transmission lines, the line parameters are distributed uniformly throughout the length of the line and cannot be represented by the nominal pi-model [7], [8].

The exact pi-model is an adopted version of the nominal pi-model for simulation of long transmission lines and even transient phenomena (at a single frequency) as it takes the distributed nature of the line impedance and admittance into account by applying correcting factors in the Z and Y . This model is discussed in Section 2.5.3.

Table 2.8 presents the applied electrical parameters for 380 kV-50 Hz OHL and cable sections of the Spaak connection. The OHL is composed of a bundle of four sub-conductors with a continuous current rating (ampacity) of 4 kA in total. The continuous current rating of a single cable is 1.5 kA, but this value can be increased to 2 kA for 24 hours.

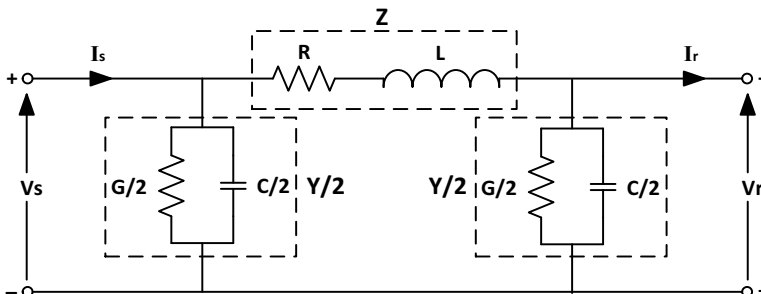


Figure 2.5: Nominal pi-model of a two-conductor transmission line.

TABLE 2.8
INPUT ELECTRICAL PARAMETERS FOR 380kV-50HZ OHL AND CABLE SECTIONS OF THE SPAAK CONNECTION

Type	Cross-section (mm ²)	R+jX (Ω/km)	C (nF/km)	Z _s ^(b) (Ω)	SIL ^(c) (MVA)	I _n ^(d) (A)	S _n ^(e) (MVA)
OHL ^(a)	2483.6	0.0148+j0.232	15.3	219.7	657.3	4000	2635
XLPE Cable	2500	0.0227+j0.1712	231.5	48.5	2976.2	1500 ^(f)	987.27

(a) Bundle of four sub-conductors
(b) Surge impedance: $Z_s = \sqrt{\frac{L}{C}}$
(c) Surge impedance loading for a three-phase system calculated at V_n=380 kV
(d) Rated current (ampacity)
(e) Apparent power at ampacity I_n (thermal power limit): $S_n = \sqrt{3}V_n I_n$
(f) This value can be increased to 2 kA for only 24 hours continuous operation.

2.5 GRID MODELLING FOR TRANSIENT STUDIES

Power system harmonic and transient simulations require models in which the frequency-dependency of system components are taken into account. Such models can be developed in specialized programs for electromagnetic transient (EMT) simulations, among which the most well-known programs are EMTP-RV, ATP-EMTP, and PSCAD/EMTDC.

The EMT simulation results are only accurate when three requirements are satisfied: firstly, the input data used for the components modelling should be accurate; secondly, the level of details put into the model of a component should be sufficient; and thirdly, the extent to which the area around the point of interest is modelled should be enough. Each of these requirements has a substantial influence on the simulation results. In the literature, the second and third requirements are referred as modelling depth.

2.5.1 MODELLING DEPTH

An important issue in simulation of electromagnetic transients is the modelling depth or depth of complexity in representation of the grid. The size and the detail level of the modelled area around the event location (disturbance location) can significantly affect both the simulation accuracy and the simulation time. The simulation results are inaccurate when the modelled area is too small or with insufficient details. On the other hand, the required simulation time can substantially increase when the size of the modelled area or the level of details are increased. Therefore, there is a trade-off between the simulation accuracy and the simulation time, which can be properly handled by determining a sufficient modelling depth.

It is recommended in the literature to represent the grid up to two busbars from the event location [9], but this is not always sufficient. In [10-12], it is proposed to divide the grid into three zones, as illustrated in Figure 2.6, where each zone is represented by a different level of details:

1. *Study zone*: this is the part of the grid near the event location, which has to be represented by detailed frequency-dependent models. OHLs and cables should be represented by distributed frequency-dependent parameter models and all cable bondings should also be included with details.

2. *External zone*: this is the part of the grid farther than the studied zone from the event location; therefore, network components can be represented by detailed or simpler models. OHLs and cables can be represented by distributed-parameter models like Bergeron model, which uses values of the line parameters at a single frequency. In this zone, only major cable bondings are represented by detailed or simplified models, e.g. the use of ideal cross-bondings when cables are cross-bonded.
3. *Distant zone (rest of the grid)*: this zone is the distant part of the grid, which is very far from the event location without contribution to the transient voltages and currents. This zone can be represented by one or two busbars depth and by lumped-parameter line models as this will reduce the simulation inaccuracy (by decreasing the chance of erroneous high voltage), but at the expense of a slightly longer simulation time. Finally, an N-port or 2-port equivalent can be used to represent the remaining parts of the grid.

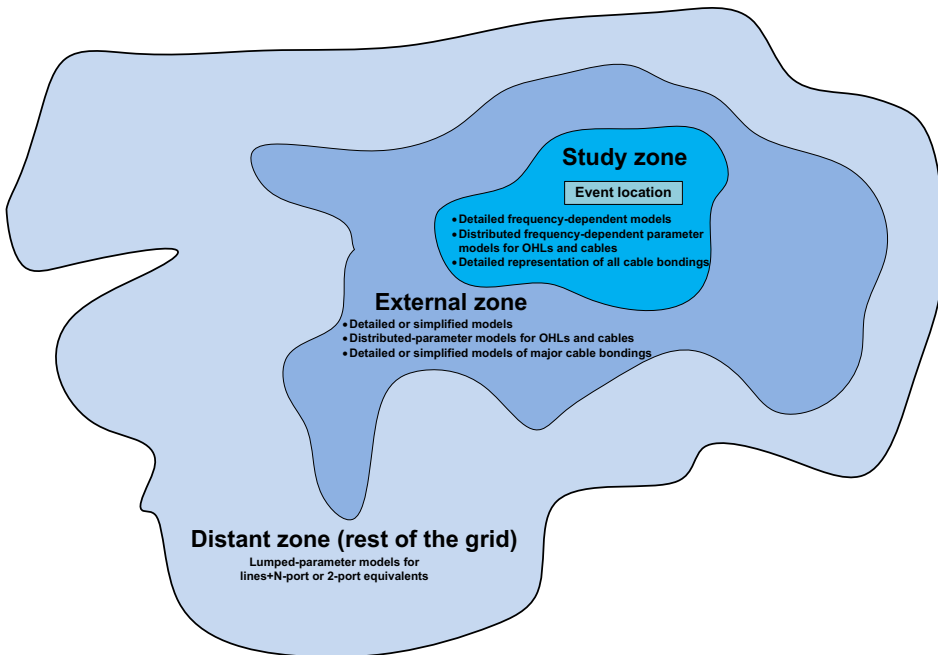


Figure 2.6: Three-level modelling of the grid for transient studies.

It should be pointed out that finding the border of these three zones is mainly based on a try and error approach, although some methods are proposed in the literature to find the extend of the detailed study zone. For example, in [11], authors proposed a method that can be used to estimate the depth of the modelling area by using the grid layout. Do note that the level of details is also strongly dependent on the type of the investigated phenomenon at the event location. To address these challenges, frequency-dependent network equivalents (FDNE) have been developed that can be used to represent the external and distant zones

[13-16]. The FDNE modules are already included in many EMT programs to accelerate simulations of large power systems.

2.5.2 OVERVIEW OF THE DUTCH 380 kV GRID MODEL

A thorough frequency-dependent model of the whole Dutch 380 kV transmission system was developed in PSCAD/EMTDC for the harmonic and transient studies [17], [18]. The whole 380 kV grid was modelled in order to ensure the maximum accuracy of the results despite of long simulation time. However, the sensitivity analyses revealed that the major part of the simulation time is spent for the cables of the Spaak connection, especially when the cables are long. This is because of the complexity of cable models and the use of a small numerical time step for the simulation of transients in cable circuits.

The Dutch 380 kV grid model includes detailed representations of substations, transmission lines, three-phase three-limb power transformers, and shunt reactors. Each generation unit was modelled by a voltage source, a series impedance, and a step-up transformer with values calculated based on a specific load-flow snapshot.

The lower voltage levels, i.e. 220 kV and below, were modelled by equivalent parallel RL or RC loads. A common approach in the harmonic and transient studies of EHV systems is to either disregard the downstream network or to model them by parallel RC or RL circuits on the secondary side of the transmission transformers, where they are sized based on the load-flow dispatch. These simplifications can decrease the required time for the modelling and EMT simulations of EHV grids with the expense of some inaccuracies in simulation results.

In [19], the authors studied the impact of the downstream network modelling on the harmonic frequency impedance (frequency scan) and switching overvoltages of the Dutch 380 kV grid, where it has been concluded that the type of the downstream network (OHL or cable) has a great influence while the parameters of end customer loads have only minor effects. In addition, it has been concluded that the lower voltage lines can be modelled by nominal pi-model without losing the accuracy of the simulated harmonic impedance and maximum overvoltage. However, the use of the parallel RC equivalent for the downstream network results in some disagreements in the harmonic frequency impedance seen from the EHV level with that of the detailed model. On the other hand, regarding the transient overvoltages, good agreement between the parallel RC equivalent and the detailed model was observed.

The following sections elaborate on the component models used for the representation of the Dutch 380 kV grid in PSCAD/EMTDC. The modelling is performed according to the guidelines and recommendations in the literature [9], [20].

2.5.3 TRANSMISSION LINES MODELLING

Transients in power systems produce travelling electromagnetic waves (i.e. voltage and current waves) with high-frequency components, where the wave travel time and propagation in transmission lines should be properly modelled to obtain a realistic simulation. In such a model, the line capacitance and inductance have to be represented

with distributed parameters as the properties of the travelling electric field are represented by means of the line capacitance and the properties of the magnetic field by the line inductance. This means the total capacitance, inductance, and resistance are equally distributed over the length of the transmission line. In addition, an accurate line model for transient studies must take the frequency dependency of the line parameters into account. This includes the frequency dependency of conductors, due to the skin and proximity effects, frequency dependency of capacitances, due to permittivity variations, and frequency dependency of the earth-return path.

A. TELEGRAPH EQUATIONS

To derive formulas for calculation of voltages and currents of a transmission line during transients, it is assumed that the parameters are distributed evenly along the line length and the line consists of an infinite number of incremental differential-length segments. This allows to represent each segment by lumped parameters and to apply Kirchhoff's voltage and current laws. Figure 2.7 depicts an equivalent circuit of a differential-length segment of a two-conductor transmission line [1], [21]. It is assumed that the line is balanced and uniform. The indicated parameters are:

R the series resistance per unit length per phase (Ω/m)

L the series inductance per unit length per phase (H/m)

G the shunt conductance per unit length per phase to neutral (S/m)

C the shunt capacitance per unit length per phase to neutral (F/m)

dx the segment length (m)

By applying the Kirchhoff's voltage law, the voltage drop on the line series resistance and inductance can be derived [1], [6], [21]:

$$V(x, t) - V(x + dx, t) = RdxI(x + dx, t) + Ldx \frac{\partial I(x + dx, t)}{\partial t} \quad (2.3)$$

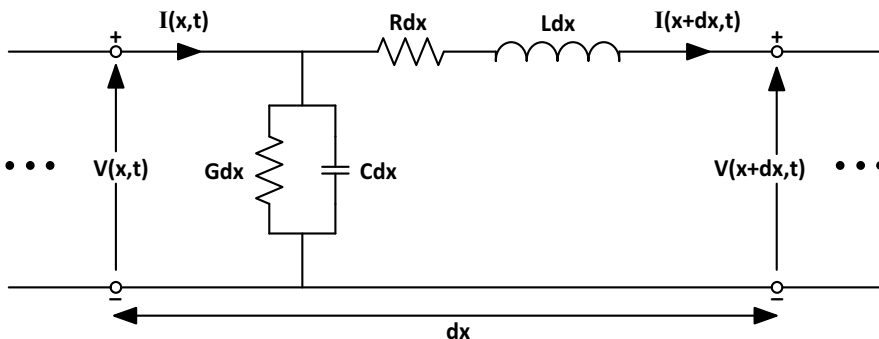


Figure 2.7: Lumped-parameter equivalent of a differential-length segment of a two-conductor transmission line (without mutual coupling to other lines).

And similarly, by applying the Kirchhoff's current law, the current flowing to the shunt conductance and the shunt capacitance can be derived:

$$I(x,t) - I(x+dx,t) = GdxV(x,t) + Cdx \frac{\partial V(x,t)}{\partial t} \quad (2.4)$$

Equations 2.3 and 2.4 are called the Telegraph Equations. Partial derivatives are used since the current and voltage are functions of both time and distance. As $dx \rightarrow 0$, these equations become:

$$-\frac{\partial V(x,t)}{\partial x} = RI(x,t) + L \frac{\partial I(x,t)}{\partial t} \quad (2.5)$$

$$-\frac{\partial I(x,t)}{\partial x} = GV(x,t) + C \frac{\partial V(x,t)}{\partial t} \quad (2.6)$$

Equations 2.5 and 2.6 can be solved in the time domain or the frequency domain, although it is common to drive the solutions in the frequency domain where the complete frequency dependencies of line parameters are easily handled [1].

TIME-DOMAIN SOLUTION FOR LOSSLESS LINES

For simplicity, it is assumed that the line is lossless, meaning that the series resistance, R , and the shunt conductance, G , are zero. By applying this assumption to equations 2.5 and 2.6 and differentiate once more with respect to x , the following equations can be obtained:

$$\frac{\partial^2 V(x,t)}{\partial x^2} = LC \frac{\partial^2 V(x,t)}{\partial t^2} \quad (2.7)$$

$$\frac{\partial^2 I(x,t)}{\partial x^2} = LC \frac{\partial^2 I(x,t)}{\partial t^2} \quad (2.8)$$

The time-domain solutions of the current and voltage waves in equations 2.7 and 2.8 are [1], [6], [21]:

$$V(x,t) = f_1\left(t + \frac{x}{v}\right) + f_2\left(t - \frac{x}{v}\right) \quad (2.9)$$

$$I(x,t) = -\frac{1}{Z_c} \left[f_1\left(t + \frac{x}{v}\right) - f_2\left(t - \frac{x}{v}\right) \right] \quad (2.10)$$

where,

$$v = \sqrt{\frac{1}{LC}} \quad \text{is the wave velocity in m/s} \quad (2.11)$$

$$Z_c = \sqrt{\frac{Z}{Y}} \text{ is the characteristic impedance} \quad (2.12)$$

Solutions of the voltage and current waves expressed by equations 2.18 and 2.19 have a physical interpretation. Assume that a line with an open end is being energized. The energizing wave propagates as a forward wave in the line until it reaches the open end, where it reflects back as a backward wave. After this instant, the total wave in the line is the summation of the forward wave (the energizing wave sent into the line) and the backward wave (the reflection of the energizing wave at the open end). In equations 2.18 and 2.19, both voltage and current waves consist of two components; a forward wave represented by the function $f_2\left(t - \frac{x}{v}\right)$, which describes the wave propagation in the positive x-direction of the line, and a backward wave represented by the function $f_1\left(t + \frac{x}{v}\right)$, which describes the wave propagation in the negative x-direction of the line. The positive x-direction of the line is typically from the sending end to the receiving end. The most important conclusion is that the total wave at a given time and in a given location on the line is the superposition of the forward and backward components [6], [21].

B. AVAILABLE COMPUTER MODELS FOR TRANSMISSION LINES

Various types of line models are available in EMT software packages for the simulation of transients in OHLs and cables. These models have been evolved over the time, resulting in more realistic and accurate transient simulations. However, it is very important to use a proper model with regards to the type of the transient phenomenon under study to assure the reliability of the simulation results. Reference [10] provides a guideline to identify the minimum recommended line model and level of details for various types of transient studies. This section presents a summary of the existing line models and advantages and disadvantages of each.

EXACT PI-MODEL OF LINE

As it was previously mentioned in Section 2.4, the exact pi-model is an adopted version of the nominal pi-model for simulation of long transmission lines and transient phenomena. This model was initially implemented in EMT programs in 1970s [22]. This model considers the distributed nature of the line impedance and admittance for the entire line length in a defined frequency. For this purpose, the Z and Y of the nominal pi-section model (Figure 2.5) are corrected by the following equations to describe the wave propagation along the line [23], [24]:

$$Z' = Z \cdot \frac{\sinh \gamma l}{\gamma l} \quad (2.13)$$

$$\frac{Y'}{2} = \frac{Y}{2} \cdot \frac{\tanh\left(\frac{\gamma l}{2}\right)}{\frac{\gamma l}{2}} \quad (2.14)$$

where l is the line length, γ is the propagation constant ($\gamma = \sqrt{ZY}$), and Z and Y are respectively the total series impedance and shunt admittance of the line. The equivalent circuit of the exact pi-model is shown in Figure 2.8.

The exact pi-model represents the distributed behaviour of the line at a single defined frequency and is often used for frequency scan validation of other cable models. Therefore, this model is only accurate for frequency-domain studies and validation of other models and not for time-domain system studies [10], [25].

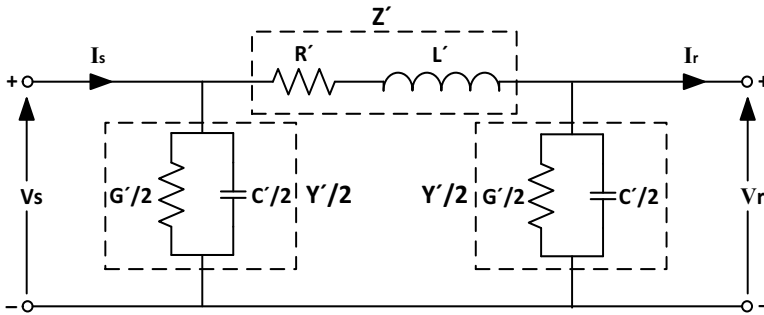


Figure 2.8: Exact pi-model of a two-conductor transmission line.

BERGERON LINE MODEL

The Bergeron line model is a constant-frequency Norton equivalent model based on the travelling wave solution in the time domain. This model is depicted in Figure 2.9. The distributed nature of the line parameters is taken into account in this model, where the line inductance and capacitance are represented by lossless Norton equivalents and the line distributed series resistance is represented as a series lumped resistance [22], [26].

In the Bergeron model, the transmission line parameters are only evaluated in one fixed frequency (e.g. fundamental frequency). Therefore, it is very important to select a right target frequency for the calculation of cable parameters when this model is used [10], [25]. In analysis of long cable systems, this model is usually recommended as the minimum model for a wide range of transient studies since the frequency of interest is normally limited to 1000 Hz due to the large charging capacity of cables [10]. In most cases, the Bergeron model produces conservative results and can be used for the initial evaluation of the system transient performance due to its numerical stability and lower computational burden compared to more accurate but sophisticated line models.

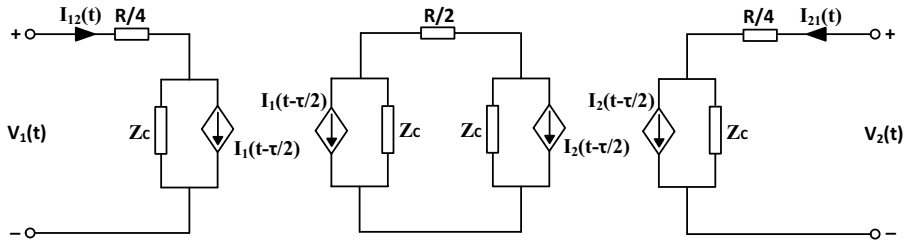


Figure 2.9: Bergeron model of a transmission line.

FREQUENCY-DEPENDENT LINE MODELS

The frequency-dependent line models take both distribution (based on the travelling wave theory) and frequency dependency of line parameters into account. These models produce more accurate and realistic results than other available models since the frequency dependencies of all line parameters are represented by them. In addition, calculations are performed in the frequency domain when these models are used, resulting in a higher accuracy since line parameters are frequency dependent [18], [25], [27-30].

When the time-domain simulations are of interest, solutions obtained in the frequency domain are transformed into the time domain by using the Fourier transform, Z-transform, or S-transform [25]. It is stated in [18]: “*transmission systems are frequency-dependent and so it makes sense to solve their parameters in the frequency domain. This is only suitable for those instances when the frequency domain characteristics are of primary interest. In order to accurately represent a frequency-dependent line when simulating with EMTDC (which of course operates in the time domain), these parameters must be convolved into their equivalent time-domain characteristics. The techniques required for this convolution are quite complex and are one of the primary attributes that differentiate the various transmission system modelling methods available today.*” A review on the existing frequency-dependent line models can be found in [25]. In general, the frequency-dependent line models can be divided into the modal-domain and phase-domain categories.

The most advanced modal-domain models are based on a frequency-dependent modal transformation matrix relating phase voltages and currents to modal voltages and currents, as presented in [31], which is based on the approach presented in [32]. In this way, equations in a multiphase line are decoupled and solved separately as a single-phase line. In other words, the modal transformation changes the system from a coupled system to a decoupled one, i.e. from the phase domain to the modal domain. The modal-domain analysis is similar to the sequence component analysis used in power systems studies. For example, there are three modal modes for a three-phase OHL circuit. The number of modal modes for an underground cable system is defined by the number of conducting layers including cores and sheaths [27], [33]. It should be mentioned that modal-domain analysis can be numerically unstable since the frequency-dependent transformation matrices cannot be handled in some cases [27].

The phase-domain models realize the frequency-dependent transfer functions of a transmission line directly in the phase-domain [27], [34], [35]. In 1999, an accurate

phase-domain model was proposed in [36], known as Universal Line Model, which is considered as the most advanced available time-domain model (especially for cables) [18], [37]. This model represents the full frequency dependency of all line parameters and the effects of a frequency-dependent transform. This model can be also used when the transformation matrix is highly frequency dependent.

In general, both frequency-dependent modal-domain and phase-domain models are reliable candidates for representation of transmission lines in transient studies, although the phase-domain models are more favourable for cables [25]. It should be mentioned that the accuracy of the frequency-dependent line models is strongly dependent on the accuracy of the calculated line electrical parameters (i.e. series impedance matrix, Z , and shunt admittance matrix, Y). The EMT programs calculate the line electrical parameters from the geometry and material properties of the line, which are inputs provided by the user. Detailed information on calculation of cable electrical parameters can be found in [22], [27], [38].

C. OHL AND CABLE MODELLING IN THE DUTCH 380 kV GRID MODEL

In the developed EMT model for the Dutch 380 kV grid, OHLs and XLPE cables have been represented by the frequency-dependent phase model of PSCAD to ensure the maximum simulation accuracy. This model is based on the Universal Line Model theory [36]. The input data of the model is based on the actual geometry and material properties of the represented transmission lines. It should be noted that the EMT programs widely use the Cable Constants routine developed in 1970s based on the study presented in [39]. EMTP-RV and ATP-EMTP use this routine while PSCAD uses an approximation of this routing according to the formulas in [29].

The basic construction of a typical XLPE cable is shown in Figure 2.10, where the function of each layer is as follows [27], [40], [41]:

1. *Conductor*: the aluminium or copper conductor carries the current and its behaviour is significantly characterized by the skin and proximity effects.
2. *Semi-conductive conductor screen*: the semi-conductive (SC) screen is placed on the conductor to prevent the electric field concentration and to provide a stress optimized transition from the conductive medium, where the electric field is nil, to the insulating medium, where the electric field is non-nil. Another purpose of the semi-conductive screen is to prevent formation of voids between the conductor and the insulation due to bending of the cable and mechanical stresses.
3. *XLPE insulation*: the insulation is one of the most important layers of a cable as it electrically insulates the conductor (HV potential) from the cable sheath (earth potential). The insulation must be able to withstand the electric field of the cable during its service life under the rated (steady-state) and the transient operating conditions.

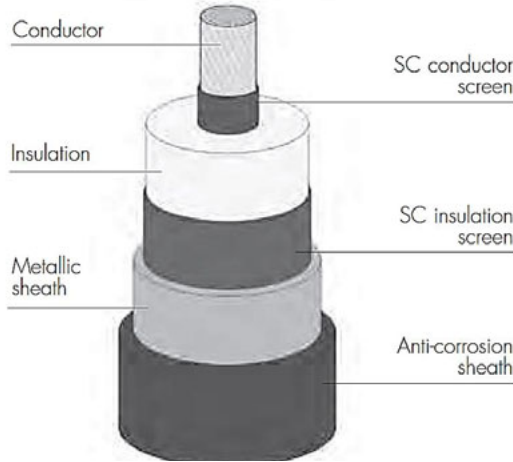


Figure 2.10: Construction and layers of a typical XLPE cable (SC: semi-conductive) [40].

4. *Semi-conductive insulation screen*: the function of this layer is similar to the function of the semi-conductive conductor screen. This layer provides a smooth electric field transition from the cable insulation to the cable metallic sheath.
5. *Metallic sheath*: the main functions of the metallic sheath are to provide a return path for the cable charging current and also a conductive path to the earth for fault currents in case of a fault in the cable. Another function of the metallic sheath is the mechanical protection of the cable and providing a radial waterproofing to avoid the contact between the insulation and water. In addition, the metallic sheath confines the electric field within the cable and nullifies it outside the cable, which is realized by connecting the sheath to the earth. This results in elimination of the capacitive coupling between cables.
6. *Outer sheath (insulation)*: the main functions of this layer are insulating the metallic sheath from the ground and surrounding medium, protection of the metallic sheath from humidity and corrosion, and contribution to the mechanical protection of the cable. The most suitable material for the outer sheath is polyethylene.

In addition to the above layers, an armour layer may be added as the outer layer on outside of the cable to increase the mechanical protection in tougher environments, where physical hazards and outside forces can damage or crush the cable.

Tables 2.9 and 2.10 show the geometry and material properties used as input parameters to model the OHLs and cables of the Spaak connection in PSCAD. The cable is a single-core 2500 mm² copper conductor cable with the XLPE insulation. The semi-conductive layers and the additional copper wire screen¹ are included in the main insulation, where the thickness, permittivity, and permeability of the insulation are modified according to the methods proposed in [42] and [43]. The proposed methods in [42] were verified in [44] too. It has been shown in [38] and [45] that the semi-conductive

¹ The copper wires of the screen are laid helical around the cable and not straight along the cable.

layers should be included in the cable model when simulating transients.

Table 2.9
GEOMETRY AND MATERIAL PROPERTIES USED TO MODEL THE OHL SECTIONS OF THE SPAAK CONNECTION

Conductor properties	
Conductor style	Solid
Outer radius	16.2 (mm)
DC resistance	0.0488 (Ω/km)
Relative permeability	1
Sag	11.1 (m)
Bundling	
Number of bundled conductors	4
Bundle configuration	Symmetrical
Bundle conductors spacing	0.5 (m)
Configuration	
Ideal transposition of circuits	Disabled
Shunt conductance	1×10^{-11} (S/m)

TABLE 2.10
GEOMETRY AND MATERIAL PROPERTIES USED TO MODEL THE CABLE SECTIONS OF THE SPAAK CONNECTION
(SINGLE-CORE 2500 MM² COPPER CONDUCTOR CABLE WITH XLPE INSULATION)

	Cable layer			
	Core conductor	1 st insulation ⁽¹⁾	Screen conductor (metallic sheath)	2 nd insulation (outer sheath)
Outer radius (mm)	30.65	63.1	63.7	71.5
Resistivity (Ωm)	1.98×10^{-8}	-	1.68×10^{-8}	-
Relative permeability	1	1.17	1	0.76
Relative permittivity	-	2.79	-	3.05
⁽¹⁾ The thickness, permittivity, and permeability of the insulation are modified to include the semi-conductive layers and the copper wire screen.				
* Earth return approximation/ resistivity/ permeability: Saad/100 $\Omega\text{m}/1$				

As previously mentioned, the cable metallic sheath should be connected to the earth to provide a path for the cable charging current and fault currents and to nullify the electric field outside the cable. A proper sheath grounding is also necessary to improve the cable performance by reducing the sheath current (thus reduction of the sheath losses and improve the cable ampacity due to the lower heat dissipation) and by reducing the sheath voltage (thus decreasing the breakdown probability of the cable insulation) [46]. In a normal operating condition, the sheath carries the cable charging current plus the current induced in it by the current of the main conductor, which results in power losses and (over)voltages in the sheath.

An effective bonding of the cable sheath to the earth at sufficient points is a very important factor in operation of long cables. By an effective bonding, the sheath current is reduced and limited to flow over a short length before going into the earth; moreover, the sheath voltage is also reduced and the electric field is completely confined within the cable. There are different methods of sheath bonding to the earth, among those the common types are single-point bonding, two-points bonding, multiple-points bonding, and cross-bonding.

The cross-bonding is the most effective and common bonding method for long cables [46-48].

When a cable circuit is cross-bonded, the cable phases are sectionalized and divided to equal lengths over the route, called minor sections. At the end of each minor section, the sheath continuities are broken and they are cross-bonded. Sheath Voltage Limiters (SVLs) are connected to the earth at these intermediate cross bonding positions (i.e. between two minor sections) to dissipate sheath voltage surges. Finally, sheaths are bonded and grounded at the ends of each major section, which is made of three minor sections. In some cases, the cable core conductors may also be transposed for further reduction of sheath currents. By using the cross-bonding technique and grounding in between, the induced sheath currents are largely cancelled out and the sheath (over)voltages are reduced. The cross-bonding affects the cable impedance and admittance matrices since the system parameters are changed by transposition and grounding of the cable sheaths. More information on the calculation of the impedance and admittance matrices of cross-bonded cables can be found in [49], [50].

Figure 2.11a shows an illustration of the applied sheath cross-bonding for the Spaak connection. This bonding method has been already used in the commissioned cable projects in the Dutch 380 kV grid (Randstad South-Ring and North-Ring projects). Therefore, the same bonding approach is considered in this research. It is assumed that each minor section is 1 km long. So, when for instance a cable section in Figure 2.3 is 30 km long, it is made of 10 major sections and 30 minor sections. In practice, cable cross-bonding joints are used to connect cable minor sections. This allows cross-bonding or termination of sheath conductors and also direct connection of core conductors without transposing.

It is very important to model the cable cross-bondings with sufficient details in order to have an accurate transient simulation. In the developed EMT model of the Dutch 380 kV grid in PSCAD, all cable cross-bondings are represented in full detail as shown in Figure 2.11a. A detailed model of each cross-bonding was applied as the discrete representation of each minor section is the most accurate way of modelling [51]. The bonding wires are represented by 1 μ H inductances at the cross-bonding joints. The grounding wires are represented by 10 μ H inductances at the straight through joints (connection of two major sections) and 1 m Ω resistances at the cable terminations [52].

Figure 2.11b shows cross-sectional layout of the cable circuits, which are laid in a flat formation in an open cable trench. The mutual electric and magnetic couplings between all 12 cables are taken into account in the developed EMT model of the Dutch 380 kV grid in PSCAD. A flat formation improves heat dissipation and thereby increases the ampacity of the cable. Other cable formations are also possible like a trefoil formation, which is advantageous in terms of space and electromagnetic field issues.

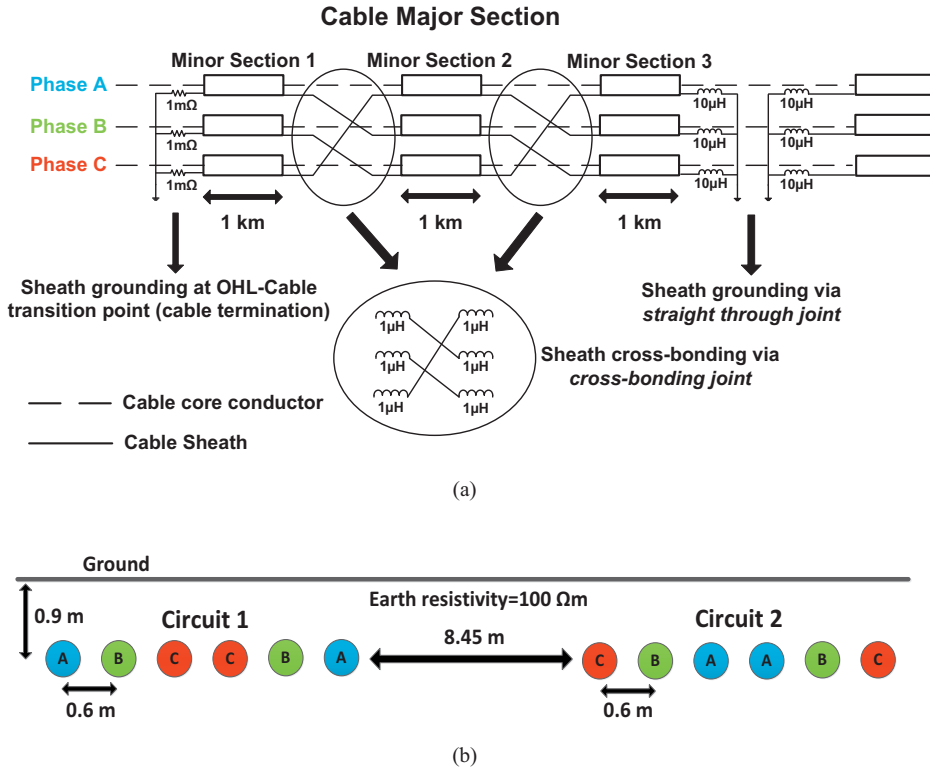


Figure 2.11: (a) Schematic of a cable major section and sheath cross-bonding, (b) Cable cross-sectional layout with flat formation in an open cable trench. The depth and distances are referred to the center of the cable.

2.5.4 TRANSFORMER AND SHUNT REACTOR MODELLING

A detailed model of the three-winding three-limb power transformers was used in the EMT model of the Dutch 380 kV grid. This model includes the core saturation and parasitic capacitances of the transformer. The air core shunt reactors are represented by a multi-layer model; however, the mutual couplings (mutual inductances) between windings of reactors are not taken into account since this is a typical simplification used when performing transient studies [53]. The transformer and shunt reactor modelling were within the scope of another Ph.D. research within the framework of the Dutch 380 kV cable research program, where more elaboration is available in [43].

2.5.5 CAPACITOR BANKS MODELLING

In the Dutch 380 kV grid, capacitor banks exist at some substations for voltage control and they are switched-in or out depending on the load-flow and the voltage level. Equivalent RLC circuits were used to represent the 380 kV capacitor banks in the EMT model of the Dutch 380 kV grid.

2.5.6 LOWER VOLTAGE GRIDS MODELLING

As it was previously mentioned in Section 2.5.2, the lower voltage levels, i.e. 220 kV and below, are represented by equivalent parallel RL or RC loads. The fixed load component in PSCAD is used for this purpose. This component models the load characteristics as a function of the voltage magnitude and frequency, where the load real and reactive powers are considered separately using the following expressions [18], [37]:

$$P = P_0 \left(\frac{V_l}{V_{l_0}} \right)^{NP} (1 + K_{PF} dF) \quad (2.15)$$

$$Q = Q_0 \left(\frac{V_l}{V_{l_0}} \right)^{NQ} (1 + K_{QF} dF) \quad (2.16)$$

where:

- P equivalent load real power (Watt)
- P_0 rated real power per phase (Watt)
- V_l load voltage (Volt)
- V_{l_0} rated load voltage (Volt)
- NP dP/dV voltage index for real power
- K_{PF} dP/dF frequency index for real power
- Q equivalent load reactive power (VAR)
- Q_0 rated reactive power per phase (VAR)
- NQ dQ/dV voltage index for reactive power
- K_{QF} dQ/dF frequency index for reactive power

2.6 CONCLUSIONS

This chapter elaborated on the research approach and the models of the Dutch transmission grid, which will be used for the analysis of the grid operation with long cables.

In the first part, the Spaak project as the case study project of this research was introduced. This project is a hypothetical future 380 kV double-circuit connection with the transmission length of 80 km. The location of the project, cable scenarios, and mixed-line configurations together with general information about the Dutch transmission grid were provided in this part.

The second part of the chapter discussed about the DIGSILENT PowerFactory and PSCAD models used to simulate and analyse the steady-state and transient operations of the grid, respectively. The PowerFactory model represents the whole Dutch transmission grid including all voltage levels (110 kV to 380 kV). The EMT model in PSCAD represents the whole Dutch 380 kV grid and equivalents of the lower voltage levels, i.e. 220 kV and below. The developed grid model uses the Universal Line Model for OHLs and cables

together with frequency-dependent models for other system components. The use of an accurate transmission line model is one of the most crucial factors in transient studies, which requires a robust distributed frequency-dependent parameter line model based on the travelling wave theory. So far, the Universal Line Model is the most accurate line model for simulation of transient voltages and currents in lines.

REFERENCES

- [1] A. Ametani, N. Nagaoka, Y. Baba and T. Ohno, *Power System Transients: Theory and Application*, CRC Press, 2014.
- [2] CIGRE Working Group C4.307, "Resonance and ferroresonance in power networks," *CIGRE Technical Brochure no. 569*, February 2014.
- [3] F. Iliceto, E. Cinieri and A. Di Vita, "Overvoltages due to open-phase occurrence in reactor compensated EHV lines," *IEEE Transactions on Power Apparatus and Systems*, vol. PAS-103, no. 3, pp. 474-482, March 1984.
- [4] F. M. Gatta and S. Lauria, "Very long EHV cables and mixed overhead-cable lines. Steady-state operation," in *IEEE Power Technology Conference*, St. Petersburg, Russia, June 2005.
- [5] L. Wu, P. A. A. F. Wouters and E. F. Steennis, "Frequency domain transient analysis of resonant behavior for different HV overhead line and underground cable configurations," in *International Conference on Power System Transients (IPST)*, Vancouver, Canada, 2013.
- [6] L. van der Sluis, *Transients in Power Systems*, Chichester, UK: Wiley, August 2001.
- [7] J. J. Grainger and W. D. Stevenson Jr., *Power System Analysis*, Singapore: McGraw-Hill, 1994.
- [8] R. Smeets, L. van der Sluis, M. Kapetanovic, D. Peelo and A. Janssen, *Switching in Electrical Transmission and Distribution Systems*, Hoboken, NJ, USA: Wiley, 2015.
- [9] CIGRE Working Group 02, Study Committee 33, "Guidelines for representation of network elements when calculating transients," *CIGRE Technical Brochure no. 39*, 2000.
- [10] CIGRE Working Group C4.502, "Power system technical performance issues related to the application of long HVAC cables," *CIGRE Technical Brochure no. 556*, October 2013.
- [11] F. F. da Silva, C. L. Bak and P. B. Holst, "Estimation of the required modeling depth for the simulation of cable switching in a cable-based network," *IEEE Transactions on Power Delivery*, vol. 27, no. 4, pp. 1902-1908, October 2012.
- [12] F. F. da Silva, C. L. Bak and P. B. Holst, "Study of harmonics in cable-based transmission networks," in *44th CIGRE Session*, Paris, France, 2012.
- [13] J. Morales, J. Mahseredjian, K. Sheshyekani, A. Ramirez, E. Medina and I. Kocar, "Pole-selective residue perturbation technique for passivity enforcement of FDNEs," *IEEE Transactions on Power Delivery*, DOI:10.1109/TPWRD.2018.2810706, March 2018.
- [14] B. Gustavsen and H. M. Jeewantha De Silva, "Inclusion of rational models in an electromagnetic transients program: Y-parameters, Z-parameters, S-parameters, transfer functions," *IEEE Transactions on Power Delivery*, vol. 28, no. 2, pp. 1164-1174, April 2013.
- [15] A. Ubolli and B. Gustavsen, "Multiport frequency-dependent network equivalencing based on Ssimulated time-domain responses," *IEEE Transactions on Power Delivery*, vol. 27, no. 2, pp. 648-657, April 2012.

- [16] K. Sheshyekani, H. R. karami, P. Dehkhoda, M. Paolone and F. Rachidi, "Application of the matrix pencil method to rational fitting of frequency-domain responses," *IEEE Transactions on Power Delivery*, vol. 27, no. 4, pp. 2399-2408, October 2012.
- [17] A. Ametani, *Numerical Analysis of Power System Transients and Dynamics*, UK: IET, Power and Energy Series 78, 2015.
- [18] Manitoba HVDC Research Centre, "User's guide on the EMTDC analysis for PSCAD power system simulation," Winnipeg, Manitoba, Canada, 2010.
- [19] F. Barakou, M. H. J. Bollen, S. Mousavi-Gargari, P. A. A. F. Wouters and E. F. Steennis, "Downstream network modeling for switching transients in EHV networks containing cables," in *IEEE Power Technology Conference*, Manchester, UK, June 2017.
- [20] IEEE Modeling and Analysis of System Transients Working Group, "Modeling guidelines for switching transients," Special Publication, Modeling and Simulation Working Group 15.08.
- [21] A. Greenwood, *Electrical Transients in Power Systems*, Hoboken, NJ, USA: Wiley, 1971.
- [22] H. W. Dommel, *Electromagnetic Transients Program Manual (EMTP Theory Book)*, Portland, OR, USA: Bonneville Power Administration, August 1986.
- [23] P. Schavemaker and L. van der Sluis, *Power System Essentials*, Chichester, UK: Wiley, 2008.
- [24] N. Tleis, *Power Systems Modelling and Fault Analysis*, Oxford, UK: Newnes, 2008.
- [25] U. S. Gudmundsdottir, "Modelling of long high voltage AC cables in transmission systems," Ph.D. dissertation, Department of Energy Technology, *Aalborg University, Aalborg, Denmark*, 2010.
- [26] H. W. Dommel, "Digital computer solution of electromagnetic digital computer solution of electromagnetic networks," *IEEE Transactions on Power Apparatus and Systems*, vol. PAS-88, no. 4, pp. 388-396, April 1969.
- [27] A. Ametani, T. Ohno and N. Nagaoka, *Cable System Transients: Theory, Modeling and Simulation*, Singapore: Wiley, July 2015.
- [28] L. M. Wedepohl and S. E. T. Mohamed, "Multi-conductor transmission lines: Theory of natural modes and Fourier integral applied to transient analysis," *Proc. of the Institution of Electrical Engineers (IEE)*, vol. 116, no. 9, pp. 1153-1563, September 1969.
- [29] L. M. Wedepohl and D. J. Wilcox, "Transient analysis of underground power transmission systems," *Proc. of the Institution of Electrical Engineers (IEE)*, vol. 120, no. 2, pp. 253-260, 1973.
- [30] N. Watson and J. Arrilaga, *Power Systems Electromagnetic Transients Simulation*, UK: IET, Power and Energy Series no. 39, 2003.
- [31] L. Marti, "Simulation of transients in underground cables with frequency-dependent modal transformation matrices," *IEEE Transactions on Power Delivery*, vol. 3, no. 3, pp. 1099-1110, July 1998.
- [32] A. Ametani, "Refraction coefficient method for switching surge calculations on un-transposed transmission line," in *IEEE Power Engineering Society (PES) Summer Meeting*, Vancouver, Canada, 1973.
- [33] F. F. da Silva and C. L. Bak, *Electromagnetic Transients in Power Cables*, London, UK: Springer, 2013.
- [34] H. Nakanishi and A. Ametani, "Transient calculation of a transmission line using superposition law," *IEE Proceedings C-Generation, Transmission and Distribution*, vol. 133, Pt. C, no. 5, pp.

- 263-269, July 1986.
- [35] T. Noda, N. Nagaoka and A. Ametani, "Phase domain modeling of frequency-dependent transmission lines by means of an ARMA model," *IEEE Transactions on Power Delivery*, vol. 11, no. 1, pp. 401-411, 1996.
- [36] A. Morched, B. Gustavsen and M. Tartibi, "A universal model for accurate calculation of electromagnetic transients on overhead lines and underground cables," *IEEE Transactions on Power Delivery*, vol. 14, no. 3, pp. 1032-1038, July 1999.
- [37] Manitoba HVDC Research Centre, "User's guide on the use of PSCAD," Winnipeg, Manitoba, Canada, 2010.
- [38] B. Gustavsen, J. A. Martinez and D. Durbak, "Parameter determination for modeling system transients-Part II: insulated cables," *IEEE Transactions on Power Delivery*, vol. 20, no. 3, pp. 2045-2050, July 2005.
- [39] A. Ametani, "A general formulation of impedance and admittance of cables," *IEEE Transactions on Power Apparatus and Systems*, vol. 99, no. 3, pp. 902-910, May 1980.
- [40] Nexan Brochure, "60-500 kV high voltage underground power cables: XLPE insulated cables," Nexan High Voltage Underground Cables.
- [41] C. L. Bak and F. F. da Silva, "High voltage AC underground cable systems for power transmission-A review of the Danish experience, part 1," *Electric Power Systems Research*, vol. 140, pp. 987-994, 2016.
- [42] B. Gustavsen, "Panel session on data for modeling system transients: insulated cables," in *IEEE Power Engineering Society (PES) Winter Meeting*, 2001.
- [43] L. Wu, "Impact of EHV/HV underground power cables on resonant grid behavior," Ph.D. dissertation, Department of Electrical Engineering, Eindhoven University of Technology, Eindhoven, The Netherlands, October 2014.
- [44] k. Steinbrich, "Influence of semiconducting layers on the attenuation behaviour of single-core power cables," *IEE Generation, Transmission and Distribution*, vol. 152, no. 2, pp. 271-276, March 2005.
- [45] A. Ametani, Y. Miyamoto and N. Nagaoka, "Semiconducting layer impedance and its effect on cable wave-propagation and transient characteristics," *IEEE Transactions on Power Delivery*, vol. 19, no. 4, pp. 1523-1531, October 2004.
- [46] "IEEE Guide for Bonding Shields and Sheaths of Single-Conductor Power Cables Rated 5 kV through 500 kV," IEEE Standard 575, 2014.
- [47] CIGRE Working Group B1.19, "General guidelines for the integration of a new underground cable system in the network," *CIGRE Technical Brochure no. 250*, August 2004.
- [48] CIGRE Working Group B1.18, "Special bonding of high voltage power cables," *CIGRE Technical Brochure no. 283*, 2005.
- [49] N. Nagaoka and A. Ametani, "Transient calculations on crossbonded cables," *IEEE Transactions on Power Apparatus and Systems*, vol. 102, no. 4, pp. 779-787, April 1983.
- [50] A. Ametani, Y. Miyamoto and N. Nagaoka, "An investigation on a wave propagation characteristic on a crossbonded cable," *IEEE Transactions on Power and Energy*, vol. 123-B, no. 3, pp. 395-401, 2003.
- [51] I. Lafaia, J. Mahseredjian, A. Ametani, M. T. Correia de Barros, I. Kocar and Y. Fillion, "Frequency and time domain response of cross-bonded cables," *IEEE Transactions on Power Delivery*, vol. 33, no. 2, pp. 640-648, April 2018.

-
- [52] U. S. Gudmundsdottir, B. Gustavsen, C. L. Bak and W. Wiechowski, "Field test and simulation of a 400-kV cross-bonded cable system," *IEEE Transactions on Power Delivery*, vol. 26, no. 3, pp. 1403-1410, July 2011.
- [53] "Insulation Co-Ordination-Part 4: Computational Guide to Insulation Co-Ordination and Modelling of Electrical Networks," IEC 60071-4, 2004.

CHAPTER 3

SHUNT COMPENSATION ALLOCATION IN HYBRID OHL-CABLE SYSTEMS

3.1 INTRODUCTION

As previously mentioned, cables have different electrical characteristics from OHLs, which results in excessive reactive power production and in some cases cable overloading when they are operated in parallel with OHLs. Several system operation problems are associated with the reactive power of long cables, which should be handled by an optimal reactive power shunt compensation and, when required, by applying countermeasures to control the loading of the cable. It is crucial to have sufficient size of shunt compensation since both under- and over-compensation increase the risk of undesirable conditions like overvoltages and the zero-current phenomenon [1], [2]. The size of shunt compensation has to be determined in the first step of system impact studies as it has a direct impact on the rest of technical issues like harmonic and transient operations.

The main goal of this chapter is to study the shunt compensation sizing in hybrid OHL-Cable transmission systems and to address the most important parameters in an optimal compensation allocation. In addition, the active power flow and the cable overloading are analysed. Simulation results show that various parameters including the cable length, shunt reactor location, mixed-line configuration, and load-flow can substantially affect the required size of shunt compensation. The outcomes of this study are important in the design process of every hybrid OHL-Cable circuit as they can be used to choose the best compensation approach. The compensation sizes obtained in this chapter will be used in the rest of the thesis for the analysis of other technical issues.

This chapter is structured as follows: Sections 3.2 and 3.3 explain the theoretical background of the cable capacitive behaviour and its impact on the system operation. Section 3.4 highlights the necessity and importance of the optimal shunt compensation in cable systems. The simulation results of the shunt compensation analysis for the case study project (Spaak project) are presented in Section 3.5, where the compensation sizing requirements and various sensitivity analyses are discussed. In addition, the impact of the

distributed compensation and the mixed-line configuration on the compensation size are treated in this section. The cable overloading is discussed in Section 3.6 and finally the most important conclusions are summarized in Section 3.7.

3.2 CABLE CAPACITIVE BEHAVIOUR

A useful parameter in the study of electrical power systems is the surge impedance loading (SIL) or natural loading. SIL of a transmission line is the megawatt (MW) loading of the line at which a natural reactive power balance occurs. In other words, SIL is the power loading at which reactive power is neither produced nor absorbed by the line and can be expressed as below [3]:

$$SIL = \frac{V^2}{Z_s}, \text{ where } Z_s = \sqrt{\frac{L}{C}} \quad (3.1)$$

where V is the system voltage and Z_s is the line surge impedance. L is the line series inductance and C is the line shunt capacitance, both per unit length.

SIL is a useful parameter to reveal the reactive power behaviour of a transmission line. When a line is loaded above its SIL, it acts like a reactor and absorbs reactive power and when it is loaded below its SIL, it acts like a capacitor and generates reactive power. Compared to an OHL, a cable has a larger shunt capacitance and a smaller series inductance, thus the surge impedance (Z_s) of the cable is several times smaller than that of the OHL and consequently SIL of the cable is several times larger than that of the OHL.

The thermal rating of a line is the power transmission capacity at its ampere capacity (ampacity). During normal operation, cables are always loaded below their SIL because the cable SIL is several times larger than its thermal rating. Hence, cables behave as capacitors and produce reactive power. On the contrary, SIL of an OHL is several times smaller than its thermal rating; therefore, OHLs are normally operated above their SIL and behave as inductors, i.e. consuming reactive power [3], [4].

3.3 NEGATIVE EFFECTS OF CABLE REACTIVE POWER

The large surplus reactive power produced by cables results in steady-state voltage rise and under-excitation of synchronous generators (in severe cases self-excitation), which can impose severe stresses on system equipment and increase the risk of system transient instability [1], [4], [5]. Another risk of long cables operation is the large capacitive current in the line circuit breakers, which can exceed the type-tested breaking capability of the breaker [4], [6-8].

Always a part of the cable ampacity is occupied by its capacitive charging current whilst this part becomes larger by increasing the cable length and consequently the remaining transfer capacity for the active power gets smaller. At a critical length, $L_{critical}$, the capacitive current equals the cable ampacity so that no transfer capacity is left for the active

power. This is one of the main limitations in the application of long AC cables, which is elaborated and analysed in [4], [9-11].

Figure 3.1 illustrates the voltage profile and the flows of current, reactive power, active power, and apparent power in a lossless cable [11]. The optimal operating condition in a lossless cable happens when the voltage of the sending (V_s) and the receiving (V_r) terminals are equal. This leads to an equal distribution of the reactive power between the two terminals. In this situation, the maximum cable length, L_{max} , is twice of $L_{critical}$ and the charging current equals to the ampacity at each end.

In Figure 3.2, the maximum transferable active power through a lossless cable is plotted versus the cable length for three voltage levels [4]. The calculated powers are for a three-phase system with 2500 m² copper conductor single-core cables. For 380 kV cables, the maximum length is around 210 km, implying that at this length the active power that can be transferred through the cable is zero. According to this figure, it is beneficial from the transfer capacity aspect to operate short cables under higher voltages and long cables under lower voltages.

The operation of a lossless cable with different terminal voltages causes an asymmetrical reactive power profile (non-optimal operation condition). This results in flow of more reactive power toward the terminal with the lower voltage. In this case, the maximum transferable active power can be calculated as a function of the sending and the receiving terminal voltages by using non-linear equations [4].

It should be noted that for a lossy cable, the optimal operating condition and the maximum active power transfer are achieved when there is a particular voltage deviation (depending on the system parameters) between the sending and receiving terminals.

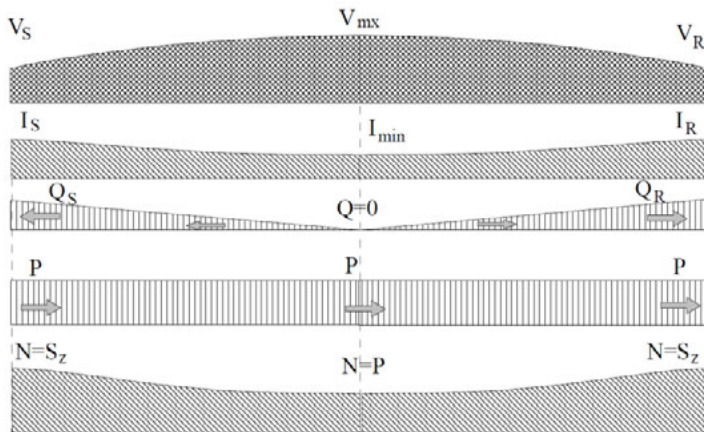


Figure 3.1: Voltage profile (V) and flows of current (I), reactive power (Q), active power (P), and apparent power (S) in a lossless EHV cable operated with equal terminal voltages (optimal operation condition) [11]. S and R denote the sending and receiving terminals, respectively.

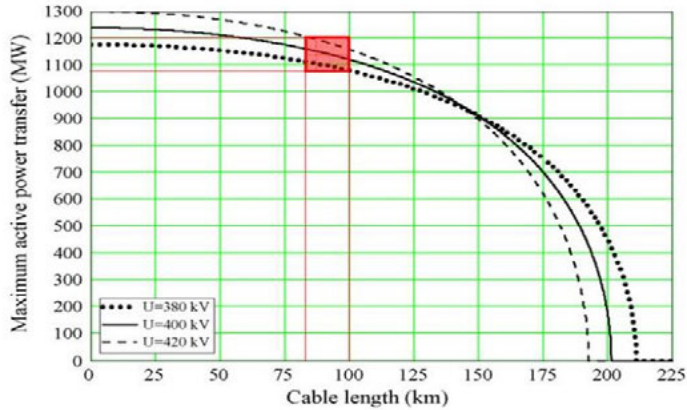


Figure 3.2: Maximum active power transfer, P_{\max} , at the thermal limit versus the cable length, calculated for different terminal voltages. The cable losses are neglected and terminals have equal voltages (optimal operation condition) [4]. The red box shows an example case.

3.4 REACTIVE POWER COMPENSATION

Taking into account the negative impacts of the cable surplus reactive power, it is necessary to allocate reactive power shunt compensation with an optimal size at proper locations. The shunt compensation is realized by using fixed- or variable-size shunt reactors and reduces the reactive power fed into the rest of the system.

As it was previously mentioned in Section 2.3.1, shunt reactors should be connected directly to the hybrid circuit at the two ends of the circuit or distributed at multiple locations along the circuit. Alternatively, for some cable lengths, shunt reactors can be installed at substation busbars or at tertiary windings of power transformers if energization overvoltages and capacitive currents are not large. When the increase of the active power transfer capacity is required, shunt reactors should be distributed along the cable especially for cables longer than the critical length. A distributed compensation can also reduce the required degree of compensation and boost the system transient stability [5], [7]; however, the distributed compensation may not be possible in some situations due to the land occupation and visual impact of reactor banks as well as reliability issues [4].

The shunt compensation can be realized by fixed-size reactors or by controllable shunt compensation devices like tapped-winding reactors, thyristor controlled reactors (TCR), and shunt-connected flexible AC transmission systems (FACTS) based on voltage-source converters, like the static synchronous compensator (STATCOM). Power electronics-based apparatus like TCRs and STATCOMs are more costly, but they give a continuous regulation capability and a fast dynamic response despite the fast response is not strictly required for the steady-state reactive power control. The continuous regulation can also be provided if a sufficient number of discrete regulation steps in the desired range are available [10]. In this aspect, tapped-winding reactors or reactor banks with sufficient number of switchable fixed-size reactors are favourable and cost-effective solutions.

In the literature, several arrangements for the location of shunt reactors are proposed. In [12], the authors proposed different arrangements for shunt reactors as shown in Figure 3.3a, where it is assumed that a load with unity power factor is supplied. The curves in Figure 3.3b show the effectiveness of the proposed arrangements by the extent to which the thermal rating of the cable is available for the active power transmission as a function of the cable length. One per unit (pu) receiving-end power means the active power equal to the thermal rating of the cable. One pu line length is the cable length at which the total charging current equals the current rating of the cable (i.e. critical length). In general, it can be concluded that the best efficiency in the active power transfer can be archived by a distributed compensation in which shunt reactors are placed at several points along the circuit. However, in practice it is usually preferred to place the shunt reactors at the ends of the hybrid circuit to minimize the land occupation and visual impacts.

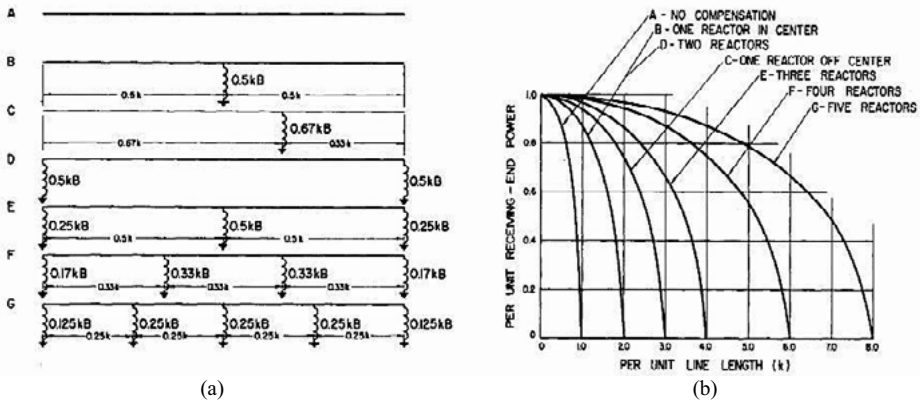


Figure 3.3: (a) Various arrangements of shunt compensating reactors, (b) Line performance with a unity power factor load, pu values [12].

3.5 STUDY OF THE SPAAK PROJECT

The steady-state study was performed for the Spaak connection with the six cable scenarios presented in Chapter 2. The mixed-line configuration under study is as shown in Figure 2.3, unless a different configuration is mentioned. The line-end compensation (LEC) with direct connection of reactors to the circuit was applied due to the reasons explained in Section 2.3.1.B. Several sensitivity analyses were performed to determine the impacts of different parameters on the steady-state design and operation of cable circuits. The steady-state simulations were carried out by the PowerFactory model of the Dutch transmission grid as described in Chapter 2.

3.5.1 SIZING CRITERIA

This research proposes a shunt compensation sizing approach based on the criteria addressed in [1], [4], [7], [9], [13], [14]. This approach is according to the technical concerns related to the operation of long EHV cables. In this regard, the following four

criteria were used for the sizing of shunt reactors, which are mainly based on the no-load open-end operation as the situation with the most severe reactive power balance:

1. *Sudden voltage step (rapid voltage change (RVC))*: RVC is a quick transition in RMS voltage between two steady-state conditions during which the voltage does not exceed the dip/swell thresholds [15]. Based on this sizing criterion, the sudden voltage jump at the sending terminal after the no-load energization should be less than 3% (according to the Dutch grid code) to reduce the disturbance to customers. In addition, the sending terminal final voltage should be less than the swell threshold of 1.1 pu.
2. *Voltage along the line*: this constraint is related to the voltage on the hybrid circuit following the no-load energization. The voltage must be less than 1.1 pu to allow line reclosure and avoid damages to line connected devices. Protection equipment like surge arrestors must be checked in terms of temporary overvoltage (TOV) capability. The voltage at all OHL-cable transition points (cable terminations) and open-end has to be smaller than 1.1 pu.

It is worth noting that due to the Ferranti effect, the voltage at the open-end is the highest voltage during the no-load energization when the shunt compensation is not utilized. However, the highest voltage along a shunt-compensated hybrid circuit may be at a point different than the open-end. Therefore, in this study the attention is given to the voltage of all points along the circuit and not only to the open-end voltage.

The Ferranti effect states that in case of the no-load operation of a transmission line, the steady-state voltage at the receiving open-end (V_r) increases beyond the sending-end voltage (V_s), which can be expressed as below:

$$V_r = \frac{V_s}{1 - \frac{\omega^2 L C l^2}{2}} \quad (3.2)$$

where L is the line series inductance per unit length, C is the line shunt capacitance per unit length, and l is the line length. ω is the system angular frequency ($\omega = 2\pi f_0$, where f_0 is the system power frequency). The source inductance (i.e. the equivalent short-circuit inductance of the system) is included in L , therefore it can be concluded that the steady-state voltage rise at the open-end is higher when the system short-circuit power is lower (i.e. larger L).

3. *Capacitive breaking current of circuit breakers*: when a large TOV occurs, the fast line switching-off at the energizing terminal is an option under the condition that the capacitive breaking current of the line circuit breaker be sufficient. When shunt compensation is applied, it must be checked that the no-load current of the hybrid circuit is not larger than the type-tested capacitive breaking current of the circuit breaker. This is an important requirement in order to avoid circuit breaker failures [8], [16]. For the sake of this study, 400 A is selected as the strictest limit as well as the preferred value according to [16], although higher limits can also be used.

4. *Cable charging current*: in situations where the cable length is longer than the critical length, shunt compensation must ensure that the cable charging current stays below the thermal limit (ampacity) of the cable. This can be realized by installing the shunt reactors at appropriate intermediate locations along the cable. In this study, 2 kA limit is chosen for this criterion since each individual cable of the Spaak connection can withstand 2 kA for 24 hours, whereas the energization only lasts for tens of seconds or maximum a few minutes.

3.5.2 LOAD-FLOW SCENARIOS

It is important to do the system studies for different load-flow scenarios such as high wind power generation or low conventional power generation. The shunt reactor sizing under different load-flow scenarios is crucial to take the impact of different power dispatches and short-circuit powers into the account.

Based on the TenneT quality and capacity plan 2013 (Kwaliteits en Capaciteits Document (KCD)), two load-flow scenarios (planning cases) were chosen for this study:

1. *Load-flow A (West-East)*: this planning case represents high generation in the Maasvlakte region (see Figure 2.1) and high import from Britain while low generation in the Eemshaven region and low power import from Germany, Norway and Denmark. In this case, a large power transport is expected from the west to the east. The assumed short-circuit powers of the Krimpen and Dodewaard substations are 29.7 and 20.4 GVA, respectively. The steady-state voltages at the Krimpen and Dodewaard substations are around 1.03 pu.
2. *Load-flow B (East-West)*: this planning case is related to the situation of high generation in the Eemshaven and high import from Germany, Norway and Denmark; meanwhile, low generation in the Maasvlakte and low import from Britain. In this case, there is a large transport of power from the north-east to the west and south-west. The assumed short-circuit powers of the Krimpen and Dodewaard substations are 20.1 and 21 GVA, respectively. The steady-state voltages at the Krimpen and Dodewaard substations are around 1.08 pu. It should be pointed that the steady-state voltage profiles are high in this load-flow.

3.5.3 GLOBAL COMPENSATION

The steady-state operation of the Spaak connection was studied under two assumptions. Firstly, according to the best-end switching approach, the hybrid OHL-Cable circuit is energized from the substation with a higher short-circuit power (the Krimpen substation in the load-flow A and the Dodewaard substation in the load-flow B). The best-end switching decreases the sudden voltage jump at the sending-end and also the steady-state overvoltage at the open-end (due to the Ferranti effect, equation 3.2), which leads to the further saving on the compensation size¹.

¹ In the case of disconnection, it is better to begin the switching from the weak-end in order to minimize sudden voltage changes.

Secondly, when both circuits should be connected, the second circuit is energized after the complete connection of the first circuit to the system at both ends. It was also assumed that the required compensation for each circuit is equally distributed at the two ends ($SR1=SR2$ and $SR3=SR4$ in Figure 2.3). In addition, the required compensation sizes for the first energized circuit and the second energized circuit can be different.

Table 3.1 presents the minimum required size of shunt compensation for different cable lengths in the circuit. The results are categorized for the two load-flow scenarios and two modes of operation, namely single-circuit and double-circuit operations. The reported sizes for the double-circuit operation are the total size of both circuits ($SR1+SR2+SR3+SR4$). The values between parentheses are the compensation degrees, calculated as below:

$$K_{sh}(\%) = \frac{Q_{sh}}{N \times \omega C l V_n^2} \times 100 \quad (3.3)$$

where Q_{sh} is the total shunt compensation size in Mvar, C is the cable capacitance in F/km, l is the cable length in km, and V_n is the system nominal voltage, which in this study is 380 kV. The factor N denotes the number of cables, which is 6 and 12 respectively for the single-circuit and the double-circuit operations. In this equation, the reactive power produced by the OHL sections of the hybrid circuit are ignored since they are negligible compared to those of the cable sections.

Figure 3.4 shows the minimum required compensation size and degree for different cable lengths and the two load-flow scenarios when both circuits are in operation. It can be noticed that the minimum required compensation size becomes higher by increasing the cable length albeit a full compensation ($K_{sh}=100\%$) not required. When the compensation degree gets closer to 100%, the resonance frequency of the circuit formed by the shunt compensation inductance and the cable capacitance gets closer to the fundamental frequency. In addition, the probability and the severity of the zero-missing phenomenon is higher when the degree of compensation is higher [2].

According to Table 3.1, the required compensation size for the double-circuit operation is slightly higher than double of that for the single-circuit operation. There is also a substantial difference between the results of the two load-flows with higher compensation degrees for the load-flow B. The main reason is the high voltage profile in the region of the Spaak connection in the load-flow B, which is already around 1.08 pu before the cable energization. Therefore, a larger compensation is required to keep the voltages within the limit.

TABLE 3.1
MINIMUM REQUIRED SHUNT COMPENSATION SIZE (Q_{sh}) AND DEGREE (K_{sh}) FOR THE SINGLE-CIRCUIT AND DOUBLE-CIRCUIT OPERATIONS OF THE SPAAK CONNECTION

Cable length (km)	Q_{sh} [Mvar] (K_{sh} [%])			
	Load-flow A		Load-flow B	
	Single-circuit	Double-circuit	Single-circuit	Double-circuit
12 (15%)	50 (19.8%)	102 (20.2%)	176 (69.8%)	366 (72.6%)
20 (25%)	214 (50.9%)	430 (51.2%)	356 (84.8%)	722 (86%)
40 (50%)	620 (73.8%)	1245 (74.1%)	750 (89.3%)	1560 (92.9%)
60 (75%)	1030 (81.7%)	2062 (81.8%)	1160 (92.1%)	2380 (94.4%)
80 (Fully Cable)	1440 (85.7%)	2883 (85.8%)	1600 (95.2%)	3226 (96%)

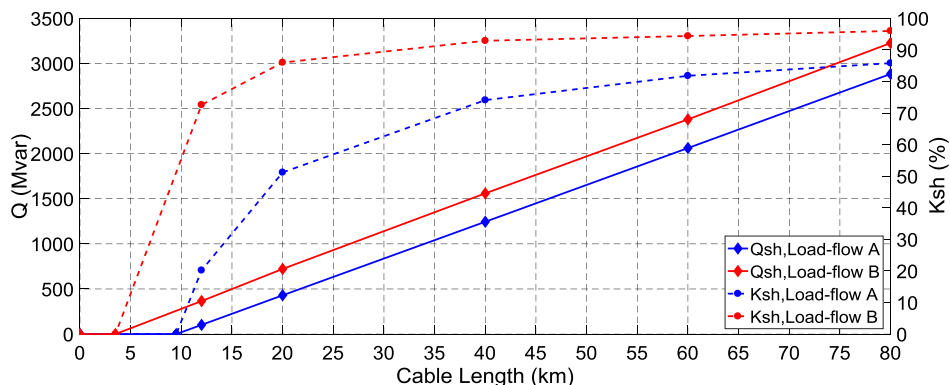


Figure 3.4: Minimum required shunt compensation size (Q_{sh}) and degree (K_{sh}) for versus the cable length for the double-circuit operation of the Spaak connection.

It has been shown that the load-flow scenario has a considerable impact on the shunt compensation size. The steady-state voltage prior to the cable energization and the short-circuit power of the substation from which the circuit is energized can significantly affect the size of shunt compensation. Hence, when operation in several load-flow scenarios is expected, a global compensation capable of satisfying the sizing criteria in all the expected scenarios is necessary. This means that the installed capacity for shunt compensation should be based on the highest calculated size among different load-flow scenarios. In this regard, in the case of the Dutch transmission system, future operation in both the load-flows A and B together with other load-flow cases could be expected. With the assumption that the most extreme cases are the load-flows A and B, the global compensation sizes are those obtained for the load-flow B as reshown in Table 3.2.

TABLE 3.2
MINIMUM REQUIRED SHUNT COMPENSATION SIZE (Q_{sh}) AND DEGREE (K_{sh}) FOR THE GLOBAL COMPENSATION OF THE SPAAK CONNECTION

Cable length (km)	Q_{sh} [Mvar] (K_{sh} [%])	
	Single-circuit operation	Double-circuit operation
12 (15%)	176 (69.8%)	366 (72.6%)
20 (25%)	356 (84.8%)	722 (86%)
40 (50%)	750 (89.3%)	1560 (92.9%)
60 (75%)	1160 (92.1%)	2380 (94.4%)
80 (Fully Cable)	1600 (95.2%)	3226 (96%)

3.5.4 MOST DECISIVE SIZING CRITERION

It is of high interest to determine the sizing criterion that requires the largest compensation size to be satisfied. Among the four sizing criteria, the cable charging current during the no-load energization is found to be the less strict criterion. The cable charging current variation by increasing the cable length prior to the shunt compensating is shown in Figure 3.5. None of the cable currents exceeds the limit (2 kA) even for longer lengths up to around 103 km in the load-flow A and around 92 km in the load-flow B. Comparing the first circuit and the second circuit energizations, the cable currents are identical for lengths up to 40 km. However, the currents get slightly different for lengths longer than 40 km with higher values for the second circuit energization.

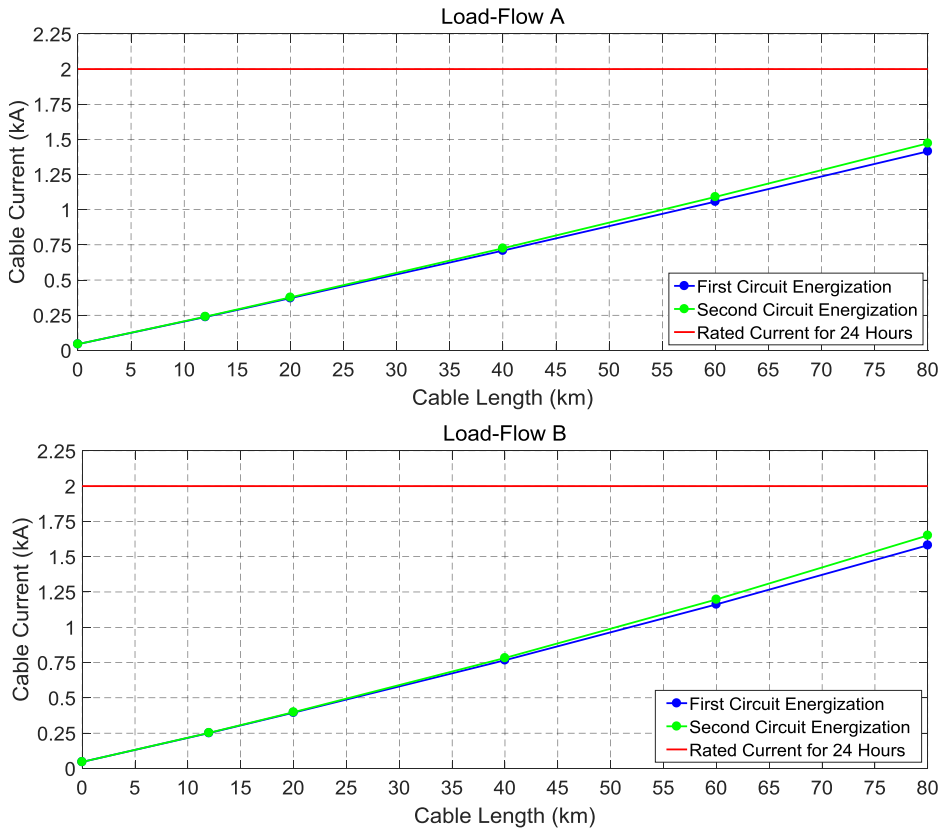


Figure 3.5: Cable charging current versus the cable length after the no-load energization of the Spaak connection without shunt compensation in the load-flows A and B. The plotted currents are for the first cable section from the sending-end, which is: Cable 1 in the load-flow A, first circuit energization; Cable 4 in the load-flow A, second circuit energization; Cable 3 in the load-flow B, first circuit energization; Cable 6 in the load-flow B, second circuit energization (see Figure 2.3).

Figure 3.6 shows the minimum required shunt compensation degree for the double-circuit operation versus the cable length calculated based on the other three sizing criteria. It can be seen that the capacitive breaking current of the circuit breaker is decisively the most determinant criterion for the load-flow A. This means that the size of compensation is dictated by this criterion and any further savings on shunt reactors can be achieved with the use of higher rated circuit breakers. However, in contrast to the load-flow A, the voltage along the hybrid circuit is the most decisive sizing criterion for the load-flow B despite of the decreasing difference between the sizing criteria by increasing the cable length. It should be noted that for the Spaak connection with 80 km transmission length, the most decisive sizing criterion is not dependent on the mixed-line configuration, compensation location, and operation mode (single-circuit or double-circuit), whereas this dependency exists when the transmission length is longer.

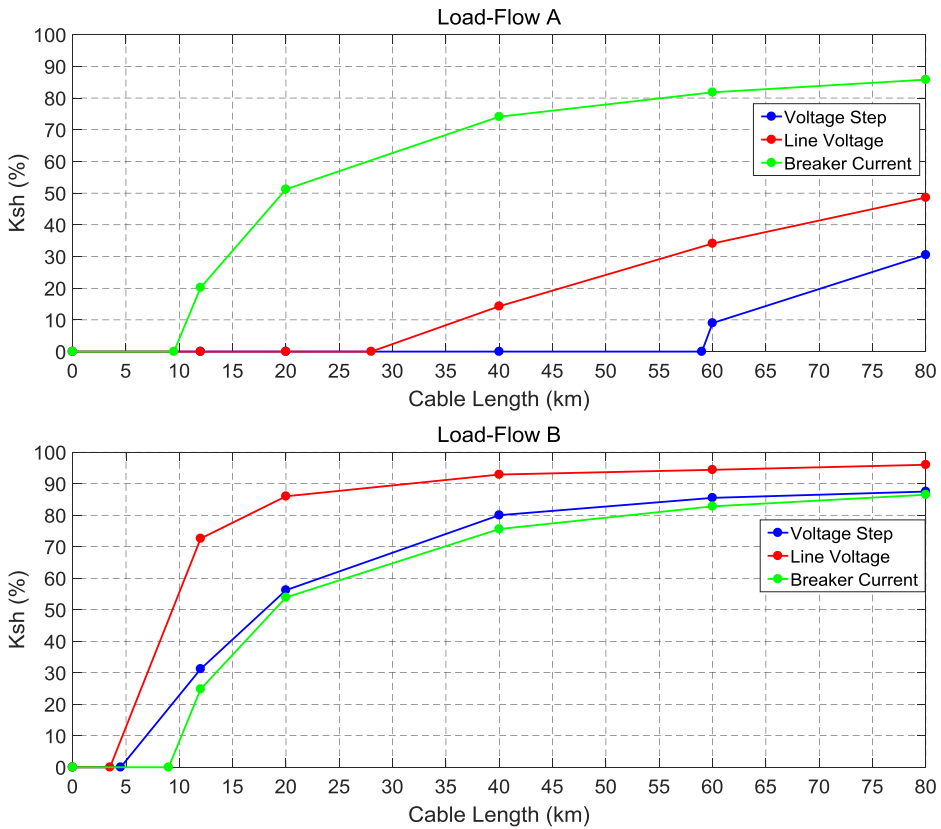


Figure 3.6: Minimum required shunt compensation degree versus the cable length calculated based on different sizing criteria for the double-circuit operation of the Spaak connection in the load-flows A and B.

It is necessary to note that the computed compensation sizes related to the capacitive breaking current criterion are based on the 400 A target value as the recommended value in the standard [16]. However, in some cases, the alternative solution to reduce the compensation size is to type test the circuit breakers for a higher capacitive current breaking and perform the sizing based on this current as the target value. This results in further saving on the shunt compensation in scenarios like the load-flow A. For instance, the capacitive current in the line circuit breaker before shunt compensating in the load-flow A is reported in Table 3.3. The circuit breaker should be either type tested for interrupting the total capacitive current of the circuit or, if it cannot interrupt the total current, shunt reactors should be sized to decrease the capacitive current down to the interrupting level of the breaker.

Figure 3.7 shows the results of the sensitivity analysis on the circuit breaker capacitive breaking current rating. The minimum required compensation degree is plotted versus the cable length for two rated values, 400 A and 500 A, when operating in the load-flow A. The utilization of a 500 A rated circuit breaker, compared to a 400 A, results in up to 20% saving in the compensation size, which can be a considerable value for long cable lengths.

TABLE 3.3
CAPACITIVE CURRENT FLOWING THROUGH THE LINE CIRCUIT BREAKER BEFORE SHUNT COMPENSATING IN THE LOAD-FLOW A

Cable length (km)	Current (A)
12	484
20	756
40	1437
60	2140
80	2862

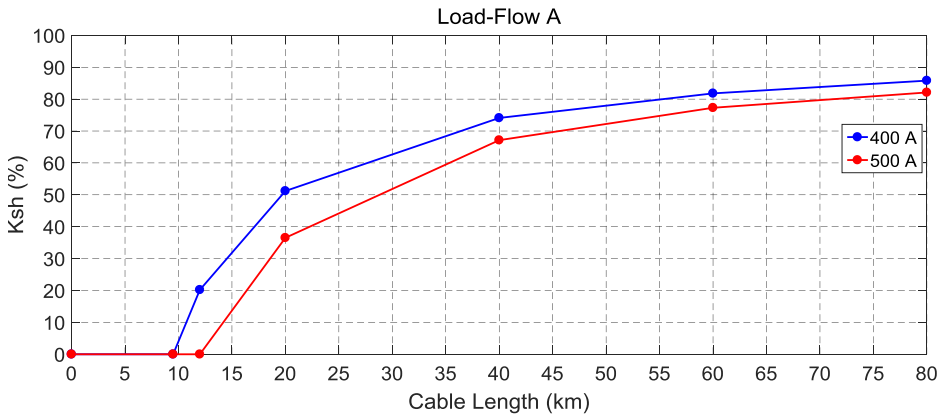


Figure 3.7: Minimum required shunt compensation degree versus the cable length for 400 A and 500 A ratings for the capacitive-breaking current of the line circuit breaker.

3.5.5 DISTRIBUTED COMPENSATION

In addition to the shunt compensation size, the location of shunt compensation impacts the steady-state and transient operations of the system. The line-end compensation was investigated in the previous sections. This type of compensation is easy to be realized in practice and well-known for system operators. There are also less-practiced compensation arrangements in which shunt reactors are distributed along the circuit. As it was previously mentioned in Section 3.4, the realization of these arrangements in practice is certainly more difficult than the line-end compensation due to the higher cost and the need for the construction of more intermediate facilities. However, the distributed compensation requires a smaller compensation size compared to the line-end compensation and it improves the system operation by increasing the active power transfer capacity and better voltage control along the circuit. In addition, the distributed compensation is more reliable in case of failure in one of the reactor banks because the rest of the reactors will remain in operation and only a percentage of the total compensation will be lost.

In this section, the performance of different distributed compensation arrangements is investigated in terms of the required compensation size. Three arrangements, which differ in the number and location of shunt reactors, are compared with the line-end compensation:

1. *Arrangement A3*: in this arrangement, two reactors are connected to the circuit at the sending and receiving ends right behind the line circuit breakers (same as LEC), plus an additional shunt reactor at the fourth OHL-Cable transition point (cable termination) of each circuit. In the case of 80 km cable (fully-cable scenario), since there is no OHL-Cable transition point, the additional reactor is located at the middle of the cable.
2. *Arrangement A6*: this arrangement is called cable-end compensation (CEC). In CEC, six reactors are located at the six OHL-Cable transition points of each circuit (i.e. one reactor per transition point of each circuit). In the case of 80 km cable (fully-cable scenario), reactors are placed at six equally distributed intermediate points along the cable with the distance of 11.43 km from each other.
3. *Arrangement A8*: this arrangement has eight reactors per circuit. It is similar to the arrangement A6, but with two more reactors at the sending and receiving ends of each circuit right behind the line circuit breakers.

Figures 3.8 shows the minimum required shunt compensation degree versus the cable length for different distributed compensation arrangements when both circuits are in operation (double-circuit operation) in the load-flows A and B. The sizes were calculated according to the most decisive sizing criterion, which is the breaker capacitive breaking current in the load-flow A and the voltage along the line in the load-flow B.

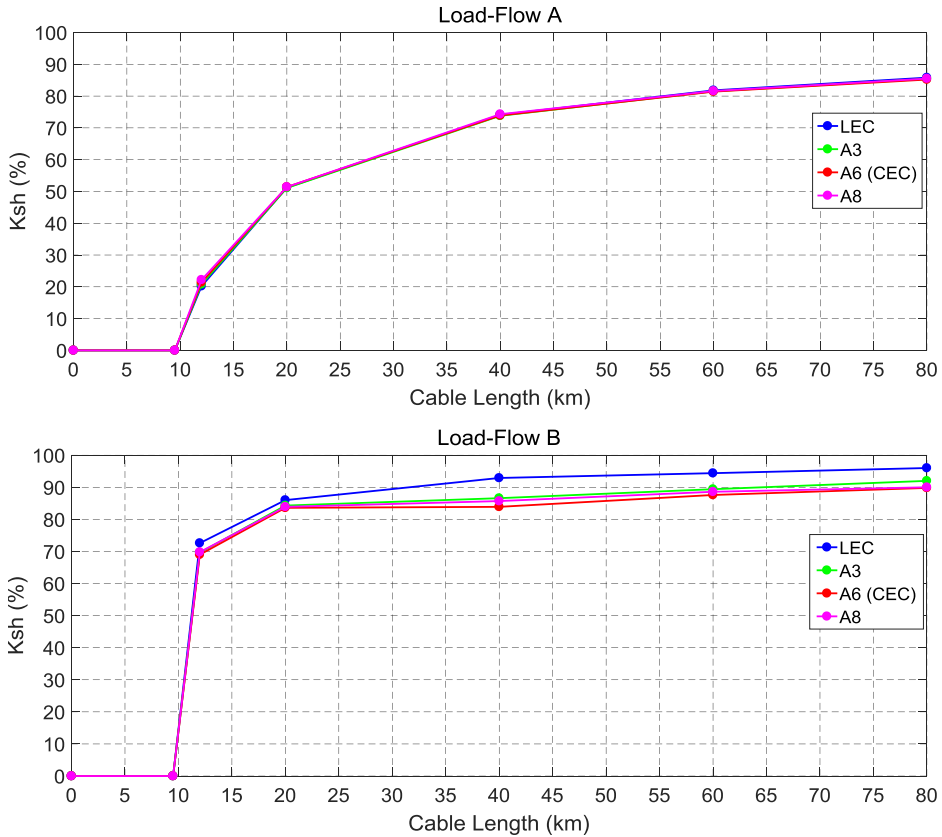


Figure 3.8: Minimum required shunt compensation degree versus the cable length for the double-circuit operation of the Spaak connection in the load-flows A and B with the line-end compensation (LEC) and three distributed compensation arrangements.

For the load-flow A, the application of the distributed compensation can result in up to 1.6% decrease in the minimum required compensation size compared to that of the line-end compensation. In addition, for the load-flow B, the application of the distributed compensation can decrease the minimum required compensation size up to 8.8%. This is due to the fact that the distributed compensation provides a very effective control on overvoltages along the hybrid circuit (especially for circuits with long cables). Such an effective control on the voltage leads to the need for a smaller compensation size compared to the line-end compensation for the cases like the load-flow B in which the voltage is the most decisive sizing criterion. For very long cables, it can be even critical to utilize the distributed compensation to effectively control the voltage and to increase the active power transfer capacity of the cable.

3.5.6 IMPACT OF MIXED-LINE CONFIGURATION

Since the number and the location of cable sections are determined in the planning and design stages of cable projects, it is important to compare various mixed-line configurations (i.e. different number and location of cable sections) from the shunt compensation

perspective. For this purpose, the four mixed-line configurations presented in Section 2.3.1.C (with the section lengths presented in Tables 2.4 to 2.7) and the symmetrical study case configuration (with the section lengths presented in Table 2.3) are compared under the condition that all these configurations are compensated at the line-ends (i.e. LEC) with sizes calculated based on the sizing criteria presented in Section 3.5.1.

The minimum required compensation degree for the five mixed-line configurations versus the cable length is shown in Figure 3.9. For the load-flow A, there is a negligible difference between the configurations, whereas the difference is considerable for the load-flow B as it can be up to 60% in some case. This means hundreds of Mvar difference in the total size of compensation. The difference between configurations is however decreasing by increasing the cable length in the circuit as it was predictable due to the decreasing dissimilarity between the configurations.

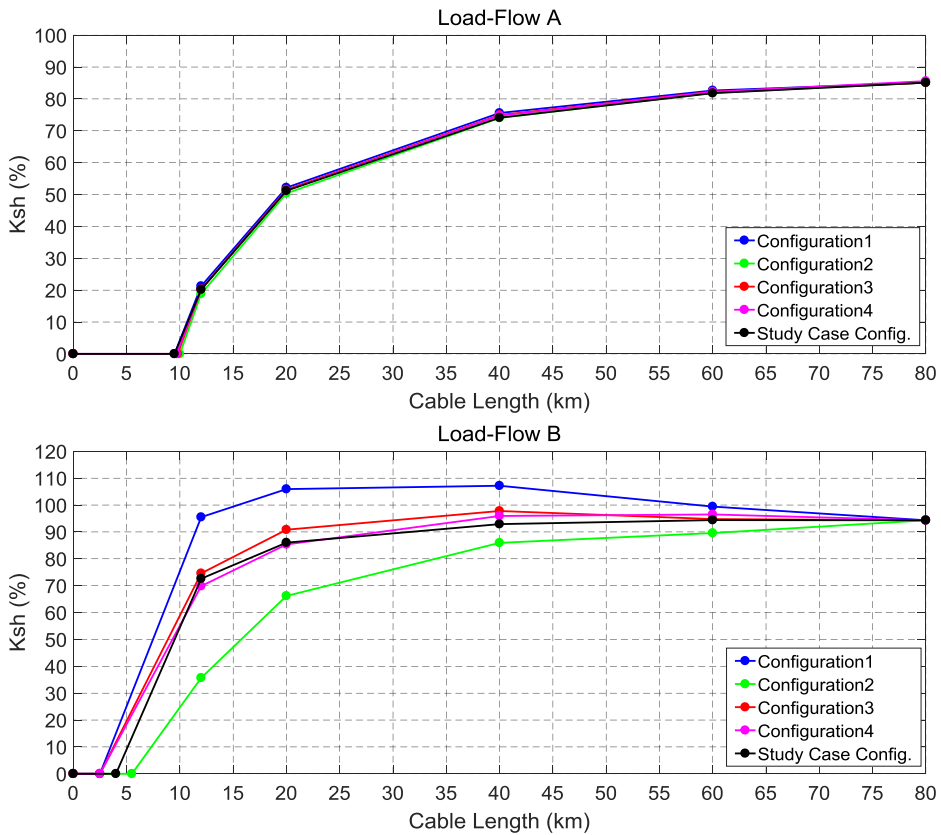


Figure 3.9: Minimum required shunt compensation degree versus the cable length for different mixed-line configurations for the double-circuit operation of the Spaak connection in the load-flows A and B.

Moreover, as shown for the load-flow B, Configuration 1 requires the highest compensation degree (even overcompensation for cable lengths between 15 km and 60 km), whereas Configuration 2 requires the lowest compensation degree. These two configurations will obviously represent an opposite behaviour when the circuit is being energized from the other end (i.e. the Dodewaard substation). Thus, it can be concluded that the location of the cable sections with respect to the substation from which the circuit is being energized can significantly affect the overvoltages on the circuit and consequently the required compensation size. This point should be always taken into account in determination of the switching sequence for the energization of cable circuits.

3.6 CABLE OVERLOADING

In addition to determination of the optimal size and location of shunt reactors, it is necessary to investigate the power flow and cable loadings when the hybrid OHL-Cable circuit is under operation. The power transferred through a hybrid circuit increases by increasing the cable length due to the decrease of the total series impedance of the circuit. It can be expected that the cable rated power be exceeded for cables longer than a particular length depending on the grid topology and the load-flow scenario [1], [13].

To investigate this issue for the Spaak connection, it is assumed that the circuits are compensated with the sizes reported in Table 3.2 and the currents at both ends of each cable section, as shown in Figure 3.10, are observed during the single-circuit and double-circuit operations. For the case of 80 km cable (fully-cable scenario), since there is only one cable section, the currents are measured at the sending terminal, the receiving terminal, and four points along the circuit with the distances of 11.43 km, 34.29 km, 45.72 km, and 68.57 km from the sending terminal.

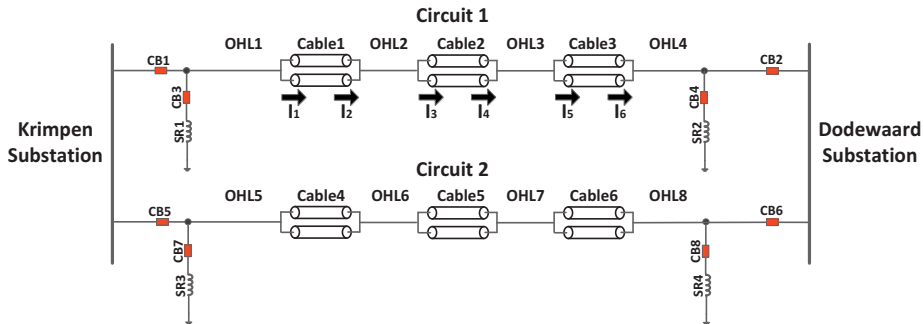


Figure 3.10: Investigated cable currents shown on the single-line diagram of the Spaak connection.

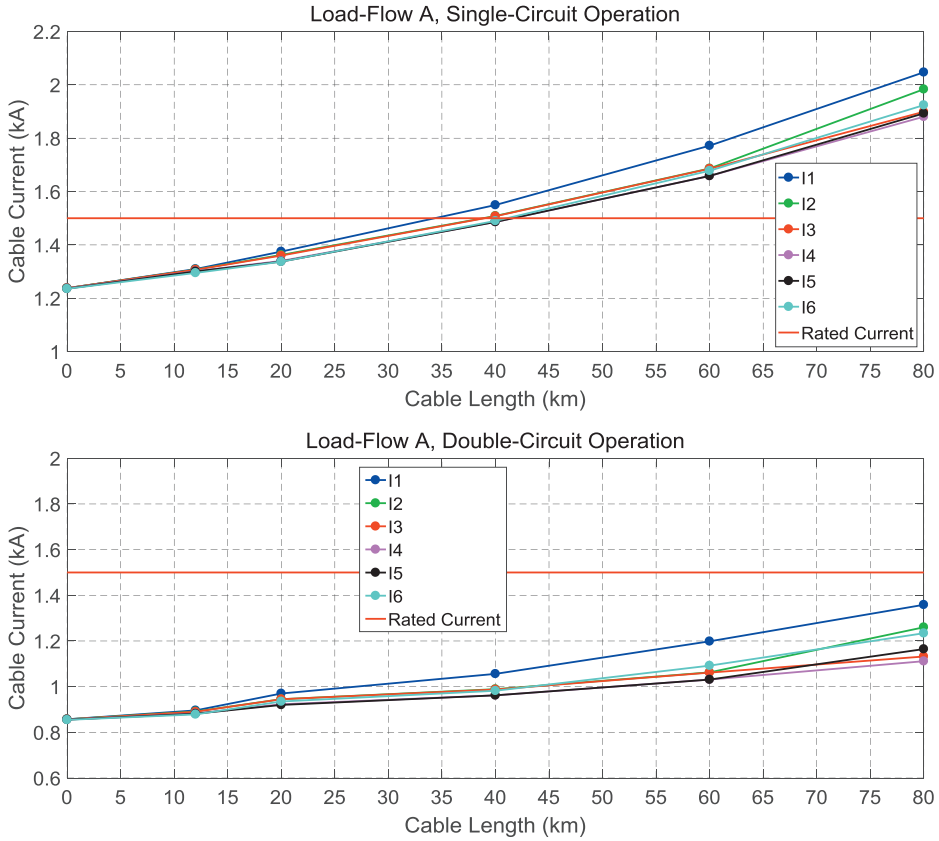


Figure 3.11: Cable currents versus the cable length for the single-circuit and double-circuit operations of the Spaak connection in the load-flow A.

Figure 3.11 shows the cable currents for different cable lengths during the single-circuit and double-circuit operations of the Spaak connection in the load-flow A. The cable currents are exceeding the rated current when the circuit is operated with a single circuit and the cable length is longer than approximately 37 km, whereas the loading in the double-circuit operation is below the rating for all the cable lengths. This means that in the double-circuit operation when one of the circuits is switched out of service, special attention should be paid to the loading of the remained connected circuit (i.e. the n-1 criterion should be checked). The control of power flow can be realized by using series reactors, phase shifting transformers or changing the dispatch scenario.

Figure 3.12 depicts the injected active power to the circuit at the sending terminal. It can be seen that the injected active power increases for longer cables as the result of the lower series impedance of the cable compared to that of OHL.

Figure 3.13 shows the cable currents versus the cable length for the single-circuit and double-circuit operations of the Spaak connection in the load-flow B. Unlike the load-flow A, the cable currents are always lower than the rated current. The injected active

power at the sending terminal is depicted in Figure 3.14, where the trend of changes in the active power flow is similar to that of the load-flow A.

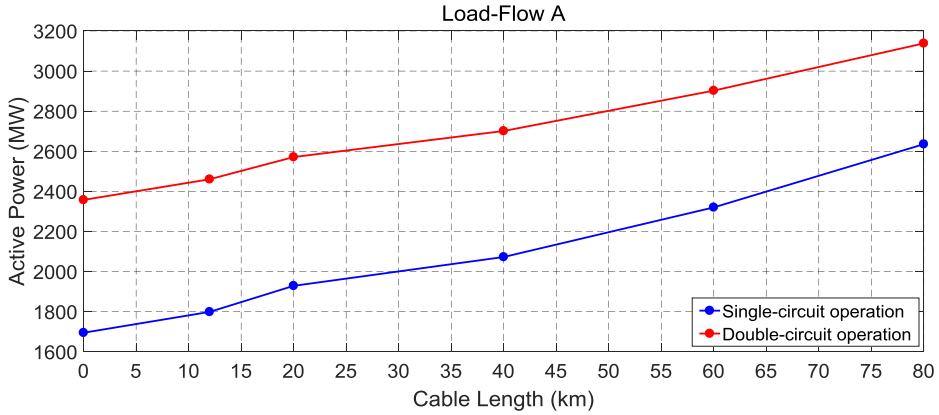


Figure 3.12: Injected active power at the sending terminal versus the cable length for the single-circuit and double-circuit operations of the Spaak connection in the load-flow A.

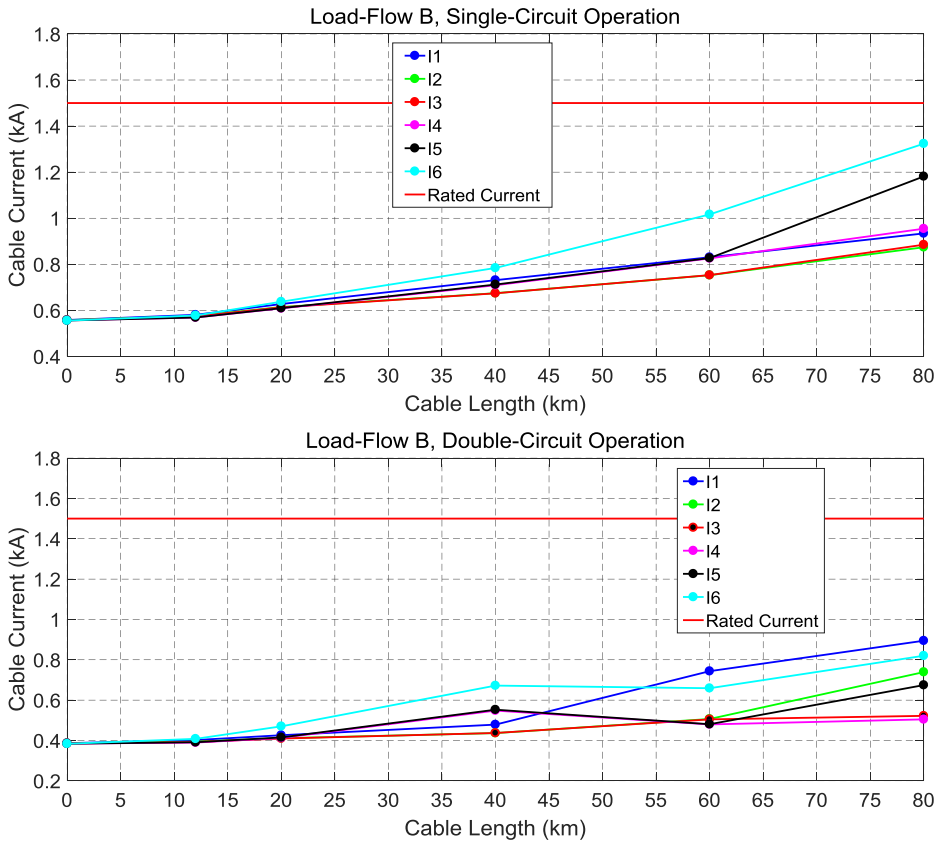


Figure 3.13: Cable currents versus the cable length for the single-circuit and double-circuit operations of the Spaak connection in the load-flow B.

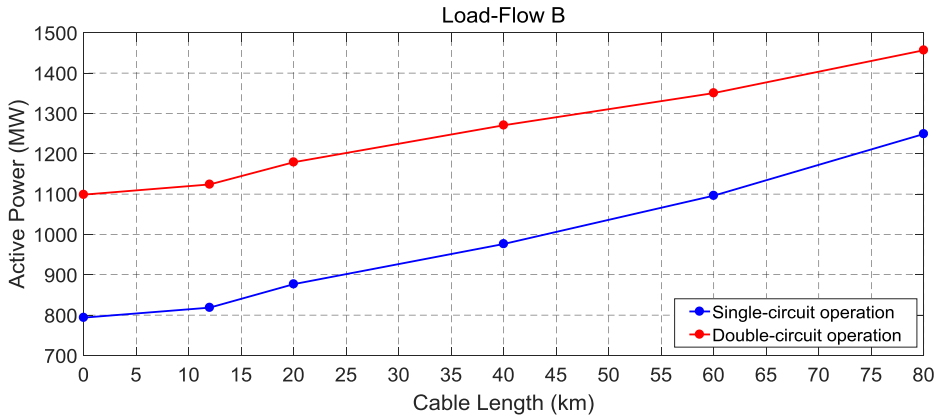


Figure 3.14: Injected active power at the sending terminal versus the cable length for the single-circuit and double-circuit operations of the Spaak connection in the load-flow B.

3.7 CONCLUSIONS

This chapter addressed the most important issues related to the steady-state operation and shunt compensation of hybrid OHL-Cable circuits. The study was carried out for different cases and involved sensitivity analysis on the influence of various parameters on the steady-state operation of power systems with long EHV cables.

Various system operation problems are associated with the reactive power of long cables, which should be handled by optimal reactive power shunt compensation. According to the simulation results, it is crucial to investigate the influence of different load-flow scenarios on the allocation of shunt reactors. The results can considerably vary from one load-flow scenario to another. In fact, the short-circuit power and voltage levels prior to the cable energization significantly affect the size of shunt compensation. Moreover, the most decisive sizing criterion is dependent on the load-flow scenario, cable length, and shunt reactors location. For a robust network like the Dutch transmission system, the most decisive sizing criterion is very likely either the capacitive breaking current of line circuit breakers or the voltage along the line during the no-load energization.

The minimum required compensation size and degree increases by increasing the cable length. For the Spaak connection, a distributed compensation can decrease the minimum required size of compensation up to 8.8% compared to the traditional type of compensation at line-ends. This is due to the fact that the distributed compensation provides a very effective voltage control along the circuit (especially in circuits with long cables), which leads to the need for a smaller compensation size. Another advantage of the distribution compensation is the increase of the cable active power transfer capacity, which is needed for very long cables when the cable has almost reached its critical length. In addition, the distributed compensation is more reliable in case of failure in one of the reactor banks because the rest of the reactors will remain in operation. Finally, the number and location of cable sections can influence the minimum required compensation degree considerably, especially when the voltage profile is high.

It is necessary to pay a special attention to the power loading of long cables. The cable overloading can occur due to the fact that the series impedance of a cable is lower than that of an equivalent OHL. According to the simulation results, the transferred active power through the hybrid circuit increases when the length of the cable increases. The location of shunt reactors (line-end or distributed) does not affect the active power flow through the circuit but it can decrease the overloading by reducing and optimizing the flow of the reactive power through the circuit.

Finally, from the steady-state operation perspective, there is no limit for the maximum cable length when sufficient reactive power compensation at optimal locations is installed. However, this can be a downside for the application of very long cables due to the need for a very large compensation and a big land use. The risk of cable overloading needs a special attention, where it can be solved by countermeasures like the use of phase shifting transformers or series reactors. The grid reinforcement by increasing the number of cables per phase or the number of parallel circuits could be also a solution. In addition, HVDC underground cables may be more robust options when the cable is very long. However, the technical possibilities of using HVDC cables should be investigated by dedicated thorough studies.

REFERENCES

- [1] CIGRE Working Group C4.502, "Power system technical performance issues related to the application of long HVAC cables," *CIGRE Technical Brochure no. 556*, October 2013.
- [2] H. Khalilnezhad, M. Popov, L. van der Sluis, J. A. Bos, J. P. W. de Jong and A. Ametani, "Countermeasures of zero-missing phenomenon in (E)HV Cable Systems," *IEEE Transactions on Power Delivery*, vol. 33, no. 4, pp. 1657-1667, 2017.
- [3] J. J. Grainger and W. D. Stevenson Jr., *Power System Analysis*, Singapore: McGraw-Hill, 1994.
- [4] F. M. Gatta, A. Geri, S. Lauria and M. Maccioni, "Steady-state operation conditions of very long EHVAC cable lines," *Electric Power Systems Research*, vol. 81, pp. 1525-1533, 2011.
- [5] H. Khalilnezhad, M. Popov, J. A. Bos and K. P. J. Jansen, "Influence of partial undergrounding on the transient stability of EHV power transmission systems," *Electric Power Systems Research*, vol. 131, pp. 126-138, 2016.
- [6] R. Smeets, L. van der Sluis, M. Kapetanovic, D. Peelo and A. Janssen, *Switching in Electrical Transmission and Distribution Systems*, Hoboken, NJ, USA: Wiley, 2015.
- [7] H. Khalilnezhad, S. Chen, M. Popov, J. A. Bos, J. P. W. de Jong and L. van der Sluis, "Shunt compensation design of EHV double-circuit mixed OHL-cable connections," in *IET International Conference on Resilience of Transmission and Distribution Networks*, Birmingham, U.K., 2015.
- [8] A. Ametani, T. Ohno and N. Nagaoka, *Cable System Transients: Theory, Modeling and Simulation*, Singapore: Wiley, July 2015.
- [9] L. Colla, F. M. Gatta, A. Geri, S. Lauria and M. Maccioni, "Steady-state operation of very long EHV AC cable lines," in *IEEE Power Technology Conference*, Bucharest, Romania, June-July 2009.

- [10] F. M. Gatta and S. Lauria, "Very long EHV cables and mixed overhead-cable lines. Steady-state operation," in *IEEE Power Technology Conference*, St. Petersburg, Russia, June 2005.
- [11] L. Colla, F. M. Gatta, F. Iliceto and S. Lauria, "Design and operation of EHV transmission lines including long insulated cable and overhead section," in *IEEE Power Engineering Conference*, November-December 2005.
- [12] J. J. Dougherty and C. S. Schifreen, "Long cable lines-Alternating Current with reactor compensation or direct current," *Transactions of the American Institute of Electrical Engineers. Part III: Power Apparatus and Systems*, vol. 81, no. 3, pp. 169-178, April 1962.
- [13] F. M. Gatta, A. Geri, S. Lauria and M. Maccioni, "Steady-state operation conditions of very long EHVAC cable lines: Two case studies," *Electric Power Systems Research*, vol. 83, pp. 160-169, 2012.
- [14] S. Lauria, F. M. Gatta and L. Colla, "Shunt compensation of EHV cables and mixed overhead-cable lines," in *IEEE Power Technology Conference*, Lausanne, Switzerland, July 2007.
- [15] "Electromagnetic Compatibility (EMC)-Part 4-30: Testing and Measurement Techniques-Power Quality Measurement Methods," IEC 61000-4-30, 2014.
- [16] "High-voltage Switchgear and Controlgear-Part 100: Alternating-Current Circuit-Breakers," IEC 62271-100, 2008.

CHAPTER 4

RESONANCE BEHAVIOUR OF HYBRID OHL-CABLE SYSTEMS

4.1 INTRODUCTION

The application of long EHV cables in existing transmission systems raises serious concerns regarding the risk of low-order resonance frequencies. The large cable capacitance together with the inductance of inductive components, like transformers and shunt reactors, may result in series and parallel resonance circuits leading to temporary overvoltages when excited. Resonance frequencies in systems with long cables can be considerably lower than those in systems without cables, especially during the periods of low short-circuit power. As a result, low resonance frequencies are considered among the most limiting factors for the large-scale application of cables in transmission systems.

This chapter investigates the impact of the Spaak connection on the resonance behaviour of the Dutch transmission system by performing the frequency-scan analysis in the PSCAD model of the grid, as described in Chapter 2. The analysis is carried out for the six cable scenarios (introduced in Chapter 2) with sensitivity analyses on the influence of the shunt compensation size, shunt compensation location, and mixed-line configuration on the resonance behaviour of the grid. The simulation results are analysed and compared based on two defined criteria: the order of first resonance frequency and the number of resonance frequencies.

This chapter is structured as follows: Section 4.2 provides a brief introduction on the resonance theory in electrical circuits. Section 4.3 describes the typical grid topologies that can lead to resonance in transmission cable systems. Afterwards, the frequency-scan results are presented and analysed in Section 4.4, where the parameter selection and the evaluation criteria used for the study are elaborated too. Finally, the conclusions are provided in Section 4.5.

4.2 RESONANCE IN ELECTRICAL CIRCUITS

Resonance is a phenomenon in electrical circuits consisting of both capacitors and inductors during which the energy stored in the electric field, i.e. in capacitors, is periodically transformed into the energy stored in the magnetic field, i.e. in inductors, and vice versa. In other words, when a resonance occurs in an electrical system, the electromagnetic energy periodically oscillates between capacitors and inductors.

Resonance in electrical circuits has two types: series and parallel. This can be simply explained by simple series and parallel RLC circuits shown in Figure 4.1. The total impedance of the circuits is:

$$Z_{series} = R + j\left(\omega L - \frac{1}{\omega C}\right) \quad (4.1)$$

$$Z_{parallel} = \frac{R}{1 + jR\left(\omega C - \frac{1}{\omega L}\right)} \quad (4.2)$$

The condition for resonance occurrence is that the stored electric and magnetic energies be equal. This condition is satisfied when the capacitive reactance equals the inductive reactance ($X_C = -X_L$), which only happens when the driving frequency is:

$$f_n = \frac{1}{2\pi\sqrt{LC}} \quad (4.3)$$

This frequency is called natural frequency or resonance frequency. When a series or parallel resonance circuit is fed by respectively a voltage or current source with a frequency equal to its natural frequency, the capacitive and inductive elements of the circuit are cancelling out each other; thus, the imaginary part of Z become zero and the total impedance of the circuit becomes a pure resistance.

In reality, electrical circuits are not as simple as shown in Figure 4.1 forming a perfect series or parallel resonance circuit. Usually circuits are more complex and involve mixed parallel and series combinations of inductors and capacitors. These circuits are known as series-parallel resonance circuits and have the ability to resonance in the series mode or the parallel mode depending on the type and frequency of the excitation.

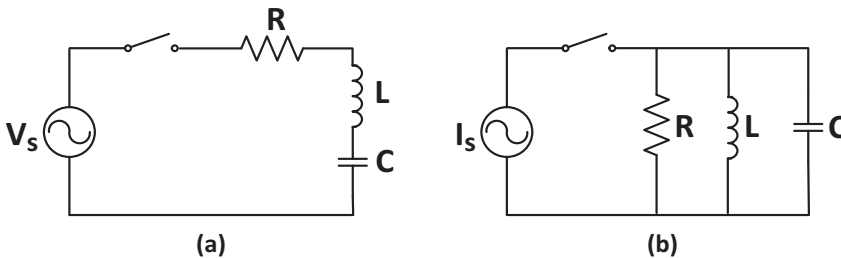


Figure 4.1: Series (a) and parallel (b) resonance circuits.

The magnitude and the phase of the driving impedance of an example series-parallel resonance circuit are shown in Figure 4.2, where they are plotted versus the frequency [1]. When the series-parallel resonance circuit is fed by an alternative voltage source, the series resonance circuit gets excited. In this case, at low frequencies the total circuit impedance given by equation 4.1 is dominated by the reactance of the capacitor and the phase angle approaches -90° (since the current is leading the voltage). This can be seen in Figure 4.2. As the frequency increases, the reactance of the inductor becomes larger so that it becomes equal to the capacitive reactance at the resonance frequency given by equation 4.3. In this situation (series resonance), the circuit series impedance is purely resistive with phase angle equal zero and the voltages across the inductor and capacitor reach high values (called resonance overvoltages) with opposing phase angles. For frequencies above the resonance frequency, the inductive reactance dominates the circuit characteristics and the phase angle approaches $+90^\circ$ (since the current is lagging the voltage).

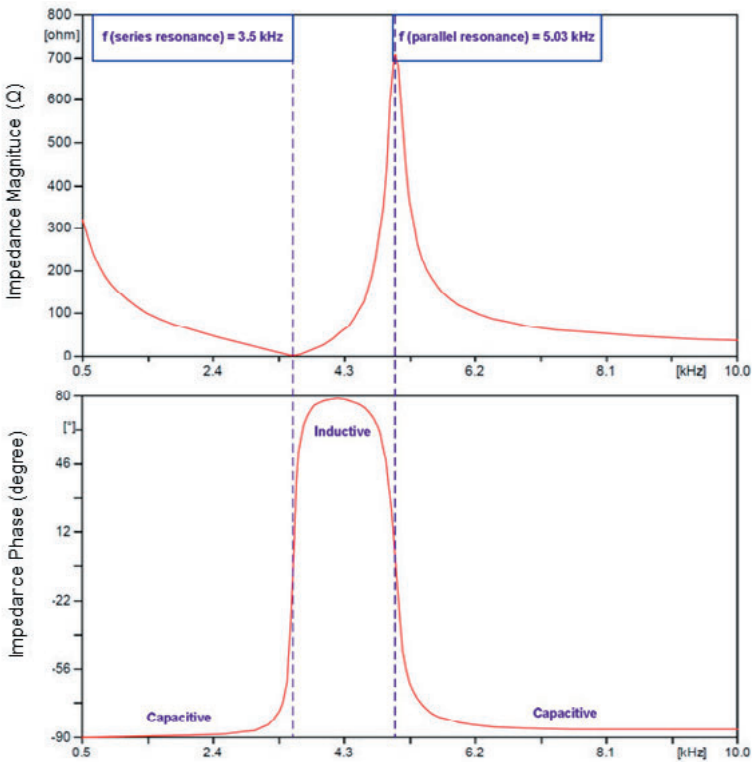


Figure 4.2: The magnitude and the angle of the driving impedance of a series-parallel resonance circuit as a function of frequency [1].

In series resonance circuits, the circuit impedance is minimum at the resonance frequency, while it is larger at lower and higher frequencies. The small impedance at the resonance frequency (dip in the plot) is the indication of a series resonance. The resistor R damps the oscillations and acts as a current limiter in the circuit, where the current can only reach up to $I_s = \frac{V_s}{R}$. Without the resistor, the lossless circuit is an ideal (undamped) series resonance circuit, where the voltages and currents increase without any restriction and reach infinity in theory.

When the series-parallel resonance circuit is fed by an alternative current source, the parallel resonance circuit gets excited. In this case, at low frequencies the total impedance given by equation 4.2 is dominated by the inductive reactance and the phase angle approaches $+90^\circ$. As the frequency increases, the reactance of the capacitor becomes larger until it becomes equal to the inductive reactance at the resonance frequency given by equation 4.3. In this case, as shown in Figure 4.2, the impedance is purely resistive with phase angle equal zero. The currents in the inductor and capacitor branches reach high values (and produce high overvoltages) with opposing phase angles during the parallel resonance. As the frequency increases above the resonance frequency, the capacitive reactance dominates the circuit characteristic and the phase angle approaches -90° .

In parallel resonance circuits, the circuit impedance is maximum at the resonance frequency, while it is smaller at lower and higher frequencies. The high impedance at the resonance frequency (peak in the plot) is the indication of a parallel resonance. The resistor R damps the oscillations and acts as a voltage limiter, where the voltage can only reach up to $V_p = I_p R$. Without the resistor, the parallel resonance circuit is undamped and voltage and currents can theoretically reach infinity.

4.3 TYPICAL GRID TOPOLOGIES LEADING TO RESONANCE IN CABLE SYSTEMS

Generally, actual power systems are much more complex than simple RLC circuits as they consist of numerous capacitors and inductors that form various paths for energy exchange between them. In other words, different paths lead to various series and parallel resonance circuits with several resonance frequencies.

Resonance overvoltages are categorized as temporary overvoltages (TOVs), as it was explained in Section 1.4 of Chapter 1 too. In power systems with long cables, the resonance frequencies are low because of the large cable capacitance. On the other hand, the system resistance is frequency dependent and will be smaller at the low-order resonance frequencies. As a result, the resulting TOVs are weakly damped and last long when the resonance occurs in a cable system. This sustained nature of resonance TOVs in cable systems can impose a high-risk situation for system equipment, where surge arresters are one of the most vulnerable components as their withstand voltages and energy absorption capabilities can be exceeded by severe TOVs.

The voltages and currents that excite the resonance circuits in an actual power system can be originated from switching actions or short-circuits in the system (damped oscillations) and/or from the existing background harmonic sources (driven oscillation) [2], [3]. In the latter case, the existing background harmonics produced by sources like frequency controllers of motors, HVDC connections, and converters can be amplified due to the resonance. The background harmonic amplification can cause power quality issues and is unequal among the three phases when the cable system is electrically asymmetrical [4].

In the following sections, some of the most common topologies in transmission cable systems that can result in resonance are described.

4.3.1 SERIES RESONANCE TOPOLOGIES

An example of a series resonance circuit in an actual power transmission system is shown in Figure 4.3, where the cable capacitance and the transformer leakage inductance form a series resonance circuit [5], [6]. When the parallel transmission line is energized, the generated transient overvoltage wave due to the energization propagates into the series resonance circuit as well as to the surrounding grid. If the part of the wave that travels into the series resonance circuit contains the natural frequency (f_n) of the circuit, the circuit gets excited and produces resonance overvoltages at the secondary side of the transformer.

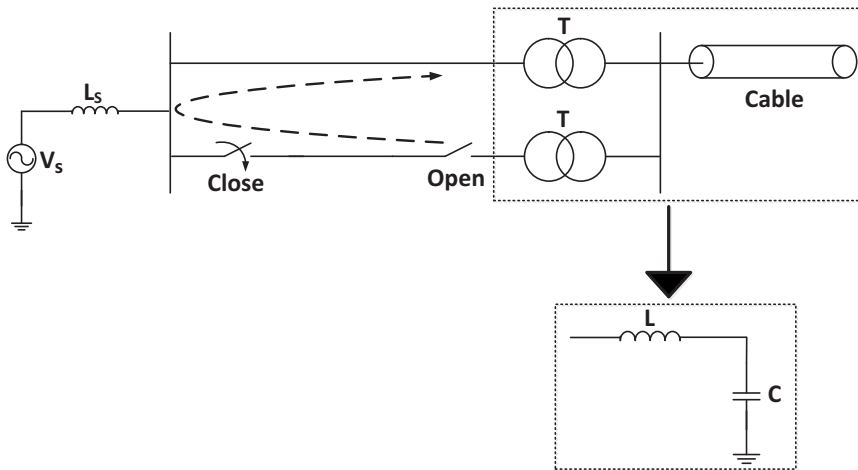


Figure 4.3: Series resonance circuit created by the transformer and cable, excited when the parallel transmission line is being energized (T: transformer) [5].

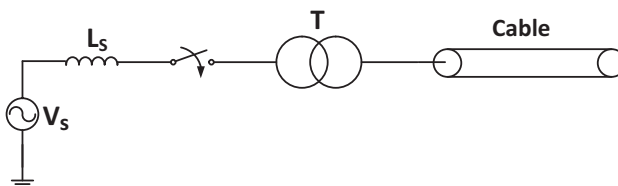


Figure 4.4: Series resonance circuit created by the transformer and cable, excited when they are energized together (T: transformer).

To determine the possibility and the severity of the series resonance occurrence, two parameters should be identified: (1) the natural frequency of the series resonance circuit, (2) the dominant frequencies contained in the transient energization overvoltage. The dominant frequencies of the transient overvoltage could be very low when the transmission line being energized is a long cable (depending on the source impedance and the cable length). Low-frequency overvoltages can travel over long distances due to the weak damping of the grid in low frequencies and therefore cause resonance overvoltages at distant locations [5], [7].

Another series resonance circuit in power systems is created when a transformer is in a series connection with a cable and they are energized together by a voltage source, as shown in Figure 4.4. This situation is not common in meshed grids as it is very unlikely to energize the cable and transformer together. However, it can occur in offshore grids where transformers and subsea cables may be energized together.

4.3.2 PARALLEL RESONANCE TOPOLOGIES

Parallel resonance circuits can be created in various ways in an actual power system and can be excited by a harmonic current. Harmonic currents are generated by the cable energization, transformer energization, power electronics, HVDC links, etc. One of the most common cases is a parallel resonance circuit excited by the inrush current of a transformer being energized. The transformer energization inrush current has high contents of harmonic frequencies, which are low order, low damped, and with a long duration [2], [5].

An example case of a parallel resonance circuit is shown in Figure 4.5a, where a transformer is energized through a cable. The cable reactive power is compensated by a shunt reactor. When the transformer is being energized, harmonic currents contained in the inrush current flow through the parallel resonance circuit, composed of the cable capacitance (C), the shunt reactor inductance (L_s), and the equivalent source inductance (L_0). This is illustrated by the harmonic equivalent circuit depicted in Figure 4.5b, in which a harmonic current source is used to express the transformer inrush current. Therefore, the voltage source is removed since it only generates the fundamental frequency voltage.

The natural frequency of the parallel resonance circuit in Figure 4.5b can be expressed as:

$$f_n = \frac{1}{2\pi} \sqrt{\frac{1}{L_s C} + \frac{1}{L_0 C}} \quad (4.4)$$

The most dominant harmonic content in a transformer inrush current is the second order harmonic (100 Hz in 50 Hz systems), which has a higher proportion compared to the other harmonic contents. The natural resonance frequency of the circuit is 50 Hz when the degree of the reactive power compensation is 100%, ignoring the equivalent source inductance (L_0). To obtain a circuit with natural resonance frequency of 100 Hz, the equivalent source impedance should be $L_0 = \frac{L_s}{3}$ [5]. However, during normal operating conditions, the equivalent source impedance is usually much smaller than $\frac{L_s}{3}$ since the typical meshed power

grids are strong. Thus, the natural frequency of 100 Hz can occur in weak networks such as in the black start operations. Severe parallel resonance overvoltages are expected in this situation since the load level is generally low in weak networks. Therefore, this type of parallel resonance can be mainly expected in weak grids [5], [8].

Another example of the parallel resonance in cable systems is the resonance during the fault clearing and system islanding, when one end of a long cable is open and a part of the grid together with the long cable is separated from the rest of the grid. However, system islanding is unlikely in today's interconnected meshed grids, but it can be expected in connections to offshore wind farms. More information regarding resonance overvoltages caused by system islanding can be found in [5], [9], [10].

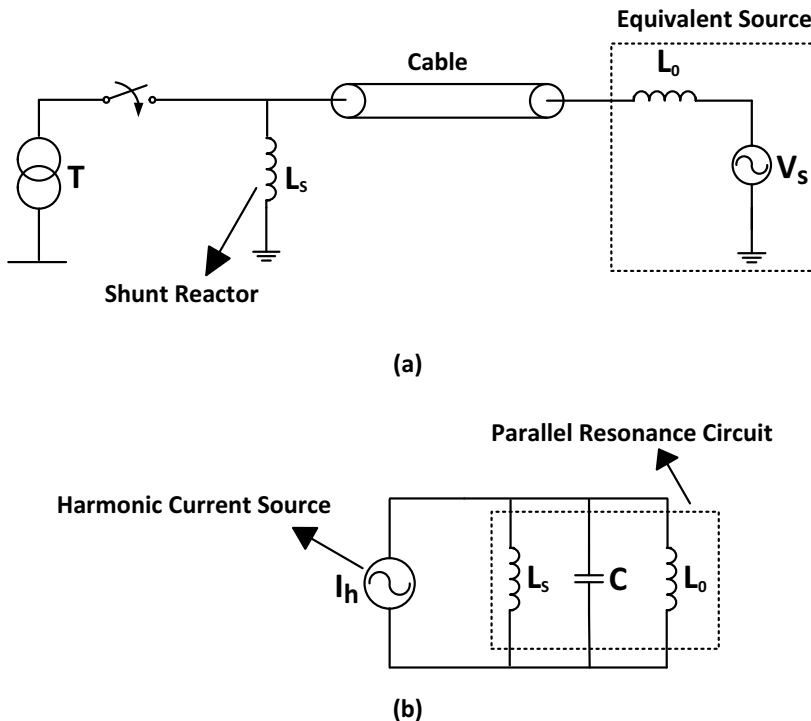


Figure 4.5: Parallel resonance circuit created by the cable and shunt reactor. The resonance circuit is excited by the transformer inrush current.

4.4 RESONANCE BEHAVIOUR OF THE DUTCH 380 kV GRID WITH THE SPAAK CONNECTION

It is of importance to investigate how the resonance behaviour of a grid would change when a long cable connection is realized in the grid. This includes determination of the resonance points, resonance frequencies, and their series or parallel nature by means of the frequency-scan analysis (sometimes called sweep frequency response analysis) of the grid.

In a frequency-scan analysis, one per-unit current with the frequency of interest is injected at a point of interest and afterwards the resulting response voltage is calculated. This voltage is equal to the per-unit impedance in the frequency domain seen from the point of interest. The scan is performed over a range of frequencies and it leads to identify resonance frequencies, sensitive locations, and the impact of different system parameters on the resonance frequencies.

In cable systems, the first resonance frequency at the point of interest can be estimated by equation 4.3, where L and C can be substituted by the following simplified equations:

$$L = \frac{V^2}{2\pi f_0 S_{system}} \quad (4.5)$$

$$C = \frac{S_{cable}}{2\pi f_0 V^2} \quad (4.6)$$

where, V is the system voltage, f_0 is the system power frequency, S_{system} is the system short-circuit power at the point of interest including the shunt compensation power, and S_{cable} is the cable reactive power. By using equations 4.5 and 4.6 in equation 4.3, equation 4.7 can be derived to estimate the first resonance frequency at the point of interest:

$$f_1 = f_0 \sqrt{\frac{S_{system}}{S_{cable}}} \quad (4.7)$$

where, f_1 is the first resonance frequency. It can be deduced from this equation that the first resonance frequency is directly proportional to the short-circuit power of the grid at the point of interest. In other words, the first resonance frequency decreases when the grid becomes weaker and vice versa [11].

In the following sections, the frequency response of the Dutch 380 kV grid is evaluated to determine the impact of long cables in the Spaak connection on the resonance frequencies of the grid. Moreover, the influence of the shunt compensation size, shunt compensation location, and mixed-line configuration on the frequency scan of the grid is investigated too.

4.4.1 PARAMETER SELECTION

The frequency scan was performed in the frequency range of 1 Hz to 2.5 kHz for the positive sequence impedance. In this research, resonance frequencies below 2.5 kHz (50th harmonic in a 50 Hz system) are of interest as the dominant harmonic frequencies are within this range. All simulations were carried out when both circuits of the Spaak connection were in operation. The mixed-line configuration is as shown in Figure 2.3 with the cable scenarios defined in Table 2.2. Shunt compensation sizes are according to the values reported in Table 3.2, which were determined by the steady-state analysis presented in Chapter 3.

4.4.2 EVALUATION CRITERIA

A set of criteria is needed to evaluate the frequency-scans of different cases with and without cables and with different system parameters. Two criteria are used here with respect to the applied analysis approaches in literature [7], [11-14]:

1. *Order of the first resonance frequency*: this is the most important criterion for the analysis of the frequency scan results. The system is more vulnerable when the first resonance frequency is low as the harmonic emissions in transmission systems are mainly at the low-order harmonic frequency range. In addition, the resulting resonance TOVs are larger and lower damped when the resonance frequency is lower.
2. *Number of resonance frequencies below 2.5 kHz*: this criterion is proposed in this research since it is very crucial to check the number of resonance frequencies in an interested frequency range. The interested frequency range for the analysis should cover the low-order harmonic frequencies since the dominant harmonic frequency emissions at transmission levels are mainly low in order. This criterion shows how the potential risk of the resonance can increase in the system when cables are installed.

4.4.3 IMPACT OF THE SPAAK CONNECTION

The frequency scan was carried out at four substations: Krimpen, Dodewaard, Maasvlakte, and Eemshaven (see Figures 2.1 and 2.2) with short-circuit powers of about 30, 20, 28, and 11 GVA in the selected snapshot, respectively. One scenario in addition to the six cable scenarios presented in Table 2.2 is the grid without the Spaak connection. The comparison of this scenario with the other scenarios reveals the influence of realizing this project as well as the influence of the increasing cable length on the frequency response of the grid.

Figure 4.6 shows the frequency scan results when the grid is scanned from the Krimpen substation for three scenarios: without the Spaak connection, with the fully-OHL Spaak connection, and with the fully-cable Spaak connection (with LEC). The magnitude and the phase of the driven impedance are plotted versus frequency. As it was previously explained, at the resonance frequencies the phase angle becomes zero (i.e. imaginary part of the impedance is zero). It can be noticed in this figure that one of the substantial influences of the increasing cable length is the decrease of the first resonance frequency and a considerable increase in the number of resonance frequencies. The first resonance frequency is 125 Hz (close to the second harmonic frequency) when the Spaak connection is realized only with cables, while it is 158 Hz without the Spaak connection and 161 Hz with the fully-OHL Spaak connection. The low first resonance frequency of the grid without the Spaak connection is because of the cables in the Randstad South-Ring and North-Ring connections, which are nearby of the Krimpen substation.

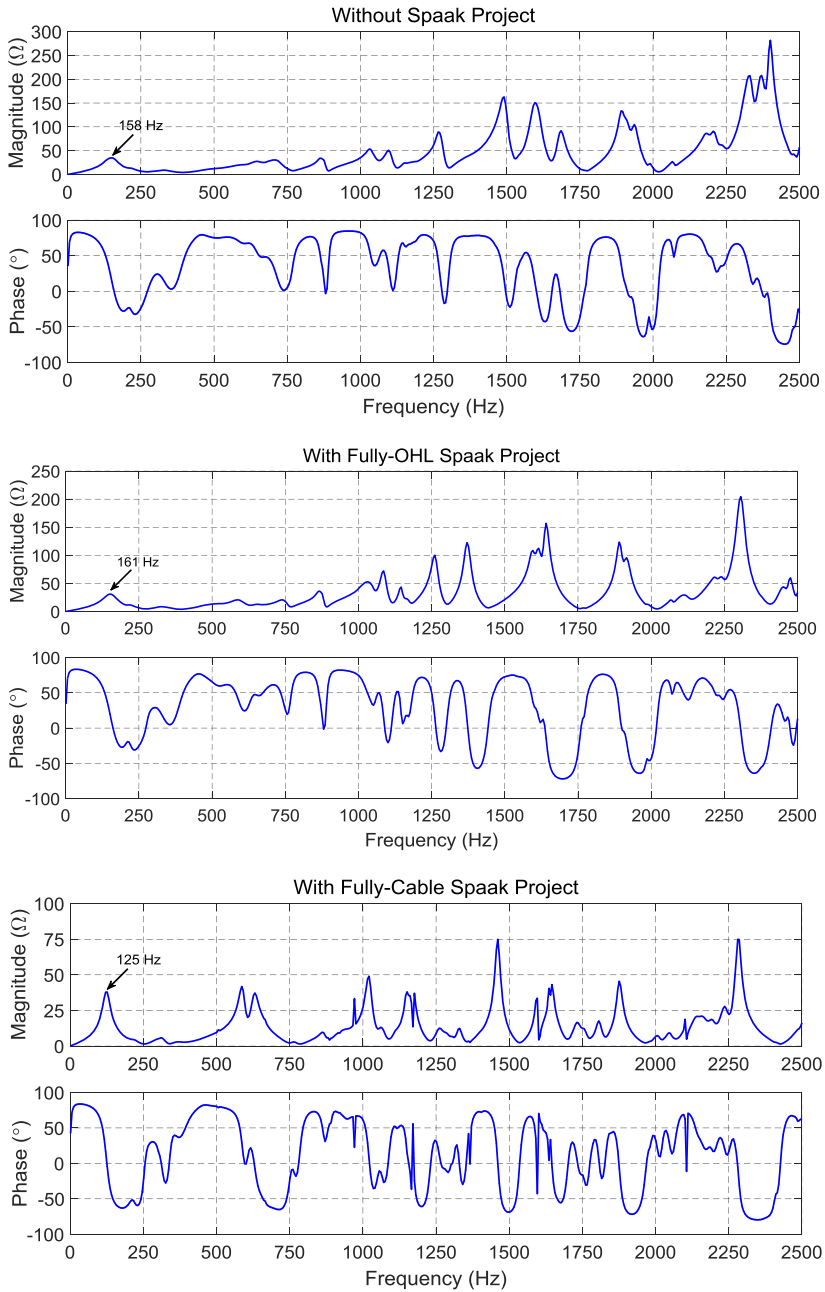


Figure 4.6: Frequency scan of the Dutch 380 kV grid from the Krimpen substation without the Spaak connection, with the fully-OHL Spaak connection, and with the fully-cable Spaak connection.

A detailed analysis of the frequency scan results for all the cable scenarios is depicted in Figure 4.7, where the first resonance frequency and the number of resonance frequencies seen from the four substations are plotted for the six cable scenarios.

It can be seen that the first resonance frequency decreases with the increasing cable length in the circuit. This decrease was expected since, according to Table 3.2, the percentual increase of the compensation degree is less than the total percentual increase of the cable length, which results in a lower first resonance frequency according to equation 4.7. In the worst case, the first resonance frequency has decreased to 125 Hz, which is for the fully-cable scenario scanned from the Krimpen substation. Moreover, compared to the other substations, the first resonance frequency seen from the Eemshaven substation is almost unchanged when the cable length is increased from 15% to 100%. This is because of the relatively far distance of the Spaak connection from the Eemshaven substation. Finally, the number of resonance frequencies below 2.5 KHz show a strong dependency on the cable length and the point of interest (the substation at which the scan is performed).

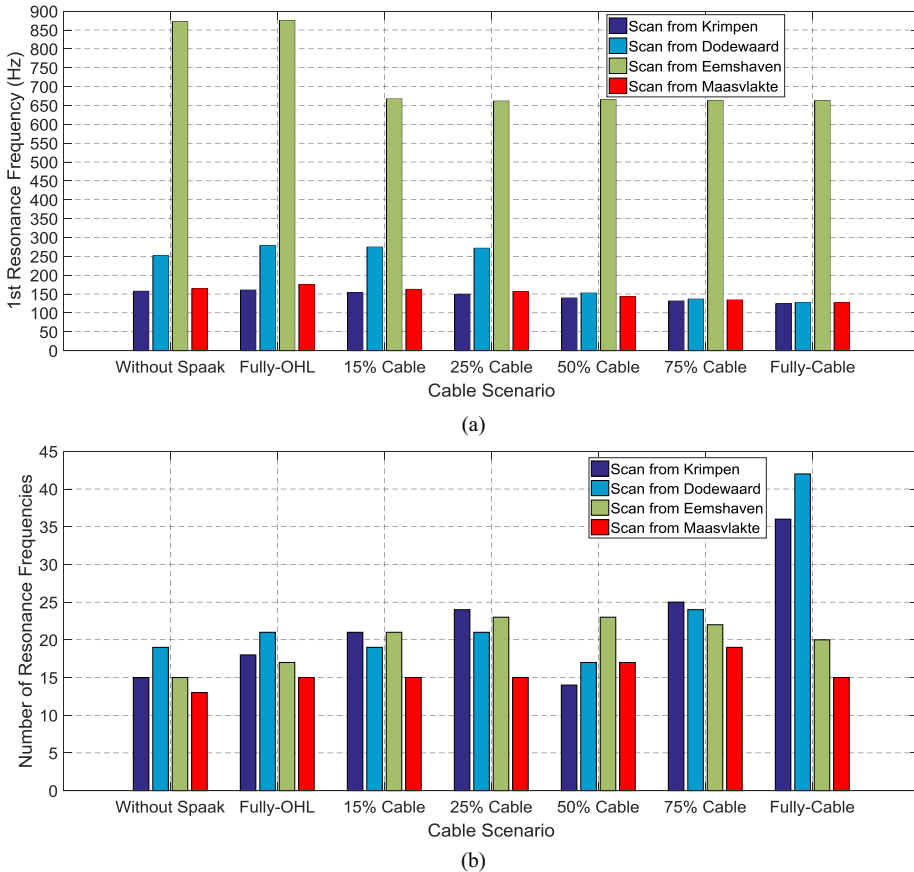


Figure 4.7: Resonance behaviour of the Dutch 380 kV grid scanned from four substations for the six cable scenarios of the Spaak connection, (a) first resonance frequency (f_1), (b) number of resonance frequencies below 2.5 kHz.

4.4.4 IMPACT OF SHUNT COMPENSATION

The shunt compensation allocation, i.e. locating and sizing shunt reactors, is one of the most important issues regarding the operation of long cables in transmission systems. The allocation should be carried out according to a detailed steady-state study, as it was explained in Chapter 3.

From the harmonic resonance perspective, it is interesting to investigate the changes in the frequency scan of the system with and without shunt reactors for reactive power compensation. Figure 4.8 shows the frequency scan of the Dutch 380 kV grid for the 50% cable and the fully-cable scenarios of the Spaak connection, both with and without shunt compensation. It can be noticed that the first resonance frequency and the number of resonance frequencies increase in both cable scenarios when the shunt reactors are added, although the increase in the first resonance frequency is very small. In addition, the difference between with and without compensation cases is larger for the fully-cable scenario compared to the 50% cable scenario.

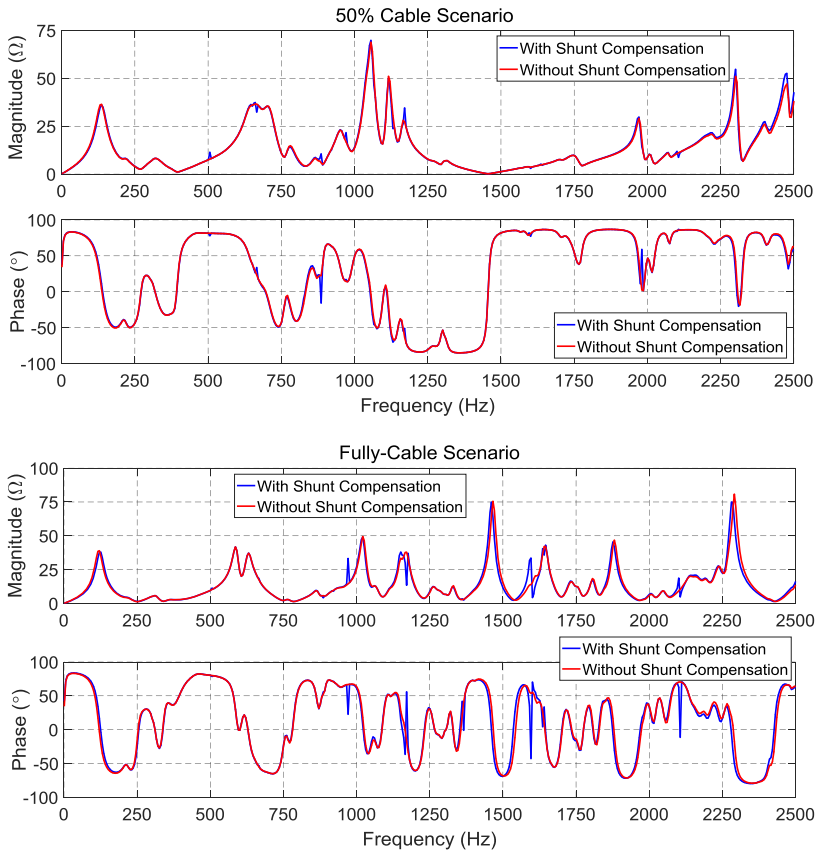


Figure 4.8: Frequency scan of the Dutch 380 kV grid for the 50% cable and the fully-cable scenarios of the Spaak connection with and without shunt compensation. The scan was performed at the Krimpen substation.

Figure 4.9 shows the first resonance frequency and the number of resonance frequencies for the six cable scenarios with and without shunt compensation scanned from the Krimpen substation. It can be seen that the existence of shunt compensation has a small impact on the first resonance frequency, while the impact becomes larger when the cable length is increased. This is because of the bigger shunt compensation size for the longer cables, which has a bigger contribution to the system short-circuit power in equation 4.7 (S_{system}) and therefore causing a higher first resonance frequency compared to the case without compensation. Furthermore, the number of resonance frequencies increases when shunt reactors are operated in the grid. This means a higher probability of resonance occurrence when cables are compensated by shunt reactors compared to the case without shunt reactors.

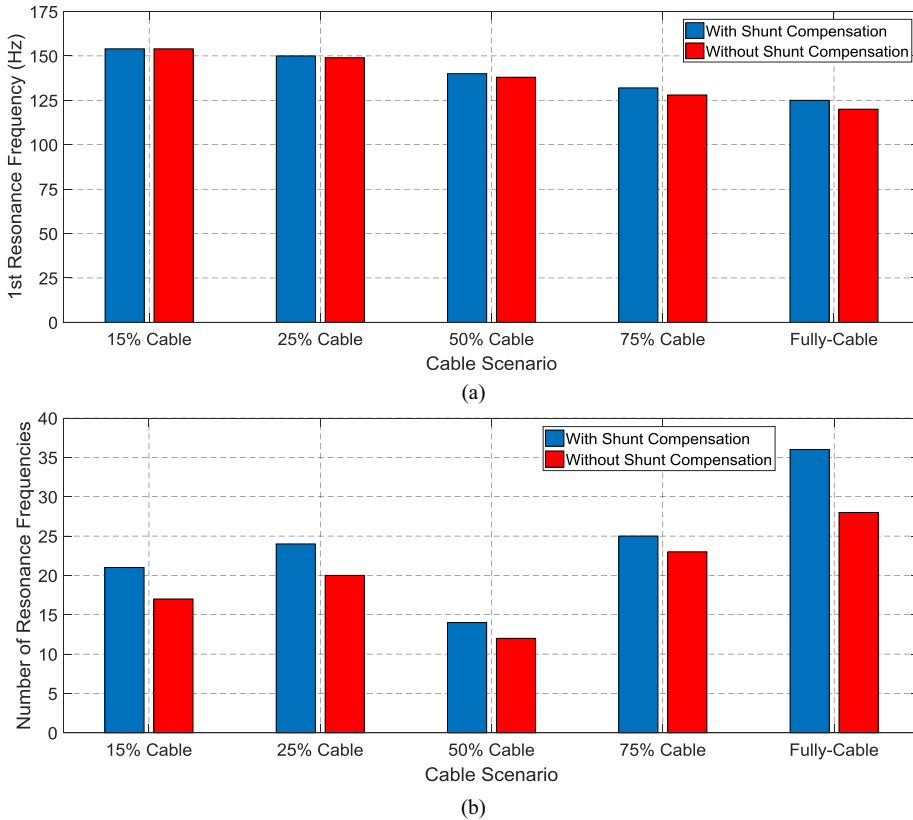


Figure 4.9: Resonance behaviour of the Dutch 380 kV grid for the six cable scenarios of the Spaak connection with and without shunt compensation, (a) first resonance frequency (f_1), (b) number of resonance frequencies below 2.5 kHz. The scan was performed at the Krimpen substation.

4.4.5 IMPACT OF SHUNT COMPENSATION LOCATION

The influence of shunt reactor locations on the frequency response of the grid is shown in Figure 4.10. Two cases are compared: (1) line-end compensation (LEC), as previously described in Chapter 2 and shown in Figure 2.3, (2) cable-end compensation (CEC), in which, as a distributed compensation, shunt reactors are located at each OHL-Cable

transition point (i.e. six reactors per circuit). The sizes for CEC are according to the reported values in Figure 3.8 for the load-flow B.

According to the simulation results, the location of shunt compensation has no impact on the first resonance frequency, whereas it can increase or decrease the number of resonance frequencies depending on the cable length.

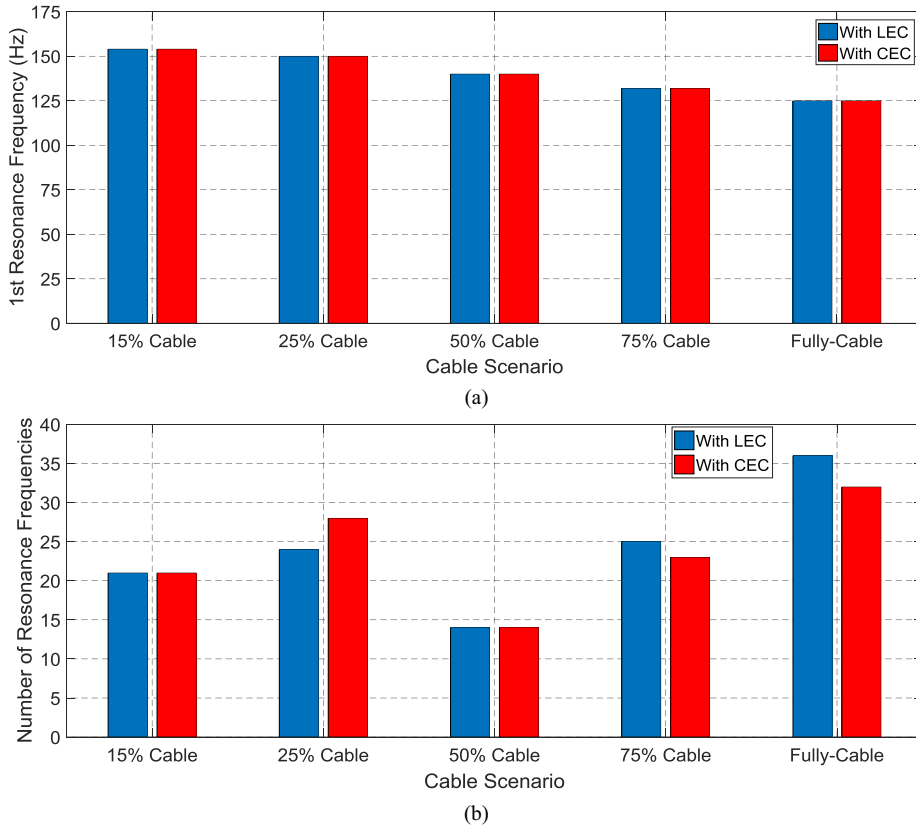


Figure 4.10: Resonance behaviour of the Dutch 380 kV grid for the six cable scenarios of the Spaak connection with LEC and CEC, (a) first resonance frequency (f_1), (b) number of resonance frequencies below 2.5 kHz. The scan was performed at the Krimpen substation.

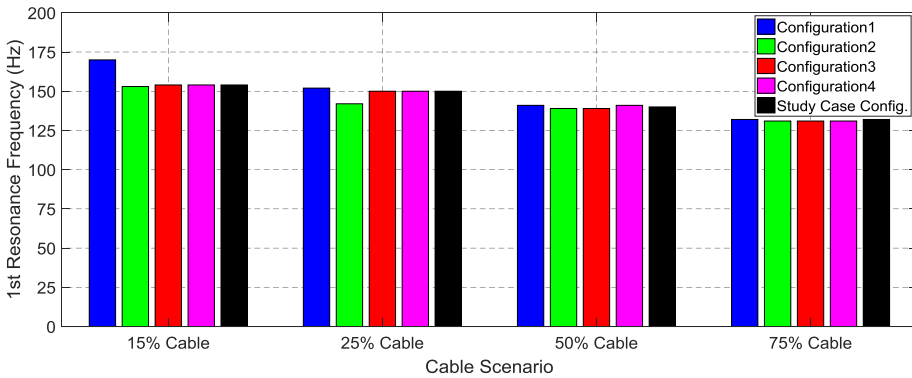
4.4.6 IMPACT OF MIXED-LINE CONFIGURATION

Similar to the steady-state analysis, it is of importance to investigate the influence of the mixed-line configuration on the resonance behaviour of the system. For this purpose, the four mixed-line configurations presented in Section 2.3.1.C (with the section lengths presented in Tables 2.4 to 2.7) and the symmetrical study case configuration (with the section lengths presented in Tables 2.3) are compared in terms of the first resonance frequency and the number of resonance frequencies. All the configurations are compensated at line-ends (LEC) with the compensation degrees reported in Figure 3.9 for the load-flow B.

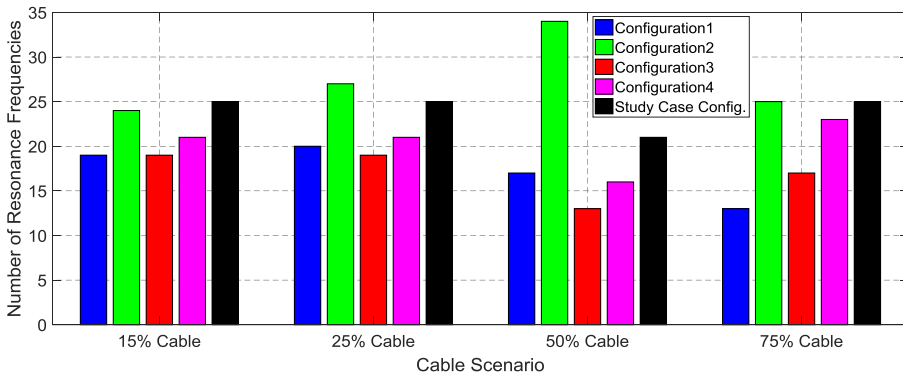
Figure 4.11 shows the impact of the five mixed-line configurations on the resonance behaviour of the Dutch 380 kV grid when the scan is performed at the Krimpen substation.

As the results show, the first resonance frequency decreases with the increasing cable length in all the five mixed-line configurations, whilst, for a given cable scenario, the difference between the resonance frequencies of the configurations is not very significant. However, the difference is larger from the number of resonance frequencies perspective, as for example the number of resonance frequencies for the 50% cable scenario in Configuration 2 is almost 3 times of those in Configuration 3.

These results can be used in the planning and design stages of cable projects for the selection of the best mixed-line configuration in terms of the resonance behaviour. For example, let’s assume that it is decided to build the project with 60 km cable (i.e. 75% cable scenario); according to the simulation results, Configuration 1 is the best option as it provides a higher first resonance frequency and a lower number of resonance frequencies compared to the other configurations.



(a)



(b)

Figure 4.11: Resonance behaviour of the Dutch 380 kV grid for the six cable scenarios of the Spaak connection with different mixed-line configurations, (a) first resonance frequency (f_1), (b) number of resonance frequencies below 2.5 kHz. The scan was performed at the Krimpen substation.

4.5 CONCLUSIONS

The influence of underground cables on the resonance behaviour of the Dutch 380 kV grid was studied in this chapter, where the frequency-scan analysis was carried out for the six cable scenarios of the Spaak connection. Results were analysed in terms of two defined criteria: the first resonance frequency and the number of resonance frequencies below 2.5 kHz. In addition, sensitivity analyses were performed to determine the impact of the shunt compensation size, shunt compensation location, and mixed-line configuration on the resonance behaviour of the grid.

According to the simulation results, increasing the cable length in the Spaak connection results in a lower first resonance frequency, where the lowest resonance frequency is 125 Hz and for the fully-cable scenario. Furthermore, the number of resonance frequencies below 2.5 kHz shows a strong dependency on the cable length and the characteristics of the point of interest (the substation at which the scan is performed), mainly the short-circuit power. In addition, the size and location of shunt compensation have a minor influence on the first resonance frequency, but they have a noticeable effect on the number of resonance frequencies. The difference between various mixed-line configurations is not very significant in terms of the first resonance frequency, but it is considerable in terms of the number of resonance frequencies.

To summarize, it can be concluded that the risk of low-order resonance frequencies is substantially higher when cables are included in the grid. From resonance point of view and for future cable projects, it is advised to investigate all available possibilities for the number, location, and length of the cable and OHL sections as well as the size and location of shunt reactors. The outcomes of such a study help to identify the mixed-line and shunt compensation topologies that cause the highest first resonance frequency and the lowest number of resonance frequencies.

REFERENCES

- [1] CIGRE Working Group C4.307, "Resonance and ferroresonance in power networks," *CIGRE Technical Brochure no. 569*, February 2014.
- [2] CIGRE Working Group B1.47, "Implementation of long AC HV and EHV cable systems," *CIGRE Technical Brochure no. 680*, March 2017.
- [3] L. Colla, S. Lauria and F. M. Gatta, "Temporary overvoltages due to harmonic resonance in long EHV cables," in *International Conference on Power System Transients (IPST)*, Lyon, France, June 2007.
- [4] C. F. Jensen, "Harmonic background amplification in long asymmetrical high voltage cable systems," in *International Conference on Power System Transients (IPST)*, Seoul, Republic of Korea, June 2017.
- [5] A. Ametani, T. Ohno and N. Nagaoka, *Cable System Transients: Theory, Modeling and Simulation*, Hoboken, NJ, USA: Wiley, July 2015.
- [6] R. Smeets, L. van der Sluis, M. Kapetanovic, D. Peelo and A. Janssen, *Switching in Electrical*

- Transmission and Distribution Systems*, Hoboken, NJ, USA: Wiley, 2015.
- [7] Tokyo Electric Power Company, "Assessment of the technical issues relating to significant amounts of EHV underground cable in the all-island electricity transmission system," November 2011.
- [8] C. L. Bak and F. F. da Silva, "High voltage AC underground cable systems for power transmission-A review of the Danish experience, part 1," *Electric Power Systems Research*, vol. 140, pp. 984-994, 2016.
- [9] V. Akhmatov, "Excessive over-voltage in long cables of large offshore windfarms," *Wind Engineering*, vol. 30, no. 5, pp. 375-383, October 2006.
- [10] T. Karasaki, T. Goto and A. Ametani, "An abnormal overvoltage due to load rejection on EHV underground transmission lines," in *International Conference on Power System Transients (IPST)*, Lisbon, Portugal, 1995.
- [11] CIGRE Working Group C4.502, "Power system technical performance issues related to the application of long HVAC cables," *CIGRE Technical Brochure no. 556*, October 2013.
- [12] H. Khalilnezhad, M. Popov, L. van der Sluis, J. A. Bos and J. P. W. de Jong, "Influence of long EHV AC underground cables on the resonance behavior of the Dutch transmission system," in *IEEE Power and Energy Society (PES) General Meeting*, Boston, MA, USA, July 2016.
- [13] M. Bollen, S. Aceby, H. Jansson and M. Jonsson, "Using transfer impedance to study harmonic resonance due to AC cables in a transmission system," in *CIGRE*, Lund, Sweden, 2015.
- [14] F. F. da Silva, C. L. Bak and P. B. Holst, "Study of harmonics in cable-based transmission networks," in *44th CIGRE Session*, Paris, France, 2012.

CHAPTER 5

ENERGIZATION OVERVOLTAGES IN HYBRID OHL-CABLE SYSTEMS

5.1 INTRODUCTION

The transient behaviour of an EHV hybrid OHL-Cable system is significantly different from an OHL-based system because of substantial differences between electrical characteristics of OHLs and cables. As a result, several questions have been raised concerning the transient operation of such systems. A very important question is how energization overvoltages would be in hybrid OHL-Cable systems and which parameters can affect their significance.

In general, energization overvoltages in EHV systems can reach very high values and are considered among the severest overvoltages stressing the insulation of system components. These overvoltages have a statistical behaviour caused by the random behaviour of the circuit breaker closing time. Thus, the required insulation level should be specified by means of a statistical approach by which the distribution of energization overvoltages is determined. The statistical distribution of energization overvoltages has been used for decades for the insulation coordination studies, as it has been recommended by the IEC 60071-2 standard too [1].

Literature has properly studied the distribution of energization overvoltages in purely OHL or cable systems, but such a study is not available for hybrid systems consisting of both OHLs and cables. It is expected that the overvoltage distributions change considerably when both OHLs and cables are used in a transmission line. This scientific gap will be addressed in this chapter, where energization overvoltages in the hybrid OHL-Cable circuits of the Spaak connection are studied. The study includes various sensitivity analyses to identify the impact of system parameters and topology on overvoltages.

This chapter begins with the analysis of time-domain voltage waveforms and afterwards the statistical distribution of energization overvoltages will be presented. Section 5.2 describes the simulation parameters and assumptions. The time-domain energization overvoltages of the Spaak connection are treated in Sections 5.3. Section 5.4 is dedicated to statistical analysis of energization overvoltages, where the results of numerous statistical

simulations and sensitivity analyses are discussed. Finally, conclusions are presented in Section 5.5.

5.2 SIMULATION CONSIDERATIONS

The transient studies were performed by the use of the distributed frequency-dependent parameter model of the Dutch 380 kV grid in PSCAD. This model was described in detail in Chapter 2. Surge arresters are not included in this model in order to simulate the worst overvoltages. The magnitude, frequency and duration of switching overvoltages are dependent on several parameters, mainly switching instant, short-circuit power, cable length, shunt compensation size and location, and mixed-line configuration.

The mixed-line configuration is shown in Figure 5.1 (which is the study case configuration defined in Chapter 2) with the cable scenarios defined in Table 2.2. Shunt compensation sizes are according to the values reported in Table 3.2. Overvoltages due to the no-load energization of circuit 1 of the Spaak connection are studied with the assumption that the parallel circuit (circuit 2) is out of service (i.e. single-circuit energization). The switching is performed from the Krimpen substation while the circuit is open at the other side, as illustrated in Figure 5.1.

When overvoltages are expressed in per unit, the base value (1 pu) is the peak value of the phase-to-earth nominal voltage (310.27 kV). The power-frequency and the transient overvoltages are the two components of the total switching overvoltage, so the obtained maximum overvoltages depend on the power-frequency voltage, which in this study is 1.076 pu (333.85 kV phase-to-ground). The short-circuit power at the Krimpen substation is 26.3 GVA (corresponding to 37.14 kA fault current or 20 mH equivalent source inductance calculated at 408.88 kV ($333.85 \text{ kV} \times \sqrt{\frac{3}{2}}$)).

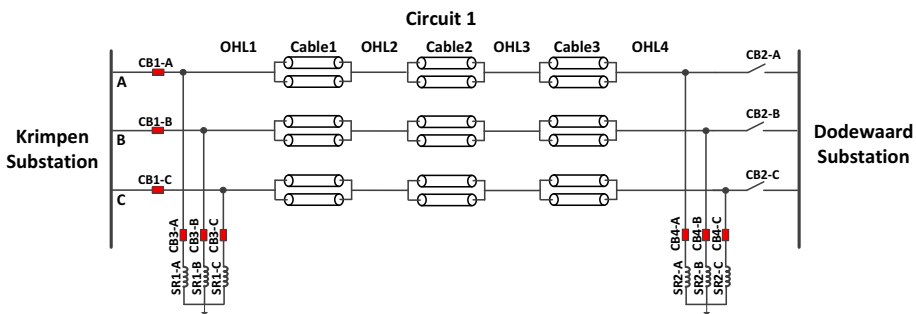


Figure 5.1: Single-circuit energization of the Spaak connection from the Krimpen substation, while the second circuit (Circuit 2) is out of service (CB: circuit breaker, SR: shunt reactor).

In the transient studies of cable systems, the determination of the right numerical integration time step is a critical factor to obtain an accurate simulation of transient voltages and currents. As a rule of thumb, the time step should be smaller than the travelling time of the wave in the shortest piece of the line. In this way, the wave propagation in all lines can be accurately simulated.

To calculate the travelling time of the shortest line piece, the wave propagation velocity should be calculated by means of equation 2.11 in Chapter 2. The inductance and capacitance of the conductor are required for calculation of the wave velocity. For a cylindrical conductor with isolation, the inductance and capacitance can be calculated by making use of the following well-known equations:

$$C = \frac{2\pi\epsilon}{\ln\left(\frac{b}{a}\right)} \quad (\text{F/m}) \quad (5.1)$$

$$L = \frac{\mu}{2\pi} \ln\left(\frac{b}{a}\right) \quad (\text{H/m}) \quad (5.2)$$

where, a and b are respectively the radius of the conductor and the insulation, ϵ is the permittivity of the insulation consisting of the relative permittivity and the vacuum permittivity ($\epsilon = \epsilon_0\epsilon_r$), and μ is the permeability of the conductor consisting of the relative permeability and the vacuum permeability ($\mu = \mu_0\mu_r$).

By substituting these values in equation 2.11, wave velocity can be obtained as below:

$$v = \sqrt{\frac{1}{LC}} = \sqrt{\frac{1}{\mu\epsilon}} = \frac{C_0}{\sqrt{\epsilon_r\mu_r}} \quad (\text{m/s}) \quad (5.3)$$

where C_0 is the light velocity in the free space (3×10^8 m/s). The wave propagation velocity in the OHL and the cable can be calculated by using the relative permittivity and permeability values in Table 2.10:

$$v_{OHL} \approx C_0 = 3 \times 10^8 \quad (\text{m/s}) \quad (5.4)$$

$$v_{cable} = \frac{C_0}{\sqrt{2.79 \times 1.17}} = 1.6605 \times 10^8 \quad (\text{m/s}) \quad (5.5)$$

The shortest line piece in the Dutch 380 kV grid model is 900 m. This is the length of the minor cable sections in the Randstad South-Ring connection nearby the Spaak connection. Therefore, the wave travelling time in these pieces is:

$$t = \frac{\text{length}}{V_{cable}} = \frac{900}{1.6605 \times 10^8} = 5.42 \quad \mu\text{s} \quad (5.6)$$

Taking this travelling time into account, the selected simulation time step for the transient studies was $4.8 \mu\text{s}$ in order to keep the balance between the simulation accuracy and the simulation time.

5.3 ENERGIZATION OVERVOLTAGES

It was assumed that in all simulations the three poles of CB1 (circuit breaker 1 in Figure 5.1) are closed simultaneously at the voltage peak of phase C ($t = 0.07099 \text{ s}$). In addition, shunt reactors were energized together with the line at the same time.

Figure 5.2 shows the voltage at the Krimpen substation after the no-load energization of the six cable scenarios. In Figure 5.2a, which shows three phase voltages for the 50% cable scenario, the overvoltage peaks are 367 kV (1.18 pu), 377 kV (1.22 pu), and 356 kV (1.15 pu) respectively for phase A, phase B, and phase C.

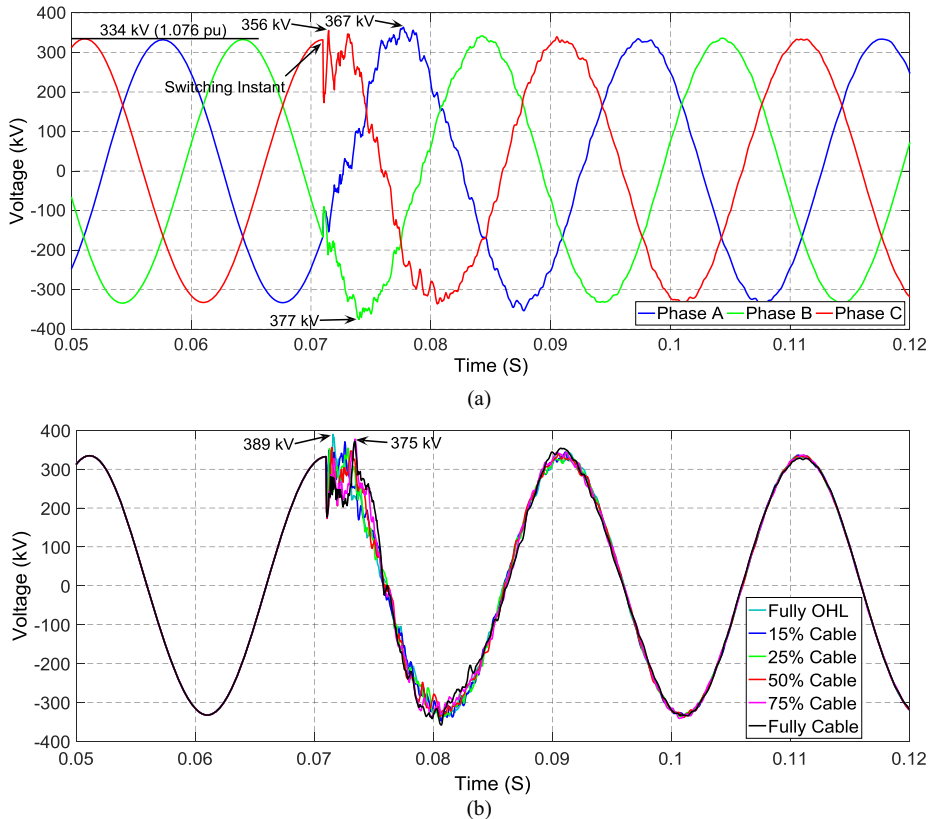


Figure 5.2: Voltage at the Krimpen substation (sending-end) after the no-load energization of the Spaak connection, (a) phase voltages for the 50% cable scenario, (b) phase C voltage for the six cable scenarios.

As depicted in Figure 5.2b, overvoltage peak in phase C is larger for other scenarios and reaches up to 389 kV (1.25 pu) for the Fully-OHL, 375 kV (1.21 pu) for the fully-cable, 373 kV (1.2 pu) for the 50% cable, and 371 kV (1.2 pu) for 15% cable scenarios. The fully-OHL scenario has the highest initial overvoltage peak due to the absence of shunt compensation and faster wave travelling time in it. However, the overvoltage damps out much faster in the fully-OHL scenario than in the scenarios with cable

Furthermore, the voltage peaks happen at different instants depending on OHL and cable section lengths, which are determining the wave propagation pattern. However, overvoltages are damped in the first few milliseconds with high-frequency low-amplitude oscillations for all the cable scenarios. The difference between final steady-state voltages in Figure 5.2b is negligible, as it was expected due to the shunt compensation sizing by steady-state analysis. Without shunt compensation, the difference between the steady-state peak values of different cable scenarios can be up to tens of kilovolts, whereas it is just in the range of a few kilovolts with the use of optimum shunt compensation. Since the overvoltages last for few milliseconds, the switching transient overvoltages can be classified as slow-front overvoltages. All overvoltage peaks are far below the phase-to-earth switching impulse withstand voltage (SIWV) proposed in [2], which is 850, 950, or 1050 kV (peak value) for equipment with 420 kV highest RMS voltage.

Immediately after switching the circuit breaker, the energizing wave propagates through the circuit resulting in reflection and refraction waveforms at the locations where the conducting medium is changing, i.e. cable joints and transition points (TP) between OHL and cable sections. Therefore, during this transient period, voltage variations along the circuit can be significant, depending on the location as it is illustrated in Figure 5.3. In this figure, the voltage of phase C at the six transition points is plotted for the 50% cable scenario.

It can be seen that all the overvoltage peaks are below the SIWV for the studied cable scenarios. In addition, each of these six transition points experiences different overvoltage peaks at different moments, depending on the distance of the transition point from the sending-end. The overvoltage peak occurs sooner and with a higher value when the transition point is further from the sending terminal. In other words, the overvoltage peak becomes higher when moving toward the open-end (as it was expected) and therefore the highest transition point overvoltage is at TP6.

Figure 5.4 shows the energization voltage at the open-end for the 50% cabling scenario, where the highest overvoltage with the amplitude of 650 kV (2.09 pu) is in phase C since the switching is performed at its peak voltage.

Figure 5.5 depicts the voltage of phase C at the open-end for the six cable scenarios. The highest overvoltage peak with an amplitude of 676 kV (2.18 pu) is for the 15% cable scenario. The amplitude and the frequency of voltage oscillations become smaller for the scenarios with higher cable share. Moreover, with the increasing cable share, it takes a longer time for the first travelling surge to reach the open-end of the circuit since the wave travelling speed in the cable is almost half of its speed in the OHL (1.66×10^8 versus $3 \times$

10⁸ m/s). This results in a longer time for the wave to reach the open-end when the cable is longer.

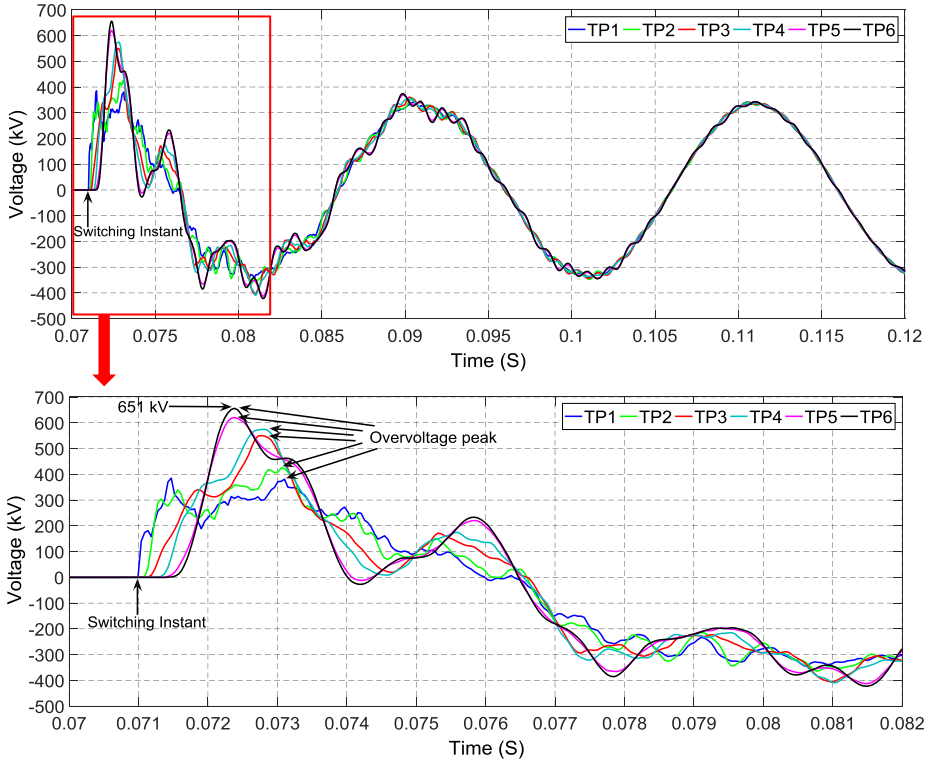


Figure 5.3: Phase C voltage at OHL-Cable transition points (TP) after the no-load energization of the 50% cable scenario.

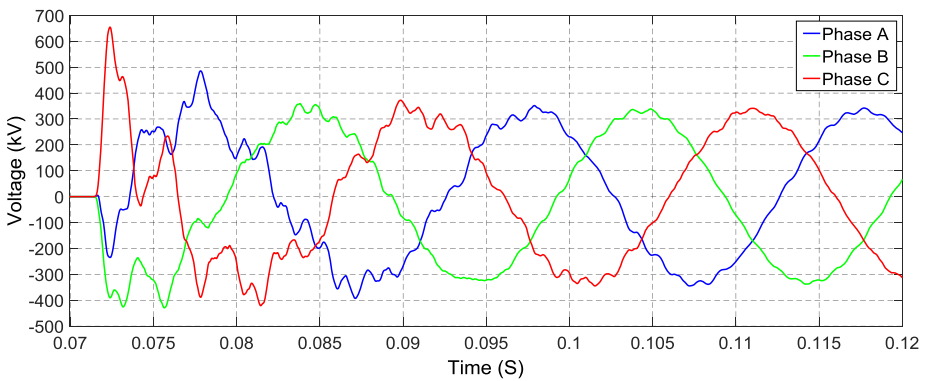


Figure 5.4: Open-end voltage after the no-load energization of the 50% cable scenario.

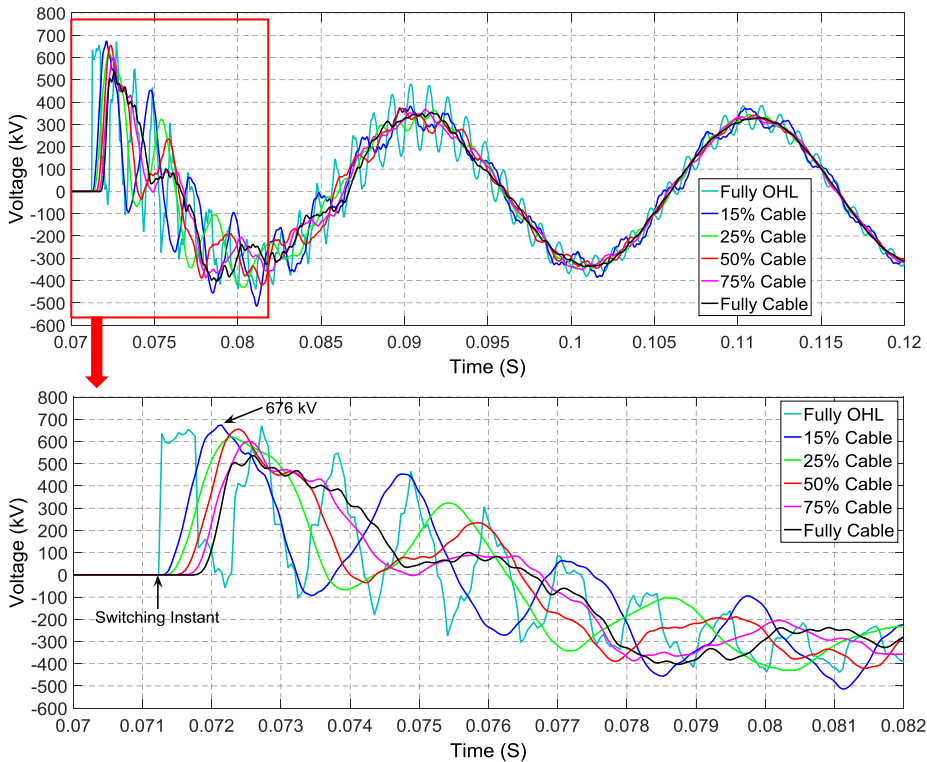


Figure 5.5: Phase C voltage at the open-end after the no-load energization of the six cable scenarios.

5.4 STATISTICAL ANALYSIS OF OVERVOLTAGES

The determination of the statistical distribution of energization overvoltages is highly recommended for the insulation coordination studies due to the statistical nature of switching actions and the insulation strength. The risk of an insulation failure can be calculated by the comparison of the overvoltage probability distribution and the insulation breakdown probability distribution [1], [3], [4].

The statistical nature of energization overvoltages is the result of the random behaviour of the circuit breaker closing time. The breaker contacts can be switched at any point on the voltage waveform with a pole closing span. The pole closing span is the time difference between the first and the last pole to close due to different stochastic variations in the operating time of poles [5], [6].

The detailed study of the statistical distribution of line energization overvoltages (OHL or cable) has been addressed in [7-16]. In [11] and [12], the statistical distribution of energization overvoltages in EHV cables and OHLs were compared, where it has been concluded that overvoltages in a cable are lower than those in an OHL. However, despite the importance of the issue, there is very limited literature related to the statistical switching analysis of hybrid circuits consisting of OHLs and cables combined.

It has been reported in [17] that energization overvoltages in a cable circuit are in general lower than those in an OHL-Cable circuit. In [18], authors concluded that energization overvoltages of a hybrid OHL-Cable circuit are less than those in a purely OHL circuit and higher than those in a purely cable circuit. However, these conclusions cannot be generalized as the studies neglected the breaker pole span and are only for one circuit topology and set of system parameters.

In this regard, a more comprehensive study is required for hybrid OHL-Cable systems where the impacts of various system topologies and parameters are investigated, notably the cable length, configuration of the hybrid OHL-Cable circuit, short cable sections, and system short-circuit power. In practice, the distribution of overvoltages can be significantly different from one system to another and this can be identified by a sensitivity analysis.

The aim of this section is to address the mentioned crucial scientific gaps and perform sensitivity analyses on the system parameters to find out how the statistical distribution of transient energization overvoltages changes in hybrid OHL-Cable circuits. In addition, overvoltages due to the presence of trapped charges (residual charges) in the cable are investigated too.

5.4.1 STATISTICAL BEHAVIOUR OF CIRCUIT BREAKER

The breaker closing time (T_{close}) is the instant at which the breaker connects a phase to the voltage source and it can be expressed as follows [5], [13]:

$$T_{close} = T_{command} + \underbrace{\Delta T_{known} + \Delta T_{stochastic}}_{\Delta T_{operating}} \quad (5.7)$$

where $T_{command}$ is the instant at which the breaker receives the closing command, and $\Delta T_{operating}$ is the breaker operating time representing the required time for the control and mechanical parts of the breaker to operate. ΔT_{known} is the known and predictable part of the operating time (from measurements and/or adaptive control) and $\Delta T_{stochastic}$ is the stochastic variation (unpredicted variation) in the operating time, which indicates the randomness of the closing time.

$\Delta T_{stochastic}$ can be different between the poles due to the separate mechanical systems and it has a random behaviour according to the normal distribution [5-16], [18]. The different stochastic variations of the operating time can result in energization of phases at different instants, which is known as the pole closing span. In other words, the pole closing span is the time difference between the first and the last pole to close.

With regards to equation 5.7, the statistical behaviour of the breaker closing time can be represented if two parameters are determined: (1) mean closing time, T_{mean} , where $T_{mean} = T_{command} + \Delta T_{known}$, (2) pole closing span or distribution of pole closing times around the mean closing time, $\Delta T_{stochastic}$. A sufficient number of these two parameters should be simulated to obtain accurate energization overvoltage distributions [13], [16], [19].

5.4.2 STATISTICAL SIMULATION APPROACH

The statistical analysis of energization overvoltages is more accurate when a larger number of switching times are simulated, but this requires a long computation time especially when a big and complex grid is modelled. For instance, each single switching simulation in the PSCAD model of the Dutch 380 kV grid can take up to a few hours to be completed, depending on the simulated cable length. Such a long simulation time is mainly caused by the small numerical integration time step ($\Delta t = 4.8 \mu s$) and a large number of cables.

In [8-10], 100 random line energizations were performed to produce the overvoltage distributions, whilst the analysis was conducted in [11] by 200 random line energizations. The literature has recommended minimum 100 simulations to obtain a sufficiently accurate overvoltage distribution [13], [16-19]. In this study, 400 energizations were carried out for each study case to maximize the accuracy of the obtained statistical distributions. The applied approach for the selection of T_{mean} and $\Delta T_{stochastic}$ (pole span) is illustrated in Figure 5.6:

1. T_{mean} : it was assumed that the line and shunt reactor breakers receive the closing command simultaneously and they have the same T_{mean} . The mean closing time can be any point of the power-frequency voltage cycle. 100 random points (with uniform distribution) were chosen by using the multiple-run feature of PSCAD.
2. $\Delta T_{stochastic}$ (pole span): for each T_{mean} , 4 sets of pole closing span were simulated for each breaker. The pole span was determined by a random number generator using the normal (Gaussian) distribution. The mean value of the normal distribution was T_{mean} and the standard deviation was 1 ms ($\sigma = 1$ ms). The normal distribution curve was truncated at -3σ and $+3\sigma$.

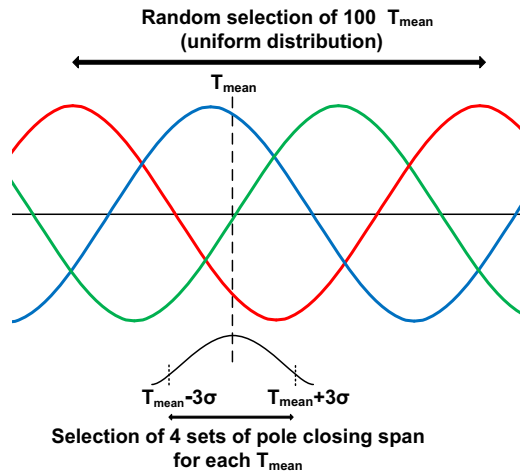


Figure 5.6: Statistical variation of the breaker closing time over a cycle of the power-frequency voltage.

The phase-peak method was applied to obtain the overvoltage probability distribution for each study case [1]. This means that from each energization simulation, the peak value of the phase-to-earth overvoltage in each phase at the point of interest was included in the overvoltage probability distribution. Therefore, the representative probability distribution for each case has 1200 overvoltage peak values (3 peak values per simulation \times 400 simulations).

5.4.3 SIMULATION RESULTS AND ANALYSIS

The effects of cable length, shunt compensation size/location, short cable sections, short-circuit power, trapped charges (residual charges), and circuit configuration on the energization overvoltages are studied in this section. The point of interest is always the line open-end, unless a different location is mentioned.

A. IMPACT OF CABLE LENGTH

The statistical switching analysis was performed on the six cable scenarios (presented in Table 2.2) to find the influence of cable length on the distribution of energization overvoltages. Figure 5.7 shows the obtained maximum overvoltages at the sending-end, open-end and all the six OHL-Cable transition points (TP). The fully-OHL and the fully-cable scenarios are excluded since the transition points do not exist for these scenarios. It can be seen that for each cable scenario the maximum overvoltage becomes higher at transition points closer to the open-end as the highest overvoltage is at the open-end.

Table 5.1 presents the maximum, mean, standard deviation, and 2% values, which are the four key values of the statistical distributions. The 2% value is the overvoltage value that the probability of this value being exceeded is 2% and is used for the insulation coordination studies [1].

The complementary cumulative distribution functions (here called cumulative probabilities) of energization overvoltages of the six cable scenarios are given in Figure 5.8. For a given overvoltage on the horizontal axis, the corresponding value on the vertical axis shows the probability that overvoltages exceed the given overvoltage.

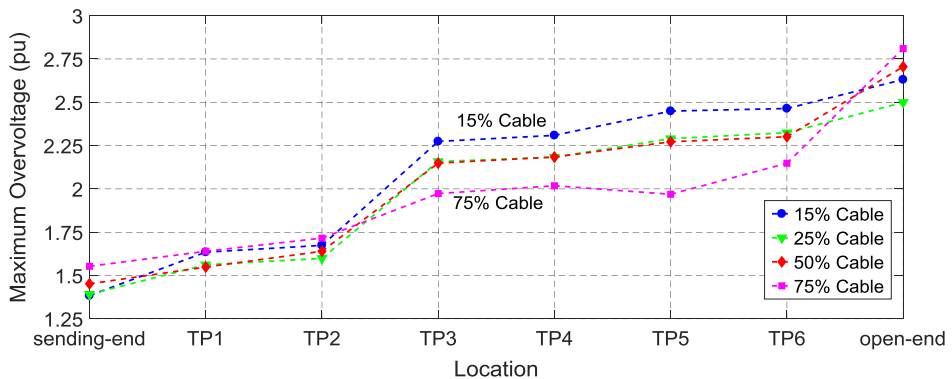


Figure 5.7: Maximum energization overvoltage at different locations along the hybrid OHL-Cable circuit.

TABLE 5.1
KEY VALUES OF THE OVERVOLTAGE DISTRIBUTIONS

Scenario	Overvoltage (pu)			
	Max.	Mean	Stand. dev.	2% value
Fully OHL	2.826	1.821	0.358	2.509
15% Cable	2.631	1.756	0.262	2.346
25% Cable	2.499	1.694	0.245	2.269
50% Cable	2.705	1.689	0.259	2.319
75% Cable	2.810	1.626	0.256	2.329
Fully Cable	1.908	1.501	0.163	1.820

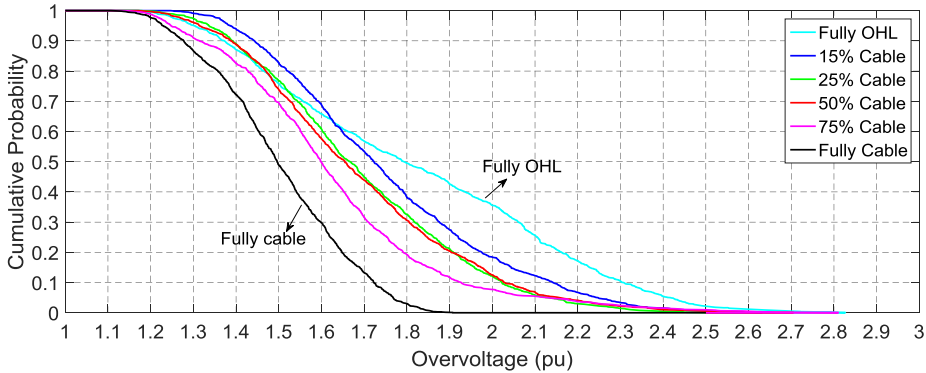


Figure 5.8: Cumulative probability distributions of energization overvoltages of the six cable scenarios.

As it is shown in Table 5.1, for the fully-OHL scenario, the maximum overvoltage (2.826 pu), mean overvoltage (1.821 pu), and 2% value (2.509 pu) are the highest among all the scenarios. In contrast, the lowest values are for the fully-cable scenario with the maximum overvoltage, mean overvoltage, and 2% value of 1.908 pu, 1.501 pu, and 1.820 pu, respectively. The standard deviation is also largest for the fully-OHL scenario and smallest for the fully-cable scenario. In addition, in Figure 5.8, the probability of overvoltages is the highest for the fully-OHL scenario (for overvoltages above 1.65 pu), whereas it is always the lowest for the fully-cable scenario. These findings coincide with the conclusions of [11] and [12] that line energization overvoltages in cables are lower than those in OHLs.

According to Table 5.1, the hybrid scenarios produce overvoltages lower than those of the fully-OHL scenario and higher than those of the fully-cable scenario. In addition, in Figure 5.8 and for overvoltages above 1.65 pu, the overvoltage probabilities of the hybrid scenarios are between those of the fully-OHL and the fully-cable scenarios.

According to the simulation results, it can be concluded that a partial or full replacement of an overhead transmission line with cables results in lower energization overvoltages. It should be noted that for the partial cabling this conclusion is a rule of thumb and may not be always valid due to its dependency on the system topology and parameters (e.g. see Sections 5.4.3.D, 5.4.3.E, and 5.4.3.G for three exceptions).

The probability distributions of energization overvoltages of the six cable scenarios with fitted normal distribution curves are shown in Figure 5.9. It is a usual approach to compare the probability distributions of random energization cases with the normal distribution. The

y-axis (height of rectangle) is the frequency with which the overvoltages in the specified range (width of rectangle) have occurred. Table 5.2 presents the skewness (S) and kurtosis (K) values of the overvoltage distributions, calculated as expressed below:

$$S = \frac{1}{1200} \sum_{i=1}^{1200} \left(\frac{x_i - \mu_v}{\sigma} \right)^3 \tag{5.8}$$

$$K = \frac{1}{1200} \sum_{i=1}^{1200} \left(\frac{x_i - \mu_v}{\sigma} \right)^4 \tag{5.9}$$

where, x_i is the overvoltage value (i.e. sample value), μ_v is the mean value of the overvoltages distribution, and σ is the standard deviation of the overvoltages distribution. There are 1200 overvoltage values in each probability distribution.

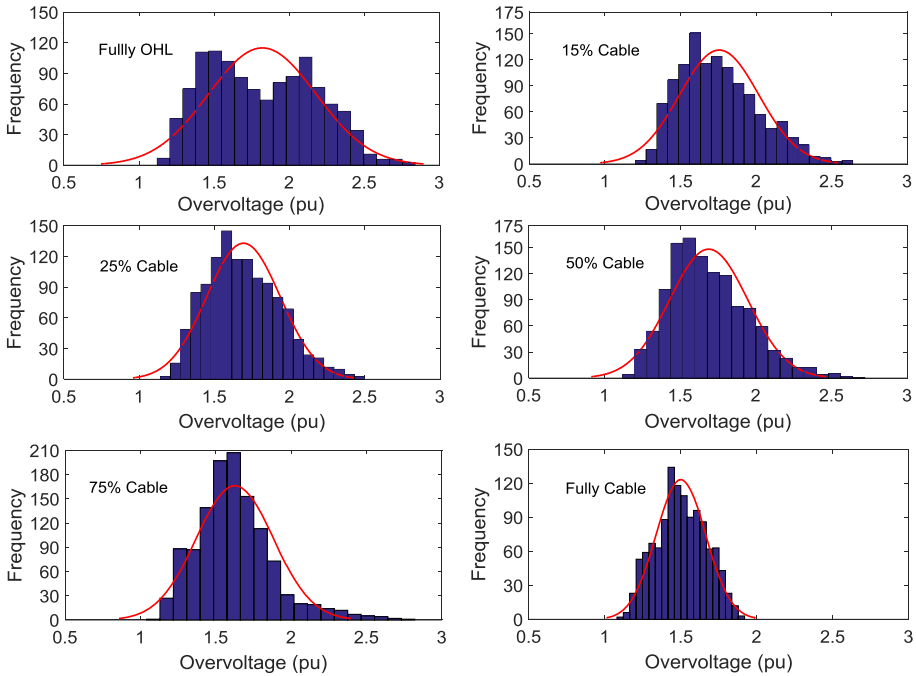


Figure 5.9: Probability distributions of energization overvoltages of the six cable scenarios with fitted normal distribution curves.

TABLE 5.2
SKEWNESS AND KURTOSIS OF THE ENERGIZATION OVERVOLTAGES DISTRIBUTIONS

Scenario	Skewness	Kurtosis
Fully OHL	0.239	2.084
15% Cable	0.581	2.867
25% Cable	0.453	2.802
50% Cable	0.640	3.262
75% Cable	1.012	4.886
Fully Cable	0.016	2.321

The skewness is a measure describing how symmetrically the data is distributed around the mean value. The skewness of any symmetric distribution like the normal distribution is zero. A negative skewness indicates that the data has a longer tail to the left side of the mean value and a positive skewness indicates that the data has a longer tail to the right side. The overvoltage probability distributions of all the scenarios have positive skewness and are spread out more to the right side of the mean values. The fully-cable scenario has the smallest skewness indicating that its overvoltages probability distribution is the most symmetrical one.

The kurtosis is a measure of how outlier-prone (heavy- or light-tailed) a distribution is. Higher kurtosis indicates that the distribution is more outlier-prone (heavier-tailed) and lower kurtosis indicates that the distribution is less outlier-prone (lighter-tailed). The kurtosis of the normal distribution is 3. According to Table 5.2, the fully-OHL scenario with the kurtosis of 2.084 is the less outlier prone scenario.

It has been observed that the energization overvoltages can substantially change when the share of cable in the circuit is varied. To interpret the simulation results, the significant physical differences between cables and OHLs, which influence the energization overvoltages, should be discussed.

The first difference between cables and OHLs is the propagation velocity and the behaviour of the modal waves. According to the modal decomposition theory, a cross-bonded three-phase single-core cable system can be decomposed into six modes: one coaxial mode, two inter-phase modes, two inter-sheath modes, and one ground mode (in contrast to only one inter-phase mode and one earth-return mode for an OHL). Each mode has its own attenuation constant and propagation velocity [20-23]. The wave propagation velocity in cables is much lower than that of OHLs as the cable coaxial mode is the fastest with the propagation velocity of $\frac{C_0}{\sqrt{\epsilon_r \mu_r}}$ m/s, where ϵ_r and μ_r are respectively the relative permittivity and the relative permeability (compared to $C_0 = 3 \times 10^8$ m/s for OHLs). For a typical cable, the propagation velocity is approximately between 1.6×10^8 m/s and 1.8×10^8 m/s. If a cable is cross-bonded, the propagation velocity is slightly lower than these values [23].

During transients, when an energizing wave propagates into the cable core conductor, all the six modal waves are excited and propagate towards the open-end while they reflect and refract at each impedance discontinuity point (impedance mismatch point), where the line surge impedance changes. Therefore, the resulting overvoltage at a given location on the circuit is the superposition of all the modal waves at that location. As it is discussed in

[12], the maximum energization overvoltage at the cable open-end is determined by the superposition of the inter-phase mode (as the dominant mode) and the coaxial mode (as the superimposed mode), where the cycle time of the inter-phase mode (dominant mode) is dependent on the short-circuit power and the cable length. The overvoltages of the cable coaxial mode are low (compared with those of the inter-phase mode in OHLs) and also the cycle time of the cable inter-phase mode is generally long. These two factors result in lower energization overvoltages for cables compared to OHLs.

The second difference between cables and OHLs is the existence of cross-bonding points for cables, which makes it more difficult for the waves to propagate to the open-end [11]. Furthermore, the third difference is the smaller surge impedance of cables compared to that of OHLs, which is leading to lower overvoltages in cables for a same switching surge current [11], [24].

In addition to the mentioned differences between cables and OHLs, explanation about the reflection and refraction of the propagating waves in hybrid OHL-Cable circuits is also useful for the interpretation of the simulation results. When an electromagnetic wave propagating along a hybrid circuit arrives to an impedance discontinuity point, as shown in Figure 5.10, a part of the incident wave is reflected back and a part of the wave is transmitted beyond the point. The impedance discontinuity point can be a sheath cross-bonding point or an OHL-Cable transition point. The reflected voltage wave (V_R) and the transmitted voltage wave (V_T) can be calculated by the following equations [25]:

$$V_R = \frac{Z_2 - Z_1}{Z_2 + Z_1} \cdot V \quad (5.10)$$

$$V_T = \frac{2Z_2}{Z_2 + Z_1} \cdot V \quad (5.11)$$

where, V is the incident voltage wave, Z_1 is the surge impedance of the first transmission line through which the incident wave is travelling, and Z_2 is the surge impedance of the second transmission line.

In the Spaak connection, the surge impedances of the OHLs and cables are around 220Ω and 50Ω , respectively. So, according to equations 5.10 and 5.11, when a voltage wave travelling through an OHL section reaches a transition point to a cable section, about 63% of the wave is reflected back with the negative polarity (with respect to the incident wave) and about 37% of the wave is transmitted to the cable. In contrary, when a wave travelling through a cable section reaches a transition point to an OHL section, about 63% of the wave is reflected back into the cable with the positive polarity (with respect to the incident wave) and 163% of the wave is transmitted to the OHL.

When a circuit consists of a cascade connection of several OHL and cable sections, like the circuits of the Spaak connection, the propagating switching surge produces reflected and transmitted waveforms at all the impedance discontinuity points. This leads to a very complex propagation pattern that can be analysed with the help of a lattice diagram [26]. In

this situation, the voltage at a given point on the circuit is determined by the superposition of all the waves at every instant of time. The highest overvoltages occur when the specific condition in terms of the system topology and parameters (e.g. the number and location of sections and the short-circuit power) are present for the superposition of the waves.

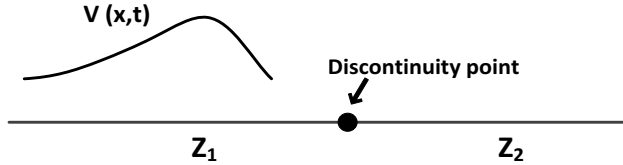


Figure 5.10: A travelling voltage wave arriving to an impedance discontinuity point at the junction of two transmission lines.

B. IMPACT OF COMPENSATION SIZE

The shunt reactors are generally sized and located based on a steady-state analysis to control the power-frequency voltage and the capacitive current in the line breakers [27]. To investigate the impact of shunt reactors on the statistical distribution of energization overvoltages, the statistical analysis was conducted without shunt compensation and the results were compared with those of the shunt-compensated circuit.

Table 5.3 presents the key values of the overvoltage distributions and Figure 5.11 shows the cumulative probabilities of energization overvoltages with and without shunt compensation. In all the cable scenarios, except the fully-cable scenario, the maximum overvoltage and the 2% value are lower when the circuit is energized without shunt compensation. In addition, for these scenarios, the probability of high overvoltages (above 1.85 pu) is lower when the circuit is energized without shunt compensation, although the post-switching steady-state overvoltages will be higher due to the Ferranti effect (see equation 3.2 in Chapter 3). This could be due to the superposition of the energization transients of the reactors and the line when they are energized together.

TABLE 5.3
KEY VALUES OF THE OVERVOLTAGE DISTRIBUTIONS WITHOUT SHUNT COMPENSATION (VALUES BETWEEN PARENTHESES ARE WITH SHUNT COMPENSATION)

Scenario	Overvoltage (pu)			
	Max.	Mean	Stand. dev.	2% value
15% Cable	2.418 (2.631)	1.748 (1.756)	0.240 (0.262)	2.267 (2.346)
25% Cable	2.393 (2.499)	1.676 (1.694)	0.217 (0.245)	2.144 (2.269)
50% Cable	2.355 (2.705)	1.699 (1.689)	0.215 (0.259)	2.153 (2.319)
75% Cable	2.134 (2.810)	1.653 (1.626)	0.185 (0.256)	2.024 (2.329)
Fully Cable	2.083 (1.908)	1.613 (1.501)	0.154 (0.163)	1.920 (1.820)

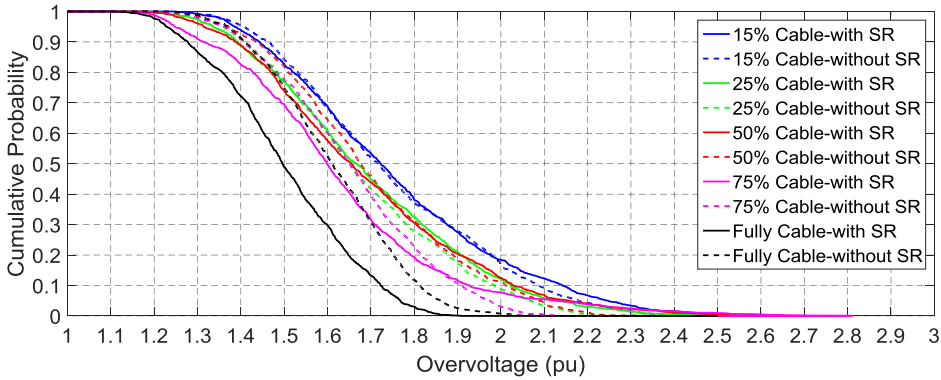


Figure 5.11: Cumulative probability distributions of energization overvoltages with shunt compensation (solid lines) and without shunt compensation (dashed lines).

C. IMPACT OF COMPENSATION LOCATION

As it was discussed in Chapter 3, the location of shunt reactors can be at the line ends (line-end compensation (LEC)) or distributed at multiple points along the route of the circuit. The technical convenience of the former or the latter has been assessed in [28], [29], where the shunt compensation allocation for different study cases has been analysed. The LEC is the most common scheme while the distributed techniques have additional advantages, most notably the increase of the available transfer capacity for the active power and the need for a lower degree of compensation [27].

To deduce the influence of compensation location on the statistical distribution of energization overvoltages, overvoltages of the cable-end compensation (CEC) were compared with those of the LEC. Therefore, instead of two reactor banks at two substations, six reactors banks (one at each cable termination) were considered with the sizes reported in Figure 3.8 for the load-flow B.

TABLE 5.4
KEY VALUES OF THE OVERVOLTAGE DISTRIBUTIONS WITH CEC (VALUES BETWEEN PARENTHESES ARE WITH LEC)

Scenario	Overvoltage (pu)			
	Max.	Mean	Stand. dev.	2% value
15% Cable	2.413 (2.631)	1.708 (1.756)	0.245 (0.262)	2.245 (2.346)
25% Cable	2.255 (2.499)	1.648 (1.694)	0.214 (0.245)	2.117 (2.269)
50% Cable	2.288 (2.705)	1.639 (1.689)	0.219 (0.259)	2.095 (2.319)
75% Cable	2.046 (2.810)	1.568 (1.626)	0.194 (0.256)	1.952 (2.329)
Fully Cable	1.876 (1.908)	1.493 (1.501)	0.155 (0.163)	1.783 (1.820)

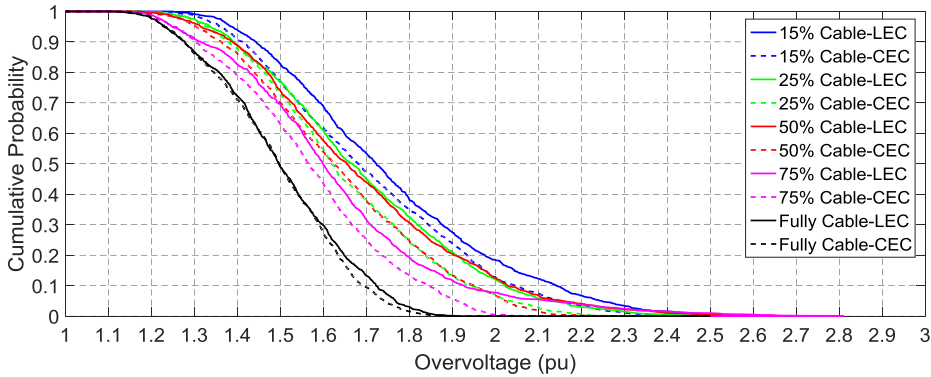


Figure 5.12: Cumulative probability distributions of energization overvoltages with LEC (solid lines) and CEC (dashed lines).

Table 5.4 presents the key values of the overvoltage distributions and Figure 5.12 shows the cumulative probabilities of energization overvoltages with CEC and LEC. The key values and cumulative probabilities of overvoltages in all CEC scenarios are lower than those of the LEC scenarios, indicating another advantage of the distributed compensation over the line-end compensation.

D. IMPACT OF SHORT CABLE SECTIONS

In practice, short cable sections may be utilized in a hybrid circuit (e.g. for water crossing). The short travelling time of the wave in short cable sections results in consecutive reflections and refractions at termination points leading to different overvoltages. To investigate this issue, six cases with short cable sections were defined for the 15% cable scenario. As illustrated in Figure 5.13, the lengths of the OHL sections are unchanged in all the cases and only the lengths of the cable sections are varied while the total cable length is constant (12 km). Case 1 is the base case as defined in Table 2.2. Cases 2, 3, and 4 have a 1 km-long cable section at the sending side, middle, and the receiving side of the circuit, respectively. Cases 5 and 6 have 1 km-long cable sections at middle plus the sending or receiving sides.

The maximum overvoltages and the cumulative probabilities of energization overvoltages are shown in Figures 5.14 and 5.15, respectively. It can be observed that Case 6 has the highest maximum overvoltage (3.3 pu) and overvoltage probability among all the cases, even higher than those of the fully-OHL scenario in Section 5.4.3.A. On the contrary, Case 5 has the lowest maximum (2.44 pu) and probability of overvoltages. In addition, after Case 6, the highest maximum and probability of overvoltages are produced by Case 4.

It can be concluded that for a given cable scenario, higher energization overvoltages are expected when very short cable sections are at the open-end of the circuit. For the studied cases, overvoltages are up to 0.86 pu (equal to 267 kV) higher than those of the cases without short cable sections. In contrast, the existence of longer cable sections at the

open-end results in lower overvoltages. This is due to the short travelling time of the propagating wave in the short cable sections and the successive reflections and refractions.

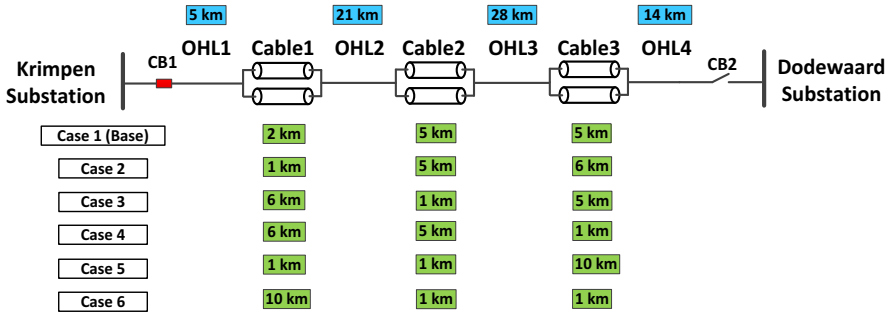


Figure 5.13: Cases of short cable sections for the 15% cable scenario (lengths of the OHL sections are unchanged).

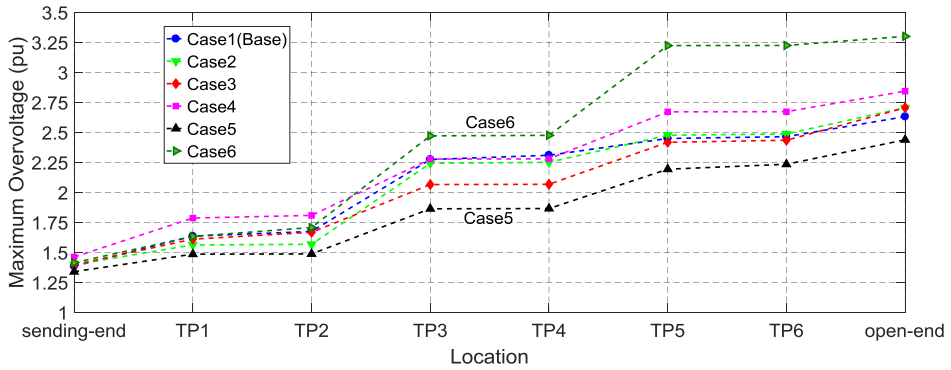


Figure 5.14: Maximum energization overvoltage at different locations along the hybrid OHL-Cable circuit for the cases in Figure 5.13.

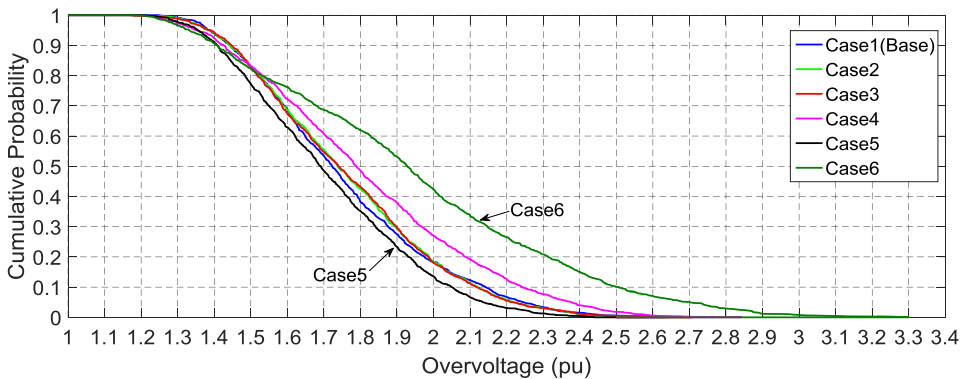


Figure 5.15: Cumulative probability distributions of energization overvoltages for the cases in Figure 5.13.

E. IMPACT OF SHORT-CIRCUIT POWER

The impact of the short-circuit power of the supply network on the statistical distribution of energization overvoltages was studied by the use of an equivalent grid model consisting of the hybrid circuit and a lumped parameter inductive source. In fact, the Thevenin equivalent was used instead of the whole grid model with distributed generation because it is more flexible and convenient to adjust the short-circuit power with the variation of the equivalent source impedance. A frequency-dependent network equivalent (FDNE) can be also an option to represent the entire grid if it can properly represent the generation and the short-circuit power of the grid [30].

In the equivalent model of the grid, the power-frequency voltage at the sending-end was adjusted to the same voltage in the whole grid model (1.076 pu). The statistical analysis was carried out for five source inductances: 15, 20, 25, 50, and 100 mH. The 20 mH source inductance is equal to the equivalent short-circuit inductance calculated at the sending substation in the whole grid model.

Figure 5.16 shows the maximum energization overvoltage and 2% value for different supply networks. For a given source inductance, the lowest and highest values are for the fully-cable and the fully-OHL scenarios, respectively. The only exception is the 50% cable scenario with 25 mH source inductance, for which the maximum overvoltage (3.36 pu) is higher than that of the fully-OHL scenario although the corresponding 2% value is still lower. In addition, for all source impedances, the hybrid scenarios produce overvoltages higher than those of the fully-cable scenario and most likely lower than those of the fully-OHL scenario. This conclusion is in line with the previous conclusions.

It can be also noticed that each cable scenario has a different behaviour than the other scenarios when the short-circuit power is varied. For the fully-OHL scenario, the maximum overvoltage decreases when the source inductance increases from 15 mH to 50 mH and thereafter slightly increases for 100 mH; but, the 2% value always decreases with increasing the source impedance (weaker supply networks). For the fully-cable scenario, both the maximum overvoltage and 2% value decrease by the increase of the source impedance. For the hybrid scenarios, the dependency of overvoltages on the supply network strength changes case-by-case.

As it was previously mentioned, the maximum energization overvoltage at the cable open-end is determined by the superposition of the inter-phase mode (as the dominant mode) and the coaxial mode (as the superimposed mode), where the cycle time of the inter-phase mode is dependent on the short-circuit power and the cable length [12]. For larger source impedances (weaker supply networks), the rate of rise of voltage is lower and the cycle time of the inter-phase mode (dominant mode) is longer. Thus, by the time the inter-phase mode reaches its maximum at the open-end, the coaxial mode has travelled back and forth to the open-end for several times and has become highly damped. As a result, the transient energization overvoltages will be likely lower when the source impedance is larger (weaker supply network).

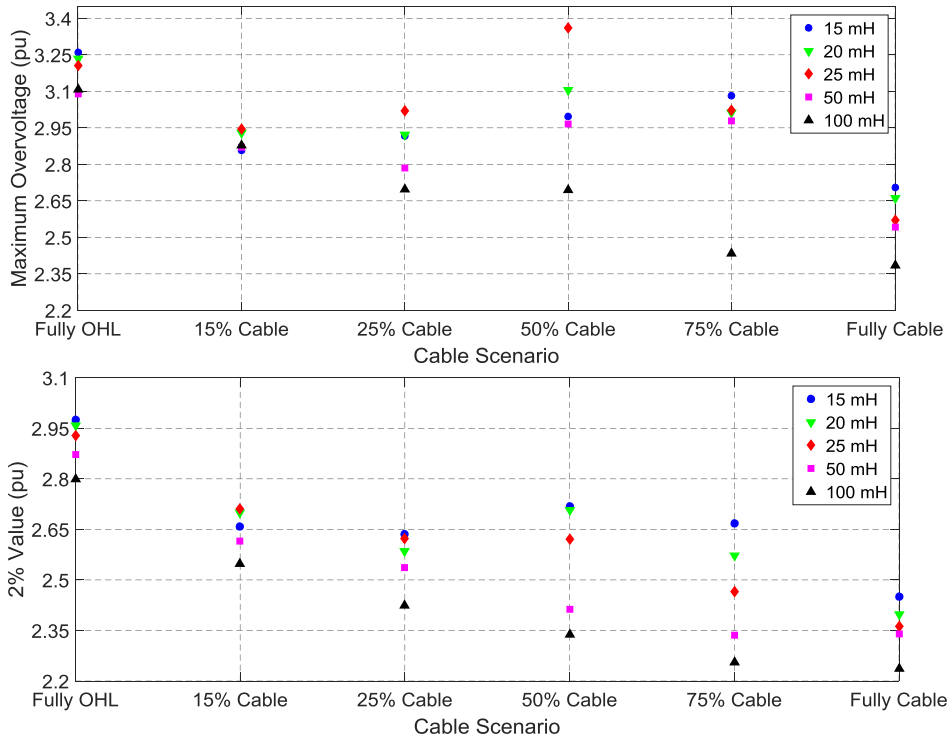


Figure 5.16: Maximum energization overvoltage and 2% value for different supply network short-circuit powers.

The comparison of the simulated overvoltages of the whole grid model in Table 5.1 with those of the equivalent model with 20 mH source inductance (as the corresponding inductance with the short-circuit power of the whole grid model) shows that the simulated overvoltages in the equivalent grid are higher. This is due to the fact that the actual damping and wave propagation to the rest of the grid are not represented by the equivalent grid.

F. IMPACT OF TRAPPED CHARGES

Trapped charges (residual charges) may exist on disconnected cables and result in very high overvoltages when the voltage of the trapped charges has opposite polarity to that of the switching surge [31]. The study was conducted by initial charging of the cables with three single-phase 30 kV dc voltage sources and then the statistical switching of the breakers whilst the dc sources were removed.

Table 5.5 and Figure 5.17 show the key values of the overvoltage distributions and the cumulative probability distributions, respectively. The maximum overvoltages are up to 0.68 pu higher than those of the cases without trapped charge, whereas the difference in 2% values is much less and only up to 0.07 pu. Moreover, the differences between the cumulative probabilities are negligible, indicating that the overvoltages are generally not higher except for particular switching instants at which the resulting switching surge and

the voltage of the trapped charges cause a very high overvoltage together. It should be noted that higher overvoltages can be expected if the residual voltage on the cables is higher than 30 kV.

TABLE 5.5
KEY VALUES OF THE OVERVOLTAGE DISTRIBUTIONS WITH TRAPPED CHARGES (VALUES BETWEEN PARENTHESES ARE WITHOUT TRAPPED CHARGES)

Scenario	Overvoltage (pu)			
	Max.	Mean	Stand. dev.	2% value
15% Cable	3.319 (2.631)	1.763 (1.756)	0.275 (0.262)	2.380 (2.346)
25% Cable	2.788 (2.499)	1.702 (1.694)	0.257 (0.245)	2.289 (2.269)
50% Cable	2.849 (2.705)	1.695 (1.689)	0.273 (0.259)	2.388 (2.319)
75% Cable	2.780 (2.810)	1.614 (1.626)	0.254 (0.256)	2.330 (2.329)
Fully Cable	2.036 (1.908)	1.498 (1.501)	0.167 (0.163)	1.828 (1.820)

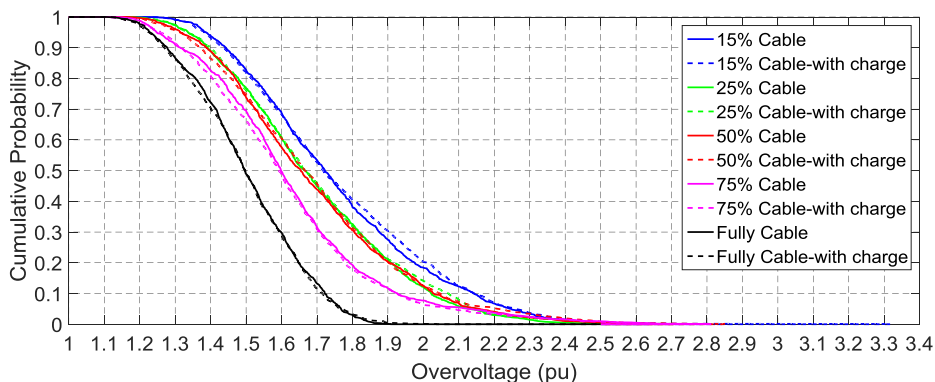


Figure 5.17: Cumulative probability distributions of energization overvoltages without trapped charges (solid lines) and with trapped charges (dashed lines).

G. IMPACT OF MIXED-LINE CONFIGURATION

It is also important to investigate the influence of the mixed-line configuration on the statistical distribution of energization overvoltages. For this purpose, the four mixed-line configurations presented in Section 2.3.1.C (with the section lengths presented in Tables 2.4 to 2.7) and the symmetrical study case configuration (with the section lengths presented in Tables 2.3) are compared. As concluded in Chapter 3, the required compensation size for each configuration is different, so the reported values in Figure 3.9 for the load-flow B were used.

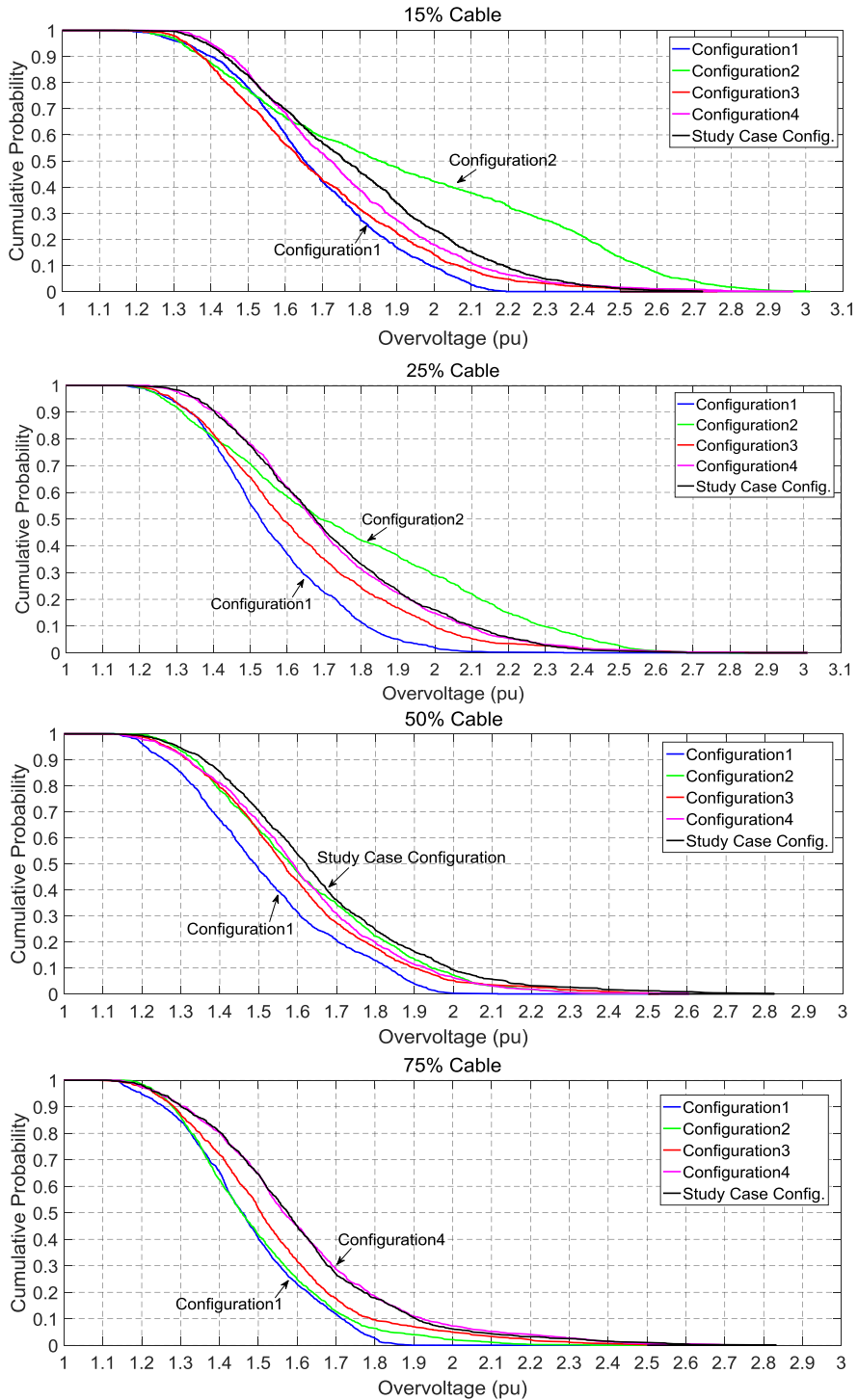


Figure 5.18: Cumulative probability distributions of energization overvoltages for different mixed-line configurations.

The cumulative probabilities of energization overvoltages are shown in Figure 5.18. It can be noticed that for a given cable scenario, the difference between the cumulative probabilities of different configurations can be up to 35%. Therefore, the number and the distribution of the OHL and cable sections can substantially affect overvoltages due to the consequent changes in the wave propagation pattern. In addition, Configuration 1, in which a long cable section is at the open-end of the circuit, produces the lowest overvoltages for all the scenarios. This finding is in line with the conclusions of Section 5.4.3.D. The reason that Configuration 1 produces lower overvoltages than the other configurations is as follows: when the travelling voltage wave through the OHL section reaches the transition point to the cable section, about 63% of the incident wave is reflected back (see equations 5.10 and 5.11) and only 37% of the incident wave is transmitted to the cable and moving towards the open-end. So, the resulting overvoltage at the open-end of the circuit will be reduced.

5.5 CONCLUSIONS

The statistical distribution of energization overvoltages plays an important role in the determination of the required insulation levels for EHV components. In this chapter, the distribution of energization overvoltages has been thoroughly studied for hybrid OHL-Cable circuits by means of numerous statistical switching simulations.

It has been found that a hybrid OHL-Cable circuit produces energization overvoltages higher than those of a fully-cable circuit and most likely lower than those of a fully-OHL circuit with the same transmission lengths. This means that the probability of experiencing high energization overvoltages and stressing system components is higher in a fully-OHL circuit than in a partial or fully undergrounded circuit.

Energization overvoltages are dependent on the number, locations, and lengths of the OHL and cable sections because of the consequent changes in the energizing wave propagation. For a given cable scenario, the existence of long cable sections at the open-end of the circuit results in lower energization overvoltages compared to the case that short cable sections are at the open-end. In addition, the difference between the overvoltage cumulative probabilities of different mixed-line configurations can be also substantial, where, as an example, it was up to 35% for the studied configurations in this paper. This shows the high impact of the number and the distribution of the OHL and cable sections on energization overvoltages.

Furthermore, energization overvoltages can be substantially affected by the system parameters, most notably the short-circuit power of the supply network and the shunt compensation size and location. The transient energization overvoltages are likely lower when the network short-circuit power is lower (i.e. weaker supply network), whereas the post-switching steady-state overvoltages will be higher due to the Ferranti effect at the open-end of the circuit. Moreover, the distributed reactive power compensation along the circuit, like CEC, results in lower overvoltages compared to the line-end compensation.

Finally, in hybrid OHL-Cable circuits, extremely high overvoltages (higher than 3 pu) may occur in specific cases such as the presence of trapped charges on the cable, the presence of very short cable sections at the open-end of the circuit, and certain short-circuit powers of the supply network. Special attention should be paid to these situations as they can lead to a component failure and/or exceeding the energy absorption capacity of surge arresters and sheath voltage limiters.

REFERENCES

- [1] “Insulation Co-Ordination-Part 2: Application Guide,” IEC 60071-2 , 1996.
- [2] “Insulation Co-Ordination-Part 1: Definitions, Principles and Rules,” IEC 60071-1, 2006.
- [3] CIGRE Working Group 21/33, “Insulation co-ordination for HV AC underground cable systems,” *CIGRE Technical Brochure no. 189*, June 2001.
- [4] A. R. Hileman, *Insulation Coordination for Power Systems*, New York, USA: Marcel Dekker, June 1999.
- [5] R. Smeets, L. van der Sluis, M. Kapetanovic, D. Peelo and A. Janssen, *Switching in Electrical Transmission and Distribution Systems*, Hoboken, NJ, USA: Wiley, 2015.
- [6] “Live Tank Circuit Breakers: Buyer’s Guide,” 6th ed., ABB, Ludvica, Sweden, 2014.
- [7] CIGRE Working Group 13.02, “Switching overvoltages in EHV and UHV systems with special reference to closing and reclosing transmission lines,” *Electra*, no. 30, pp. 70–122, 1973.
- [8] CIGRE Working Group 13.05, “The calculation of switching surges,” *Electra*, no. 19, pp. 67-78, 1971.
- [9] CIGRE Working Group 13.05, “The calculation of switching surges-II. Network representation for energization and re-energization studies on lines fed by an inductive source,” *Electra*, no. 32, pp. 17-42, 1974.
- [10] CIGRE Working Group 13.05, “The calculation of switching surges-III. Transmission line representation for energization and re-energization studies with complex feeding networks,” *Electra*, no. 62, pp. 45-78, 1979.
- [11] T. Ohno, C. L. Bak, A. Ametani, W. Wiechowski and T. K. Sorensen, “Statistical distribution of energization overvoltages of EHV cables,” *IEEE Transactions on Power Delivery*, vol. 28, no. 3, pp. 1423-1432, July 2013.
- [12] T. Ohno, A. Ametani, C. L. Bak, W. Wiechowski and T. K. Sørensen, “Analysis of the statistical distribution of energization overvoltages of EHV cables and OHLs,” in *International Conference on Power System Transients (IPST)*, Vancouver, Canada, July 2013.
- [13] P. Mestas and M. C. Tavares, “Relevant parameters in a statistical analysis-application to transmission-line energization,” *IEEE Transactions on Power Delivery* , vol. 29, no. 6, pp. 2605-2613, December 2014.
- [14] A. H. Hamza, S. M. Ghania, A. M. Emam and A. S. Shafy, “Statistical analysis of switching overvoltages and insulation coordination for a 500 kV transmission line,” in *18th International Middle East Power Systems Conference*, Cairo, Egypt, December 2016.
- [15] M. Z. Daud, P. Ciufu and S. Perera, “Statistical analysis of overvoltages due to the energization of a 132 kV underground cable,” in *6th ECTI Conference*, Pattaya, Thailand, May 2009, pp. 54-57.

- [16] J. A. Martinez, R. Natarajan and E. Camm, "Comparison of statistical switching results using Gaussian, uniform and systematic switching approaches," in *IEEE Power Engineering Society Summer Meeting*, Seattle, USA, July 2000, pp. 884-889.
- [17] Y. Itoh, N. Nagaoka and A. Ametani, "Transient analysis of a crossbonded cable system underneath a bridge," *IEEE Transactions on Power Delivery*, vol. 5, no. 2, pp. 527-532, April 1990.
- [18] H. Khalilnezhad, M. Popov, J. A. Bos, J. P. W. de Jong and L. van der Sluis, "Investigation of statistical distribution of energization overvoltages in 380 kV hybrid OHL-cable systems," in *International Conference on Power System Transients (IPST)*, Seoul, Republic of Korea, June 2017.
- [19] A. I. Ibrahim and H. W. Dommel, "A knowledge base for switching surge transients," in *International Conference on Power System Transients (IPST)*, Montreal, Canada, 2005.
- [20] I. Lafaia, J. Mahseredjian, A. Ametani, M. T. Correia de Barros, I. Kocar and Y. Fillion, "Frequency and time domain response of cross-bonded cables," *IEEE Transactions on Power Delivery*, vol. 33, no. 2, pp. 640-648, April 2018.
- [21] F. F. da Silva and C. L. Bak, *Electromagnetic Transients in Power Cables*, London, UK: Springer, 2013.
- [22] C. F. Jensen, U. S. Gudmundsdottir, C. L. Bak and A. Abur, "Field test and theoretical analysis of electromagnetic pulse propagation velocity on crossbonded cable systems," *IEEE Transactions on Power Delivery*, vol. 29, no. 3, pp. 1028-1034, June 2014.
- [23] A. Ametani, T. Ohno and N. Nagaoka, *Cable System Transients: Theory, Modeling and Simulation*, Singapore: Wiley, July 2015.
- [24] CIGRE Working Group B1.30, "Cable systems electrical characteristics," *CIGRE Technical Brochure no. 531*, April 2013.
- [25] A. Greenwood, *Electrical Transients in Power Systems*, Hoboken, NJ, USA: Wiley, 1971.
- [26] L. van der Sluis, *Transients in Power Systems*, Chichester, UK: Wiley, August 2001.
- [27] H. Khalilnezhad, S. Chen, M. Popov, J. A. Bos, J. P. W. de Jong and L. van der Sluis, "Shunt compensation design of EHV double-circuit mixed OHL-cable connections," in *IET International Conference on Resilience of Transmission and Distribution Networks*, Birmingham, UK, 2015.
- [28] S. Lauria, F. M. Gatta and L. Colla, "Shunt compensation of EHV cables and mixed overhead-cable lines," in *IEEE Power Technology Conference*, Lausanne, Switzerland, July 2007.
- [29] R. Benato and A. Paolucci, "Operating capability of long AC EHV transmission cables," *Electric Power System Research*, vol. 75, pp. 17-27, 2005.
- [30] J. Morales, J. Mahseredjian, K. Sheshyekani, A. Ramirez, E. Medina and I. Kocar, "Pole-selective residue perturbation technique for passivity enforcement of FDNEs," *IEEE Transactions on Power Delivery*, DOI:10.1109/TPWRD.2018.2810706, March 2018.
- [31] F. Ghassemi, "Effect of trapped charges on cable SVL failure," *Electric Power Systems Research*, vol. 115, pp. 18-25, 2014.

CHAPTER 6

ZERO-MISSING PHENOMENON IN CABLE SYSTEMS

6.1 INTRODUCTION

As it was mentioned in the previous chapters, the operation of long cables requires reactive power compensation by means of shunt reactors. In most situations, shunt reactors should be directly connected to the hybrid circuit and energized together with the cable to minimize post-switching steady-state overvoltages and to control the capacitive current in the line breaker [1], [2].

The simultaneous energization of the cable and reactors may cause the zero-missing phenomenon, which is the situation that the current through the line breaker does not cross the zero value for several cycles (even up to several seconds). In this situation, it is difficult or even impossible to safely open the healthy phases if a fault occurs in the circuit during energization when the zero-missing current is still present. Therefore, the system is more vulnerable and unprotected against faults when proper countermeasures are not devised at the design stage of the cable project.

Several countermeasures are available for the zero-missing phenomenon, while each of those has advantages and disadvantages depending on the grid topology and specifications. Synchronized switching at the voltage peak, sequential switching, and the use of circuit breakers equipped with pre-insertion resistors are the mostly studied countermeasures in the literature [3-6].

In [3], switching at the voltage peak was applied to avoid the zero-missing phenomenon based on an insulation coordination study. In [4], the authors studied the use of pre-insertion resistors to minimize the zero-missing current, where they proposed a simple formula to approximate the resistor value. The expanded version of [4] has been presented in [5], where extra countermeasures of the zero-missing phenomenon have been also discussed. In addition, an iterative process for more accurate determination of the pre-insertion resistor size has been provided in [5]. In [6], a general overview of the countermeasures and a more detailed study of the sequential switching countermeasure can be found.

There are three important aspects regarding countermeasures of the zero-missing phenomenon that have not been addressed in the literature: (a) the resulting transient

overvoltages and inrush currents after applying a countermeasure, (b) the impact of the circuit breaker mechanical delay on the effectiveness of an applied countermeasure, (c) the influence of hybrid OHL-Cable circuits and the cable length on the effectiveness of an applied countermeasure.

Furthermore, several additional countermeasures to the studied measures in the literature are available, which have not been investigated so far. Under some circumstances, these measures can be more effective solutions for the zero-missing phenomenon. Therefore, it is required to carry out a comprehensive study, which implements all countermeasures on a reference system and does a comparison based on a set of system operation criteria.

The goal of this chapter is to address the mentioned scientific gaps by performing an in-depth investigation on countermeasures of the zero-missing phenomenon and determining the requirements, benefits, and deficiencies of each method. Countermeasures are compared in terms of resulting currents and voltages after their implementation. High transient overvoltages, a voltage dip/swell, and high inrush currents may occur when a particular countermeasure is applied. Applying a countermeasure should result in neither switching overvoltages nor inrush currents over the permissible limits.

Countermeasures were applied for the Spaak connection, for which six cable scenarios were defined in Chapter 2 and shunt compensation sizes were calculated in Chapter 3. It is of high importance to take the impact of the cable length into account since a countermeasure may be the optimal solution only for a certain range of the cable length, depending on system specifications. Moreover, the switching sequence of breakers is determined for each countermeasure. This can be implemented in practice by applying the controlled switching (also known as synchronized or point-on-wave switching) in combination with single-pole operated circuit breakers.

This chapter is structured as follows: Section 6.2 explains the zero-missing phenomenon and parameters affecting it. The defined operation criteria and the studied countermeasures are presented in Sections 6.3 and 6.4, respectively. Section 6.5 is dedicated to the simulation results, where countermeasures are analysed and compared with respect to the operation criteria. The paper methodology and findings are discussed in Section 6.6, and finally, conclusions are presented in Section 6.7.

6.2 ZERO-MISSING PHENOMENON

The zero-missing phenomenon can be simply illustrated by the cable system (i.e. the cable and the shunt reactor) shown in Figure 6.1. The cable system is energized by a voltage source.

When the reactor is being energized, its charging current has two components, an AC-component and a decaying DC-component:

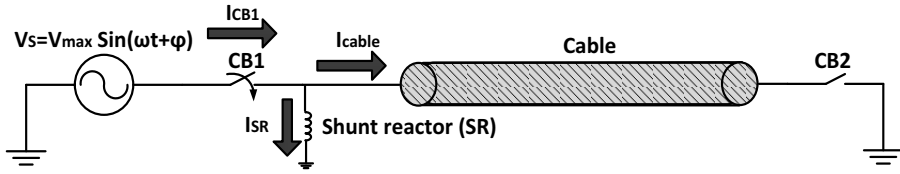


Figure 6.1: Single-line diagram of a simple shunt-compensated cable system (CB: circuit breaker).

$$I_{SR}(t) = e^{-\left(\frac{R}{L}\right)t} \left[\underbrace{\frac{-V_{\max}}{|Z|} \sin(\varphi - \theta)}_{\text{DC component } (I_{SR,dc})} \right] + \underbrace{\frac{V_{\max}}{|Z|} \sin(\omega t + \varphi - \theta)}_{\text{AC component } (I_{SR,ac})} \quad (6.1)$$

where R , L , and Z are respectively resistance, inductance, and impedance of the reactor. V_{\max} is the voltage amplitude, φ is the initial phase angle of the voltage (i.e. the point on the voltage waveform at which the breaker is closed), and θ is the load angle. As it is seen, the initial value of the DC-component depends on the initial phase angle and its decaying time depends on the time constant, expressed by $\tau = \frac{L}{R}$. The DC-component is maximum (equal to the amplitude of the AC-component at $t = 0$) when $\varphi - \theta$ is 90° , and is zero when $\varphi - \theta$ is zero.

The current through the line circuit breaker (CB1) when the circuit is being energized is as below:

$$\begin{aligned} I_{CB1}(t) &= I_{SR}(t) + I_{cable}(t) \\ &= \underbrace{I_{SR,dc}(t)}_{\text{DC comp.}} + \underbrace{(I_{SR,ac}(t) + I_{cable}(t))}_{\text{AC component}} \end{aligned} \quad (6.2)$$

$$I_{SR,ac}(t) = -K_{sh} \times I_{cable}(t) \quad (6.3)$$

where I_{CB1} is the current through the circuit breaker, I_{SR} is the energization current of the shunt reactor, and I_{cable} is the cable charging current. K_{sh} is the shunt compensation degree and shows the percentage of the cable reactive power which is compensated by the shunt reactor (as explained in Chapter 3). Due to simplicity reasons, it is assumed that in equations 6.2 and 6.3 the cable is a pure capacitor and the resistance of the shunt reactor is zero in the AC-component (these simplifications have a negligible influence).

As it is shown in equation 6.3, the AC-component of the reactor current has an opposite phase angle with the cable charging current. Therefore, in equation 6.2, the AC-component of the reactor current is partially (or completely if the compensation degree is 100%) cancelling out the cable charging current. When the compensation degree is higher than 50%, the AC-component in equation 6.2 may become smaller than the DC-component, so that the total current (I_{CB1}) does not cross the zero point until the DC-component is sufficiently damped. Thus, the zero-missing phenomenon can occur if two conditions are

satisfied: (1) energization of the shunt reactor together with the cable, (2) shunt compensation degree larger than 50% ($K_{sh} > 50\%$).

Assume that the length of the cable in Figure 6.1 is 60 km and the shunt compensation degree is 92.1% (according to the compensation sizing results presented in Chapter 3, Table 3.2). The system is energized in two cases: (1) closing each phase at the zero voltage, (2) closing each phase at the voltage peak. Note that this can be realized in practice by means of the controlled switching and single-pole operated circuit breakers. Resulting currents and voltages after energization at the zero voltage and at the voltage peak (obtained by PSCAD simulations) are respectively shown in Figures 6.2 and 6.3.

Figures 6.2a and 6.2b respectively show the cable charging current (I_{cable}) and the shunt reactor current (I_{SR}) when each phase is energized at the zero voltage. The DC-component of the shunt reactor current is maximum since $\varphi=0$ and $\theta \approx 90^\circ$ (see equation 6.1). However, the reactor current always touches the zero point because its maximum DC-offset is equal to the amplitude of its AC-component. Figure 6.2c shows the current through the circuit breaker ($I_{CB1} = I_{cable} + I_{SR}$). The total AC-component is very small due to the cancelation of 92.1% of the cable charging current by the AC-component of the reactor current. Thus, the total current flowing through the circuit breaker is mainly DC and is not crossing the zero point. The main benefit of switching at voltage zero is that the cable charging inrush currents (Figure 6.2a) and the transient switching overvoltages (Figure 6.2d) are minimized.

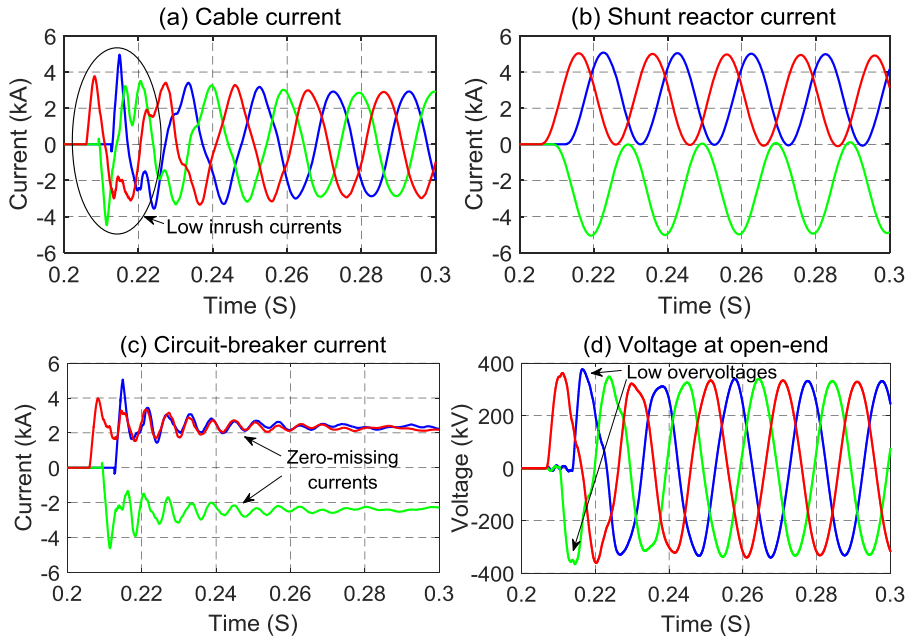


Figure 6.2: Currents and open-end voltages after the energization of the circuit in Figure 6.1 at the zero voltage (60 km cable, $K_{sh} = 92.1\%$).

In contrast, the DC-component is zero if each phase is closed at the voltage peak ($\varphi = 90^\circ$ and $\theta \approx 90^\circ$ in equation 6.1), as shown in Figure 6.3b. This means that the zero-missing phenomenon does not occur (Figure 6.3c). However, in comparison to the switching at the zero voltage, the cable charging inrush currents (Figure 6.3a) and the transient switching overvoltages (Figure 6.3d) are higher.

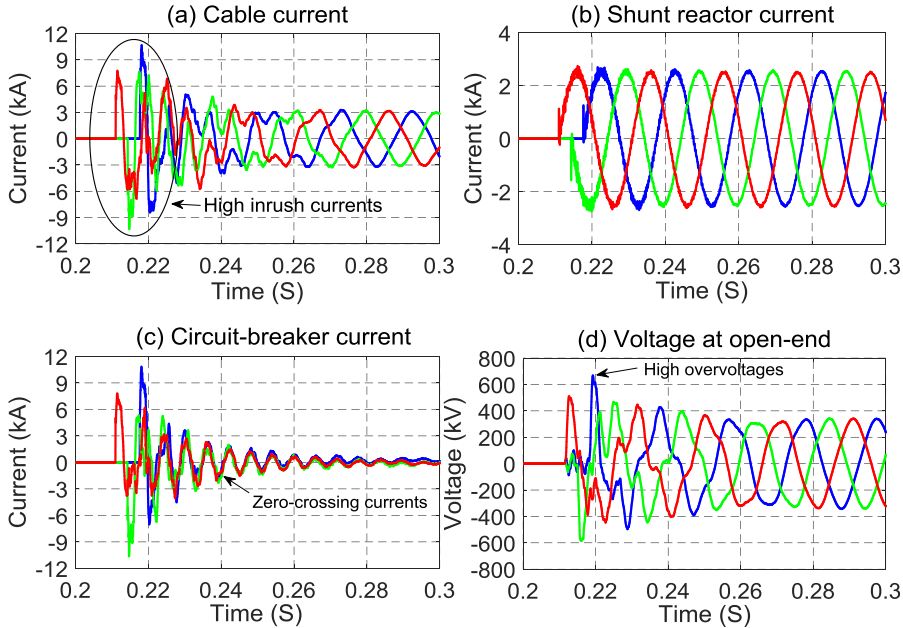


Figure 6.3: Currents and open-end voltages after the energization of the circuit in in Figure 6.1 at the voltage peak (60 km cable, $K_{sh} = 92.1\%$).

6.3 OPERATION CRITERIA

The implementation of a countermeasure can cause high and very steep inrush currents and/or transient switching overvoltages. High inrush currents and voltage surges increase dielectric and mechanical stresses on circuit breakers and other system components. These stresses can cause immediate or gradual damages of equipment and affect the system reliability [7].

It is important to define clear criteria based on the system operation limits and standards to evaluate voltages and currents after implementation of a countermeasure. Therefore, three criteria are defined based on the specified requirements for circuit breakers, insulation coordination, and power quality by manufacturers, the IEC standards, and the grid code. These criteria are:

1. *Amplitude and frequency of inrush current*: the countermeasure should not cause high inrush currents recognized to be harmful for breakers and other components [7], [8]. For capacitor banks, standardized peak value and frequency of capacitive inrush

currents are 20 kA and 4.25 kHz, respectively [8], [9]. These values are used in this paper since the cable energization inrush current is almost similar to that of an equivalent capacitor bank. However, it should be noted that the amplitude and the rate-of-rise of the cable inrush current are normally lower than those of an equivalent capacitor bank due to the relatively higher surge impedance of cables [7].

2. *Transient switching overvoltages*: the peak values of the phase-to-earth transient energization overvoltages after implementation of a countermeasure should remain below the switching impulse withstand voltage (SIWV) of 3.38 pu (1050 kV), as the specified value in [10] for 380 kV equipment¹.
3. *RMS voltage step*: the IEC standard [11] and the Dutch grid code impose limits for the quick changes in the RMS voltage between two steady-states. This criterion is mainly related to the power quality and minimization of the disturbance to consumers. After switching, RMS voltages should be within the voltage dip and swell thresholds of 0.9 pu (342 kV) and 1.1 pu (418 kV), respectively. In addition, the rapid voltage change (RVC) should be smaller than 3% (11.4 kV). The time frame for the calculation of the RMS value is half of the power-frequency cycle (10 ms in 50 Hz systems).

6.4 COUNTERMEASURES

The main goal of this chapter is to analyse and compare various countermeasures of the zero-missing phenomenon. The countermeasures fall into one of the following three categories:

1. *Prevention methods*: the zero-missing current will be avoided by the application of these countermeasures.
2. *Mitigation methods*: these measures do not prevent the occurrence of the zero-missing current, but they minimize the decaying time of the DC-component by increasing the system damping (i.e. smaller time constant), so that the current through the breaker crosses the zero point faster.
3. *Handling methods*: these measures are neither helping to avoid nor to mitigate the zero-missing current. However, they help system operators to safely open the breakers when a fault occurs in the hybrid circuit at the instant of, or after, energization when the zero-missing phenomenon is still present.

In this study, the following six countermeasures are analysed and compared, where detailed elaborations on them can be found in the next section:

1. Simultaneous cable and reactors energization at the voltage peak
2. In advance cable energization
3. In advance reactor energization

¹ The IEC 60071-1 standard has specified 850, 950, or 1050 kV (peak value) for the phase-to-earth switching impulse withstand voltage of equipment with 420 kV highest RMS voltage.

4. Sequential switching
5. Opening of the faulted phase(s)
6. Increasing the DC-offset damping

6.5 SIMULATION RESULTS

This section presents the simulation results when the countermeasures are tested on the Spaak connection. The mixed-line configuration is as shown in Figure 2.3 with the cable scenarios defined in Table 2.2. Shunt compensation sizes are according to the values reported in Table 3.2, which are determined by the steady-state analysis presented in Chapter 3. The energization of one of the circuits from the Krimpen substation was simulated and analysed by the use of the developed grid model in PSCAD, as the model was described in Chapter 2. Transient overvoltages are expressed in per unit, where the base value (1 pu) is the peak value of the phase-to-earth nominal voltage (310.27 kV). Overvoltages were recorded at the open-end (unless differently specified) since the highest overvoltages are occurring there.

In the first step, it is important to investigate the influence of the cable length on the severity of the zero-missing phenomenon. Figure 6.4 shows the current through the line breaker for the six cable scenarios when each phase is energized by the controlled switching at the zero voltage. With the increasing cable share, the zero-missing phenomenon becomes more severe in terms of the amplitude of the DC-component and the required time for the first zero crossing. This is due to a larger DC-component (because of bigger compensation size, i.e. smaller $|Z|$, in equation 6.1) and a smaller AC-component (because of higher degree of compensation) when the cable length is increased. As the result, the current through the line breaker is dominantly a high-amplitude and low-damped DC current.

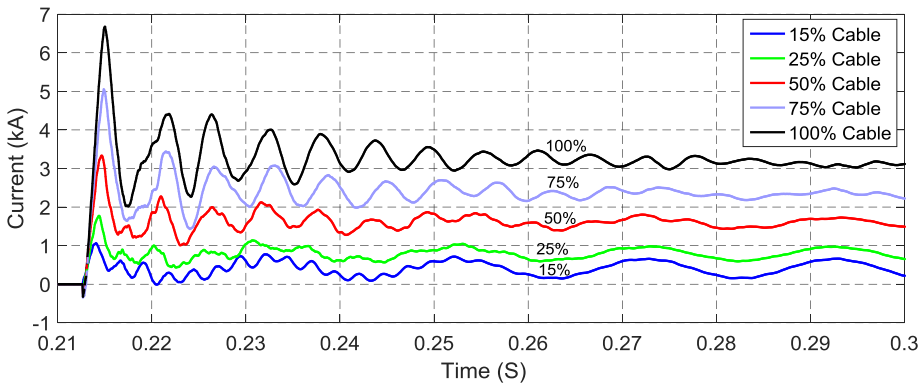


Figure 6.4: Line breaker current (I_{CBI} , phase A) for the six cable scenarios when each phase is energized at the zero voltage.

6.5.1 SIMULTANEOUS CABLE AND REACTORS ENERGIZATION AT THE VOLTAGE PEAK

This technique proposes to energize each cable phase together with shunt reactors of that phase at its voltage peak (requires controlled switching and single-pole operated breakers). This is a prevention countermeasure, but higher switching overvoltages and higher inrush currents are expected due to the energization at the voltage peak. Figure 6.5 shows the resulting current when this measure is applied. With increasing the cable length, the inrush current peak value becomes higher (around 13 kA for the 100% cable (fully-cable) scenario) due to the larger circuit capacitance; however, the peak values and the frequencies of the inrush currents are still within the specified limits.

Table 6.1 shows the maximum overvoltage at the open-end of the circuit when energization is performed at the voltage peak (i.e. when this countermeasure is applied) and at the zero voltage. It can be seen that in some cases the resulting overvoltages by switching at the voltage peak are almost double of those resulted by switching at the zero voltage. Although the overvoltages are higher, they are still below the specified limit of 3.38 pu for the studied cable scenarios.

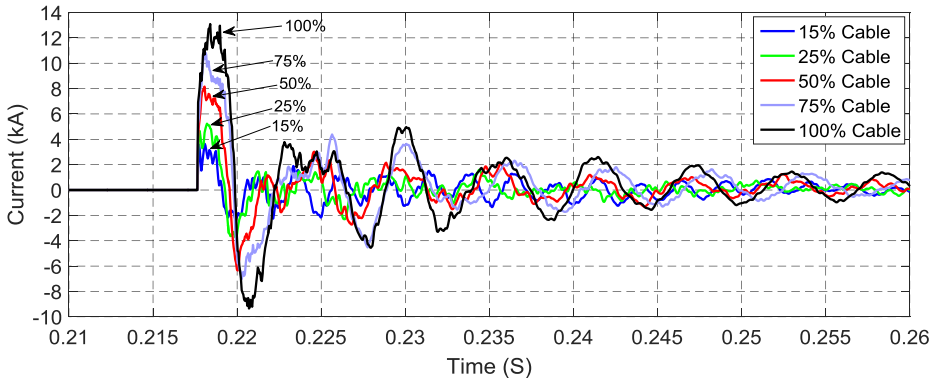


Figure 6.5: Line breaker current (I_{CB1} , phase A) for the six cable scenarios when each phase is energized at the voltage peak (Countermeasure 6.5.1).

TABLE 6.1
OVERVOLTAGES AT THE CIRCUIT OPEN-END AFTER CLOSING EACH PHASE AT THE VOLTAGE PEAK AND THE ZERO VOLTAGE

Scenario	Maximum overvoltage (pu)					
	Synchronized switching at zero voltage			Synchronized switching at voltage peak		
	Phase A	Phase B	Phase C	Phase A	Phase B	Phase C
15% Cable	1.128	1.186	1.199	2.159	1.650	2.182
25% Cable	1.125	1.202	1.141	1.973	2.056	1.724
50% Cable	1.128	1.193	1.147	2.224	2.111	1.682
75% Cable	1.215	1.180	1.170	2.153	1.892	1.647
100% Cable (Fully Cable)	1.209	1.135	1.151	2.063	1.763	1.615

It should be pointed out that the resulting overvoltages are dependent on the system topology and parameters such as the number/location/length of OHL and cable sections, the steady-state voltage prior to the switching, and the system short-circuit power. The distribution and length of OHL and cable sections can significantly affect the resulting overvoltages due to the changes in reflections and refractions of the propagating wave at the transition points. These remarks were proved in Chapter 5 by the statistical analysis of energization overvoltages.

This countermeasure requires an accurate controlled switching to close each pole of the breaker at its voltage peak. As it was previously mentioned in Chapter 5, breakers are in practice not ideal and they show variations in their operating times [7], [9]. Variations in the operating time are either predictable or stochastic. Predictable variations (e.g. long-term aging) do not affect the effectiveness of the controlled switching and can be compensated by an adaptive control. However, stochastic variations (inherent scatter) of the operating time can result in energization of the cable and reactors at a point different than the voltage peak. This limitation of the controlled switching can be described by the statistical distribution function of the scatter [7].

A statistical analysis was carried out to find the influence of stochastic variations in the breaker closing time on the probability distribution of energization overvoltages. For each breaker pole, the closing time was varied by a normal (Gaussian) distribution. The mean value was the instant at which the voltage peak of that pole occurs, the standard deviation (σ) was 1 ms, and the distribution curve was truncated at -3σ and $+3\sigma$. 50 closing times were simulated for each pole to obtain an accurate set of statistical data [3], [7], [12]. The statistical simulations were implemented in PSCAD by the use of the multiple-run feature and random number generators based on the normal distribution.

Table 6.2 shows the maximum, mean, standard deviation, and 2% values of the obtained overvoltage distributions for the six cable scenarios. The 2% value is the overvoltage value that the probability of this value being exceeded is 2% [13]. From each energization simulation, the peak value of the phase-to-earth overvoltage on each phase at the circuit open-end was included in the overvoltage probability distribution (known as the phase-peak method [12]). It can be seen that for the studied scenarios, the maximum recorded overvoltage is 2.406 pu, which is below the specified limit of 3.38 pu.

TABLE 6.2
KEY VALUES OF THE ENERGIZATION OVERVOLTAGE DISTRIBUTIONS WHEN COUNTERMEASURE 6.5.1 IS APPLIED

Scenario	Overvoltage (pu)			
	Max.	Mean	Standard deviation (σ)	2% value
15% Cable	2.406	1.879	0.279	2.393
25% Cable	2.378	1.755	0.271	2.283
50% Cable	2.355	1.861	0.216	2.134
75% Cable	2.188	1.850	0.248	2.181
100% Cable (Fully Cable)	2.151	1.818	0.218	2.132

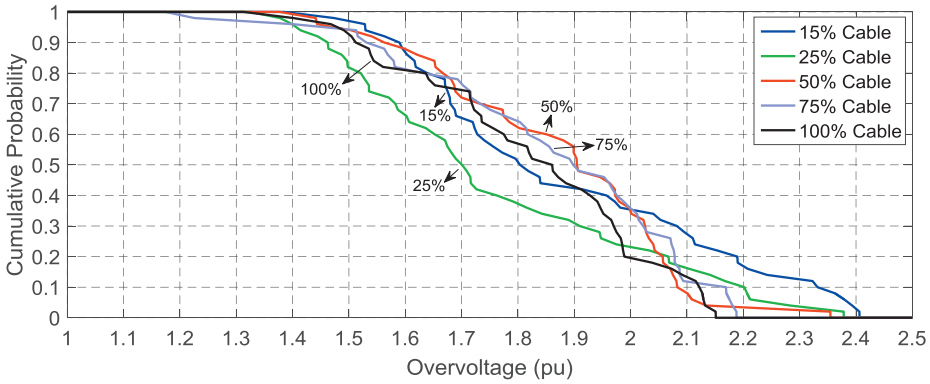


Figure 6.6: Cumulative probability distributions of overvoltages at the circuit open-end due to stochastic variations in the breaker closing time when Countermeasure 6.5.1 is applied.

Figure 6.6 shows the cumulative probability of overvoltages obtained by the statistical variation of the closing time. For a given voltage level, the vertical axis shows the cumulative probability of overvoltages exceeding that voltage level.

When the stochastic variation in the pole closing time exceeds a threshold, the cable and reactors are energized at a point on the voltage waveform at which the DC-component of the line breaker current is larger than the AC-component. This means that the zero-missing current occurs although it was supposed to be avoided by energizing at the voltage peak as the aimed closing point. Therefore, this countermeasure will be successful only if the stochastic variation in the breaker closing time is not exceeding the threshold. This threshold is named here breaker closing variation threshold (BCVT).

The BCVT shows the maximum variation in the breaker closing time (ΔT_{BCVT}) around the instant of the voltage peak (T_{peak}), for which the breaker current crosses the zero point before a given time limit. If the pole is not closed at $T_{peak} - \Delta T_{BCVT} < T < T_{peak} + \Delta T_{BCVT}$, the absolute value of the DC-component of the current through the line breaker will be larger than the absolute value of the AC-component, thus the total current does not cross the zero point before the given time limit. The time limit can be defined based on the preference of the system operator.

To calculate the BCVT, first the line breaker current should be calculated as a function of the breaker closing time. This can be done by the use of system parameters including the OHL and cable impedances, shunt reactor impedance, and shunt compensation degree. Then, the maximum variation in the breaker closing time around the instant of the voltage peak, for which the line breaker current has a first zero-crossing before the given time limit, is calculated by an iterative process. This means that the BCVT is calculated under the condition that the zero-missing current should not occur, or, when it occurs, it should disappear within the given time limit after the closing time.

TABLE 6.3
BCVT FOR DIFFERENT TIME LIMITS AND THE FIVE CABLE SCENARIOS OF THE SPAAK CONNECTION

Scenario	Time limit										
	10 ms	20 ms	40 ms	60 ms	80 ms	100 ms	500 ms	1 s	2 s		
15% Cable	±0.71ms (±12.8°)	±1.42ms (±25.6°)	±1.43ms (±25.7°)	±1.43ms (±25.8°)	±1.44ms (±25.9°)	±1.45ms (±26°)	±1.54ms (±27.7°)	±1.67ms (±30°)	±1.67ms (±30°)		
25% Cable	±0.21ms (±3.7°)	±0.57ms (±10.3°)	±0.57ms (±10.3°)	±0.58ms (±10.4°)	±0.58ms (±10.4°)	±0.58ms (±10.5°)	±0.64ms (±11.6°)	±0.72ms (±13°)	±0.87ms (±15.7°)		
50% Cable	±0.13ms (±2.3°)	±0.38ms (±6.8°)	±0.38ms (±6.9°)	±0.38ms (±6.9°)	±0.39ms (±7°)	±0.39ms (±7.1°)	±0.46ms (±8.3°)	±0.55ms (±9.9°)	±0.69ms (±12.5°)		
75% Cable	±0.08ms (±1.5°)	±0.27ms (±4.8°)	±0.27ms (±4.9°)	±0.27ms (±4.9°)	±0.28ms (±5°)	±0.28ms (±5.1°)	±0.35ms (±6.3°)	±0.43ms (±7.7°)	±0.53ms (±9.6°)		
100% Cable (Fully Cable)	±0.04ms (±0.8°)	±0.15ms (±2.7°)	±0.16ms (±2.8°)	±0.16ms (±2.8°)	±0.16ms (±2.9°)	±0.16ms (±2.9°)	±0.21ms (±3.8°)	±0.27ms (±4.8°)	±0.32ms (±5.8°)		

Table 6.3 shows the calculated BCVT for different time limits and for the five cable scenarios of the Spaak connection. The values between parentheses are the corresponding angles in degrees. As it is shown, for a given cable scenario, BCVT increases when the time limit increases.

For a given time limit, the BCVT is smaller for longer cables since the higher degree of compensation required for longer cables results in a line breaker current with a small AC-component but a large DC-component (see Figure 6.4). The dominant DC-component is very low-damped (due to the large time constant of shunt reactors) and sensitive to variations of the closing time. In other words, in equation 6.1, any change in $\sin(\varphi - \theta)$ is magnified by $\frac{V_{max}}{|Z|}$, which is larger for longer cables due to bigger compensation size (i.e. smaller $|Z|$). Thus, for longer cables, any variation in the closing time has a more noticeable impact on the DC-component of the line breaker current.

Knowing the BCVT is crucial because it specifies the required accuracy of breakers used for this countermeasure. In some cases, this countermeasure is not a reliable solution when the breaker delay can exceed the BCVT.

6.5.2 ENERGIZATION IN SEQUENCE

The main drawbacks of the previous countermeasure, in which both the cable and reactors were energized together at the voltage peak, were high transient overvoltages and inrush currents. However, the zero-missing phenomenon can be also avoided when the shunt reactors are energized with an intentional delay before or after the instant of cable energization. In this countermeasure, with a controlled time delay between energizations, the transient overvoltages are minimized by energizing the cable at the zero voltage and the zero-missing current is avoided by energizing the reactors at the voltage peak.

The key parameter for the success of this countermeasure is to keep the time delay between the cable energization and the shunt reactors energization as short as possible. Otherwise, a long delay may lead to a voltage dip/swell, RVC larger than 3%, and under/over excitation of nearby generators [2].

This prevention countermeasure can be realized in two ways, depending on whether cable or reactor is energized first. They are named *in advance cable energization* and *in advance reactor energization* countermeasures. The application of these methods requires the controlled switching and single-pole operated breakers. Breakers planned to close at voltage peaks (i.e. reactor breakers) should be tested to comply with the BCVT to ensure that the zero-missing current is avoided. However, breakers switching at the zero voltage should not necessarily comply with the BCVT requirement since they do not affect the DC-offset of the current.

A. IN ADVANCE CABLE ENERGIZATION

In this countermeasure, each cable phase is energized at the zero voltage and a quarter of a cycle later (5 ms in 50 Hz systems), at the voltage peak, the reactors of that phase are energized. The voltage at the open-end and the line breaker current after applying this

countermeasure for the 75% cable scenario (60 km cable) are shown in Figure 6.7. The results are compared with those of Countermeasure 6.5.1 (i.e. simultaneous cable and reactor energization at the voltage peak). The transient overvoltage and the inrush current are considerably lower with this countermeasure since the cable is energized at the zero voltage. Thus, the main advantage of this measure is the minimization of the stress on the line breaker and system components.

The results in Figure 6.7 are for the case in which the time delay between cable energization and reactors energization is 5 ms (optimal case); however, the delay may be longer in practice. The RVC and voltage swell can exceed the limits when the time delay becomes long.

Figure 6.8 shows the RMS voltage step at the Krimpen substation after energizing the 75% cable scenario (60 km cable) with three time delays between the cable and reactors energizations: 5 ms, 65 ms ($3+1/4$ of a cycle), and 1.05 s ($5+1/4$ of a cycle). It can be seen that the voltage step exceeds the 3% limit and goes beyond the swell threshold of 1.1 pu ($1.1 \times 380 \text{ kV} = 418 \text{ kV}$) with both 65 ms and 1.05 s delays. Such a high sensitivity to delay is the result of the high steady-state voltage of 1.076 pu before the energization, leaving a margin of 0.024 pu for the voltage step.

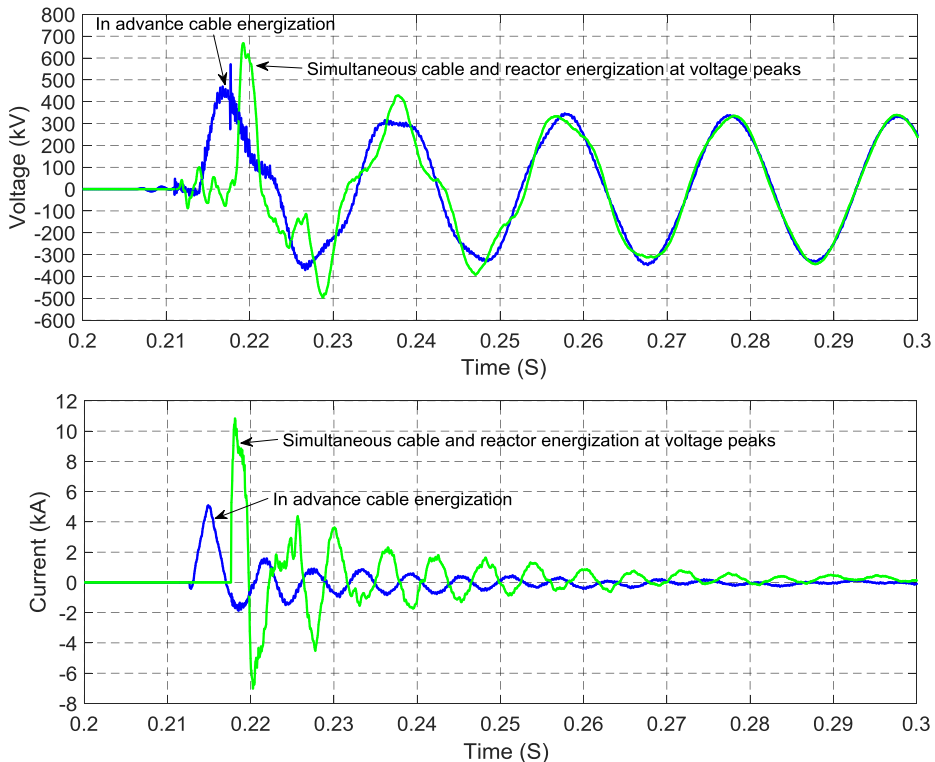


Figure 6.7: Open-end voltage (phase A) and line breaker current (I_{CB1} , phase A) after the implementation of Countermeasure 6.5.2.A (with 5 ms delay) and Countermeasure 6.5.1 (75% cable scenario, $K_{sh} = 92.1\%$).

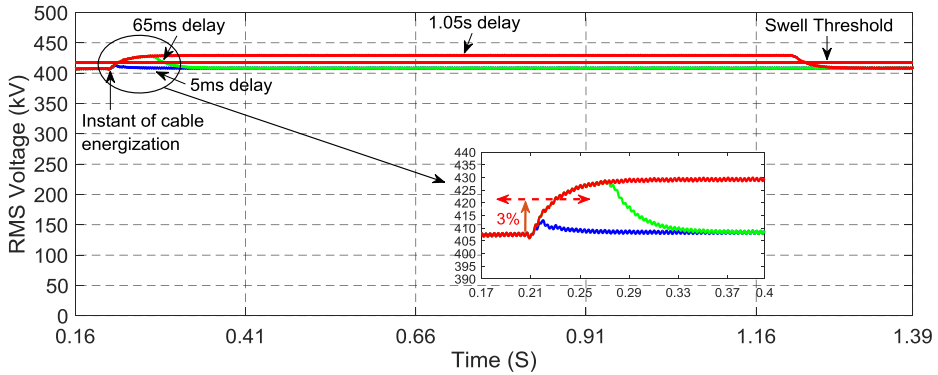


Figure 6.8: RMS voltage step at the Krimpen substation after the implementation of *Countermeasure 6.5.2.A* with three different time delays (75% cable scenario, $K_{sh} = 92.1\%$).

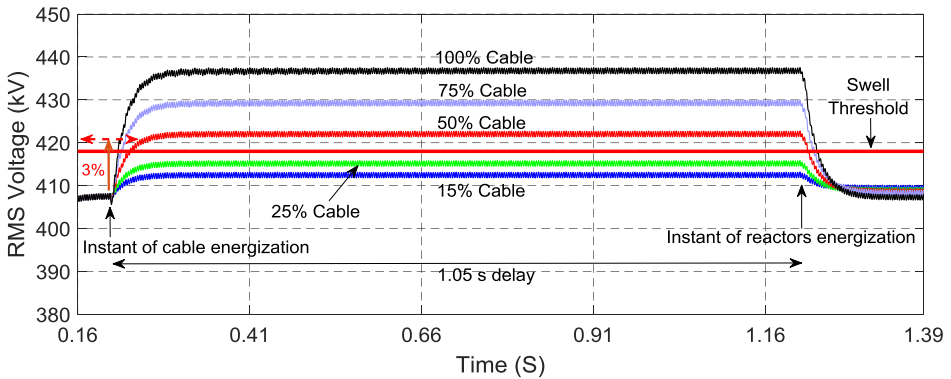


Figure 6.9: RMS voltage step at the Krimpen substation after energizing the six cable scenarios with *Countermeasure 6.5.2.A*. The time delay is 1.05 s.

In addition to the initial voltage before the energization, the cable length and the short-circuit strength of the substation from which the circuit is energized affect the amplitude of the voltage step. The effect of cable length on voltage step, when the time delay is 1.05 s, is shown in Figure 6.9. Only voltage steps in the 15% and 25% cable scenarios are below the 3% and 1.1 pu limits, whereas the step exceeds both limits with increasing the cable length. Therefore, the main limitation of this countermeasure is the expected large voltage step due to a long delay between the cable energization and reactors energization.

B. IN ADVANCE REACTOR ENERGIZATION

The implementation of this countermeasure requires two additional single-pole operated breakers to be installed at the both sides of the hybrid circuit, as shown in Figure 6.10. This allows that breakers 1 and 3 be closed at the voltage peak to energize reactor 1 (SR1) before the cable is energized. After 5 ms delay, the additional breaker, which is installed at the beginning of OHL1, will be closed at the zero voltage to energize the cable. At the next voltage peak after the cable energization, reactor 2 (SR2) is energized by closing breaker 4 and the other additional breaker, which is installed at the end of OHL4. Since both reactors are energized at the voltage peak, the zero-missing phenomenon is prevented.

Figure 6.11 shows the open-end voltage and the line breaker current after the energization of the 75% cable scenario (60 km cable) when this countermeasure is applied. It is evident that the transient overvoltage and the inrush current are lower compared to those of the previous countermeasures.

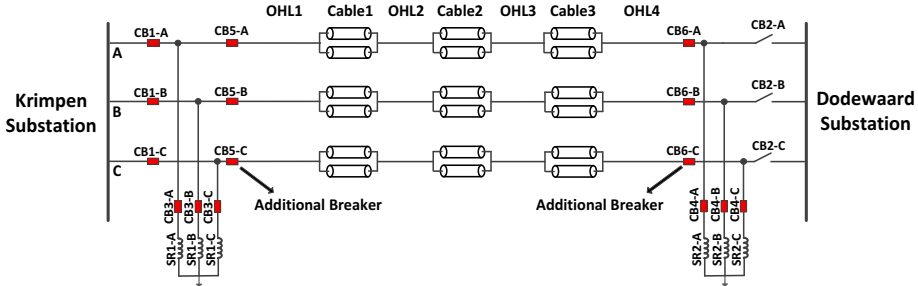


Figure 6.10: Structure of the shunt-compensated hybrid OHL-Cable circuit with Countermeasure 6.5.2.B (CB: circuit breaker, SR: shunt reactor).

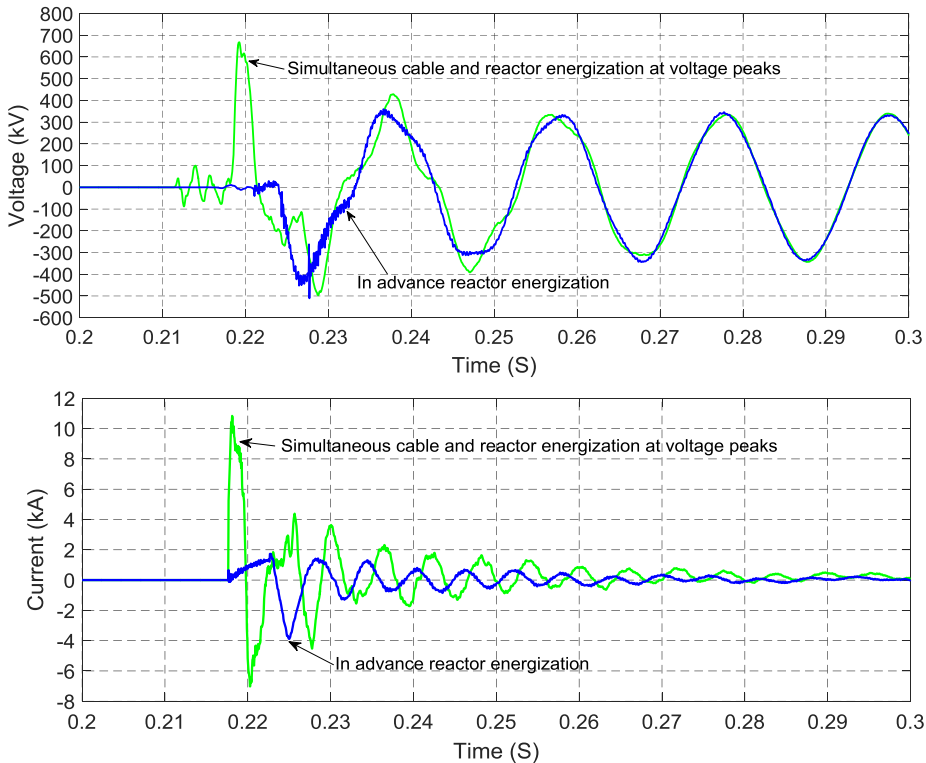


Figure 6.11: Open-end voltage (phase A) and line breaker current (I_{CB1} , phase A) after the implementation of Countermeasure 6.5.2.B (with 5 ms delay) and Countermeasure 6.5.1 (75% cable scenario, $K_{sh} = 92.1\%$).

Figure 6.12 shows the voltage step at the Krimpen substation after the energization of the 75% cable scenario with time delays of 5 ms, 65 ms, and 1.05 s between the cable and reactors energizations. Unlike Countermeasure 6.5.2.A (in advance cable energization), the voltage step is not exceeding the 3% limit and is also far above the dip threshold (0.9 pu). The reason for not exceeding the 3% limit is the size of reactor 1, which according to Table 3.2 is between 34.9% (for the 50% cable scenario) to 47.6% (for the 100% cable scenario) of the total cable reactive power. Thus, in advance energization of SR1 has a much smaller influence on the voltage than the case of cable energization in advance. The reason for not exceeding the dip threshold, in addition to the comparatively small size of SR1, is the high steady-state voltage before the energization (1.076 pu). As Figure 6.13 shows, the 3% limit is only exceeded when the cable share is 100% (80 km). It can be concluded that this countermeasure has fewer negative consequences than the previous measures in the circumstances that the pre-switching steady-state voltage is high.

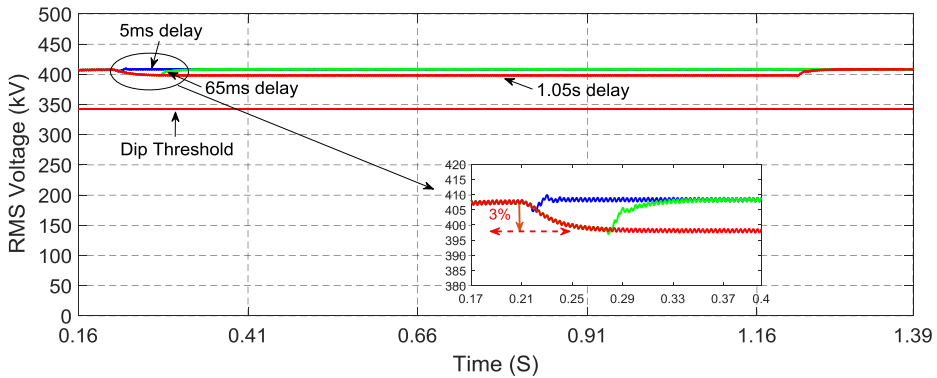


Figure 6.12: RMS voltage step at the Krimpen substation after the implementation of *Countermeasure 6.5.2.B* with three different time delays (75% cable scenario, $K_{sh} = 92.1\%$).

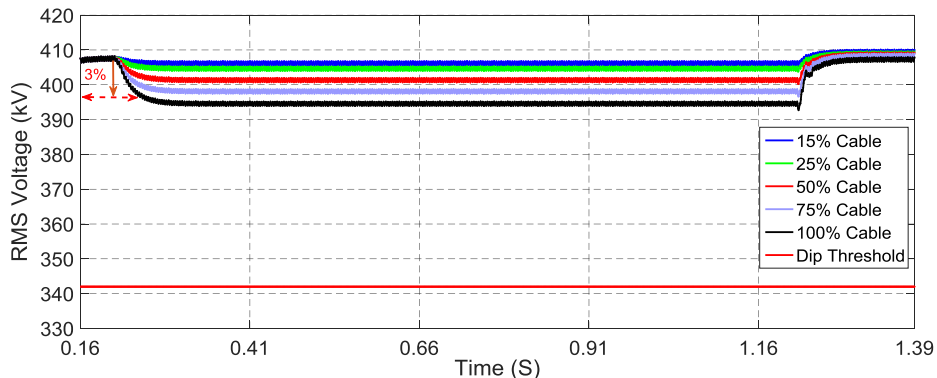


Figure 6.13: RMS voltage step at the Krimpen substation after energizing the six cable scenarios with *Countermeasure 6.5.2.B*. The time delay is 1.05 s.

6.5.3 SEQUENTIAL SWITCHING

The sequential switching is a handling countermeasure, which applies remedial switching actions to protect the system in the case that a fault occurs in the circuit during the zero-missing phenomenon [6]. By applying this measure, the cable and reactors are energized together at the zero voltage (by the use of controlled switching and single-pole operated breakers) to minimize the transient overvoltages and the inrush currents.

When a fault occurs in the circuit during energization, the line breaker(s) of the faulted phase(s) can interrupt the current since it crosses the zero point. In fact, the fault current is superimposed on the AC-component of the current through the line breaker and therefore the total AC-component becomes larger than the DC-component. However, the line breaker(s) of healthy phase(s) cannot interrupt the current due to the zero-missing phenomenon.

In order to open the line breaker(s) of healthy phase(s), the degree of compensation should be decreased to 50% or less. When the compensation degree is dropped to 50% or less, the AC-component of the line breaker current becomes larger than the DC-component, so the line current crosses the zero point. The decrease of the compensation degree to 50% is the preferred case; in fact, the leading current through the line breaker and overvoltages along the circuit are more reduced compared to the case in which the degree of compensation is lower than 50%. Moreover, to limit the overvoltages, it is preferable not to disconnect the reactors at the open-end.

The line breakers should be type-tested for higher capacitive (leading) current interruption capability since the capacitive current flowing through the line breaker can be large after the decrease of the compensation degree to 50% or less (e.g. for 60 km cable with 50% compensation, the capacitive current through the line breaker is about 1 kA). A drawback of this countermeasure is that the zero-missing problem is transferred to the next set of breakers when the line breaker of a healthy phase fails. Current differential relays are also required for realization of this countermeasure [6].

As an example of this countermeasure, assume that the Spaak connection with 75% cable (60 km cable) and the shunt reactors are energized together at the zero voltage. A single-line-to-ground (SLG) fault is applied at $t = 0.32$ s in phase B of OHL3 (see Figure 2.3). Figure 6.14 shows the current through the line breaker when the sequential switching countermeasure is applied. The breaker of phase B (CB1-B) is opened by the protection scheme 120 ms after the fault occurrence. The application of this countermeasure does not cause high transient overvoltages and inrush currents since the cable and reactors are energized at voltage zero.

It is worth mentioning that the currents through the reactor breakers of the faulted phase(s) are not crossing the zero point since reactors are discharging into the fault. This is shown in Figure 6.15. So, as a common practice [14], reactor breakers do not operate until the reactor currents cross the zero point.

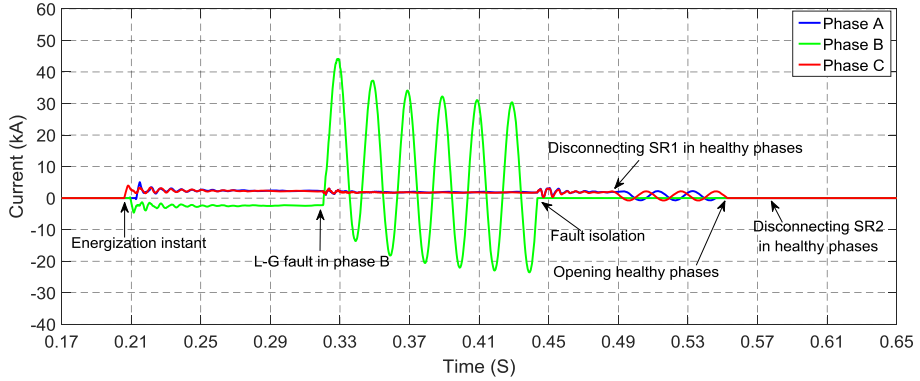


Figure 6.14: Line breaker current (I_{CBI}) when the *sequential switching* countermeasure is applied (75% cable scenario, $K_{sh} = 92.1\%$).

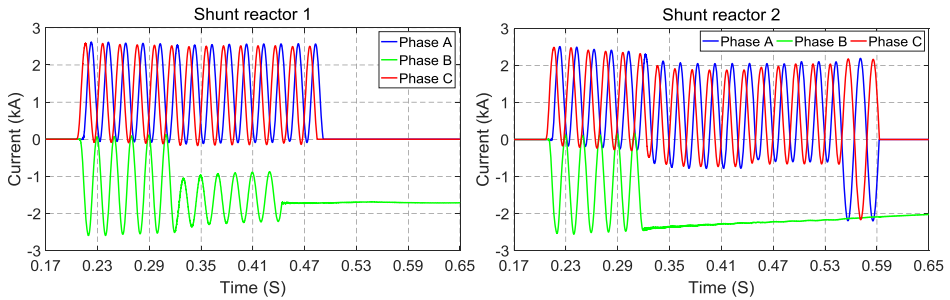


Figure 6.15: Current through shunt reactor 1 (I_{SR1}) when the *sequential switching* countermeasure is applied (75% cable scenario, $K_{sh} = 92.1\%$).

6.5.4 OPENING FAULTED PHASE(S)

In this handling countermeasure, only the line breaker(s) of the faulted phase(s) is/are opened when a fault occurs in the circuit. The healthy phase(s) is/are opened after the DC-offset is sufficiently damped and the line breaker current crosses the zero point.

The main benefit of this countermeasure is that it is cheap and only needs single-pole operated breakers, which are already commonly used in transmission systems. However, the waiting time for damping of the DC-component in healthy phase(s) can be up to several seconds due to the large time constant of shunt reactors. Leaving healthy phase(s) connected to the system may cause resonance in the disconnected phase(s) after the fault is removed [15]. In addition, applying this measure on cable projects near a generator may not be possible as this measure causes a prolonged unbalanced operation [6].

6.5.5 INCREASING DC-OFFSET DAMPING

In the cable systems, the total X/R ratio is typically large, which is resulting in a low damped DC-offset. In this mitigation countermeasure, the X/R ratio and as a result the DC-offset damping time are decreased by using an additional resistor. In addition, the cable and reactors are energized together at the zero voltage to minimize the overvoltages and the inrush currents.

One way of adding the resistor is to use a breaker equipped with the pre-insertion resistor (closing resistor) for the line or shunt reactors [7], [9]. The resistor (which its size can be in the order of the line surge impedance [14]) is connected through an auxiliary contact in parallel with the main contact (breaking chamber), as it is shown in Figure 6.16a. The circuit is energized through the resistor for a few milliseconds (e.g. approximately 8-12 ms for ABB breakers [9]) before closure of the arcing contact. These breakers are more expensive than the ordinary breakers and controlled switching. The cost can be even much higher if a new breaker is needed to be developed.

As an alternative case, a separate resistor can be connected in series with an ordinary breaker. The resistor is bypassed by a parallel disconnector or breaker as it is illustrated in Figure 6.16b. The breaker can be a lower voltage breaker with 380 kV insulation since it is not supposed to interrupt a fault current. The main advantage of this topology is the controllability of the resistor bypass time. However, an additional cost for the purchase of an extra breaker/disconnector and the resistor is imposed.

Figure 6.17 shows the influence of the pre-insertion resistor size on the DC-component of the line breaker current when each phase of the Spaak connection with 75% cable (60 km cable) is energized at the zero voltage. The DC-component decreases faster with increasing the resistor size; however, it is crucial to find the optimum size of the resistor to increase the effectiveness and to minimize the cost. Large resistors act as an open-circuit and small resistors do not cause any improvement in the DC-offset damping.

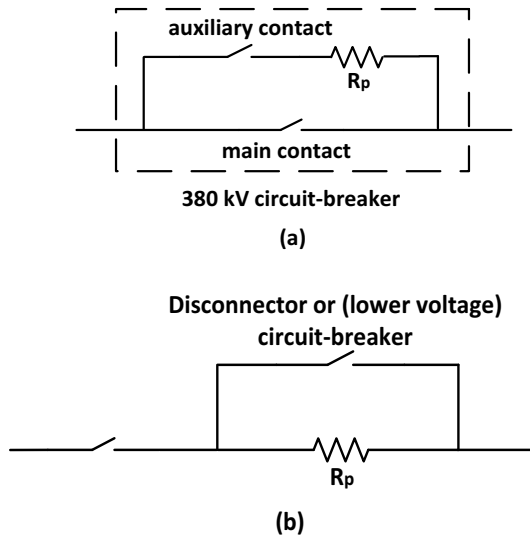


Figure 6.16: Use of resistors to mitigate the zero-current phenomenon, (a) a circuit breaker equipped with the pre-insertion resistor, (b) a resistor in series with an ordinary circuit breaker.

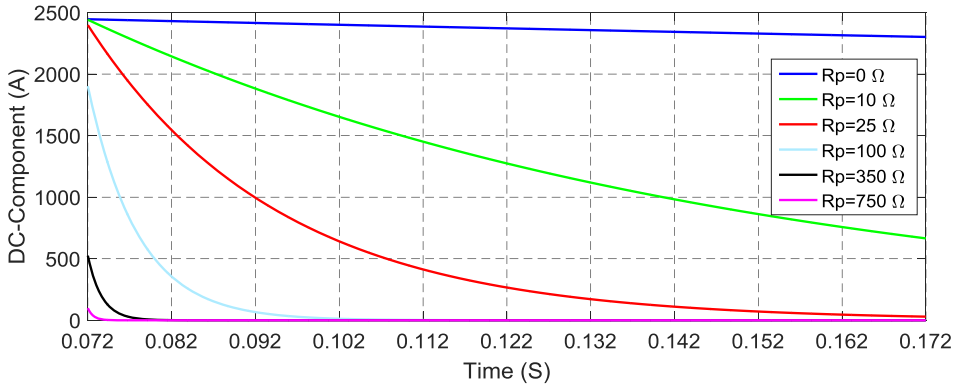


Figure 6.17: DC-component of the line breaker current (I_{CBI}) for different pre-insertion resistor sizes when each phase is energized at the zero voltage (75% cable scenario, $K_{sh} = 92.1\%$).

Reference [5] has proposed an iterative process to solve differential equations for the calculation of the pre-insertion resistor size. A formula based on energy equations (energy that the pre-insertion resistor should dissipate) is also proposed in [4] and [5]. This formula gives an approximation of the resistor value without being required to perform the iterative process, although is not always accurate due to simplifications.

If a breaker equipped with the pre-insertion resistor (Figure 6.16a) is used, the resistor should be sized so that the zero-missing phenomenon disappears by the moment that the resistor is bypassed. Figure 6.18 shows the DC-component after 10 ms (average of 8-12 ms [5], [9]) versus the size of pre-insertion resistor for the six cable scenarios when each phase is closed at the zero voltage. When the resistor size is increased, the DC-component experiences a steeper drop for the scenarios with a higher cable share. This is due to the smaller X/R ratio of the hybrid circuits with higher cable share (as a result of the smaller X/R ratio of cables compared to OHLs), in which adding an additional resistance has a more remarkable impact.

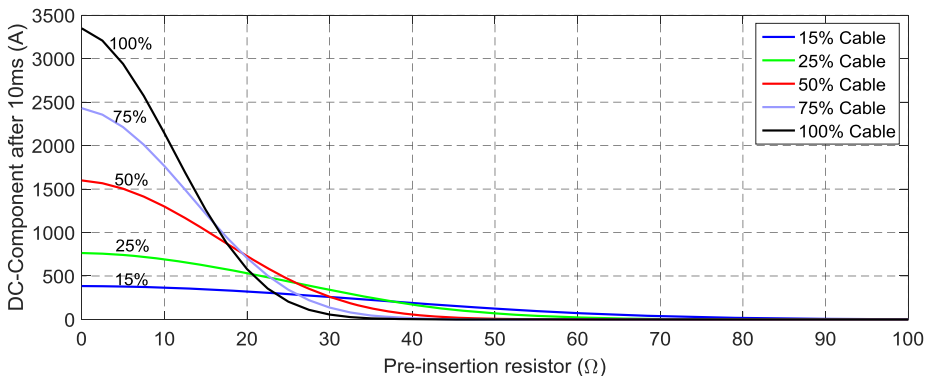


Figure 6.18: DC-component of the line breaker current (I_{CBI}) after 10 ms versus the size of the pre-insertion resistor for the six cable scenarios. Each phase is energized at the zero voltage.

The main limitation of this countermeasure is the thermal design of the resistor. The dissipated power in the resistor is shown in Figure 6.19. This countermeasure requires special designed resistors to tolerate huge power dissipation for a couple of milliseconds. This imposes extra costs and complexity to the countermeasure.

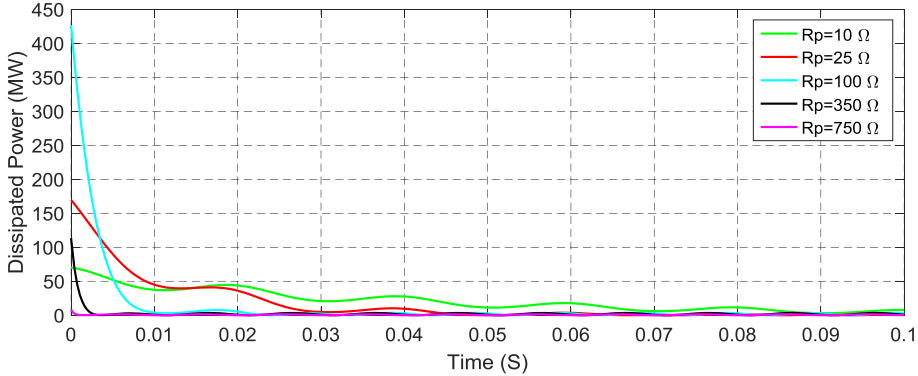


Figure 6.19: Dissipated power in different pre-insertion resistor sizes when each phase is energized at the the zero voltage (75% cable scenario, $K_{sh} = 92.1\%$).

6.6 DISCUSSIONS

Several countermeasures of the zero-missing phenomenon were analysed and compared. The applied methodology and findings are applicable on any network since the study is based on practical assumptions like the use of a hybrid OHL-Cable circuit and the three system operation criteria. Moreover, simulation results were obtained by electromagnetic transient (EMT) studies on the model of an actual power transmission grid. It should be stressed that the influence of the system topology and parameters (like the configuration of hybrid OHL-Cable circuit, power-frequency voltage, short-circuit power, etc.) on the effectivity of a countermeasure should always be considered.

Table 6.4 presents a summarized comparison between the technical advantages and disadvantages of the investigated countermeasures. Some of the countermeasures need special designed circuit breakers, control strategies and resistances, which can impose extra costs and complexity on the system design and operation. The implementation of Countermeasures 6.5.2.A (in advance cable energization) and 6.5.2.B (in advance reactor energization) is more sophisticated than commonly applied techniques like Countermeasure 6.5.1 (simultaneous cable and reactors energization at the voltage peak) since they require multiple control systems, which are coordinated together with a communication system. The advantages of these countermeasures over a traditionally-used measure, in terms of resulting overvoltages and inrush currents, were validated in Figures 6.7 and 6.11, where the results were compared with those of Countermeasure 6.5.1.

TABLE 6.4
ADVANTAGES AND DISADVANTAGES OF THE COUNTERMEASURES OF THE ZERO-MISSING PHENOMENON

Countermeasure	Advantages	Disadvantages
Simultaneous cable and reactors energization at the voltage peak (Countermeasure 6.5.1)	<ul style="list-style-type: none"> • Prevention countermeasure • Well-known by system operators • Easy to implement 	<ul style="list-style-type: none"> • Requires controlled switching • Very high overvoltages and inrush currents for long cables • Breaker operation delay should not exceed the BCVT
In advance cable energization (Countermeasure 6.5.2.A)	<ul style="list-style-type: none"> • Prevention countermeasure • Minimized overvoltages and inrush currents for long cables 	<ul style="list-style-type: none"> • Requires controlled switching • Requires a control mechanism to handle the switching sequence of the cable and reactors • Breaker operation delay should not exceed the BCVT¹ • Risk of voltage dip/swell for long cables
In advance reactor energization (Countermeasure 6.5.2.B)	<ul style="list-style-type: none"> • Prevention countermeasure • Minimized overvoltages and inrush currents for long cables 	<ul style="list-style-type: none"> • Requires controlled switching • Requires a control mechanism to handle the switching sequence of the cable and reactors • Breaker operation delay should not exceed the BCVT¹ • Risk of voltage dip/swell for long cables • Requires two additional three-phase breakers
Sequential switching (Countermeasure 6.5.3)	<ul style="list-style-type: none"> • Minimized overvoltages and inrush currents for long cables • Implemented by some system operators 	<ul style="list-style-type: none"> • Requires controlled switching • Handling countermeasure (no prevention) • Requires breakers with higher capacitive current interruption capability • Risk of transferring the zero-missing problem to the next set of breakers if the line breaker of a healthy phase fails
Opening faulted phases(s) (Countermeasure 6.5.4)	<ul style="list-style-type: none"> • Minimized overvoltages and inrush currents • Easy to implement 	<ul style="list-style-type: none"> • Requires controlled switching • Handling countermeasure (no prevention) • Leaves the system unprotected for a very long time when the cable is long • Risk of resonance in the disconnected phase(s) • May not be possible to be utilized near a generator due to causing a prolonged unbalance operation
Increase DC-offset damping (Countermeasure 6.5.5)	<ul style="list-style-type: none"> • Lowered overvoltages and inrush currents (minimized if controlled switching at zero voltage is applied) • Known by system operators 	<ul style="list-style-type: none"> • Mitigation countermeasure (no prevention) • Requires pre-insertion resistors with very high thermal design when the cable is long

⁽¹⁾ Only the breakers operating at the voltage peak should comply with the BCVT.

6.7 CONCLUSIONS

This chapter studied the effectiveness of six countermeasures of the zero-missing phenomenon in (E)HV cable systems. It was shown that the zero-missing phenomenon becomes more severe by increasing the cable length in a hybrid OHL-Cable circuit.

Simultaneous cable and reactors energization at the voltage peak is a well-known prevention countermeasure; however, the resulting transient overvoltages and inrush currents should be carefully analysed. In addition, the impact of stochastic variations in the breaker closing time as well as the breaker compliance with the BCVT should be investigated.

To decrease the transient overvoltages and inrush currents, *energization of the cable and shunt reactors in sequence (in advance cable or reactor energization)*, as a prevention countermeasure, can be utilized. A voltage dip/swell is the main risk of applying this countermeasure for long cable lengths. As an example, for the Spaak connection and in the studied load-flow profile, this situation occurs for cables longer than 50 km when the cable is energized first. In addition, breakers operating at the voltage peak should be tested for BCVT.

Other countermeasures are *sequential switching* (handling countermeasure), *opening of the faulted phase(s)* (handling countermeasure), and *increasing the DC-offset damping* (mitigation countermeasure). These methods result in low transient overvoltages and inrush currents. The later one is a costly measure for which the thermal design of the resistor is a challenge.

For the Spaak connection and in the studied load-flow profile, *in advance reactor energization* and *sequential switching* can be concluded as the most effective and less risky countermeasures resulting in low transient overvoltages and low inrush currents.

Finally, the countermeasure effectiveness should always be investigated for each cable project by a similar study since the system specifications may change from one case to another affecting the consequent voltages and currents.

REFERENCES

- [1] CIGRE Working Group C4.502, "Power system technical performance issues related to the application of long HVAC cables," *CIGRE Technical Brochure no. 556*, October 2013.
- [2] H. Khalilnezhad, M. Popov, J. A. Bos and K. P. J. Jansen, "Influence of partial undergrounding on the transient stability of EHV power transmission systems," *Electric Power Systems Research*, vol. 131, pp. 126-138, 2016.
- [3] U. S. Gudmundsdottir and P. B. Holst, "Solving zero-missing with cable energization at voltage peak, based on insulation coordination study results," in *International Conference on Power System Transients (IPST)*, Vancouver, Canada, July 2013.
- [4] F. F. da Silva, C. L. Bak, U. S. Gudmundsdottir, W. Wiechowski and M. R. Knardrupgard, "Use of a pre-insertion resistor to minimize zero-missing phenomenon and switching overvoltages," in *IEEE Power & Energy Society (PES) General Meeting*, Calgary, Canada, October 2009.
- [5] F. F. da Silva, C. L. Bak, U. S. Gudmundsdottir, W. Wiechowski and M. R. Knardrupgard,

- “Methods to minimize zero-missing phenomenon,” *IEEE Transactions on Power Delivery*, vol. 25, no. 4, pp. 2923-2930, October 2010.
- [6] A. Ametani, T. Ohno and N. Nagaoka, *Cable System Transients: Theory, Modeling and Simulation*, Hoboken, NJ, USA: Wiley, July 2015.
- [7] R. Smeets, L. van der Sluis, M. Kapetanovic, D. Peelo and A. Janssen, *Switching in Electrical Transmission and Distribution Systems*, Hoboken, NJ, USA: Wiley, 2015.
- [8] “High-voltage Switchgear and Controlgear-Part 100: Alternating-Current Circuit-Breakers,” IEC 62271-100, 2008.
- [9] “Live Tank Circuit Breakers: Buyer’s Guide,” 6th ed., ABB, Ludvica, Sweden, 2014.
- [10] “Insulation Co-Ordination-Part 1: Definitions, Principles and Rules,” IEC 60071-1, 2006.
- [11] “Electromagnetic Compatibility (EMC)-Part 4-30: Testing and Measurement Techniques-Power Quality Measurement Methods,” IEC 61000-4-30, 2014.
- [12] T. Ohno, C. L. Bak, A. Ametani, W. Wiechowski and T. K. Sorensen, “Statistical distribution of energization overvoltages of EHV cables,” *IEEE Transactions on Power Delivery*, vol. 28, no. 3, pp. 1423-1432, July 2013.
- [13] “Insulation Co-Ordination-Part 2: Application Guide,” IEC 60071-2 , 1996.
- [14] “Live Tank Circuit Breakers: Application Guide,” 1.2 ed., ABB, Ludvica, Sweden, 2013.
- [15] CIGRE Working Group C4.307, “Resonance and ferroresonance in power networks,” *CIGRE Technical Brochure no. 569*, February 2014.

CHAPTER 7

DE-ENERGIZATION TRANSIENTS OF HYBRID OHL-CABLE SYSTEMS

7.1 INTRODUCTION

In the previous chapters, energization transients of hybrid OHL-Cable circuits were studied. Transient voltages and currents are also initiated when a circuit breaker is opened to de-energize a circuit or a component. De-energization transients are associated with several transient phenomena, which may become more severe when the circuit is fully or partially undergrounded with cables.

The aim of this chapter is to analyse de-energization transients in the hybrid OHL-Cable circuits of the Spaak connection. The voltages on the disconnected phases and the transient recovery voltages (TRV) across the contacts of line circuit breakers are assessed, as the analysis is performed for two cases: with and without reactors connected to the disconnected phases. The TRV is a very important parameter to determine how significant the risk of breaker re-ignition or restrike after the current interruption is.

This chapter is organized as follows: Section 7.2 briefly explains the electrical phenomena related to the capacitive current interruption. Afterwards, in Section 7.3, de-energization transients of the Spaak connection are studied. Finally, conclusions are discussed in Section 7.4.

7.2 CAPACITIVE CURRENT INTERRUPTION

The interruption of capacitive currents can be challenging for circuit breakers. Figure 7.1 shows a simple circuit with a capacitive load. When the capacitive current is interrupted at current zero, the voltage is at its peak if 90° phase shift between the voltage and current is assumed. As it is illustrated in Figure 7.2, at the instant of current interruption, the capacitor is fully charged with the voltage $U_c = E + \Delta U$, where E is the peak of the source voltage. This means that the load voltage is higher than 1 pu of the source voltage because of the Ferranti rise at the load side prior to the breaker opening. The voltage difference, ΔU , can be calculated as follows [1]:

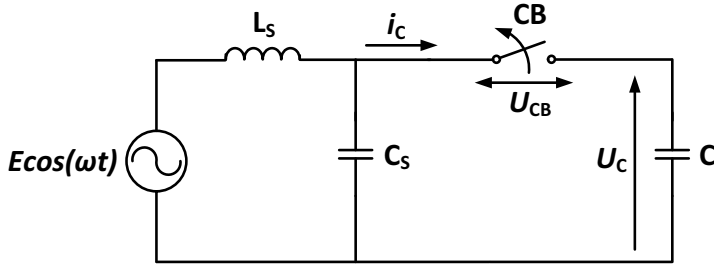


Figure 7.1: A simple circuit for a single-phase capacitive load switching.

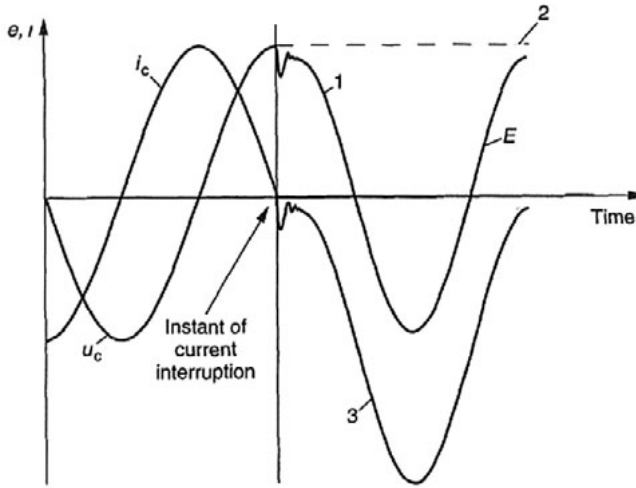


Figure 7.2: Current and voltages after the capacitive current interruption; 1: source voltage, 2: capacitor voltage, 3: voltage across the breaker terminals, E is the peak value of the source voltage [2].

$$\Delta U = \frac{1}{1 - \omega^2 L_s C} - 1 \approx \frac{Q}{P} = \frac{I_{cap}}{I_{sc,loc}} \quad (\text{pu}) \quad (7.1)$$

where L_s is the source inductance and C is the load capacitance, as shown in Figure 7.1. ω is the system angular frequency ($\omega = 2\pi f_0$, where f_0 is the system power frequency). P is the local short-circuit active power, Q is the reactive power of the capacitor, $I_{sc,loc}$ is the local short-circuit current, and I_{cap} is the capacitive current. It can be deduced from this equation that a larger capacitor (i.e. a larger capacitive current) results in a larger load voltage.

As it can be seen in Figure 7.2, after the current interruption, the capacitor voltage remains constant while the source-side voltage makes a transient excursion from $E + \Delta U$ to E and then continues its power-frequency course. A half cycle later, the source voltage reaches the next peak with a reversed polarity, so the voltage across the breaker terminals (U_{CB}) becomes approximately twice of the source-side peak voltage ($U_{CB} = 2E + \Delta U \approx 2 \text{ pu}$) [2].

The recovery voltage across the breaker terminals after the current interruption has two successive parts: the TRV part where high frequency oscillations occur followed by the steady-state voltage where transients are decayed and power-frequency oscillations are present. The TRV is dependent on the parameters of the circuit being interrupted, mainly the RLC circuit behaviour and the travelling waves in the circuit. A re-ignition or restrike occurs when the TRV exceeds the breakdown voltage of the dielectric between the contacts of the circuit breaker. The re-ignition is a breakdown occurring within a quarter of a power-frequency cycle (i.e. 5 ms in a 50 Hz system) after the current interruption and the restrike is a breakdown occurring later. Re-ignition breakdowns involve a lower amount of energy than restrike breakdowns since they occur at relatively low recovery voltage levels, so they are in general harmless and considered as a part of the interruption process. However, restrike breakdowns are associated with a considerable amount of energy in the breakdown and are the main hazards (with severe consequences) of the capacitive current interruption [1].

Figure 7.3 shows the current and voltages after a capacitive current interruption followed by multiple restrikes. If a restrike occurs near the peak of the recovery voltage, the capacitive load suddenly discharges itself via the arc channel, leading to a restrike current with a peak value of $2E\sqrt{\frac{C}{L_s}}$ and a frequency of $f = \frac{1}{2\pi\sqrt{L_s C}}$. At the first zero crossing of the transient current, the capacitor voltage is $+3E$ (while it was $-E$ at the instant of restrike). If the circuit breaker interrupts the transient current at the first zero crossing of the current (in general at an odd number of restrike-current half-cycles), the TRV increases to $4E$ in a

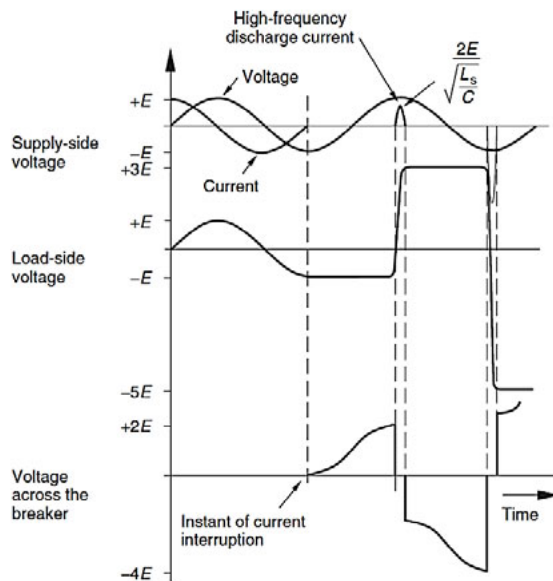


Figure 7.3: Current and voltages after a capacitive current interruption followed by multiple restrikes [2].

half cycle later. A second restrike may occur at this instant if this high recovery voltage exceeds the breakdown voltage of the dielectric between the breaker contacts. If that occurs and the breaker interrupts the transient current again at the first current zero crossing (or at odd number of restrike-current half-cycles), the voltage at the load side of the breaker becomes $5E$ and the peak recovery voltage becomes $6E$. The next restrike is very likely to take place at this moment as the TRV would be much higher than the withstand capability of the circuit breaker. Multiple restrikes are very dangerous as they lead to the capacitive voltage escalation with a high risk of severe damages to the cable and surrounding system equipment [1-3].

The above described phenomenon should be studied when cables are disconnected from the grid since a cable has almost a similar behaviour as a large capacitor. In fact, the natural discharge of a cable can be explained using the simple equations of a parallel RC-circuit [4]. This applies to the situation where the capacitive current is being interrupted at one end while the other end of the cable is already open. The capacitive current interruption becomes more challenging for breakers when the charging current of a long cable is not sufficiently compensated by shunt reactors directly connected to the cable [5]. This is due to the fact that the difference between the cable voltage and the source voltage will be large (i.e. ΔU in equation 7.1).

In [6], the preferred values for the capacitive current interruption capability of circuit breakers have been defined. However, manufacturers can build and supply breakers with higher capacitive current interruption capabilities based on the customer need. An important point is that breakers which have to perform capacitive current switching should have low or very low probability of restrike to minimize the risk of restrike overvoltages [7].

7.3 DE-ENERGIZATION TRANSIENTS OF THE SPAAK CONNECTION

In this section, transient voltages and currents after the de-energization of Circuit 1 of the Spaak connection, while Circuit 2 is assumed to be out-of-service, are presented and analysed. Two cases can be distinguished: (1) disconnection of both the circuit and shunt reactors, (2) disconnection of the circuit while the shunt reactors are left connected to the circuit. Transient voltages and currents are substantially different between these two cases due to the consequent changes in the electrical behaviour of the circuit caused by the connection or disconnection of the shunt reactors.

The cable scenarios and shunt compensation sizes are according to the presented values in Tables 2.2 (Chapter 2) and 3.2 (Chapter 3), respectively. For all simulations, at $t = 0.15$ s the open command was given to the breakers at both sides, where the breakers were assumed to be ideal and interrupt the current at the first current zero crossing.

7.3.1 SWITCHING-OFF BOTH THE CIRCUIT AND SHUNT REACTORS

Figure 7.4 shows the voltage at the Krimpen substation after the de-energization of the shunt reactors and the hybrid circuit with the 50% cable scenario (i.e. all the line and shunt reactor breakers are open). It can be seen that the source voltage does not experience a change and continues its power-frequency course since around 90% of the cable reactive power is compensated in this scenario.

When the line and shunt reactor breakers are opened, the voltage on the disconnected circuit is a decaying DC-voltage, as shown in Figure 7.5. The initial voltage caused by the voltage jump is different between the phases, which is due to the sequence of current interruption in the phases (normally about 3.33 ms time difference between the phase disconnections) and the mutual capacitive coupling between the OHL phases. The unloaded circuit has a dominant capacitive behaviour and the magnetic coupling between the phases can be ignored.

Figure 7.6 shows the voltages of phases A and C after the de-energization of the six cable scenarios. The required time for the complete discharge of the trapped voltage increases by increasing the cable length (up to tens of seconds or minutes depending on the cable length). When inductive voltage transformers (VT) are present, the cable discharge

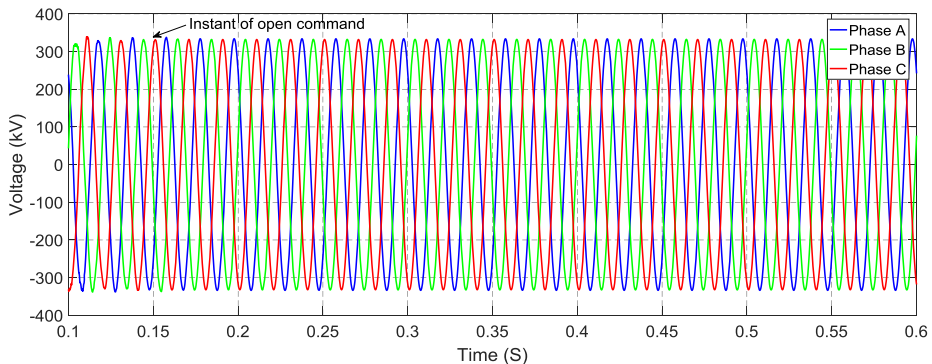


Figure 7.4: Voltage at the Krimpen substation after the de-energization of the 50% cable scenario and opening the shunt reactor breakers.

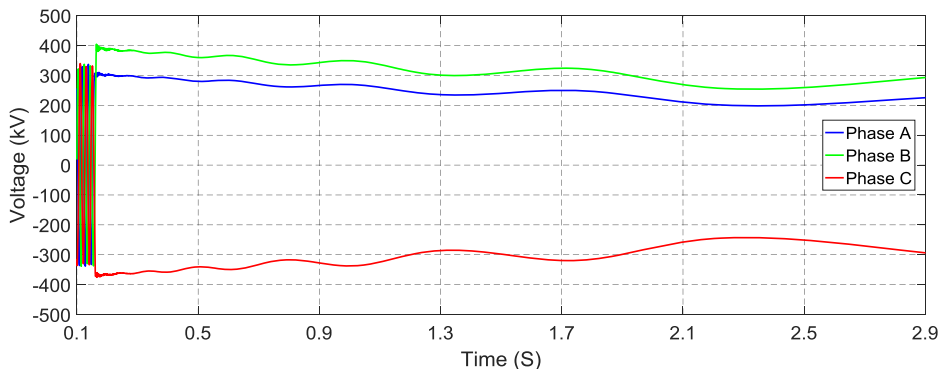


Figure 7.5: Voltage at the end of the disconnected circuit (Krimpen side) after the de-energization of the 50% cable scenario and opening the shunt reactor breakers.

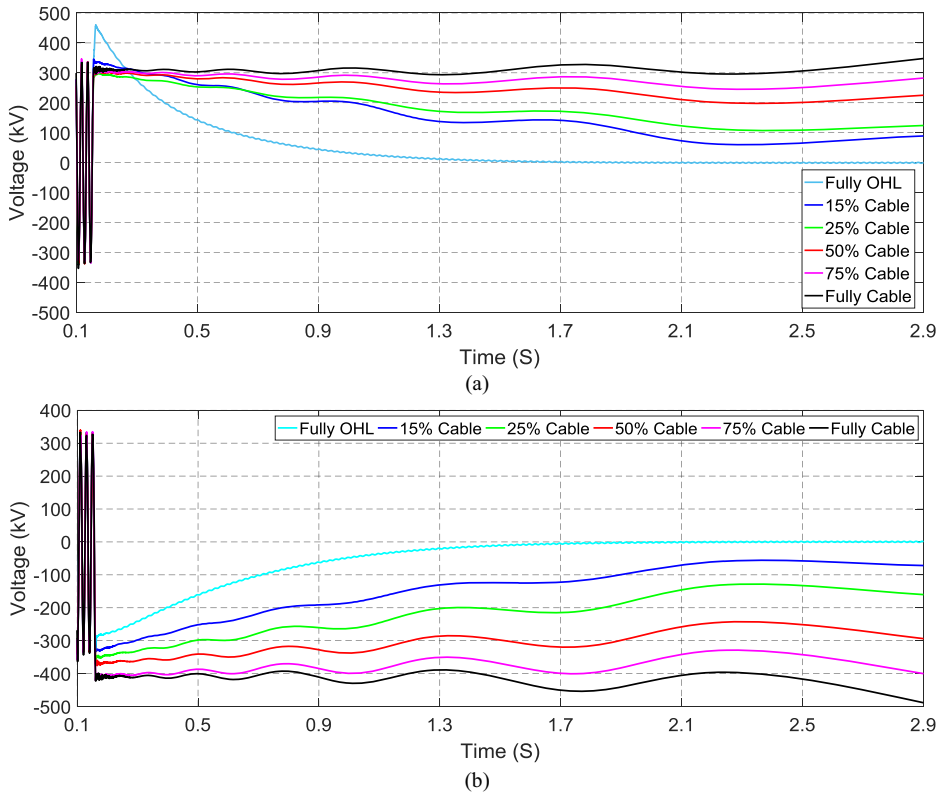


Figure 7.6: Voltage at the end of the disconnected circuit (Krimpen side) after the de-energization of the six cable scenarios and opening the shunt reactor breakers, (a) phase A, (b) phase C.

is much faster, around several hundred milliseconds, due to the quick saturation of VTs [8]. This can be easily justified by using the following equations representing the transient voltage of a capacitor (V_c) in a parallel RC-circuit during the discharge:

$$V_c(t) = V_{\max} e^{-t/\tau}, \text{ where } \tau = RC \quad (7.2)$$

where V_{\max} is the initial voltage of the capacitor at the de-energization instant, τ is the time constant of the circuit, R is the resistance, and C is the capacitance. By means of this equation, the required time to discharge the cable from $V(t_1)$ to $V(t_2)$ can be found:

$$\Delta t = t_2 - t_1 = \tau \ln \left(\frac{v(t_1)}{v(t_2)} \right) \quad (7.3)$$

The time constant of a cable is much larger than that of an OHL due to the very large cable capacitance. Thus, the time constant of the hybrid circuit increases when the cable share is increased, resulting in a much longer time for a complete discharge according to equation 7.3.

Figure 7.7 depicts the recovery voltages across the contacts of circuit breaker 1 (CB1) after the de-energization of the 50% cable scenario. The highest peak of the recovery voltage is in phase B and about 2.33 pu (724 kV), which is the result of the higher initial voltage of this phase compared to that of the other phases in the disconnected circuit (see Figure 7.5). This is a rather high value, so the withstand capability of the dielectric between the breaker contacts and the risk of restrike should be analysed. Figures 7.8 and 7.9 show the recovery voltage across phases A and C of circuit breaker 1 after the de-energization of the six cable scenarios, respectively.

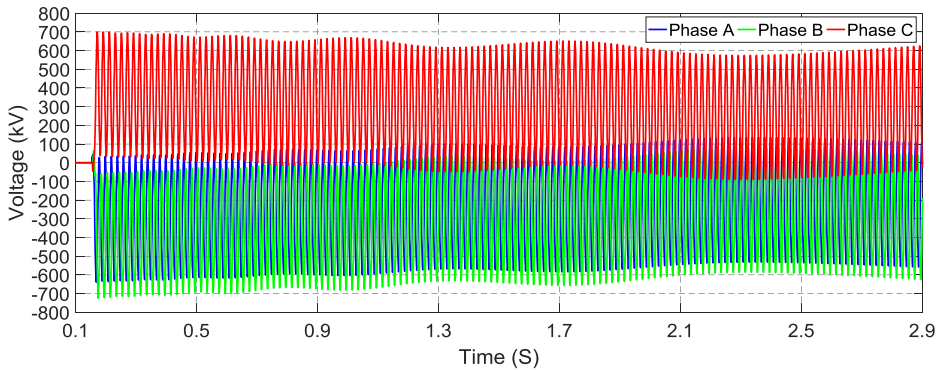


Figure 7.7: Recovery voltage across circuit breaker 1 (CB1) after the de-energization of the 50% cable scenario and opening the shunt reactor breakers.

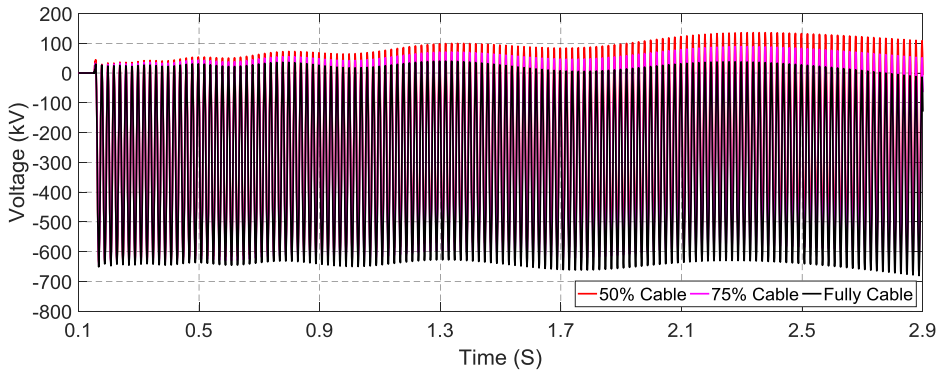
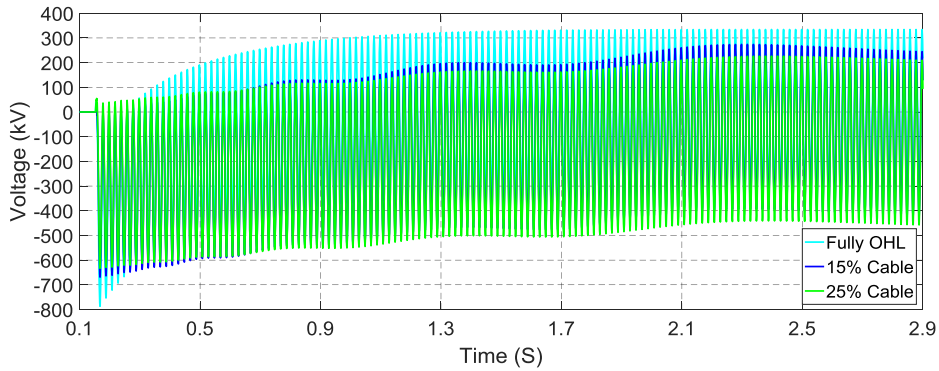


Figure 7.8: Recovery voltage across phase A of circuit breaker 1 (CB1) after the de-energization of the six cable scenarios and opening the shunt reactor breakers.

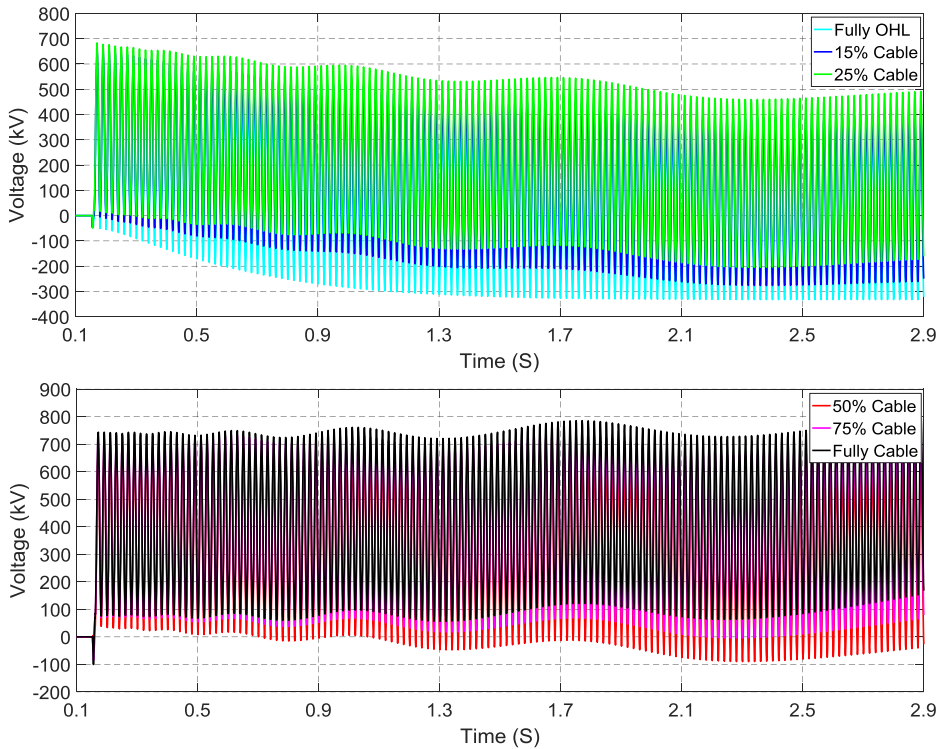


Figure 7.9: Recovery voltage across phase C of circuit breaker 1 (CB1) after the de-energization of the six cable scenarios and opening the shunt reactor breakers.

7.3.2 SWITCHING-OFF THE CIRCUIT

When a hybrid OHL-Cable circuit is de-energized while shunt reactors are left connected to the phases (i.e. only line breakers are opened), the residual voltages on the disconnected phases are no longer decaying DC-voltages and are instead decaying oscillatory AC-voltages with superimposed frequencies.

A de-energized reactor-connected cable phase oscillates with its natural frequency, determined by the cable capacitance and the shunt reactor inductance. The natural resonance frequency is almost 50 Hz if the degree of compensation is close to 100%, which is the typical case for circuits with long cables, and it will be lower than 50 Hz if the shunt compensation degree is lower. When the circuit is even slightly unsymmetrical, each phase has a slightly different resonance frequency. Due to the mutual inductive coupling (between shunt reactor phases) and capacitive coupling between circuit phases, the resulting voltage in each phase is superimposed as the sum of its own voltage and the two induced voltages by the other phases. In this situation, adding up three different voltages with different frequencies and phase shifts results in voltage amplification or attenuation [9], [10].

Figure 7.10a shows the voltage at the end of the disconnected circuit (Krimpen side) after the de-energization of the 15% cable scenario while the shunt reactors are still connected. The phase voltages will all drop to almost zero after a few seconds, where each

phase experiences a different voltage transition pattern. The maximum voltage peak is 1.29 pu (400 kV) in phase A. As it was mentioned in Chapter 2, the mutual inductances between the shunt reactor phases were not considered in the EMT model of the Spaak connection. These mutual inductances may lead to a higher voltage increase in one or more of the phases, as addressed in [11], [12].

The cable discharge is much faster when reactors remain connected to the disconnected circuit as it only takes a few seconds [4], [5], [8]. In fact, shunt reactors provide a lower resistive path to the ground and accelerate the cable discharge process. Therefore, the required time for the complete discharge of the cable depends on the system configuration and its characteristics, mainly the connection of shunt reactors and VTs.

Figure 7.10b shows the recovery voltage across the contacts of circuit breaker 1, where the peak voltage is 2.35 pu (728 kV) in phase A. This is a rather high value. The recovery voltage reaches the nominal power-frequency value within 1.5 seconds after the current interruption as the voltage on the disconnected circuit has being damped out.

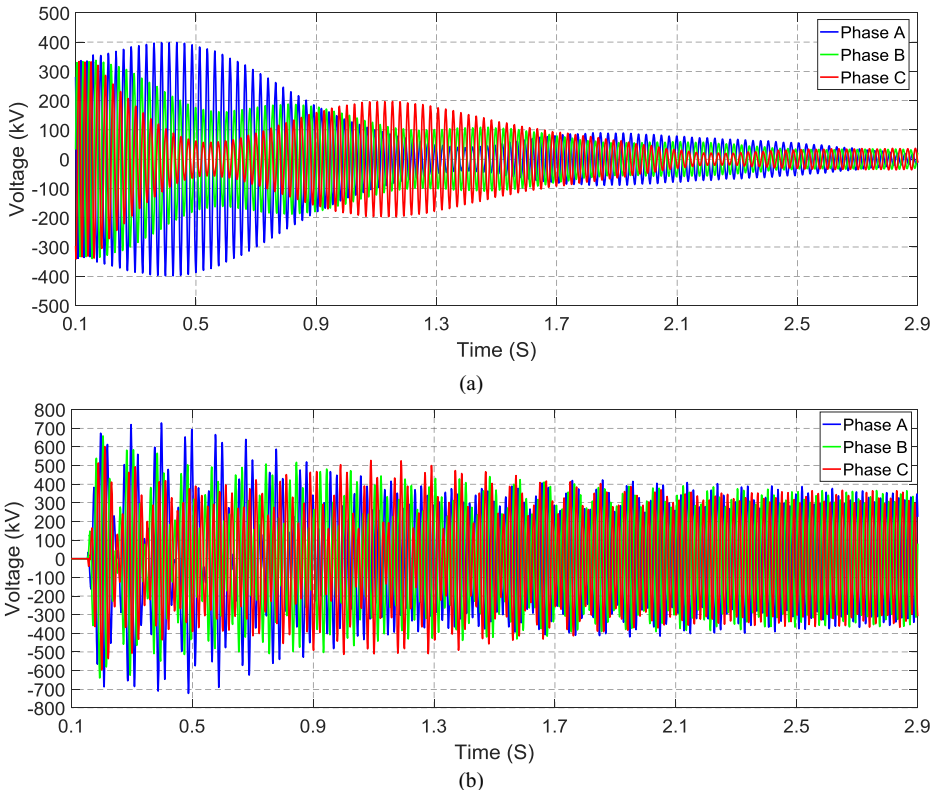


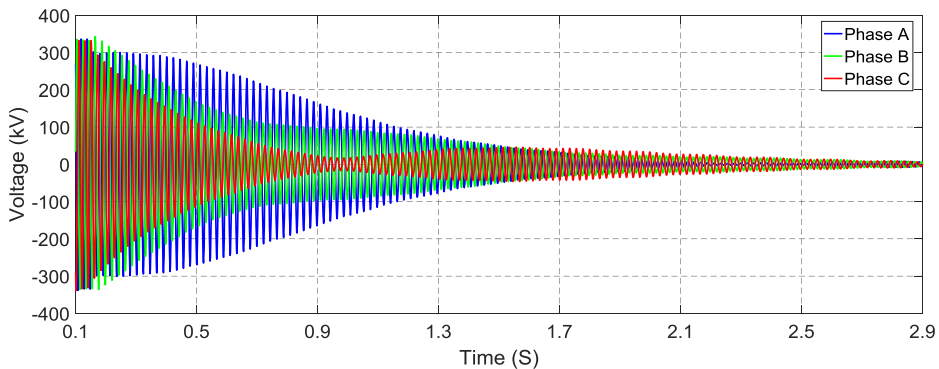
Figure 7.10: Voltage after the de-energization of the 15% cable scenario while the shunt reactors are still connected, (a) at the end of the disconnected circuit (Krimpen side), (b) across circuit breaker 1 (CB1).

As it was also mentioned in Chapter 2, resonance overvoltages are also expected in disconnected shunt-compensated hybrid OHL-Cable circuits. A resonance may occur between the reactor inductance, inter-phase/inter-circuit capacitance, and cable capacitance if reactors remain connected to the disconnected phase(s) in uneven open-phase conditions (e.g. one phase is open and the other two are closed) or to a fully three-phase disconnected circuit. In other words, the induced power-frequency voltage in the disconnected phase by the capacitive coupling with energized phases can trigger the resonance circuit formed by the cable capacitance, the shunt reactor inductance, and the capacitive coupling between the de-energized phase and the energized phases. Ferroresonance may also occur when magnetic-core shunt reactors are used for the reactive power compensation. These risks can be minimized by connecting the shunt reactors via breakers to the circuit so that they can be disconnected from the de-energized phases [13], [14].

The voltage on the disconnected circuit and the recovery voltage across the breaker contacts for the rest of the cable scenarios are shown in Figures 7.11 to 7.14. Figure 7.15 compares the phase A voltage for all the six cable scenarios.

It can be seen that with the increasing cable share in the circuit, the voltages of the disconnected phases become less modulated and more symmetrical between the phases. This is due to the smaller capacitive coupling between the phases when the OHL share in the circuit has been decreased. In fact, the capacitive coupling only exists between the OHL sections, whereas it is almost zero between the cable sections as the cable sheath is grounded.

In addition, it can be also seen in Figure 7.15.b that the maximum recovery voltage becomes lower with the increasing cable share in the circuit. The maximum TRV has decreased from 2.35 pu (728 kV in phase A) for the 15% cable scenario to 1.3 pu (404 kV in phase B, see Figure 7.14b) for the fully-cable scenario. The rate of rise of the recovery voltage is also lower when the cable length in the circuit is longer. The reason is that for the higher cable shares, the voltage of the disconnected phase becomes a decaying AC-voltage with less superimposed frequencies (because of the smaller coupling with the other phases) and with a lower oscillation frequency between the cable capacitance and the reactor inductance.



(a)

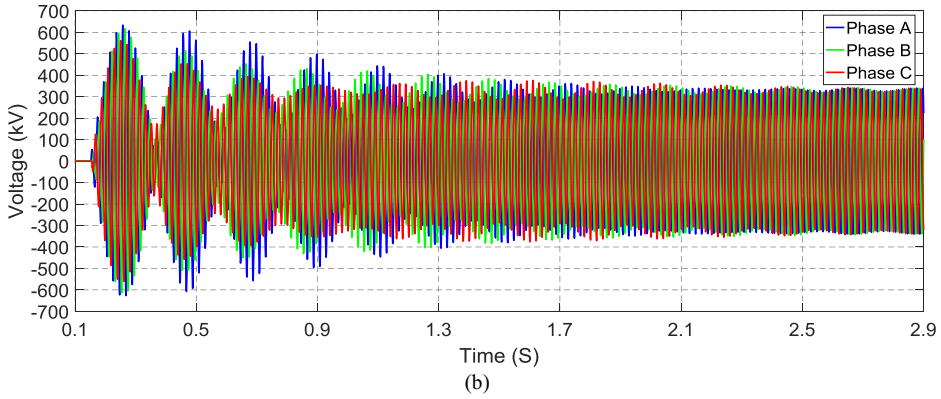


Figure 7.11: Voltage after the de-energization of the 25% cable scenario while the shunt reactors are still connected, (a) at the end of the disconnected circuit (Krimpen side), (b) across circuit breaker 1 (CB1).

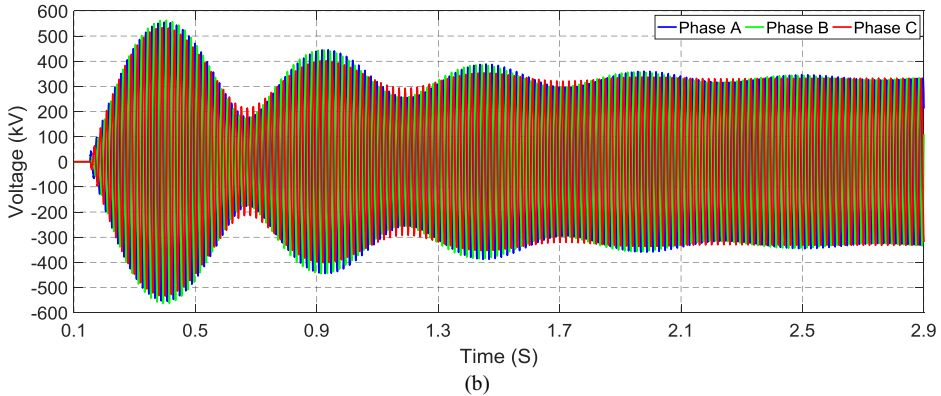
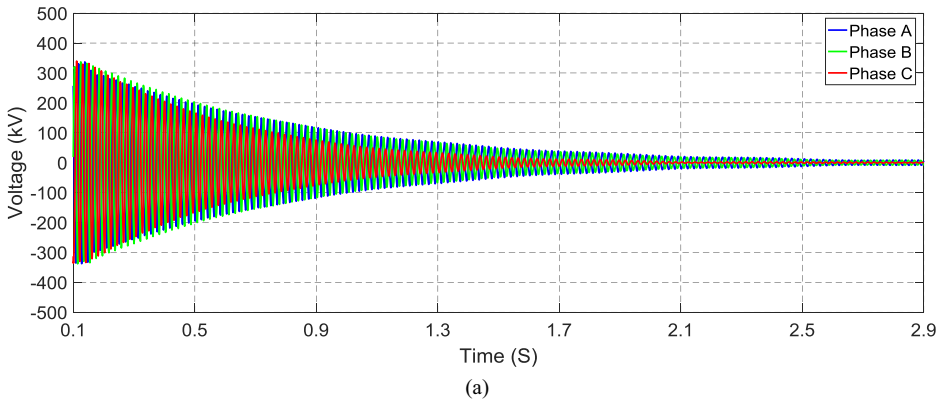


Figure 7.12: Voltage after the de-energization of the 50% cable scenario while the shunt reactors are still connected, (a) at the end of the disconnected circuit (Krimpen side), (b) across circuit breaker 1 (CB1).

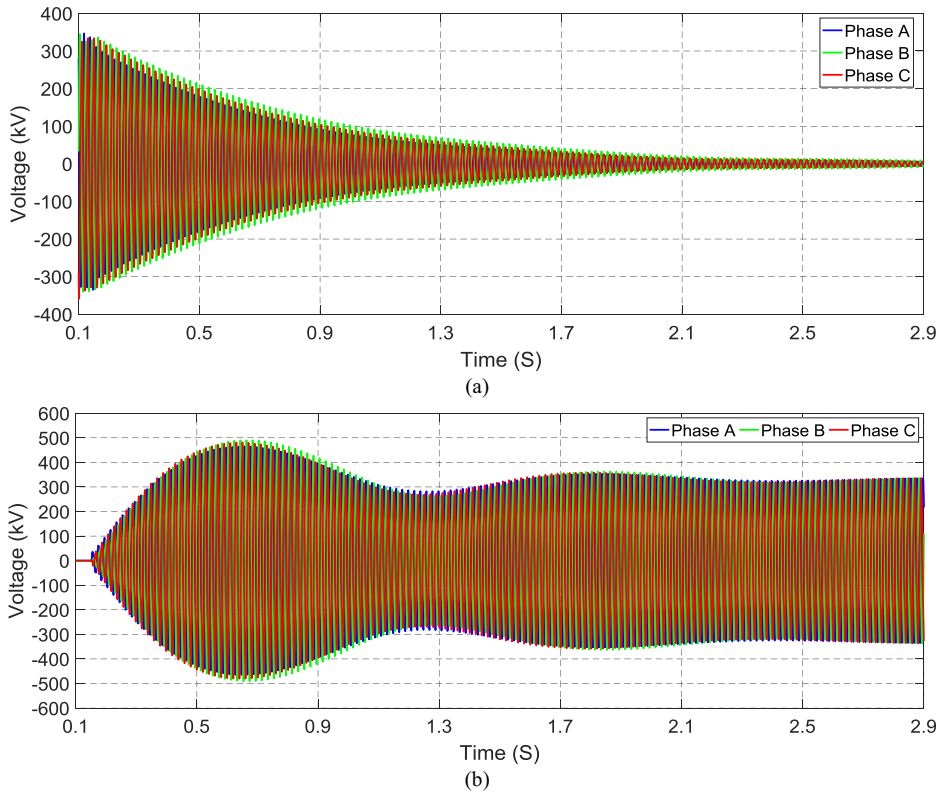
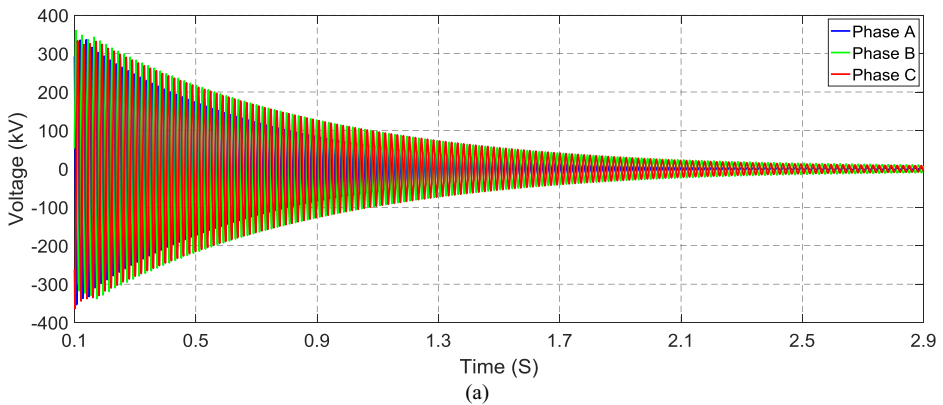


Figure 7.13: Voltage after the de-energization of the 75% cable scenario while the shunt reactors are still connected, (a) at the end of the disconnected circuit (Krimpen side), (b) across circuit breaker 1 (CB1).



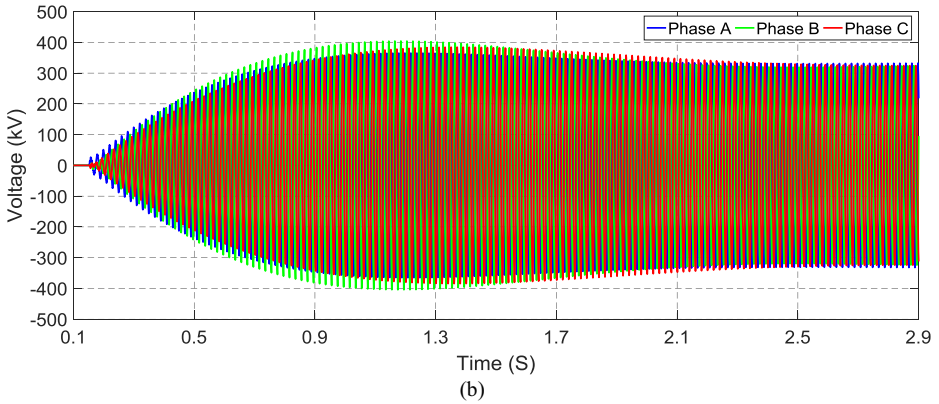


Figure 7.14: Voltage after the de-energization of the fully-cable scenario while the shunt reactors are still connected, (a) at the end of the disconnected circuit (Krimpen side), (b) across circuit breaker 1 (CB1).

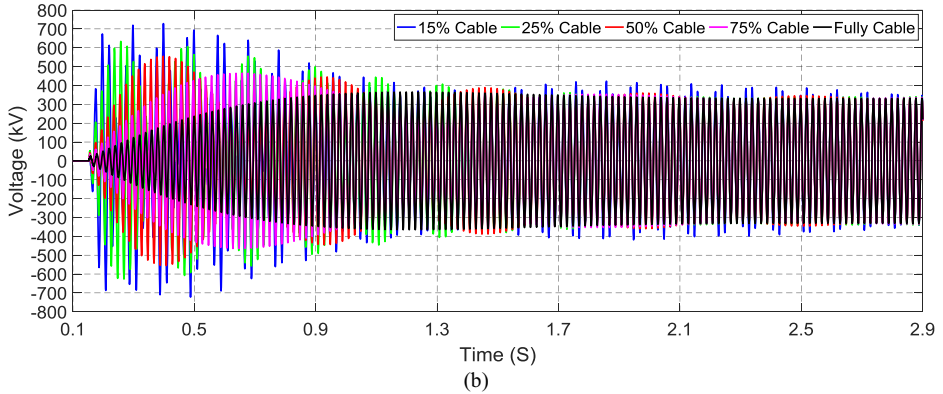
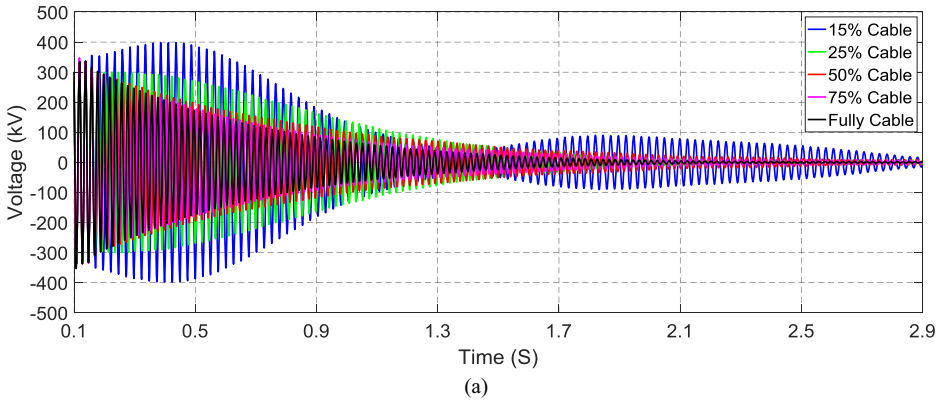


Figure 7.15: Voltage of phase A after the de-energization of the six cable scenario while the shunt reactors are still connected, (a) at the end of the disconnected circuit (Krimpen side), (b) across circuit breaker 1 (CB1).

7.4 CONCLUSIONS

De-energization transients of hybrid OHL-Cable circuits were studied in this chapter, where one of the circuits of the Spaak connection was disconnected from the grid with and without shunt reactors connected to it.

It was discovered that when both the cable and shunt reactors are de-energized, the cable behaviour is very similar to that of a parallel RC-circuit. This means that the trapped voltage on the disconnected cable is a decaying DC-voltage, which discharges through the insulation resistance (and VTs if present). The required time for a complete discharge of a long cable is very long (up to tens of seconds or minutes depending on the cable length) and it becomes even longer by increasing the cable length since the time constant of the circuit increases. When VTs are present, the cable discharge is much faster due to the quick saturation of VTs.

When a hybrid OHL-Cable circuit is de-energized while shunt reactors have been left connected to the phases, the residual voltages on the disconnected phases are decaying oscillatory AC-voltages with superimposed frequencies instead of decaying DC-voltages. In this situation, the cable discharge is much faster compared to the discharge of a stand-alone cable. However, resonance overvoltages (or ferroresonance when reactors are magnetic-core) may occur in the disconnected phases when a capacitive coupling exists with the other energized phases. These risks can be minimized by connecting the shunt reactors via breakers to the circuit so that they can be disconnected from the de-energized phases. It was also observed that by increasing the cable share in the circuit, the voltage of the disconnected circuit becomes less modulated and more symmetrical between the phases, where the maximum overvoltage becomes lower too. This is due to the smaller capacitive coupling between the phases when the OHL share in the circuit has been decreased.

In the simulated scenarios, high TRVs across the terminals of the line circuit breaker were observed, especially for shorter cable scenarios. In fact, the peak TRV is lower due to the smaller capacitive coupling between the phases when the cable share in the circuit is increased. High TRVs increase the probability of the breaker restrike due to the breakdown of the dielectric between the circuit breaker contacts. Since restrike overvoltages can be very dangerous and harmful for power system components, an in-depth study is required to evaluate the restrike risks. In general, breakers which perform the capacitive current switching should have low or very low probability of restrike to minimize the risk of restrike overvoltages.

REFERENCES

- [1] R. Smeets, L. van der Sluis, M. Kapetanovic, D. Peelo and A. Janssen, *Switching in Electrical Transmission and Distribution Systems*, Hoboken, NJ, USA: Wiley, 2015.
- [2] L. van der Sluis, *Transients in Power Systems*, Chichester, UK: Wiley, August 2001.
- [3] F. F. da Silva, C. L. Bak and P. B. Holst, "Switching restriks in HVAC cable lines and hybrid HVAC cable/OHL lines," in *International Conference on Power System Transients (IPST)*,

- Delft, The Netherlands, June 2011.
- [4] I. Lafaia, F. Ghassemi, A. Ametani, J. Mahseredjian, S. Dennis, A. M. Haddad and S. Robson, "Experimental and theoretical analysis of cable discharge," *IEEE Transactions on Power Delivery*, vol. 32, no. 4, pp. 2022-2030, August 2017.
 - [5] A. Ametani, T. Ohno and N. Nagaoka, *Cable System Transients: Theory, Modeling and Simulation*, Hoboken, NJ, USA: Wiley, July 2015.
 - [6] "High-voltage Switchgear and Controlgear-Part 100: Alternating-Current Circuit-Breakers," IEC 62271-100, 2008.
 - [7] "IEEE Guide for the Application of Capacitance Current Switching for AC High-Voltage Circuit Breakers Above 1000 V," IEEE Standard C37.012, 2014.
 - [8] CIGRE Working Group C4.502, "Power system technical performance issues related to the application of long HVAC cables," *CIGRE Technical Brochure no. 556*, October 2013.
 - [9] C. L. Bak, W. Wiechowski, K. Sogaard and S. D. Mikkelsen, "Analysis and simulation of switching surge generation when disconnecting a combined 400 kV cable/overhead line with shunt reactor," in *International Conference on Power System Transients (IPST)*, Lyon, France, June 2007.
 - [10] C. L. Bak, H. Baldursson and A. M. Oumarou, "Switching overvoltage in 60 kV reactor compensated cable grid due to resonance after disconnection," in *8th International Conference on Electric Power Systems, High Voltages, Electric Machines (POWER '08)*, 2008.
 - [11] F. M. F. da Silva, "Analysis and simulation of electromagnetic transients in HVAC cable transmission grids," Ph.D. dissertation, Department of Energy Technology, Aalborg University, Aalborg, Denmark, 2011.
 - [12] F. F. da Silva and C. L. Bak, *Electromagnetic Transients in Power Cables*, London, UK: Springer, 2013.
 - [13] CIGRE Working Group C4.307, "Resonance and ferroresonance in power networks," *CIGRE Technical Brochure no. 569*, February 2014.
 - [14] F. Iliceto, E. Cinieri and A. Di Vita, "Overvoltages due to open-phase occurrence in reactor compensated EHV lines," *IEEE Transactions on Power Apparatus and Systems*, vol. PAS-103, no. 3, pp. 474-482, March 1984.

CHAPTER 8

CONCLUSIONS AND RECOMMENDATIONS

8.1 SOCIAL AND SCIENTIFIC RELEVANCE

During recent years, the utilization of long EHV underground cables in transmission grids has gained lots of attention among transmission system operators. This tendency is due to the widespread public and governmental support to limit the use of overhead transmission lines as they cause visual effect, land occupation, possible environmental impacts, and property price decrement when they cross through populated or environmentally sensitive areas.

Building full or partial cable-based grid connections with long sections of underground cables, at least in sensitive locations like populated areas and national parks, can be a solution to remove or limit the disadvantages of OHLs. Grids with such connections are known as hybrid OHL-Cable grids, where transmission connections are composed of OHLs in non-sensitive areas and underground cables in sensitive (and maybe non-sensitive) areas. Some advantages of cables over OHLs are: faster attenuation of the electromagnetic field with distance from the installation, limited visual impact, no audible noise, and a narrower right-of-way. These advantages enable system operators to develop transmission grids with reduced societal and environmental impacts.

Although the utilization of long EHV cables¹ in transmission grids is very encouraging from the societal and environmental perspectives, new challenges can arise mainly from the technical point of view. The large-scale operation of long cables in transmission grids is not a well-practiced technique by system operators. Underground cable connections are more expensive to construct compared to OHLs, however they are easier to maintain. Cables have been so far widely used in distribution grids but rarely used in transmission grids. In addition, cables are very different from OHLs from electrical, thermal, and mechanical perspectives. These differences may lead to several undesirable operating conditions, which increase the chance of damage to system components and reduce the reliability of the

¹ Cables that need reactive power shunt compensation are generally considered as long cables. For a three-phase 380 kV cable circuit with a single cable per phase, a long cable is associated to cables roughly longer than 10 km transmission length.

power supply. Therefore, it is required to have an in-depth knowledge and a set of guidelines for planning, designing, and operating of transmission systems with a large share of cables.

So far, numerous studies have been carried out by researchers and system operators to investigate the impact of long cables on the performance of transmission systems, where they have addressed the technical challenges and solutions of various phenomena related to cables. However, there are still several crucial scientific gaps that need to be tackled, especially in relation to systems composed of both OHLs and cables (hybrid OHL-Cable systems).

The aim of this thesis was to address the most important scientific gaps and unanswered questions in this area with the use of a reliable model and a rigorous approach, which make the findings of this thesis applicable to any transmission system. The research was conducted for a hypothetical 80 km double-circuit connection in the future Dutch 380 kV grid, called the Spaak project. For this purpose, accurate steady-state and electromagnetic transient (EMT) models of the entire Dutch 380 kV grid were used to ensure the maximum simulation accuracy.

8.2 SCIENTIFIC CONTRIBUTIONS

This thesis resulted in a set of original findings, which are the knowledge and techniques needed for a reliable design and operation of a hybrid OHL-Cable transmission system. These findings can be applied in practice to determine the possible hazards of future undergrounding and, if necessary, design countermeasures to eliminate or minimize them. In this regard, the main scientific contributions of this thesis are as follows:

1. Studying a hybrid OHL-Cable system with different cable scenarios and circuit configurations with an extensive sensitivity analysis on the system parameters to determine their impact on the system operation and performance.
2. Proposing and applying a method for precise shunt compensation sizing and locating for double-circuit hybrid OHL-Cable connections, where the impacts of the circuit configuration and shunt reactor locations on the required size of compensation were determined (Chapter 3).
3. Investigation of the harmonic resonance behaviour of hybrid grids for different system topologies in terms of two indicators: the lowest resonance frequency and the number of resonance frequencies (Chapter 4).
4. Determination of the statistical distribution of energization overvoltages in hybrid OHL-Cable systems by the use of extensive statistical simulations and rigorous sensitivity analysis on various parameters of the hybrid systems. As a result, the potential risks in hybrid systems with respect to the energization overvoltages were identified (Chapter 5).
5. Determination and analysis of several countermeasures for the zero-missing phenomenon, where as a result, a guideline for the selection of the most suitable and robust countermeasure was proposed. In addition, presenting an in-depth analysis on

the point-on-wave switching and defining the permissible breaker closing variation threshold (BCVT) that is needed to avoid the zero-missing phenomenon when synchronised switching at voltage peak is applied (Chapter 6).

6. Simulation and analysis of de-energization transients and transient recovery voltages due to the disconnection of a hybrid OHL-Cable circuit (Chapter 7).

8.3 FINDINGS AND CONCLUSIONS

Throughout the thesis, several conclusions regarding the design and system impacts of hybrid OHL-Cable systems have been made. In this section, a summary of the most important conclusions will be presented.

The first investigated technical issue was the steady-state operation and the shunt compensation allocation of hybrid OHL-Cable systems. This is a crucial issue in the design and impact study of cable projects as it leads to find the optimal size and location of the shunt reactors. Various technical problems are associated with the reactive power of long cables, where these problems should be prevented or mitigated by an optimal shunt compensation of the reactive power. The most significant problems are the decrease of the cable transfer capacity, steady-state voltage rise, under-excitation of synchronous generators (in severe cases self-excitation), and large capacitive currents in the line circuit breakers.

According to the simulation results, it is crucial to investigate the influence of different load-flow scenarios on the allocation of shunt reactors. The results could significantly vary from one load-flow to another as the short-circuit power and voltage levels change. Moreover, the most decisive sizing criterion is dependent on the load-flow scenario, the cable length, and the shunt reactors location. It was also discovered that both the minimum required compensation size and degree increase by increasing the cable length while a 100% compensation degree can be only needed for very long cables in systems operated at voltages higher than approximately 1.05 pu. Moreover, it is necessary to investigate the risk of cable overloading in case of parallel operation with OHLs or operation in a meshed network. Larger amount of power tends to flow through the cable connections due to the lower series impedance of cables compared to OHLs. The cable overloading can be avoided or mitigated by countermeasures like the use of phase shifting transformers or series reactors.

For long cables, shunt reactors should be connected to the circuit and behind the line breakers as it limits post-switching steady-state energization overvoltages in the circuit (especially at the open-end of the circuit due to the Ferranti effect) and minimizes the capacitive current through the line breaker during energization. These benefits are not achieved when shunt reactors are connected to busbars or to tertiary windings of power transformers at substations. However, for some cable lengths, shunt reactors can be connected to busbars or to tertiary windings if energization overvoltages and capacitive currents are not very large. It was also concluded that shunt reactors should be energized at the same time or with a short delay (depending on the cable length) after the cable

energization to limit the capacitive current, reactive power injection to the system, and steady-state overvoltages.

Furthermore, a distributed compensation along the circuit can decrease the minimum required size of compensation in comparison to the traditional type of compensation at the two remote ends of the circuit. This is due to the fact that the distributed compensation provides a very effective voltage control along the circuit (especially in circuits with long cables), which leads to the need for a smaller compensation size. Another advantage of the distributed compensation is the increase of the active power transfer capacity of the cable, which is needed for very long cables when the cable has almost reached its critical length. In addition, the distributed compensation is more reliable in the case of failure in one of the reactor banks because the rest of the reactors will remain in operation. To summarize, it is necessary to apply a distributed compensation for very long cables (and recommended for long cables) to achieve the mentioned advantages.

The second investigated technical issue was the resonance behaviour of hybrid OHL-Cable systems. This is a very important issue as the higher risk of low-order resonance overvoltages raises serious concerns regarding the large-scale application of cables. In fact, the application of long cables can significantly decrease the resonance frequencies to low-order ranges. According to the simulation results, the risk of resonance frequencies close to the second and third harmonics is substantially higher when long cables are operated in the grid. In addition, the resonance impedance magnitudes and the number of resonance frequencies increase when cables are applied. Another concern is the amplification of the existing background harmonics above the accepted limits, which can cause overvoltages and power quality issues.

Moreover, temporary overvoltages produced by a resonance in a cable system are weakly damped and last long, where such sustained resonance overvoltages can impose hazardous operating conditions for system components with the risk of failure. Surge arresters are one of the most vulnerable components since they are not intended to mitigate TOVs and therefore their energy absorption capabilities can be exceeded.

From the resonance point of view and for future cable projects, it is advised to investigate all available possibilities for the number, locations, and lengths of the cable and OHL sections as well as the size and location of the shunt reactors. It was shown that these parameters have impact on the resonance behaviour of the grid. The short-circuit power has also a direct impact on the order of the resonance frequency, where a higher short-circuit power leads to a higher first resonance frequency. In near future, a short-circuit power decrease is expected due to the increasing share of renewable power generation and the decreasing share of conventional generation, which will result in lower resonance frequencies.

The third investigated technical issue was the energization overvoltages phenomenon. Energization overvoltages in high voltage systems can reach very high values and are considered among the severest overvoltages stressing the insulation of system components. Therefore, the significance of these overvoltages should be precisely determined for the insulation coordination studies. It has been strongly advised in the literature and by IEC

standards that the insulation coordination study should be based on a statistical simulation to derive and to assess the statistical distribution of energization overvoltages and their significance.

By means of extensive statistical simulations, it was found that a hybrid OHL-Cable circuit with a given transmission length produces energization overvoltages higher than those of a fully-cable circuit and most likely lower than those of a fully-OHL circuit with the same transmission lengths. This means that the probability of experiencing high energization overvoltages and stressing system components is higher in a fully-OHL circuit than in a partial or fully undergrounded circuit.

Energization overvoltages are also very dependent on the number, locations, and lengths of the OHL and cable sections because of the consequent changes in the energizing wave propagation. For a given cable scenario, the existence of long cable sections at the open-end of the circuit results in lower energization overvoltages compared to the case that short cable sections are at the open-end. The cable energization with trapped charges on the cable can generate even higher overvoltages on both the core and sheath conductors and increase the risk of equipment failure.

Furthermore, energization overvoltages can be substantially affected by the system parameters, most notably the short-circuit power of the feeding network and the shunt compensation size and location. The transient energization overvoltages will be likely lower when the network short-circuit power is lower (i.e. weaker supply network), whereas the post-switching steady-state overvoltages will be higher due to the Ferranti effect at the open-end of the circuit. Moreover, a distributed reactive power compensation along the circuit, like cable-end compensation, results in lower transient overvoltages compared to the line-end compensation.

It should be again noted that extremely high overvoltages (higher than 3 pu) may occur in hybrid OHL-Cable circuits for specific situations like the presence of trapped charges on the cable, the existence of very short cable sections at the open-end of the circuit, and certain short-circuit powers. A special attention should be paid to these situations as they can lead to a component failure and/or exceeding the energy absorption capacity of surge arresters and sheath voltage limiters.

Finally, with respect to the energization transients, it is worth noting that a particular attention should be given to high inrush currents due to the back-to-back energization of cable circuits (parallel cables energization). This is a similar phenomenon to the back-to-back capacitor banks switching, although the amplitude, frequency, and the rate-of-rise of the cable inrush current are normally lower than those of an equivalent capacitor bank due to the relatively higher surge impedance of cables. However, in some cases the cable inrush current can obtain very large values, where mitigation measures should be considered when the circuit breaker ratings are exceeded.

The fourth studied issue was the zero-missing phenomenon in cable systems. The simultaneous energization of the cable and reactors may cause a zero-missing current, which means that the current through the line breaker does not cross the zero value for several cycles (even up to several seconds). In this case, it is difficult or even impossible to

safely open the healthy phases if a fault occurs in the circuit during the energization when the zero-missing current is still present. Therefore, the system is more vulnerable and unprotected against faults when proper countermeasures are not devised at the design stage of the cable project. Several countermeasures are available to prevent, mitigate, or handle the zero-missing phenomenon, where the effectivity of each countermeasure is strongly dependent on the system parameters and topology like the configuration of the hybrid OHL-Cable circuit, the power-frequency voltage, and the short-circuit power.

Six countermeasures of the zero-missing phenomenon were introduced and analysed in this thesis. The applied methodology and findings are applicable on any grid since the study is based on realistic assumptions for the system parameters and topology. It should be stressed that the influence of system topology and parameters (like the configuration of hybrid OHL-Cable circuit, power-frequency voltage, short-circuit power, etc.) on the effectivity of a countermeasure should always be considered. Some of the countermeasures need special designed circuit breakers, control strategies and resistances, which can impose extra costs and complexity on the system design and operation.

The simultaneous energization of the cable and reactors at voltage peak is a common prevention countermeasure; however, the resulting transient overvoltages and inrush currents should be carefully analysed. The impact of stochastic variations in the breaker closing time as well as the breaker compliance with the BCVT (breaker closing variation threshold) should be investigated. To decrease the transient overvoltages and inrush currents, energization of the cable and reactors in sequence, as a prevention countermeasure, can be applied. A voltage dip/swell is the main risk of applying this countermeasure for long cable lengths. In addition, breakers operating at voltage peak should be tested for BCVT. Other countermeasures are sequential switching (handling countermeasure), opening of the faulted phase(s) (handling countermeasure), and increasing the DC-offset damping by resistors (mitigation countermeasure). These methods result in lower transient overvoltages and inrush currents. The DC-offset damping by resistors is a costly but relatively robust measure for which the thermal design of the resistor is a challenge.

The fifth investigated technical issue was the de-energization transients of cables, which is associated with several phenomena. It was found that when both the cable and shunt reactors are de-energized, the cable behaviour is very similar to that of a parallel RC circuit. This means that the trapped voltage on the disconnected cable is a decaying DC-voltage, which discharges through the insulation resistance. The required time for a complete discharge of a long cable is very long (up to tens of seconds or minutes depending on the cable length) and it becomes even longer with the increasing cable length since the time constant of the circuit increases. When inductive voltage transformers (VTs) are present, the cable discharge is much faster due to the quick saturation of VTs.

When a hybrid OHL-Cable circuit is de-energized while shunt reactors have been left connected to the phases, the residual voltages on the disconnected phases are decaying oscillatory AC voltages with superimposed frequencies instead of decaying DC-voltages. In this situation, the cable discharge is much faster compared to the discharge of a stand-alone cable. However, resonance overvoltages (or ferroresonance when reactors have a

magnetic-core) may occur in the disconnected phase(s) when a capacitive coupling exists with the other energized phases. In fact, the induced power-frequency voltage in the disconnected phase(s) by the capacitive coupling with the energized phase(s) can trigger the resonance circuit formed by the reactor inductance, the inter-phase/inter-circuit capacitance, and the cable capacitance.

It is always advised to install separate breakers for the shunt reactors that are directly connected to the circuit. This results in an added switching flexibility as well as minimizing the risk of line resonance/ferroresonance by decoupling the reactors from the disconnected phase(s).

In the simulated scenarios, high transient recovery voltages across the terminals of the line circuit breaker were observed, especially for the scenarios with shorter cable. In fact, the peak transient recovery voltage is lower due to the smaller capacitive coupling between the phases when the cable share in the circuit is higher. High transient recovery voltages increase the probability of the circuit breaker restrike due to the breakdown of the dielectric between breaker contacts. Restrike overvoltages can be very dangerous and harmful for power system components and therefore breakers which have to perform capacitive current switching should have low or very low probability of restrike.

OVERALL CONCLUSIONS

The overall conclusion based on the findings of this thesis is that the large-scale application of underground cables in a transmission system is technically possible under the condition that all technical phenomena and issues are properly addressed in the planning and designing phases of each project. A case-by-case study for cable projects is a “must” as each project has its own electrical and geographical characteristics. System parameters and topology are different in different areas and consequently the severity of phenomena and challenges will be different.

In this regard, it is not possible to determine a specific cable length that can be applied in a grid. The maximum cable length and the optimal topology of the hybrid OHL-Cable circuit must be determined for each cable project by means of the simulation and analysis of all relevant phenomena. If undesirable system behaviour is observed, the necessary countermeasures should be determined in order to avoid or minimize that behaviour. Countermeasures of different phenomena have been addressed in this thesis and literature. They can be either installation of extra components in the system, redesign of the system like varying the number, the location and the length of cable sections, or the use of more robust components by an equipment design study. The decision to choose the right countermeasure is highly dependent on the specifications of the project under study.

For each cable project, it is always recommended to perform a step-by-step study similar to the presented approach in this thesis, in which all the relevant phenomena from the steady-state operation to the electromagnetic transient behaviour are investigated. Such a study should follow the guidelines, grid code, manufacturer requirements, and the most recent standards to guarantee that all requirements for a reliable system operation are met

accordingly. A study flowchart for the technical performance assessment and design of long EHV underground cable connections is presented in Appendix A.

Moreover, a prerequisite of a reliable study is to simulate the system behaviour by means of an accurate, up-to-date, and stable grid model in a proper software package, which depends on the type of the under-investigation phenomenon. In fact, each software package provides specific parameters and models suitable for studying a set of phenomena. For example, the transient phenomena should be always simulated by frequency-dependent models of system components, which are available in EMT programs like PSCAD-EMTDC, ATP-EMTP, and EMTP-RV. In this regard, it is important to keep in mind that programs sometimes use different approaches and formulas to model a given electrical component. These differences should be taken into account in the grid modelling as they may influence the simulation results and conclusions.

An important issue in the simulation of electromagnetic transients is the depth of complexity in the grid representation. The size and the detail level of the modelled area around the location under study can significantly affect both the simulation accuracy and the simulation time. The simulation results are inaccurate when the modelled area is too small or with insufficient details. On the other hand, the required simulation time can substantially increase when the size of the modelled area or the level of details are increased. Therefore, there is a trade-off between the simulation accuracy and the simulation time, which should be properly handled by determining a sufficient modelling depth.

To build reliable component models, it is required to use the most recent and advanced techniques to guarantee the maximum simulation accuracy. Usually, the main challenge is to access the right data for each component as it is not always available or known in the system impact study phase. In these situations, it is recommended to use the standard parameters available from similar projects, literature, and manufacturer datasheets. The necessary guidelines and references to model different system components were discussed in Chapter 2. Cable modelling was extensively covered in this chapter, where it was emphasized that frequency-dependent models based on the Universal Line Model theory are currently the most reliable cable models for electromagnetic transient studies.

8.4 RECOMMENDATIONS FOR FUTURE RESEARCH

Based on the studies of this thesis, several recommendations can be proposed for future research to develop and improve our understanding about the technical performance of systems with long cables:

1. As it was previously discussed, the background harmonic amplification is one of the risks of long cables application in transmission systems. To have a precise understanding of the significance of this risk, it is required to have harmonic measurements at the interested points of the grid, by which the impact of long cables on the harmonic amplification can be analysed. In fact, the severity of the background harmonic amplification should be investigated to get assured that it

complies with the voltage and power-quality standards. When it doesn't comply with the standard limits, proper countermeasures should be taken into account to prevent or minimize background harmonic amplifications. Since harmonic measurements were not available at the time of this research, it is recommended to perform the study in future when the measurement data is available.

2. During transient events, the produced overvoltage surges propagate in both the cable core conductor and the cable sheath. The common practice is to minimize the sheath overvoltages by sheath grounding at ends of every cable major section and at cross-bonding points between minor sections. The later one is realized by the use of sheath voltage limiters (SVL) at cross-bonding points to minimize the transient overvoltages and absorb the excessive energy when severe transients occur. It is recommended to carry out a dedicated study on sheath overvoltages and the energy absorption capability of SVLs in hybrid OHL-Cable circuits. The study will be very similar to that of Chapter 5 for overvoltages in the core conductor and only needs inclusion of SVL model to the cross-bonding points.
3. Lightning transients in cable systems are in general of less concern compared to other transient phenomena like energization and de-energization transients. However, it was experienced that lightning strikes produced very high and steep fast-front overvoltages in the circuit and caused insulating joint breakdown and equipment failure. This phenomenon becomes more complex for hybrid OHL-Cable circuits with cascade connection of OHL and cable sections. The successive reflections and refractions at surge impedance mismatch points can lead to higher lightning overvoltages. It is of interest to analyse the consequences of a possible lightning incident by transient studies in the frequency-dependent model of the system in an EMT program. Such an analysis requires a detailed representation of the grounding systems and high voltage towers.
4. In this thesis, surge arresters were not included in the EMT model of the system in order to simulate and analysis the worst transient overvoltages that can be expected in hybrid OHL-Cable systems. In practice, surge arresters are typically installed at the two remote ends of the circuit or at more locations to limit transient overvoltages due to energizations and lightning events. It is recommended to study the performance and energy absorption capability of surge arresters by including their models into the EMT model of the system. In addition, special attention should be paid to the vulnerability of surge arresters to resonance temporary overvoltages. Sensitivity analysis on parameters is required since temporary overvoltages and their damping rate depend on the system parameters.
5. Restrike overvoltages were discussed in Chapter 7, where it was mentioned that their probability of occurrence and the severity of consequent overvoltages are much higher when cables are being disconnected from the grid. It is absolutely necessary to determine the probability and the effect of restrikes in the system through an in-depth study on this specific phenomenon. This needs an accurate model with the arc representation for circuit breakers.

6. Protection of hybrid OHL-Cable circuits can sometimes be more challenging and more sophisticated than the protection of traditional OHLs. It is recommended to take this technical issue into account in the future studies.

APPENDIX A

STUDY FLOWCHART FOR THE TECHNICAL PERFORMANCE ASSESSMENT AND DESIGN OF LONG EHV CABLE CONNECTIONS

Figure A.2 shows a study flowchart for the technical performance assessment and design of long underground cable connections in EHV power transmission systems. As it has been concluded in the thesis, the maximum cable length and the optimal topology of the hybrid OHL-Cable circuit must be determined for each project by means of simulation and analysis of all relevant phenomena. If undesirable system behaviour is observed, the necessary countermeasures should be determined in order to avoid or minimize that behaviour.

The presented flowchart in Figure A.2 recommends a step-by-step study approach to identify the impact of a transmission connection with long cables on the technical performance of the system. The study determines the optimal cable section lengths, circuit topology, and countermeasures. Some example countermeasures for each technical issue are mentioned in the box under the chart. The flowchart covers the most important system-level phenomena from the steady-state operation to the electromagnetic transients (EMT) and the reliability studies. Each study should follow specific design criteria addressed by the guidelines, grid code, manufacturer requirements, and the most recent standards in order to guarantee that all requirements are met accordingly.

Furthermore, for each phenomenon, an appropriate software package and analysis tool should be used since each phenomenon needs to be simulated by specific parameters and models. For example, the transient and harmonic resonance phenomena should be always simulated by EMT programs like PSCAD-EMTDC, ATP-EMTP, and EMTP-RV.

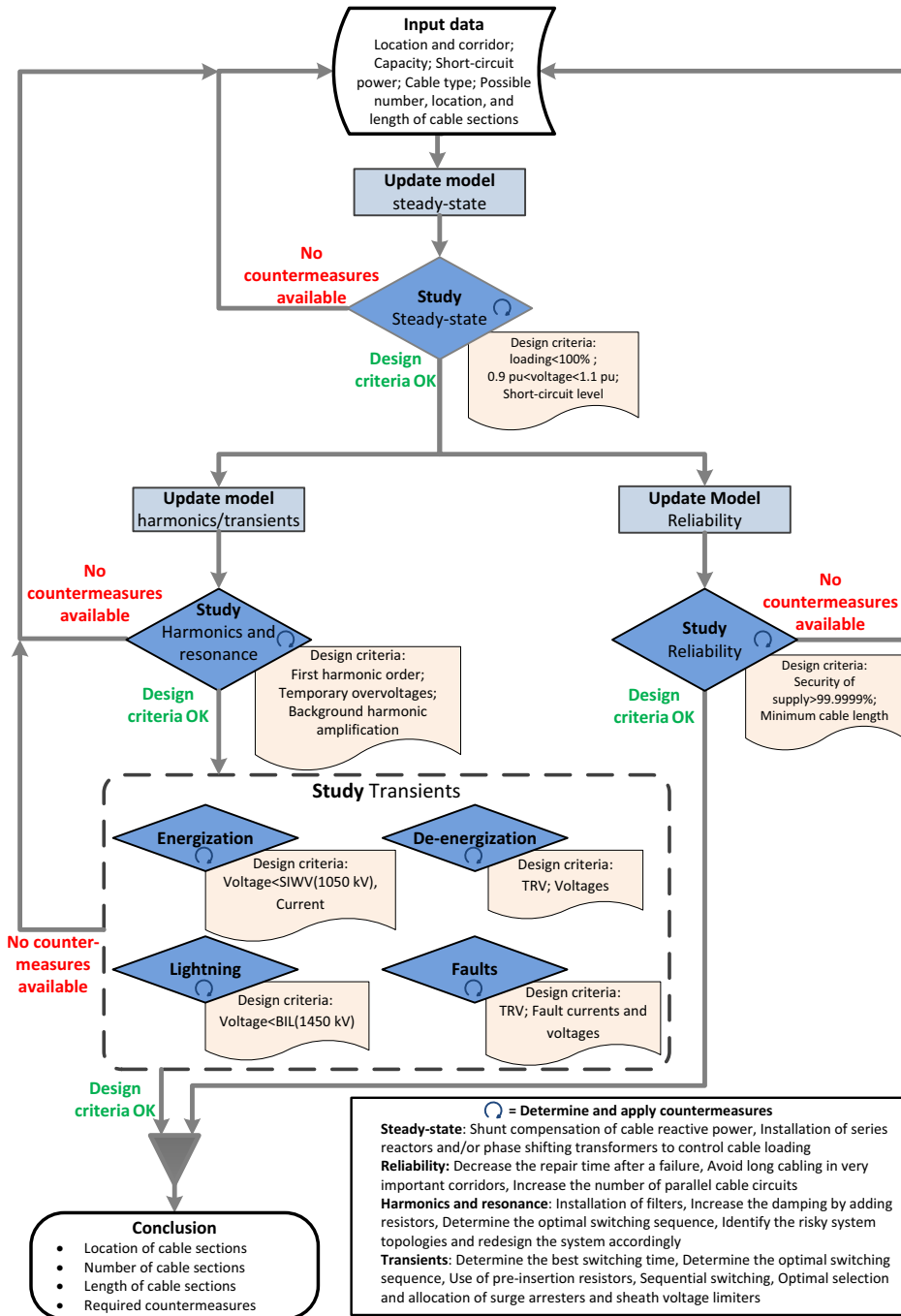


Figure A.1: A study flowchart for the technical performance assessment and design of long underground cable connections in EHV power transmission systems.

GLOSSARY

LIST OF ABBREVIATIONS

AC	Alternating current
Ampacity	Ampere capacity
BCVT	Breaker closing variation threshold
CB	Circuit breaker
CEC	Cable-end compensation
DC	Direct current
EHV	Extra high voltage
EMT	Electromagnetic transient
FACTS	Flexible AC transmission systems
FDNE	Frequency-dependent network equivalent
FFO	Fast-front overvoltage
LEC	Line-end compensation
OHL	Overhead line
PU	Per unit
RVC	Rapid voltage change
SC	Semi-conductive
SFO	Slow-front overvoltage
SIL	Surge impedance loading
SIWV	Switching impulse withstand voltage
SLG	Single-line-to-ground
SR	Shunt reactor
STATCOM	Static synchronous compensator
SVL	Sheath voltage limiter
TCR	Thyristor controlled reactors
TOV	Temporary overvoltage
TP	Transition point
TRV	Transient recovery voltage
TSO	Transmission system operator
VFFO	Very-fast front overvoltage
VT	Voltage transformer
XLPE	Cross-linked polyethylene

LIST OF SYMBOLS AND NOTATIONS

CHAPTER 2

C	Capacitance
dx	Length segment
f_0	System power frequency (nominal frequency)
G	Conductance
I_s	Sending terminal current
I_r	Receiving terminal current
I_n	Rated current (ampacity)
K_{PF}	dP/dF frequency index for real power
K_{QF}	dQ/dF frequency index for reactive power
L	Inductance
NP	dP/dV voltage index for real power
NQ	dQ/dV voltage index for reactive power
P	Equivalent load real power
P_0	Rated real power per phase
Q	Equivalent load reactive power
Q_0	Rated reactive power per phase
R	Resistance
S_n	Apparent power at ampacity (thermal power limit)
V_s	Sending terminal voltage
V_r	Receiving terminal voltage
V_n	System nominal voltage
V_l	Load voltage
V_{l_0}	Rated load voltage
Y	Shunt admittance
Z	Series impedance
Z_s	Surge impedance
Z_c	Characteristic impedance
ω	Angular frequency
v	Wave velocity
γ	Propagation constant

CHAPTER 3

K_{sh}	Shunt compensation degree
L_{max}	Maximum cable length

$L_{critical}$	Critical cable length
l	Cable length
N	Number of cables
P	Active power
P_{max}	Maximum active power transfer
Q	Reactive power
Q_{Sh}	Shunt compensation size
S	Apparent power
V	System voltage
V_r	Receiving open-end voltage

CHAPTER 4

f_1	First resonance frequency
f_n	Natural frequency (resonance frequency)
L_S	Shunt reactor inductance
L_0	Equivalent source inductance
S_{system}	System short-circuit power
S_{cable}	Cable reactive power
X_C	Capacitive reactance
X_L	Inductive reactance
Z_{series}	Series impedance of the circuit
$Z_{parallel}$	Parallel impedance of the circuit

CHAPTER 5

a	Conductor radius
b	Insulation radius
C_0	Light velocity in the free space
K	Kurtosis
S	Skewness
T_{close}	Breaker closing time
$T_{command}$	Instant of breaker closing command
T_{mean}	Breaker mean closing time
V_R	Reflected voltage wave
V_T	Transmitted voltage wave
μ	Permeability
ε	Permittivity
μ_0	Vacuum permeability
ε_0	Vacuum permittivity

μ_r	Relative permeability
ε_r	Relative permittivity
v_{OHL}	Wave propagation velocity in the OHL
v_{cable}	Wave propagation velocity in the cable
\approx	Approximately equal to
ΔT_{known}	Predictable part of the breaker operating time
$\Delta T_{stochastic}$	Stochastic variation in the breaker operating time
$\Delta T_{operating}$	Breaker operating time
σ	Standard deviation
x_i	Sample overvoltage value
μ_v	Mean value of the overvoltages distribution

CHAPTER 6

I_{SR}	Shunt reactor current
$I_{SR,dc}$	DC component of the shunt reactor current
$I_{SR,ac}$	AC component of the shunt reactor current
I_{CB}	Circuit breaker current
I_{cable}	Cable current
T_{peak}	Instant of the voltage peak
V_{max}	Voltage amplitude
φ	Initial phase angle of the voltage
θ	Load angle
τ	Time constant
ΔT_{BCVT}	Maximum variation in the breaker closing time

CHAPTER 7

E	Peak value of the source voltage
$I_{sc,loc}$	Local short-circuit current
I_{cap}	Capacitive current
L_S	Source inductance
P	Local short-circuit active power
Q	Reactive power of the capacitor
U_{CB}	Voltage across the breaker terminals
V_c	Capacitor voltage
V_{max}	Initial capacitor voltage at the de-energization instant

ACKNOWLEDGEMENTS

The five-year work on this thesis was an absolute memorable journey for me. It was a unique opportunity for me to work with exceptional friends and colleagues who have always supported and motivated me. I would like to express my gratitude to all of them in the following remarks.

First and foremost, my special gratitude goes to my promotors at TU Delft, Prof. Lou van der Sluis and Dr. Marjan Popov. I greatly appreciate their trust in my competencies and giving me the opportunity to conduct this Ph.D. research. This thesis would not be accomplished without their support. Working with Lou and Marjan was indeed a rewarding experience that I will carry with myself for the rest of my life. Lou, thank you for the guidance and advices you gave me during past years. You are a very nice person with a positive attitude. Thank you Marjan for always being there to support me with your consistent guidance. We have worked together since 2011 and every moment of that has been a pleasure for me. I will always remember our interesting social conversations and scientific discussions in Delft and during our trips in Boston and Seoul. I learnt many valuable things from you, which I appreciate more than you know.

I would also like to deeply thank my supervisors at TenneT: ir. Jorrit Bos, ir. Jan P. W. de Jong, ir. Jacco Smit, and ir. Kees Jansen. Thank you all for your generous support and collaboration. Working with you was a unique opportunity for me to gain a valuable insight into the field of electrical power engineering and to improve the quality of this thesis. I enjoyed every moment of our fruitful discussions during the monthly meetings in Arnhem. Jorrit, I have had the opportunity to work with you since January 2012 when I started working on my M.Sc. graduation project at TenneT. I am delighted to say that you were fantastically supportive and disciplined. I will be always thankful for your kindness and attitude.

Furthermore, many thanks to all the members of my doctoral examination committee for their effort to review and evaluate my thesis. Their feedback and comments helped me to improve the quality of the thesis. It has been an absolute pleasure for me to have them on board.

My very special thanks and deepest gratitude go to my beloved family for their kind support in my whole life. It would not be possible to finish this journey without them. My amazing parents have been always next to me in hard times and helped me to follow my dreams with their limitless love. Thank you my sisters, Parisa and Pardis, and my brother, Reza, for being always very good friends for me. My confidence and motivation have been always boosted with the love and the energy that I have received from you.

I am also thankful to my wonderful friends in the Netherlands, with whom I have had very lovely memories and experiences. First, I express my gratitude to Babak, Mahshid,

Nakisa, Abdi, Farhad, Ayda, Poolad, Shekofeh, Farzaneh, Javad, Bahar, Bahram, Ahura, Sarah, Shaghayegh, Reyhan, Behnam, Hasti, Hadi Jamali, Farhad Sarabchi, and Elyas. You have been great friends for me and I appreciate all your kindness and support. We have had very joyful and unforgettable moments together for which I am very thankful. I am incredibly fortunate to have friends like you in my life.

My special thanks also go to Swasti, Rishab, Matija, Tina, Lian, Lynn, and Katy for being exceptional friends for me. I am very happy that our life paths crossed each other in Delft. We have had very fun and sweet moments together and I am sure that we will always remain very good friends for each other. Moreover, I thank all my colleagues and friends at the IEPP group for having nice conversations and creating a pleasurable working atmosphere.

My sincere appreciation also goes to my manager at Stedin, Dr. Yakup Koc, for his impressive support during the last year. Yakup is a wonderful boss, colleague, and friend. Working with him has been a privilege for me to shape my professional life and strength my skills. Thank you Yakup!

Last but not the least, I would like to thank the secretary of the IEPG group, Mrs. Ellen Schwencke-Karlas, for her valuable administrative supports. Ellen, thank you for your kindness and responsibility. You are a very good-hearted and lovely person. I also thank Mrs. Sharmila Rattansingh for the fun conversations that we had at her office. I have always received a lot of energy from her.

At the end, I would like to thank all of my friends and colleagues whom I didn't have the chance to mention their names here. Thank you all.

Hossein Khalilnezhad
Delft, November 2018

BIOGRAPHY AND PUBLICATIONS

Hossein Khalilnezhad was born in Iran in 1987. He received his B.Sc. degree in electrical engineering from the Shiraz University of Technology, Shiraz, Iran, in 2010, and the M.Sc. degree (*cumlaude*) in electrical power engineering from the Delft University of Technology, Delft, the Netherlands, in September 2013. Immediately after graduation, he started working toward the Ph.D. degree at the Delft University of Technology, where he studied EHV underground cable systems. In March 2014, he won the Shell Master Award for the best M.Sc. thesis in the field of innovation and technology. He was also awarded the IEEE Power Engineering Society (PES) Travel Grant at the POWERCON conference in Wollongong, Australia, in September 2016.



He is currently working with one of the major Dutch distribution system operators, Stedin Group, as power system and energy transition analyst at the Asset Management department.

PH.D. PUBLICATIONS

JOURNAL PAPERS

1. **H. Khalilnezhad**, M. Popov, L. van der Sluis, J. A. Bos and A. Ametani, “Statistical analysis of energization overvoltages in EHV hybrid OHL-cable systems,” *IEEE Transactions on Power Delivery*, DOI: 10.1109/TPWRD.2018.2825201, April 2018.
2. **H. Khalilnezhad**, M. Popov, L. van der Sluis, J. A. Bos, J. P. W. de Jong and A. Ametani, “Countermeasures of zero-missing phenomenon in (E)HV cable systems,” *IEEE Transactions on Power Delivery*, vol. 33, no. 4, pp. 1657-1667, August 2018.
3. **H. Khalilnezhad**, M. Popov, J. A. Bos and K. P. J. Jansen, “Influence of partial undergrounding on the transient stability of EHV power transmission systems,” *Electric Power Systems Research*, vol. 131, pp. 126-138, February 2016.

CONFERENCE PAPERS

1. **H. Khalilnezhad**, M. Popov, J. A. Bos, J. P. W. de Jong and L. van der Sluis, “Investigation of statistical distribution of energization overvoltages in 380 kV hybrid OHL-cable systems,” in *IEEE International Conference on Power Systems Transients (IPST)*, Seoul, South Korea, June 2017.

2. **H. Khalilnezhad**, M. Popov, L. van der Sluis, J. P. W. de Jong, N. Nenadovic and J. A. Bos, "Assessment of line energization transients when increasing cable length in 380 kV power grids," in *IEEE International Conference on Power Systems Technology (POWERCON)*, Wollongong, Australia, September 2016.
3. **H. Khalilnezhad**, F. Barakou, N. Kandalepa, J. Wu, L. Wu, M. Popov, E. F. Steennis, P. A. A. F. Wouters, S. Mousavi Gargari, J. A. Bos, J. P. W. de Jong, C. P. J. Jansen, J. Smit and R. Kuik, "Shunt compensation sizing, reliability analysis, and condition monitoring measurements and simulations for an EHV mixed OHL-cable connection," in *46th CIGRE General Session*, Paris, France, August 2016.
4. **H. Khalilnezhad**, M. Popov, L. van der Sluis, J. A. Bos and J. P. W. de Jong, "Influence of long EHV AC underground cables on the resonance behavior of the Dutch transmission system," in *IEEE Power & Energy Society (PES) General Meeting*, Boston, USA, July 2016.
5. **H. Khalilnezhad**, S. Chen, M. Popov, J. A. Bos, J. P. W. de Jong and L. van der Sluis, "Shunt compensation design of EHV double-circuit mixed OHL-cable connections," in *IET International Conference on Resilience of Transmission and Distribution Networks*, Birmingham, UK, September 2015.
6. **H. Khalilnezhad**, M. Popov and J. A. Bos, "Influence of 380 kV AC underground cables on the dynamic stability of Dutch transmission system," in *CIGRE International Conference on Innovation for Secure and Efficient Transmission Grids*, Brussels, Belgium, March 2014.

OTHER PUBLICATIONS

JOURNAL PAPERS

1. M. Gitizadeh, **H. Khalilnezhad** and R. Hedayatzadeh, "TCSC allocation in power systems considering switching loss using MOABC algorithm," *Electrical Engineering*, vol. 95, no. 2, pp. 73-85, June 2013.

CONFERENCE PAPERS

1. M. Gitizadeh and **H. Khalilnezhad**, "Phase shifter transformers optimum allocation in power systems using a combinational method," in *IEEE International Conference on Power and Energy (PECon)*, pp. 886-90, Kuala Lumpur, Malaysia, November 2010.
2. M. Gitizadeh and **H. Khalilnezhad**, "Power system loss reduction through TCSC economic installation considering switching loss," in *45th IEEE International Universities Power Engineering Conference (UPEC)*, pp.1-4, Cardiff, UK, September 2010.



During recent years, the utilization of long underground cables in extra high voltage (EHV) power transmission grids has gained lots of attention among system operators. This tendency is due to the widespread support to limit the use of overhead transmission lines in populated or environmentally sensitive areas. Although the utilization of long underground cables in transmission grids is very encouraging from the societal and environmental perspectives, new challenges arise mainly from the technical point of view. The operation of long EHV cables is not a well-practiced technique by system operators and there are still several scientific gaps that need to be investigated. This thesis tackles this issue and provides concrete and comprehensive answers to the most crucial scientific gaps and addresses the required techniques for the reliable operation of cable projects. These techniques can be used in practice by system operators as they are based on realistic assumptions and reliable simulations on an accurate model of an actual power transmission system.